

Nitric oxide signalling in hippocampal synaptic plasticity

Beatrice Marina Pigott

Thesis submitted in fulfilment of the degree of Doctor of Philosophy, University College London (UCL).

I, Beatrice Marina Pigott, confirm that the work presented in this thesis is my own. Where information has been derived from other sources, I confirm that this has been indicated in the thesis.

Some of the data presented in **Chapter 3** has been published in abstract form (Pigott and Garthwaite, 2009).

October, 2011

Abstract

Nitric oxide (NO) is a freely diffusible transmitter acting throughout the mammalian nervous system via guanylyl cyclase activation and cGMP production. Since neuronal NO synthesis is linked to NMDA receptor activation, much research has focused on the role of NO in NMDA receptor-dependent long-term potentiation (LTP). The proposed role predicts that exogenous NO, paired with a standard LTP induction protocol, should restore the NO-dependent component of LTP when NMDA receptors are blocked. Surprisingly, however, tests of this prediction have not been reported. Here, it was found that exogenous NO, paired with a 1-s, 100-Hz tetanus during NMDA receptor blockade yielded a slowly-rising, long-lasting potentiation of CA1 field EPSPs in hippocampal slices. Like NO-dependent LTP, this potentiation required the tetanus and was guanylyl cyclase-dependent. Contrary to predictions, however, the NO-induced potentiation was additive with subsequent LTP. At CA1 and other synapses, NO is viewed as a putative retrograde transmitter, generated postsynaptically and acting presynaptically. Discordant with this role, the NO-induced potentiation was not associated with a persistent change in paired-pulse facilitation, an index of presynaptic function. However, endogenous NO did appear to facilitate neurotransmitter release under conditions of basal stimulation. In this case, NO generated by endothelial cells was responsible, perhaps explaining the requirement for endothelium-derived NO in LTP. An NMDA receptor-independent form of LTP involving L-type voltage-gated Ca²⁺ channels has previously been described at CA1 synapses. Unexpectedly, we found that this type of LTP also required NO, apparently derived solely from neurons. Unfortunately, supposed inhibitors of neuronal NO synthesis, though widely used, were found to be inadequately selective to be of use diagnostically. Finally, presynaptic effects of NO, such as those described above, have been reported to require the guanylyl cyclase $\alpha 1$ subunit. Accordingly, immunohistochemistry was used to investigate the location of this subunit in the hippocampus.

Acknowledgements

I would like to express my sincere gratitude to my supervisor, Professor John Garthwaite, for his help, guidance and advice throughout this project and for sharing his knowledge, time and enthusiasm with me. I am especially grateful to Doctor Andrew Batchelor for so generously giving me his time, for sharing his expertise and for all of his input, and Doctor Giti Garthwaite for lending me her invaluable help, and for her constant encouragement and support throughout my studies. I would also like to thank Kathryn Harris for her kind assistance with a number of aspects of this project, and Doctor Jeff Vernon, for sharing all his useful tips and hints. Lastly I would like to acknowledge Doctor Frances Edwards for her input and to thank everyone in the Garthwaite group for making the laboratory such a friendly and enjoyable place to learn.

I cannot over express my gratitude to my parents, Marina and Charles, my sister, Florence, and the rest of my family, especially my grandmothers, Despina and Hannah, for their love, support and encouragement, without which I would not have reached this stage in my education. For their unrelenting friendship and faith, I would like to express my heartfelt appreciation to Bill, Holly and too many other people to list here. Lastly, I am indebted to John Hanks for introducing me to neuroscience.

This work was supported by the Wellcome Trust (London, UK) and the Biotechnology and Biological Sciences Research Council (Wiltshire, UK). Funding for conferences was generously provided by Guarantors of Brain (London, UK) and the UCL graduate school (London, UK).

Table of Contents

Chapter 1: General introduction

| | | |
|------|--|----|
| 1.1 | Discovery of endogenous NO..... | 15 |
| 1.2 | Synthesis of endogenous NO..... | 19 |
| 1.3 | NO signal transduction..... | 29 |
| 1.4 | Characteristics of NO/cGMP signals..... | 37 |
| 1.5 | Major cGMP targets..... | 41 |
| 1.6 | Pharmacology of NOS and NO-targeted guanylyl cyclase..... | 53 |
| 1.7 | Endogenous activators of NO-targeted guanylyl cyclase other than NO..... | 54 |
| 1.8 | NO-targeted guanylyl cyclase-independent NO signal transduction..... | 55 |
| 1.9 | NO signalling in brain..... | 56 |
| 1.10 | NO and synaptic plasticity in adults..... | 58 |
| 1.11 | LTP, NO and learning and memory..... | 65 |
| 1.12 | The hippocampus..... | 72 |
| 1.13 | General aim..... | 80 |

Chapter 2: General materials and methods

| | | |
|-----|----------------------|----|
| 2.1 | Materials..... | 83 |
| 2.2 | General Methods..... | 93 |

Chapter 3: NO-induced long-lasting potentiation at hippocampal CA1 synapses

| | | |
|-----|-------------------|-----|
| 3.1 | Introduction..... | 103 |
| 3.2 | Aim..... | 108 |
| 3.3 | Methods..... | 109 |
| 3.4 | Results..... | 112 |
| 3.5 | Discussion..... | 144 |
| 3.6 | Conclusion..... | 154 |

Chapter 4: Modulation of basal synaptic efficacy by NO in area CA1 of the hippocampus

| | | |
|-----|-------------------|-----|
| 4.1 | Introduction..... | 157 |
| 4.2 | Aim..... | 159 |
| 4.3 | Methods..... | 160 |
| 4.4 | Results..... | 163 |
| 4.5 | Discussion..... | 172 |
| 4.6 | Conclusion..... | 175 |

Chapter 5: NO and NMDA receptor-independent, L-type voltage-gated Ca²⁺ channel-dependent LTP

| | | |
|-----|-------------------|-----|
| 5.1 | Introduction..... | 179 |
| 5.2 | Aim..... | 186 |
| 5.3 | Methods..... | 186 |
| 5.4 | Results..... | 190 |
| 5.5 | Discussion..... | 204 |
| 5.6 | Conclusion..... | 210 |

Chapter 6: Evaluation of nNOS inhibitors using intact tissues

| | | |
|-----|-------------------|-----|
| 6.1 | Introduction..... | 213 |
| 6.2 | Aim..... | 215 |
| 6.3 | Methods..... | 218 |
| 6.4 | Results..... | 220 |
| 6.5 | Discussion..... | 229 |

Chapter 7: The location of NO-targeted guanylyl cyclase in adult mouse hippocampus

| | | |
|-----|-------------------|-----|
| 7.1 | Introduction..... | 234 |
| 7.2 | Aim..... | 236 |
| 7.3 | Methods..... | 237 |
| 7.4 | Results..... | 244 |
| 7.5 | Discussion..... | 261 |

Chapter 8: Summary

| | | |
|-----|--|-----|
| 8.1 | NO and NMDA receptor-dependent LTP | 268 |
| 8.2 | NO and NMDA receptor-independent LTP | 271 |
| 8.3 | Some general outstanding issues..... | 273 |

Appendix 1: Intracellular recording of synaptic activity in area CA1 using sharp electrodes..... 276

Appendix 2: Mechanism of K⁺-induced, NOS-dependent cGMP accumulation in hippocampus..... 282

References..... 288

List of Figures

| | | |
|------|---|-----|
| 1.1 | Domain structures of the mammalian NOS isozymes..... | 21 |
| 1.2 | Suggested pathway of electron flow through NOS..... | 22 |
| 1.3 | Reaction for NO synthesis by NOS..... | 22 |
| 1.4 | Scheme for regulation of eNOS by caveolin 1..... | 23 |
| 1.5 | The domain structure of NO-targeted guanylyl cyclase..... | 32 |
| 1.6 | Proposed means of cGMP synthesis from GTP by NO-targeted guanylyl cyclase..... | 33 |
| 1.7 | Two-step model for NO-targeted guanylyl cyclase activation by NO..... | 34 |
| 1.8 | Predicted structure of PKGI..... | 42 |
| 1.9 | Predicted structure of PDE 5..... | 45 |
| 1.10 | Predicted topology of CNG and HCN channel subunits..... | 49 |
| 1.11 | Role of HCN channel activity in oscillatory activities in excitable cells..... | 51 |
| 1.12 | NMDA receptor-dependent LTP induction and possible expression through NO..... | 64 |
| 1.13 | Current taxonomy of memory..... | 66 |
| 1.14 | Location of the hippocampus in human and rodent brain..... | 73 |
| 1.15 | Strata of the hippocampus..... | 75 |
| 1.16 | Major connections of the hippocampal formation..... | 78 |
| 2.1 | General NONOate structure..... | 90 |
| 2.2 | Predicted profiles of NO release from two NONOates..... | 91 |
| 2.3 | The location of the hippocampus within the rodent brain and the orientation of transverse slices..... | 94 |
| 2.4 | Stimulating and recording from Shaffer collateral-CA1 synapses in transverse hippocampal slices..... | 96 |
| 2.5 | An example of absorbance at 562 nm by a series of BSA standards following the BCA protein assay..... | 97 |
| 2.6 | An example standard curve obtained by radioimmunoassay..... | 99 |
| 3.1 | Genotyping wild-type and α CaMKII ^{T286A} mice..... | 111 |
| 3.2 | Characterisation of HFS-induced LTP..... | 112 |
| 3.3 | Requirement of LTP for NMDA receptor channel opening..... | 114 |
| 3.4 | Involvement of NOS in LTP..... | 116 |
| 3.5 | Dependency of LTP on extracellular L-arginine..... | 117 |
| 3.6 | Effect of PAPA/NONOate application during HFS and NMDA receptor blockade on synaptic efficacy..... | 120 |
| 3.7 | Impact of the NO-induced potentiation on subsequent HFS-induced LTP..... | 122 |
| 3.8 | Correlation between the magnitude of the NO-induced potentiation and subsequent HFS-induced LTP..... | 124 |
| 3.9 | LTP saturation subsequent to NO-induced potentiation..... | 126 |
| 3.10 | The number of HFS required to saturate LTP and the effect of exogenous NO on | |

| | |
|--|-----|
| saturated LTP..... | 128 |
| 3.11 Effect of exogenous NO on control LTP..... | 129 |
| 3.12 Activity-dependence of NO-induced potentiation..... | 130 |
| 3.13 Impact of L-VGCC inhibition on NO-induced potentiation..... | 132 |
| 3.14 Requirement of NO-induced potentiation for NOS..... | 133 |
| 3.15 Dependence of NO-induced potentiation on NO-targeted guanylyl cyclase..... | 134 |
| 3.16 Involvement of α CaMKII in NO-induced potentiation..... | 136 |
| 3.17 PPF of CA1 fEPSPs..... | 138 |
| 3.18 Effect of 2-Cl-adenosine and forskolin on PPF..... | 139 |
| 3.19 Changes in PPF subsequent to NO-induced potentiation..... | 141 |
| 3.20 Control HFS-induced LTP and PPF..... | 143 |
| 3.21 Working scheme for the involvement of NO in NMDA receptor-dependent LTP..... | 150 |
| 4.1 A typical example of PPF..... | 161 |
| 4.2 Genotyping wild-type and eNOS ^{-/-} mice..... | 162 |
| 4.3 Involvement of endogenous NO in basal PPF..... | 165 |
| 4.4 Contribution of NO-targeted guanylyl cyclase to basal PPF..... | 167 |
| 4.5 Effect of NOS inhibition on the magnitude of PPF in slices from eNOS ^{-/-} mice..... | 169 |
| 4.6 NMDA receptor-dependency of basal PPF in wild-type mice..... | 171 |
| 5.1 Predicted subunit structure and composition of L-VGCCs based on channels purified from skeletal muscle..... | 179 |
| 5.2 Example extracellular recordings of synaptic activity made in one area of the stratum pyramidale..... | 187 |
| 5.3 LTP induced by high frequency (200 Hz) burst stimulation..... | 191 |
| 5.4 Effect of NMDA receptor and L-VGCC inhibition on LTP induced by 200 Hz burst stimulation..... | 192 |
| 5.5 Involvement of NOS in NMDA receptor-independent, L-VGCC-dependent LTP..... | 195 |
| 5.6 Requirement of L-VGCC-dependent, NMDA receptor-independent LTP for NO-targeted guanylyl cyclase..... | 196 |
| 5.7 NMDA receptor-independent, L-VGCC-dependent LTP in eNOS ^{-/-} mice..... | 198 |
| 5.8 K ⁺ -induced cGMP accumulation in hippocampal slices..... | 201 |
| 5.9 Effect of L-VGCC modulators on K ⁺ -induced cGMP accumulation..... | 202 |
| 5.10 Estimating V _m and E _k as a function of [K ⁺] _o | 204 |
| 6.1 Effect of L-VNIO on NMDA-induced cGMP accumulation and nNOS-dependent LTP in adult mouse hippocampal slices..... | 221 |
| 6.2 Chemical analysis of L-VNIO..... | 223 |
| 6.3 Effect of 1400-W on NMDA-induced cGMP accumulation in adult mouse hippocampal slices..... | 224 |
| 6.4 Chemical analysis of 1400-W..... | 225 |
| 6.5 Characterisation of the putative nNOS inhibitors, FX-5043 and JK-5, using immature | |

| | |
|--|-----|
| rat cerebellar slices..... | 227 |
| 6.6 Effect of 100 μ M FX-5043 and JK-5, pre-incubated for 90 min, on NMDA-induced cGMP accumulation in rat cerebellar slices..... | 228 |
| 6.7 Effect of 100 μ M FX-5043 and JK-5, pre-incubated for 90 min, on ACh-induced cGMP accumulation in rat aortic rings..... | 229 |
| 7.1 Immunoperoxidase staining for the NO-targeted guanylyl cyclase α 1 subunit in transverse hippocampal sections fixed with 4 % PFA..... | 245 |
| 7.2 Immunoperoxidase staining for the NO-targeted guanylyl cyclase α 1 subunit in transverse hippocampal sections fixed with 1 % PFA..... | 247 |
| 7.3 Toluidine blue staining of a section of the same tissue as Figure 7.2..... | 248 |
| 7.4 Immunoperoxidase staining for β 1 in transverse hippocampal sections fixed with 4 % PFA using an antibody provided by Prof. S. Behrends..... | 250 |
| 7.5 Immunoperoxidase staining for β 1 in transverse hippocampal sections fixed with 4 % PFA using a primary antibody obtained from Cayman..... | 251 |
| 7.6 Immunoperoxidase staining for nNOS..... | 253 |
| 7.7 Western blots of rat and mouse cerebellum and forebrain lysates for α 1..... | 254 |
| 7.8 Western blot analysis of NOGC α 1 ^{-/-} cerebellum lysate..... | 255 |
| 7.9 Immunoperoxidase staining of NOGC α 1 ^{-/-} and wild-type tissue for the NO-targeted guanylyl cyclase α 1 subunit..... | 257 |
| 7.10 Immunoperoxidase staining of NOGC α 1 ^{-/-} and wild-type tissue for the NO-targeted guanylyl cyclase α 1 subunit..... | 259 |
| 7.11 Immunoperoxidase staining for α 1 in NOGC α 1 ^{-/-} (KO) and wild-type (WT) cortex (transverse sections) fixed with 4 % PFA..... | 260 |
| 9.1 Intracellular recording of pyramidal cell activity in hippocampal slices using sharp electrodes..... | 277 |
| 9.2 PPF of pyramidal cell EPSPs and fEPSPs in hippocampal slices..... | 278 |
| 9.3 LTP of adjacent fEPSPs and pyramidal neuron EPSPs..... | 279 |
| 10.1 Pharmacological profile of high [K ⁺] _o -evoked cGMP accumulation in hippocampal slices..... | 286 |

List of Tables

| | |
|---|----|
| 1.1 Key findings relating to the discovery that NO is an effector of activated macrophage cytotoxicity..... | 18 |
| 1.2 Potential PKG substrates..... | 44 |
| 1.3 cGMP-hydrolysing PDEs..... | 47 |
| 1.4 Major pharmacological tools used for the manipulation of NO/cGMP signalling..... | 53 |
| 2.1 Pharmacological compounds used..... | 83 |

| | | |
|------|---|-----|
| 2.2 | Antibodies used..... | 86 |
| 2.3 | Primers used for PCR..... | 87 |
| 2.4 | Special chemicals, reagents and enzymes used..... | 87 |
| 2.5 | Suppliers of materials..... | 89 |
| 2.6 | Structure and properties of PAPA/NONOate..... | 90 |
| 3.1 | Evidence consistent with retrograde NO transmission during NMDA-receptor dependent LTP in CA1..... | 104 |
| 3.2 | LoxP primers used for PCR of α CaMKII ^{T286A} mouse DNA..... | 110 |
| 4.1 | PCR primers used for genotyping eNOS ^{-/-} mice..... | 161 |
| 5.1 | Summary of the pharmacological properties, tissue distribution and function of L-VGCC subtypes..... | 181 |
| 6.1 | Summary of NOS inhibitors discussed..... | 217 |
| 7.1 | Antibodies used for immunoperoxidase staining, their concentration and supplier..... | 239 |
| 7.2 | Summary of antibodies used for Western blotting, their concentration and supplier..... | 243 |
| 7.3 | Summary of results..... | 261 |
| 10.1 | Inhibitors used to identify the molecular mechanism of K ⁺ -induced, nNOS-dependent cGMP accumulation in hippocampal slices..... | 283 |

Abbreviations

| | |
|-------------------|---|
| 1400-W | [N-(3-aminoethyl)benzyl]-acetamide |
| 200 Hz HFS | 10 200 ms, 200 Hz trains delivered every 5 s at a stimulus intensity that evokes a 0.5-1 mV population spike in the stratum pyramidale. |
| 8-Br-cGMP | 8- Bromoguanosine- 3', 5'- cyclic monophosphate |
| ACh | Acetylcholine |
| aCSF | Artificial cerebrospinal fluid |
| AMPA | α -amino-3-hydroxyl-5-methyl-4-isoxazole-propionate |
| ANOVA | Analysis of variance |
| ATP | Adenosine-5'-triphosphate |
| BCA | Bicinchoninic acid |
| BDNF | Brain derived neurotrophic factor |
| CA | Cornu Ammonis |
| CaM | Calmodulin |
| CAMK | Calcium/calmodulin-activated kinase |
| cAMP | Cyclic adenosine monophosphate |
| cGMP | Cyclic guanosine monophosphate |
| CNBD | Cyclic nucleotide binding domain |
| CNG | Cyclic nucleotide-gated |
| CNQX | 6-cyano-7-nitroquinoxaline-2,3-dione |

| | |
|------------------------------------|---|
| CNS | Central nervous system |
| CO | Carbon monoxide |
| CREB | cAMP response element binding |
| D-AP5 | D-(-)-2-Amino-5-phosphonopentanoic acid |
| DEA/NONOate | 2-(N,N-Diethylamino)-diazenolate-2-oxide diethylammonium salt |
| DMSO | Dimethyl sulfoxide |
| DNA | Deoxyribonucleic acid |
| DPX | Di-N-Butyle Phthalate in Xylene |
| early-LTP | Early phase (within 1 hr of induction) LTP |
| EC₅₀ | Value of half-maximal activation |
| EDRF | Endothelium-derived relaxing factor (NO) |
| EDTA | N,N'-1,2-Ethanedylbis[N-(carboxymethyl)]glycine |
| EGTA | Ethylene glycol-bis(2-aminoethylether)-N,N,N',N'-tetraacetic acid |
| E_k | Potassium equilibrium potential |
| eNOS | Endothelial nitric oxide synthase |
| eNOS^{-/-} | Endothelial nitric oxide-deficient |
| EPSC/P | Excitatory postsynaptic current/potential |
| fEPSP | Field excitatory postsynaptic potential |
| FX-5043 | 6-[[[(3R,4R)-4-(2-[[2,2-difluoro-2-(3-fluorophenyl)ethyl]amino)ethoxy]pyrrolidin-3-yl)methyl]-4-methylpyridin-2-amine |
| GABA | γ-Aminobutyric acid |
| GMP | Guanosine monophosphate |
| GTP | Guanosine-5'-triphosphate |
| HCN | Hyperpolarisation-activated, cyclic nucleotide-gated |
| HEK | Human embryonic kidney |
| HFS | High frequency stimulation (1-s, 100-Hz tetanus) |
| Hsp | Heat shock protein |
| IC₅₀ | Value of half-maximal inhibition |
| I_h | HCN channel current |
| iNOS | Inducible nitric oxide synthase |
| IPSC/P | Inhibitory postsynaptic current/potential |
| ISI | Inter-stimulus interval |
| JK-5 | 6-[[[(3R,4R)-4-(2-[[2-(3-chloro-5-fluorophenyl)-2,2-difluoroethyl]amino)ethoxy]pyrrolidin-3-yl)methyl]-4-methylpyridin-2-amine trihydrochloride |
| K_i | Dissociation constant for inhibitor binding |
| [K⁺]_o | Concentration of extracellular K ⁺ |
| late-LTP | Late phase (> 3 hr post induction) LTP |

| | |
|-----------------------------|---|
| L-NAME | N ^G -nitro-L-arginine-methyl ester |
| L-NMMA | L-N ^G -monomethyl arginine |
| L-NNA | NG-Nitro-L-arginine |
| LTD | Long-term depression |
| LTP | Long-term potentiation |
| L-VGCC | L-type voltage gated calcium channel |
| L-VNIO | N5-(1-Iminio-3-butenyl)-L-orthinine |
| MK-801 | 5-methyl-10,11- dihydro-5H-dibenzo[a,d]cyclohepten-5,10-imine |
| mRNA | Messenger RNA |
| NADPH | Nicotinamide adenine dinucleotide phosphate |
| NANC | Non-adrenergic, non-cholinergic |
| NEO | Neomycin |
| NMDA | N-methyl-D-aspartic acid |
| nNOS | Neuronal nitric oxide synthase |
| NO | Nitric oxide |
| NOGC^{α1-/-} | NO targeted guanylyl cyclase α1 subunit deficient |
| NOGC^{α2-/-} | NO targeted guanylyl cyclase α2 subunit deficient |
| NONOate | 1-substituted diazen-1-ium-1,2-diolate |
| NOS | Nitric oxide synthase |
| NOSIP | NOS interacting protein |
| OCT | Optimal cutting temperature |
| ODQ | 1H-[1,2,4]Oxadiazolo[4,3-a]quinoxalin-1-one |
| P | Probability |
| PAPA/NONOate | (Z)-1-[N-(3-Ammoniopropyl)-N-(n-propyl)amino]diazen-1-ium-1,2-diolate |
| PB | Phosphate buffer |
| PCR | Polymerase chain reaction |
| PDE | Phosphodiesterase |
| PFA | Paraformaldehyde |
| pKa | Acid dissociation constant |
| PKA | cAMP-dependent protein kinase |
| PKG | cGMP-dependent protein kinase |
| PNS | Peripheral nervous system |
| PPF | Paired-pulse facilitation |
| PPR | Paired-pulse ratio |
| PSD | Postsynaptic density |
| PTP | Post-tetanic potentiation |
| SDS | Sodium dodecyl sulphate |
| SEM | Standard error of the mean |
| SERCA | Sarco/endoplasmic reticulum Ca ²⁺ ATPase |

| | |
|-----------------------------|--|
| SPM | Synaptic plasticity and memory |
| TAE | Tris base, acetic acid and EDTA |
| TBS | Tris-buffered saline |
| TBS-T | Tris-buffered saline containing triton |
| TBS-tween | Tris-buffered saline containing tween 20 |
| TTX | Tetrodotoxin |
| UV | Ultra-violet |
| $V_{0.5}$ | Voltage of half-maximal activation |
| VASP | Vasodilator-stimulated phosphoprotein |
| VGCC | Voltage-gated calcium channel |
| V_m | Membrane potential |

Chapter 1:
General introduction

Nitric oxide (NO) is a free radical gas. It is an air pollutant found in cigarette smoke and car exhaust fumes, and yet is also an endogenously produced, freely-diffusible transmitter active throughout the body. The effects of endogenous NO signalling typically fall into three categories: vasodilation, neurotransmission and immune defence. By extension, NO is involved in huge number of physiological processes including, amongst others, neurodevelopment, platelet aggregation, phototransduction, digestion, respiration, cardiovascular function and reproduction. Accordingly, disordered NO signalling has been implicated in myriad pathologies, such as arthritis, asthma, hypertension, diabetes, stroke and Alzheimer's disease.

In the nervous system, a major role of NO that appears to have been evolutionarily conserved is in the regulation of synaptic plasticity, which is thought to underlie various aspects of neurodevelopment, as well as learning and memory in the adult. Since neuronal NO synthesis is linked to NMDA receptor channel opening, the involvement of NO in NMDA-receptor dependent long-term potentiation (LTP) has received much attention. LTP is a form of synaptic plasticity that can be induced in the laboratory and is a putative correlate of learning. In the mammalian brain, NMDA receptor-dependent LTP is archetypal at hippocampal Schaffer collateral-CA1 synapses. Under various conditions, this LTP is NO-dependent. However, the precise role of NO remains ill-defined, and some long-standing hypotheses, most notably that NO is a retrograde messenger, are poorly evidenced. In this project, NO-dependent plasticity at CA1 synapses in the hippocampus has been investigated, paying particular attention to the role of NO in LTP.

1.1 Discovery of endogenous NO

NO was first described by Joseph Priestly, who also discovered oxygen, as a colourless, toxic gas with a short half-life (Priestley, 1775). Indeed, toxic effects of inhaled NO were reported early on in the study of the molecule: first in 1800 by the anaesthetist, Sir Humphrey Davy (Davy, 1800), whose research interests lay in nitrous oxide (N₂O); then in 1967 after N₂O contaminated with NO killed patients in the Bristol Royal Infirmary, UK (Clutton-Brock, 1967). The first indication that NO is a by-product of normal metabolism was the observation made by Mitchell *et al.*

(1916) that healthy male volunteers were capable of excreting more nitrate (NO_3^-), a metabolite of NO, than they consume. However, it was not until the 1980s that the roles of endogenous NO as a vasodilator, neurotransmitter and cytotoxin were discovered.

Beginning in 1977, Ferid Murad published a series of papers revealing that various nitrate-based vasodilators, such as nitroglycerine, caused an increase in guanylyl cyclase activity in tissues including brain, kidney and liver. Nitroglycerine had been manufactured by Alfred Nobel (the founder of the Nobel prize) as an explosive and used since the mid-19th century to relieve angina; although, the mechanism underlying its action was unknown (reviewed by Marsh and Marsh, 2000). Murad found that in pre-contracted smooth muscle preparations, such as guinea pig trachea, cGMP increase was associated with relaxation. Both the increase in cGMP and the relaxation could be mimicked by nitrate-based vasodilators, NO donors, such as sodium nitroprusside, and exogenous NO (Arnold *et al.*, 1977; Katsuki *et al.*, 1977a; Katsuki *et al.*, 1977b; Ignarro *et al.*, 1981). The vasodilatory properties of exogenous NO and concomitant increase in cGMP were then confirmed by a group led by Louis Ignarro using pre-contracted strips of bovine coronary artery (Gruetter *et al.*, 1980a; Gruetter *et al.*, 1980b).

At roughly the same time as this work, Robert Furchgott discovered an apparently freely-diffusible, endothelium-derived relaxing factor (EDRF) responsible for acetylcholine (ACh)-mediated smooth muscle relaxation in aorta (Furchgott and Zawadzki, 1980). Subsequently, numerous similarities between exogenous NO and EDRF were reported. For example, EDRF signalling was cGMP-dependent (Rapoport *et al.*, 1983). Then, in 1987, definitive evidence that endogenously-produced NO was EDRF was reported by 2 groups. One group, led by Ignarro, showed that EDRF derived from bovine pulmonary artery and vein, and exogenous NO applied to endothelium-denuded tissues, elicited identical cGMP production and vasorelaxation. Using a colorimetric assay, they showed that NO is produced and released from artery and vein upon stimulation with a Ca^{2+} ionophore. Moreover, using spectrophotometry, NO and EDRF were demonstrated to react with a complex molecule (reduced haemoglobin) to form an identical product (nitrosylhaemoglobin),

thus providing chemical evidence consistent with NO being EDRF (Ignarro *et al.*, 1987). At the same time, a group led by Salvador Moncada showed that NO, detected using a chemiluminescent assay, was produced by cultured porcine endothelial cells upon stimulation with the hormone, bradykinin, and was sufficient to account for the vasodilatory effects of EDRF produced by the porcine endothelial cells on rabbit aorta (Palmer *et al.*, 1987). Thus, for the first time, a free radical, freely-diffusible transmitter was found to be active in the mammalian body, and the active component of nitrate-based vasodilators was elucidated.

The identification of NO as an intercellular transmitter in brain occurred in 1988. Years prior to the identification of EDRF as NO, it had been found that various agents known to depolarise excitable cells, including K^+ , the Na^+/K^+ -ATPase inhibitor, ouabain, the Na^+ channel enhancer, veratridine, and glutamate (Ferrendelli *et al.*, 1973; Ferrendelli *et al.*, 1974; Ferrendelli *et al.*, 1976) elicited Ca^{2+} -dependent cGMP accumulation in cerebellar and cortical brain slices. In 1977, 2 groups had shown that exogenous NO activated guanylyl cyclase in cerebellar and cortical homogenates, leading to cGMP accumulation (Arnold *et al.*, 1977; Miki *et al.*, 1977). Later, L-arginine was identified as an endogenous activator of a guanylyl cyclase that had been partially purified from the soluble fraction of neuroblastoma cells. NO was also found to activate the cyclase in a manner that was non-additive with the effect of L-arginine (Deguchi and Yoshioka, 1982). In 1985, John Garthwaite found that glutamate-induced cGMP accumulation in dissociated cerebellar cells was NMDA receptor-dependent (Garthwaite, 1985). By selectively ablating different cell types in cerebellar slices, it was discovered that the NMDA-induced cGMP accumulation required an intercellular transmitter, because, although granule cells were necessary for ~ 90% of depolarisation-induced cGMP accumulation in whole slices, the neurons were not required for cGMP accumulation in response to exogenous NO (Garthwaite and Garthwaite, 1987). A year later, Garthwaite characterised the missing transmitter as NO/EDRF and found it to be released from brain slices in a Ca^{2+} -dependent manner following NMDA receptor activation (Garthwaite *et al.*, 1988).

At the same time that endogenous NO was identified as a neurotransmitter, research by several groups combined to assert a role for (higher concentrations of) NO as a cytotoxin used for host defence upon immune challenge. **Table 1.1** summarises the major findings that led to the realisation that activated macrophages are capable of sustained NO synthesis, leading to the generation of supra-physiological NO concentrations and the apoptosis of surrounding cells (including macrophages themselves) by the inhibition of DNA synthesis, mitochondrial respiration and aconitase (for review see MacMicking *et al.*, 1997).

| Publication | Finding |
|--|---|
| Mitchell <i>et al.</i> (1916) Green <i>et al.</i> (1981a; 1981b) | Urinary levels of nitrate exceeded dietary intake in healthy men and germfree rats, suggesting nitrates are endogenously produced by mammals. |
| Hegesh and Shliloah (1982) Wagner <i>et al.</i> (1983) | Urinary nitrate levels were increased in children with fever and diarrhoea and in rats upon injection with <i>Escherichia coli</i> (<i>E. Coli</i>) lipopolysaccharides (LPS), suggesting that nitrate biosynthesis is increased during illness. |
| Stuehr and Marletta (1985) | Experiments conducted <i>in vitro</i> implied that macrophages were sufficient to account for <i>E. Coli</i> LPS-induced nitrate and nitrite synthesis in mice. Nitrite was suggested to be involved in the production of cytotoxins used for host defence. |
| Hibbs <i>et al.</i> (1987) Iyengar <i>et al.</i> (1987) | Nitrite/nitrate synthesis by <i>E. Coli</i> LPS-activated macrophages, as well as cytotoxic effects of macrophages on cultured tumour cells, were found to depend upon L-arginine and result in the co-synthesis of L-citrulline. |
| Hibbs <i>et al.</i> (1988) | Exogenous NO was shown to reproduce the cytotoxic effects of activated macrophages on tumour cells <i>in vitro</i> and to be synthesised by activated macrophages from L-arginine in a reaction that yields L-citrulline. It is concluded that NO is the precursor of nitrite/nitrate synthesised by macrophages and it is hypothesis that it acts as a cytotoxin via formation of iron-NO complexes and degradation of iron-sulphur prosthetic groups. |

Table 1.1 Key findings relating to the discovery that NO is an effector of activated macrophage cytotoxicity.

After the 1980's, a huge amount of research on the physiology of endogenous NO was conducted. In 1992, NO was named molecule of the year by *Science*. In 1998, Furchgott, Ignarro and Murad won the Nobel Prize in Physiology and Medicine for

their discoveries relating to the vasodilatory effects of NO, a fitting award since Alfred Nobel (the founder of the prize) was among the first people to recognise nitroglycerine as a vasodilator (Marsh and Marsh, 2000). Now, NO is one of the most researched signalling molecules active in the mammalian body. Research on the physiology of organisms such as slime moulds (Golderer *et al.*, 2001), jellyfish (Moroz *et al.*, 2004), molluscs (Park *et al.*, 1998), fireflies (Dudzinski *et al.*, 2006) and even plants (reviewed by Wojtaszek, 2000), has combined to show that NO signalling has been highly evolutionary conserved. In accordance with histological data showing a wide distribution of the enzymes responsible for NO synthesis and signal transduction throughout the mammalian body (see **1.2.2** and **1.3.2**), it is accepted that NO has a huge number of consequences for mammalian health and disease. Furthermore, the NO signalling pathway is highly researched as a putative target of therapeutic strategies. Some successful outcomes of this research include anti-anginals, sildenafil (Viagra) and the use of inhaled NO to treat neonates with respiratory failure.

1.2 Synthesis of endogenous NO

Soon after NO was identified as EDRF, an assay based on the conversion of L-arginine to L-citrulline and NO was used to isolate the enzyme responsible for NO synthesis, NO synthase (NOS), from rat cerebellum and identify it as nicotinamide adenine dinucleotide phosphate (NADPH)- and calmodulin (CaM)-dependent (Bredt and Snyder, 1990). This led to the cloning of brain-derived NOS (Bredt *et al.*, 1991b) and its localisation to vascular endothelial cells, nerves of the peripheral nervous system (PNS) and discrete populations of neurons throughout the brain (Bredt *et al.*, 1990; Bredt *et al.*, 1991a).

There are now three identified mammalian NOS isozymes, each coded for by a distinct gene. Two, the neuronal NOS (nNOS) and endothelial NOS (eNOS), are constitutively expressed throughout the nervous system and relate NO production to intracellular changes in Ca^{2+} by their dependence on Ca^{2+} /CaM binding for catalytic activity. The third, inducible NOS (iNOS), is the isoform expressed in immune cells such as macrophages and microglia in response to products of infection (such as

endotoxins) and inflammatory mediators (such as cytokines). Since iNOS expression is only prevalent under pathological states, it will not be considered in detail here (reviewed by Stuehr, 1999; Alderton *et al.*, 2001; Daff, 2010). The existence of a distinct, constitutively expressed mitochondrial NOS is under debate (see Lacza *et al.*, 2006 for a review).

All three well-known NOS isozymes synthesise NO from L-arginine by two steps of monooxygenation and share a common general structure with 50-60 % homology (**Figure 1.1**). Each is conferred with distinct functionality, not only by differences in tissue distribution, but also by multiple differences in the regulation of their activity.

1.2.1 NOS structure and reaction mechanism

Functional NOS exists as a homodimer, each monomer consisting of an N-terminal oxygenase domain, comprising binding sites for the cofactors haem and tetrahydrobiopterin (BH₄), and the substrate L-arginine, and a C-terminal reductase domain, containing sites for flavin adenine dinucleotide (FAD), flavin mononucleotide (FMN) and NADPH binding. The oxygenase and reductase domains are linked by a series of amino acids constituting a Ca²⁺/CaM-binding domain (**Figure 1.1**).

The N-terminal of the most abundantly expressed (> 90 % of total) nNOS splice variant in the brain (Huang *et al.*, 1993), nNOS α , contains a PDZ domain which allows its physical association with various proteins, most notably the NR2B NMDA receptor subunit, via the adaptor protein, post-synaptic density 95 (PSD-95; Brenman *et al.*, 1996; Christopherson *et al.*, 1999). The N-terminal of eNOS contains consensus sequences for myristoylation and cysteine palmitoylation that allow its association with the membrane of endothelial cells, specifically at their caveolae, which are protein-rich invaginations of the membrane. Inducible NOS lacks the ability to associate with membranes and is cytosolic (see Alderton *et al.*, 2001; Daff, 2010 for reviews).

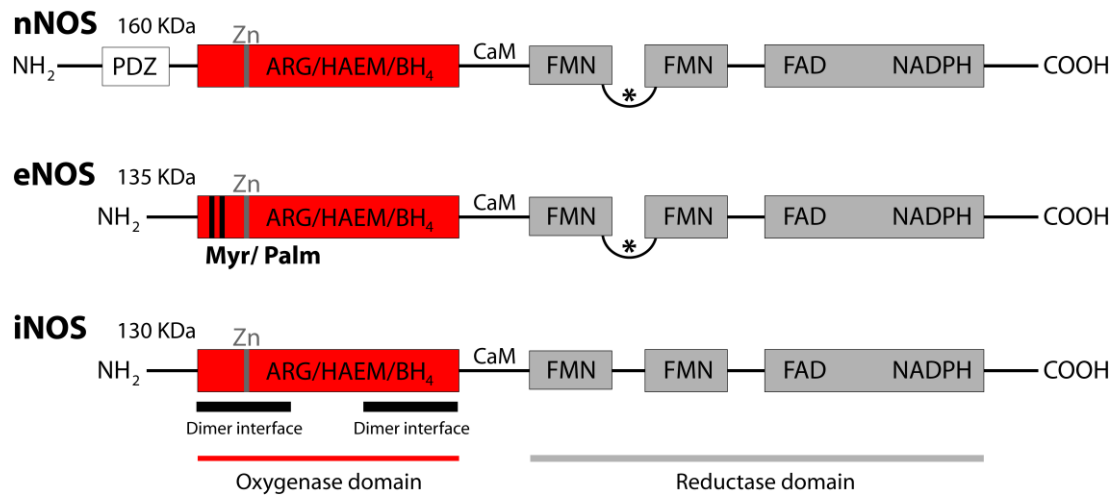


Figure 1.1 Domain structures of the mammalian NOS isozymes. Key: Arg = Arginine; Myr/Palm = sites for myristoylation and palmitoylation; PDZ = PDZ domain; Zn = zinc ligating cysteine; * = autoinhibitory loop. Molecular masses of each monomer are given in KDa. Figure adapted from Alderton et al. (2001).

Homodimerisation of NOS monomers creates an extensive interface between the oxygenase domains of the two subunits. This may be promoted or stabilised by the zinc iron indicated in **Figure 1.1** and the haem, L-arginine, BH₄ and CaM cofactors (see **1.2.3 NOS regulation** for more on the role of CaM). There remain several unknowns as to the exact mechanism of NO synthesis by NOS. However, modelling of the NOS reductase domain on the NADPH-microsomal cytochrome P450 reductase, which also catalyses monooxygenation and contains a diflavin reductase domain, as well as x-ray crystallography studies of the eNOS and iNOS oxygenase domains, have led to a general consensus for the mechanism of NOS action. It is hypothesised that Ca²⁺/CaM binding causes a conformational change in the NOS dimer that facilitates electron transfer through the enzyme from the reductase domain of one monomer to the haem iron of the oxygenase domain of the other monomer. Electron transfer occurs via the sequential reduction of the bound cofactors, NADPH, FAD and FMN (**Figure 1.2**).

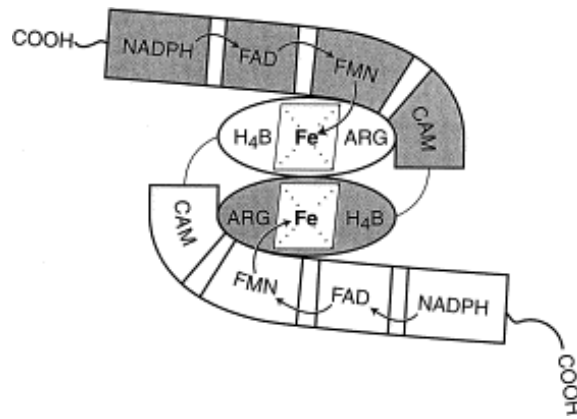


Figure 1.2 Suggested pathway of electron flow through NOS. Monomers are grey and white. Flavins in the reductase domain accept electrons from NADPH and, in the presence of $\text{Ca}^{2+}/\text{CaM}$, pass them to the haem group of the other monomer. Taken from Stuehr (1999). Reproduced by kind permission of Elsevier.

The subsequent reduction of Fe^{3+} to Fe^{2+} in the bound haem allows molecular oxygen to bind, which is then cleaved, resulting in the monooxygenation of bound L-arginine to N^{ω} -hydroxy-L-arginine. Upon a second cycle of monooxygenation, N^{ω} -hydroxy-L-arginine is converted into an unstable compound which collapses, producing L-citrulline and NO (**Figure 1.3**).

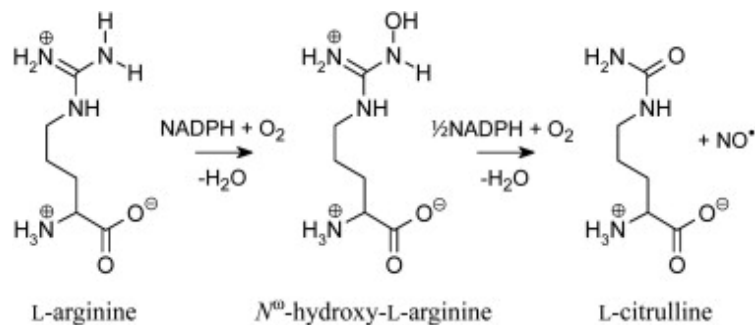


Figure 1.3 Reaction for NO synthesis by NOS. NO is synthesised from L-arginine by two stages of monooxygenation. Taken from Daff (2010). Reproduced by kind permission of Elsevier.

1.2.2 Location of NOS in brain and its intracellular distribution

nNOS

The first studies of the location of NOS in brain used NADPH-diaphorase staining (Vincent and Kimura, 1992; Southam and Garthwaite, 1993), which relies upon the reduction of tetrazolium salts to visible formazans in a NADPH- and NOS-dependent manner. Since then, immunohistochemistry (Bredt *et al.*, 1991a; Rodrigo *et al.*, 1994; de Vente *et al.*, 1998; Burette *et al.*, 2002) and *in situ* hybridisation (Keilhoff *et al.*, 1996) have also been used to locate nNOS protein and mRNA, and this has led to the consensus that nNOS is expressed throughout the entire rodent and primate brain, albeit at varying levels in different areas. In the cerebellum, most neurons are immunopositive for nNOS (Bredt *et al.*, 1990; Southam *et al.*, 1992). Areas such as the hippocampus and olfactory bulb also appear rich in the enzyme (Southam and Garthwaite, 1993). In other brain regions, nNOS appears to be restricted to populations of interneurons, as in the cerebral cortex. However, even in these areas, a dense network of nNOS positive fibres has been discovered, suggesting that the majority of brain cells could be contacted by NO (Vincent and Kimura, 1992; Rodrigo *et al.*, 1994).

The intracellular distribution (and physiology) of nNOS is largely dictated by its interaction with PDZ-containing proteins, such as PSD-95. PDZ domains are motifs for protein-protein interaction. By binding with a PDZ domain in the N-terminal of nNOS α , and another in the C-terminal domain of the NMDA receptor NR2B subunit, PSD-95 physically links the synthase to the NMDA receptor (Christopherson *et al.*, 1999). In this way, nNOS is anchored to a major site of activity-dependent Ca²⁺ influx to cells and is therefore thought to be preferentially activated by NMDA receptor opening. Consistent with this, NMDA causes NO synthesis *in vitro* (Garthwaite *et al.*, 1988; Garthwaite *et al.*, 1989) and *in vivo* (Wood *et al.*, 1990). In tissue supernatants prepared from various brain regions, Ca²⁺-dependent NO synthesis has been shown to be nNOS-dependent (Huang *et al.*, 1993), and suppression of PSD-95 in cultured cortical neurons by an anti-sense oligonucleotide has been found to inhibit NMDA-induced cGMP production by > 60% (Sattler *et al.*,

1999). Neuronal NOS and PSD-95 co-localise throughout the brain (Brenman *et al.*, 1996), and in the hippocampus, immunofluorescent staining has shown that nNOS, NR2 and PSD-95 co-localise in PSDs (Burette *et al.*, 2002).

In addition to nNOS α , there are two other splice variants of nNOS: β and γ . These lack a PDZ domain and are cytosolic. The γ variant appears to be inactive, though the β may be functional in several brain areas, including cortex, hippocampus, olfactory bulb and cerebellum (Brenman *et al.* 1996; Eliasson *et al.*, 1997; Huang *et al.*, 1993).

eNOS

An initial immunohistochemical study of the location of eNOS in the brain found it to be expressed in hippocampal pyramidal neurons (Dinerman *et al.*, 1994) but this result has not been replicated. Rather, data collected using *in situ* hybridisation (Seidel *et al.*, 1997; Demas *et al.*, 1999; Blackshaw *et al.*, 2003), immunohistochemistry (Stanarius *et al.*, 1997; Topel *et al.*, 1998) and polymerase chain reaction (PCR) of DNA from dissociated hippocampal neurons (Chiang *et al.*, 1994) has combined to assert the consensus that eNOS is exclusively expressed in the endothelium of blood vessels.

As discussed above, eNOS has been found to associate with the membrane of endothelial cells, specifically in the cells' caveolae (Garcia-Cardena *et al.*, 1996). Caveolae are enriched in cholesterol and lipids. It is thought that their limited fluidity draws proteins together, thereby promoting protein-protein interactions (Razani *et al.*, 2002). Binding of eNOS to caveolae membranes is thought to occur via the enzyme's N-terminal, which contains consensus sequences for myristoylation, which is irreversible, and palmitoylation, which is reversible (Garcia-Cardena *et al.*, 1996; Alderton *et al.*, 2001). Palmitoylation of eNOS may be subject to dynamic regulation, since prolonged stimulation of eNOS has been reported to cause the enzymes de-palmitoylation and translocation into the cytosol, this presumably limiting the opportunity for eNOS activation (see **1.2.3**).

1.2.3 NOS regulation

Physiological NO signalling necessitates extremely subtle and dynamic NOS regulation because NO is lipid soluble and, therefore, cannot be stored prior to its release. As such, every molecule of NO released by a cell must be synthesised as directed by changing stimuli. The efficacy of normal NOS regulation is illustrated by the range of pathologies in which disordered NO production has been implicated (reviewed by Gross and Wolin, 1995; Hobbs *et al.*, 1999; Vallance and Leiper, 2002) and the diversity of endogenous NO signals (for example, Hopper and Garthwaite, 2006).

Regulation by Ca²⁺/CaM binding

As discussed above, NOS is CaM-dependent. Upon binding to NOS, CaM facilitates the rate of electron transfer through the enzymes' reductase domain and into the oxidase domain. Since CaM is activated by Ca²⁺, NO synthesis is Ca²⁺-dependent and can be directed by alterations in cell activity.

The activity of each NOS isoform varies, and this can be partially explained by differences in their Ca²⁺-dependence. Inducible NOS can become active at low Ca²⁺ levels because it has high affinity for CaM. This confers iNOS with the ability for continuous activity even in the absence of Ca²⁺ and allows it to generate supra-physiological concentrations of NO. The constitutive isoforms, eNOS and nNOS, require higher Ca²⁺ concentrations for activity than iNOS because they contain an autoinhibitory loop (see **Figure 1.1**; Alderton *et al.*, 2001). It has been reported that purified mutant nNOS lacking the autoinhibitory loop can spontaneously oxidise haem and generate NO in the absence of Ca²⁺, suggesting that the loop normally acts to destabilise CaM binding and inhibit electron transfer from FMN to haem at low Ca²⁺ concentrations (Daff *et al.*, 1999). At higher than basal concentrations of Ca²⁺ (EC₅₀ of purified rat brain NOS for Ca²⁺ = 200 nM; Bredt and Snyder 1990), CaM binding to NOS may displace the loop and initiate catalysis (Alderton *et al.*, 2001).

Regulation by phosphorylation

The original cloning of NOS revealed several potential phosphorylation sites that are putative sources of dynamic NOS regulation. Regarding nNOS, some interesting examples of this have been provided by Rameau *et al.* (2004; 2007). Using cultured cortical and hippocampal neurons, they have shown that upon glutamate (5 μM)-induced NMDA receptor (and therefore probably nNOS) activation, phosphorylation of nNOS at serine-847 by Ca^{2+} /CaM kinase II (CaMKII) leads to a slow (taking ~ 15 min) but persistent inhibition of the synthase. This phosphorylation may be indicative of negative feedback on NO synthesis. Following the application of higher glutamate concentrations ($\geq 100 \mu\text{M}$), serine-847 becomes de-phosphorylated. This presumably relieves nNOS of inhibition and may contribute towards NO over-production during glutamate excitotoxicity (Rameau *et al.*, 2004). Rameau *et al.* have also found that the slow inhibition by CaMKII may be preceded by a rapid, NMDA receptor-dependent phosphorylation of nNOS at serine-1412 by Akt (protein kinase B) that is necessary for NO synthesis (Rameau *et al.*, 2007).

The cyclical phosphorylation of two sites, serine-1179 and threonine-497, is of particular relevance to the regulation of eNOS (reviewed by Alderton *et al.*, 2001; Garthwaite, 2005). Phosphorylation of serine-1179, which is close to the eNOS C-terminal, reduces the dependence of eNOS on Ca^{2+} and increases its catalytic rate. Conversely, phosphorylation of threonine-497 in the CaM binding domain increases the synthase's requirement for Ca^{2+} /CaM. Under basal conditions, phosphorylation at threonine-497 predominates over phosphorylation of serine-1179. Upon stimulation of eNOS, threonine-497 is de-phosphorylated and serine-1179 phosphorylated, leading to a persistent (over hours) enhancement of eNOS activity, even in the absence of Ca^{2+} . This Ca^{2+} -independent eNOS activity is thought to underpin the low-level, activity-independent, endothelium-derived NO tone that has been discovered in tissues including optic nerve (Garthwaite *et al.*, 2006) and hippocampus (Chetkovich *et al.*, 1993; Hopper and Garthwaite, 2006). *In vivo*, the PI3 kinase-Akt pathway is probably the primary means of generating serine-1179 phosphorylation, although other kinases, including cAMP-regulated protein kinase A (PKA), cGMP-regulated protein kinase (PKG) and CaMKII may also be responsible.

These kinases, as well as Akt, may be activated in response to stimuli including shear stress, oestrogens, insulin and vascular endothelial growth factor (Garthwaite, 2008).

Regulation by protein-protein interaction

As discussed above, protein-protein interactions, for example, between nNOS and PSD-95, serve to anchor the constitutive NOS isoforms to cell membranes where they may be switched on by a rise in intracellular Ca^{2+} . Importantly, the binding of e- and nNOS to cell membranes is reversible. Indeed, the intracellular distributions of e- and nNOS, and thus the capacity for their activation, are subject to dynamic regulation by various other binding proteins.

The C-terminal PDZ ligand of NOS (CAPON), is an adaptor protein that was identified by a yeast two-hybrid screen with nNOS. Immunohistochemistry for CAPON shows that it is expressed throughout the brain in a distribution overlapping that of nNOS. It contains a C-terminal domain which competes with PSD-95 for binding to the PDZ domain of the synthase. This causes the translocation of nNOS away from the PSD and therefore, may limit neuronal NO synthesis (Jaffrey *et al.*, 1998). In presynaptic terminals, interaction between a phosphotyrosine binding domain in the N-terminal of CAPON and synapsin 1 may direct nNOS to the membrane (Jaffrey *et al.*, 2002) where nNOS may be activated by voltage-gated Ca^{2+} channels (VGCCs), as in the PNS (reviewed by Vincent, 2010).

NOS interacting protein (NOSIP) was also discovered by yeast two-hybrid screening with nNOS and may also modulate nNOS by altering its intracellular distribution. Dreyer *et al.* (2004) have found that NOSIP and nNOS can be co-immunoprecipitated from rat brain lysates, and co-occur in multiple brain areas including the hippocampus, cortex and cerebellum. They also report that expression of NOSIP leads to a reduction in Ca^{2+} -induced NO synthesis in an immortalised cell line containing nNOS, and a (moderate) shift in the location of nNOS from the dendrites to the soma of dissociated hippocampal neurons.

Other protein regulators of nNOS include ‘protein-inhibitor of nNOS’, a dynein light chain that may bind to and regulate the axonal transport of nNOS (Rodriguez-Crespo *et al.*, 1998) and heat shock protein 90 (Hsp90), which has been shown to facilitate nNOS activity *in vitro*, likely by increasing its affinity for CaM (Song *et al.*, 2001).

Endothelial NOS is also regulated by various proteins, most notably caveolin-1. Caveolin-1 is a membrane scaffolding protein and constitutes the main component of caveolae. It has been reported that eNOS and caveolin-1 co-immunoprecipitate from endothelial cell lysates and co-localise in endothelial cells from bovine lung (Garcia-Cardena *et al.*, 1996). Using site-directed mutagenesis, it has been found that the N- and C-terminal domains of caveolin-1 directly interact with the eNOS oxygenase domain, resulting in the inhibition of NO synthesis in a manner reversible by $\text{Ca}^{2+}/\text{CaM}$ (Garcia-Cardena *et al.*, 1997; Michel *et al.*, 1997b). Accordingly, it has been found that transfection of mouse aorta with caveolin-1 inhibits NO synthesis and eNOS-dependent vasodilation *in vivo* (Bucci *et al.*, 2000), whereas mice lacking caveolin-1 exhibit increased NO-induced vasodilation (Drab *et al.*, 2001). It is now thought that the inhibition of eNOS by caveolin-1 is cyclical, being interrupted by activity-induced CaM binding to the synthase which causes eNOS activation, and the translocation of the synthase from the caveolae membrane to the cytoplasm (Michel *et al.*, 1997a; Feron *et al.*, 1998).

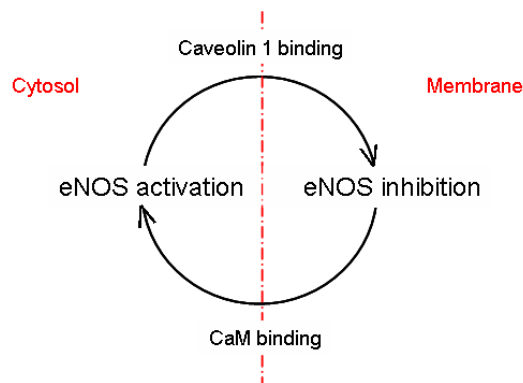


Figure 1.4 Scheme for regulation of eNOS by caveolin-1. Binding of caveolin-1 to eNOS inhibits NO synthesis and anchors it to the caveolae membrane. The interaction between eNOS to caveolin-1 may be disrupted by CaM, which may directly compete for the binding site in eNOS, leading to the activation of eNOS and re-distribution of the enzyme from the membrane to the cytosolic fraction (Feron *et al.*, 1998).

Hsp90 may also bind directly to eNOS in a Ca^{2+} -dependent manner. It has been found to co-immunoprecipitate from endothelial cells with eNOS and caveolin-1 (Gratton *et al.*, 2000), and has been hypothesised to facilitate the displacement of caveolin-1 from eNOS by CaM. Indeed, the EC_{50} of Ca^{2+} and CaM for eNOS is reduced in the presence of Hsp90 (Takahashi and Mendelsohn, 2003a). Additionally, physiological stimuli for eNOS, such as vascular endothelial growth factor or shear stress, have been reported to increase the interaction of Hsp90 and eNOS in isolated cells, whereas an antibiotic-based Hsp90 inhibitor has been found to inhibit eNOS-dependent ACh-induced vasodilation of rat aortic rings (Garcia-Cardena *et al.*, 1998). Co-immunoprecipitation studies also suggest that Hsp90 may facilitate a physical interaction between eNOS and Akt (Garcia-Cardena *et al.*, 1998), consistent with findings that the effects of Hsp90 and Akt on eNOS activity are synergistic at low Ca^{2+} concentrations (Takahashi and Mendelsohn, 2003b).

In caveolae, eNOS may also directly interact with bradykinin B_2 receptors, which, are upstream of the phospholipase C-phosphatidylinositol 4,5-bisphosphate (PIP_2) pathway, and the arginine transporter, cationic amino acid transporter, which may facilitate eNOS activity (reviewed by Nedvetsky *et al.*, 2002). NOSIP may also regulate eNOS in the same way that it does nNOS: Dedio *et al.* (2001) have found that the co-expression of eNOS and NOSIP in Chinese hamster ovary cells causes a reduction in NO synthesis and the redistribution of eNOS from the caveolae membrane to the cytoplasm.

1.3 NO signal transduction

The identification of NO as EDRF was preceded by the discovery that NO elicits cGMP accumulation in tissues such as aorta, lung and brain, and that a rise in cGMP accompanies the relaxation of smooth muscle (see **1.1 Discovery of endogenous NO**). About 20 years prior to this, cGMP had been detected in mammalian urine and various tissues. At around the same time, cAMP, produced by adenylyl cyclases, was recognised as a biological second messenger. This spurred research which led to the discovery of two major variants of guanylyl cyclase that synthesise cGMP from

GTP: one that is membrane-bound and consists of seven isoforms, each of which contain an extracellular binding domain for ligands such as natriuretic peptides and are unresponsive to NO; and another that does not span the membrane and contains a prosthetic haem group able to bind NO (reviewed by Potter, 2011; Schulz *et al.*, 1989). The latter cyclase was initially termed ‘soluble’, but it is now known to associate with membranes under some conditions (see **1.3.2**) and therefore has been renamed ‘NO-targeted’ or ‘NO-activated’.

To date, NO is the only known physiological activator of NO-targeted guanylyl cyclase. Cyclic GMP accumulation via the activation of this enzyme is the only accepted means of physiological NO signal transduction (see **1.8** and Garthwaite, 2008). Amongst the research that has led to this consensus are findings that mice lacking eNOS or the NO-targeted guanylyl cyclase are incapable of NO-induced vasodilation (Huang *et al.*, 1995; Friebe *et al.*, 2007) and that NADPH diaphorase histochemistry for NOS in rodent brain is remarkably coincident with immunohistochemistry for exogenous NO-induced cGMP accumulation (Southam and Garthwaite, 1993).

1.3.1 NO-targeted guanylyl cyclase structure and reaction mechanism

Isoforms of NO-targeted guanylyl cyclase

NO-targeted guanylyl cyclase is an obligate heterodimer comprising one β and one α subunit (Nakane *et al.*, 1990; Buechler *et al.*, 1991; Harteneck *et al.*, 1991). To date, two endogenous, functional isoforms of NO-targeted guanylyl cyclase have been discovered: the $\alpha 1\beta 1$ - and $\alpha 2\beta 1$ -containing enzymes. The isoforms appear to have a similar sensitivity to exogenous NO, capacity for cGMP production and pharmacology (Russwurm *et al.*, 1998; Gibb *et al.*, 2003), but different intracellular distributions (see **1.3.2**). The $\alpha 1\beta 1$ isoform was first purified from rat and bovine lung and subsequently both participating subunits were cloned and sequenced (Koesling *et al.*, 1988; Nakane *et al.*, 1988; Koesling *et al.*, 1990; Nakane *et al.*, 1990; Russwurm *et al.*, 1998). The $\alpha 2$ subunit was identified by homology screening with the $\alpha 1$ subunit. Subsequently, functional $\alpha 2\beta 1$ dimers were reported to form in

cells transfected with both subunits (Harteneck *et al.*, 1991) and, in 1998, were discovered in human placenta (Russwurm *et al.*, 1998). Message for the $\alpha 1$, $\alpha 2$ and $\beta 1$ subunits has now been found throughout the mammalian body and brain (Gibb and Garthwaite, 2001; Mergia *et al.*, 2003).

Two other NO-targeted guanylyl cyclase subunits, namely $\alpha 3$ and $\beta 3$, have been cloned but identified as human variants of the $\alpha 1$ and $\beta 1$ subunits (Zabel *et al.*, 1998). Messenger RNA for a $\beta 2$ NO-targeted guanylyl cyclase subunit has also been detected in rodents, and in various organs (Mergia *et al.*, 2003). The expression of this subunit with $\alpha 1$ in COS-7 cells has been reported to result in a functional cyclase, although with reduced sensitivity to NO compared to the $\alpha 1\beta 1$ and $\alpha 2\beta 1$ isoforms (Gupta *et al.*, 1997; Gibb *et al.*, 2003). However, the transfection of other types of cells with $\alpha 1$ and $\beta 2$ NO-targeted guanylyl cyclase subunits has failed to yield a functional enzyme (Gibb *et al.*, 2003). Furthermore, message for the $\beta 2$ subunit in brain and other organs is negligible, and there have been no reports of an endogenous functional $\beta 2$ -containing NO-targeted guanylyl cyclase (Gibb and Garthwaite, 2001; Mergia *et al.*, 2003).

General structure of heterodimers

Each functionally relevant NO-targeted guanylyl cyclase subunit contains a C-terminal, catalytic domain, a dimerisation domain and an N-terminal, regulatory domain (see **Figure 1.5**). The catalytic domain appears to have been highly conserved across each NO-targeted guanylyl cyclase subunit, and, within the functional enzyme, is so homologous to that of adenylyl cyclase that substitution of three amino acids produces a NO-targeted, cAMP-synthesising enzyme (Sunahara *et al.*, 1998). It is highly likely that the catalytic domain contains the site for GTP binding, and consistent with this, studies using site-directed mutagenesis have found the catalytic domain to be sufficient for un-stimulated cGMP production (Wedel *et al.*, 1995).

The N-terminal regulatory domain of each heterodimer binds one haem prosthetic group, primarily through an interaction with the haem Fe^{2+} and His-105 of the $\beta 1$

subunit (Wedel *et al.*, 1994). The α subunits, which differ significantly from each other within the N-terminal region, may also be necessary for haem binding (Wedel *et al.*, 1995; Foerster *et al.*, 1996; although see Koglin and Behrends, 2003), thus partly explaining why NO-targeted guanylyl cyclase is an obligate heterodimer. The haem is the NO-binding site within the cyclase. It has long been known that NO binds to haem; indeed its interaction with reduced haemoglobin was critical to the identification of NO as EDRF (Ignarro *et al.*, 1987). As such, the haem component of NO-targeted guanylyl cyclase was discovered relatively soon after initial attempts to purify the enzyme (Craven and DeRubertis, 1978; Gerzer *et al.*, 1981) and was immediately identified as a putative NO binding site. Now the evidence in favour of this is convincing. Studies have shown, for example, that haem loss (Foerster *et al.*, 1996), truncation of the N-terminal domain (Wedel *et al.*, 1995; Foerster *et al.*, 1996) or substitution of His-105 with phenylalanine (Wedel *et al.*, 1994) renders the guanylyl cyclase NO-insensitive.

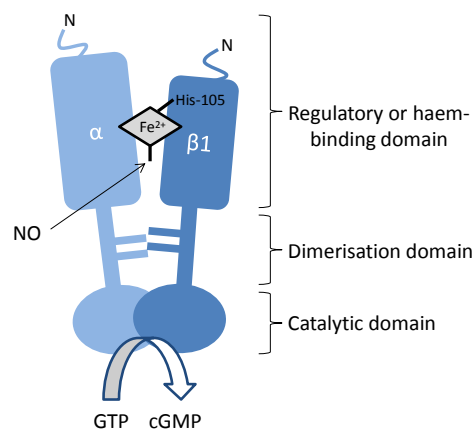


Figure 1.5 The domain structure of NO-targeted guanylyl cyclase. The haem is shown in grey.

Adapted from Bartus (2009).

NO-targeted guanylyl cyclase activation and catalytic mechanism

Soon after NO-targeted guanylyl cyclase was purified from lung, mass spectrometry and high-performance liquid chromatography were used to determine the reaction by which the enzyme synthesises cGMP. The accepted scheme is shown in **Figure 1.6**. NO-targeted guanylyl cyclase is thought to synthesise cGMP by the expulsion of pyrophosphate from GTP (Senter *et al.*, 1983). A basic amino acid residue (labelled

X in the figure), the identity of which is currently unknown, is required to accept a proton from GTP during the reaction.

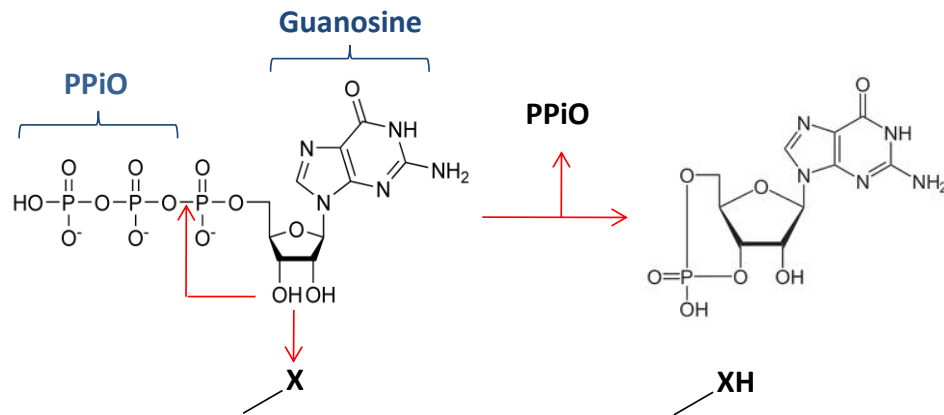


Figure 1.6 Proposed means of cGMP synthesis from GTP by NO-targeted guanylyl cyclase. A basic residue in the NO-targeted guanylyl cyclase (shown as X) accepts a proton from the hydroxyl group at position five of the ribose moiety of GTP. This leads to the displacement of pyrophosphate (PPiO) from the molecule and the formation of cGMP.

Detailed structure-function studies are required to elucidate how NO binding to the NO-targeted guanylyl cyclase haem catalyses this reaction. However, studies on a homologous cyanobacterial NO detector, in conjunction with the analysis of UV-visible absorbance spectra for different haem species formed during NO binding, have led to a general scheme in which the cyclase passes through inactive, NO-bound and active states (**Figure 1.7**; Bellamy and Garthwaite, 2002). When the enzyme is inactive, the haem appears to be five-coordinated, its Fe^{2+} centre covalently bound to the cyclase via His-105 in the N-terminal of the $\beta 1$ subunit. NO binding to the haem, which is thought to be so rapid that it is almost diffusion-limited, forms a six-coordinated haem and is thought to cause the haem to pivot, leading to the rapid (within 1 ms) translocation and subsequent rupture of the bond between it and His-105. Rupture of the bond is assumed to cause a conformational change in the cyclase that propagates to the catalytic domain by some unknown mechanism and causes up to a 1000-fold increase in the rate of cGMP synthesis. The propagation of this conformational change is thought to be the rate-limiting step in activation of the enzyme and is hypothesised to facilitate access of GTP to the catalytic site.

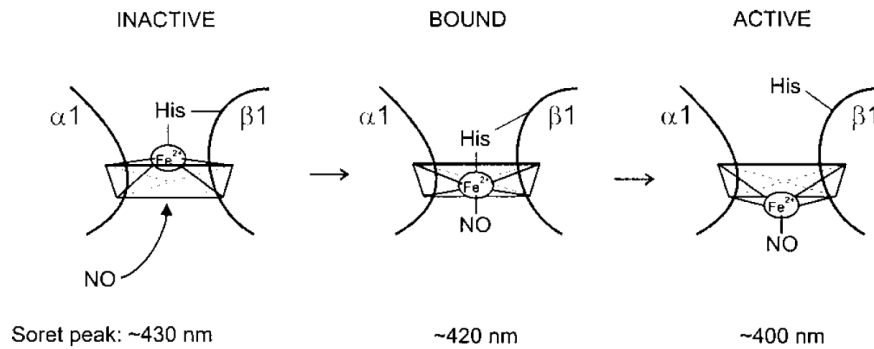


Figure 1.7 Two-step model for NO-targeted guanylyl cyclase activation by NO. In its inactive state, the haem group is five coordinated and bound to His-105 of the cyclase $\beta 1$ subunit. Upon NO binding, a 6 co-ordinate haem is formed. This strains the bond between His-105 and haem, resulting in its cleavage and the formation of the active NO-targeted guanylyl cyclase. Absorbance maximum or Soret peaks for each species are given. Taken from Bellamy and Garthwaite (2002). Reproduced by kind permission of Springer Science and Business Media.

1.3.2 Location of NO-targeted guanylyl cyclase in brain and its intracellular distribution

As assessed using quantitative reverse transcription PCR, message for the NO-targeted guanylyl cyclase is present throughout the body, and is particularly abundant in the lung and brain (Mergia *et al.*, 2003). In the latter organ, *in situ* hybridisation (Matsuoka *et al.*, 1992; Gibb and Garthwaite, 2001), immunohistochemistry (Ding *et al.*, 2004), quantitative PCR and Western blot analysis (Mergia *et al.*, 2003) suggest that all three functionally relevant NO-targeted guanylyl cyclase subunits ($\alpha 1$, $\alpha 2$ and $\beta 1$) are present, although in an uneven distribution. Overall, the amount of mRNA for each of the α subunits appears to be equal and \sim half the total measured for $\beta 1$, consistent with, though not in direct confirmation of, $\beta 1$ being common to both of the functional NO-targeted guanylyl cyclase isoforms so far identified (Mergia *et al.*, 2003). In some brain areas, for example, the cerebellum, hippocampus and olfactory bulbs, the cyclase appears to be densely expressed. In other areas, such as neocortex and brain stem, fewer NO-targeted guanylyl cyclase positive cells are observable. However, in every region NOS and NO-targeted guanylyl cyclase appear to co-occur. Indeed, NADPH diaphorase histochemistry for NOS in rat brain shows a remarkably coincident distribution with cGMP immunohistochemistry following *in*

in vivo perfusion of the NO donor, sodium nitroprusside (Southam and Garthwaite, 1993).

Message for the β subunit is almost always accompanied by mRNA for one or, more typically, both of the α subunits. Some areas appear to contain more RNA for one α subunit than the other. For example, the hippocampus and cerebellum appear richer in $\alpha 2$, whereas the caudate putamen and nucleus accumbens appear richer in $\alpha 1$ (Gibb and Garthwaite, 2001). These trends have been confirmed by quantitative real-time PCR (Mergia *et al.*, 2003).

Within cells, the $\alpha 1\beta 1$ and $\alpha 2\beta 1$ appear to differ in their location. This arises due to the ability of the $\alpha 2$ subunit to interact with PDZ-containing synaptic proteins, including PSD-95 and synapse associated protein-97, through its C-terminal (Russwurm *et al.*, 2001). In this way, the $\alpha 2\beta 1$ isoform may be anchored to the membrane and in remarkable proximity to sites of NO synthesis. In contrast, the $\alpha 1\beta 1$ isoform appears to be mainly cytosolic, although, in platelets and lung endothelial cells, it has been found to translocate to the membrane upon raised concentrations of intracellular Ca^{2+} . Translocation to the membrane has been found to increase the sensitivity of the cyclase to NO (Zabel *et al.*, 2002), perhaps by placing the cyclase closer to sites of NO synthesis.

1.3.3 Regulation of NO-targeted guanylyl cyclase

Compared to NOS, relatively little is known about how NO-targeted guanylyl cyclase activity is regulated. Some putative examples of regulation are given below, although more work is needed to clarify whether these are physiologically relevant and what effect they have on NO-induced cGMP accumulation.

Regulation by co-factors

Several co-factors are required for the conversion of GTP to cGMP. Two Mg^{2+} per cyclase are required for catalytic activity and may facilitate the binding of GTP to the cyclase. Additionally, ATP inhibits NO-targeted guanylyl cyclase, perhaps by

binding to a regulatory site in competition with GTP (Ruiz-Stewart *et al.*, 2004; Roy and Garthwaite, 2006). Apart from the regulation of the $\alpha 1\beta 1$ intracellular distribution by Ca^{2+} (see 1.3.2), this cation also inhibits cGMP synthesis under physiological conditions (Kazerounian *et al.*, 2002).

Regulation by phosphorylation

Both the α and β subunits contain several putative phosphorylation sites that might confer the cyclase with dynamic regulation (reviewed by Pyriochou and Papapetropoulos, 2005). The effect of kinases including PKA and protein kinase C on NO-targeted guanylyl cyclases have been researched, although studies have yielded contradictory results. Two studies have shown that PKG may inhibit NO-targeted guanylyl cyclase, thereby providing cGMP production with negative feedback (Ferrero *et al.*, 2000; Murthy, 2001). Murthy (2001) found that the NO donor, sodium nitroprusside, caused an increase in PKG-dependent ^{32}P incorporation into NO-targeted guanylyl cyclase in gastric smooth muscle that was accompanied by a reduction in cGMP synthesis. Ferrero *et al.* (2000) have reported that NO-targeted guanylyl cyclase is phosphorylated under basal conditions by PKG in chromaffin cells (neuroendocrine cells of the sympathetic nervous system) and that a cGMP analogue or PKG activation leads to the activation of a phosphatase, dephosphorylation of NO-targeted guanylyl cyclase and a subsequent decrease in sodium nitroprusside-induced cGMP synthesis.

Regulation by protein-protein interactions

Several proteins may regulate the intracellular distribution of the NO-targeted guanylyl cyclases. For example, in endothelial cells, Hsp90 may physically link the NO-targeted guanylyl cyclase $\beta 1$ subunit to eNOS (Venema *et al.*, 2003).

1.4 Characteristics of NO/cGMP signals

In the brain, NO may act as a neurotransmitter (discussed **1.9.1**). Research suggests that bursts of NO are synthesised by nNOS in response to synaptic stimuli that cause a rise in intracellular Ca^{2+} (Park *et al.*, 1998; Batchelor *et al.*, 2010). However, unlike classical neurotransmitters, immunohistochemistry for NOS and NO-targeted guanylyl cyclase, in accordance with functional studies of NO transmission, suggest that NO may act as anterograde (for example, Park *et al.*, 1998), retrograde (for example, Arancio *et al.*, 1995; Arancio *et al.*, 1996; Arancio *et al.*, 2001), and/or intracellular transmitter (for example, Burette *et al.*, 2002). These effects may be synapse specific (see below). Tonic NO signals synthesised by continuous eNOS activity have also been found to effect paracrine transmission between blood vessels and groups of neurons (for example, Garthwaite *et al.*, 2006; Hopper and Garthwaite, 2006). To describe the ability of a ‘cloud’ of NO to diffuse freely from a source and potentially affect all receptive structures contacted by a physiologically relevant concentration, the term ‘volume signalling’ has been used. Despite intense research on the dynamics of NO signalling, details that are vital to our understanding of how NO is capable of such diverse signalling, such as what constitutes a physiological or pathological concentration of NO, or how far a physiological concentration of NO can spread through brain tissue from a site of synthesis, remain unclear.

1.4.1 Concentration of physiological NO signals

Initial attempts to measure endogenous NO employed NO/cGMP assays and NO electrodes, which translate a chemical reaction between NO and the electrode tip into an electric potential. Unfortunately, these approaches have many drawbacks, and have led to a wide spread of measurements (from femtomolar to low micromolar values). More recently, NO biosensors have been used to measure the concentration of endogenous NO signals elicited by physiological stimuli. These biosensors are composed of cGMP binding sites connected to fluorescent proteins. Cyclic GMP binding causes a conformational change in the protein and concomitant change in its fluorescence. This type of biosensor takes advantage of the amplification of NO signals by cGMP production and the high selectivity of cGMP-binding proteins over

cAMP and GTP (reviewed by Hall and Garthwaite, 2009). Using a fluorescence resonance energy transfer-based biosensor incorporating the cGMP-binding domain of NO-targeted guanylyl cyclase, Sato *et al.* have detected 1 nM endogenous NO inside un-stimulated endothelial cells. Approximately 100 pM NO was detected inside a cell placed next to hippocampal neurons under the influence of spontaneous, oscillatory network activity or endothelial cells stimulated with ATP (Sato *et al.*, 2005; Sato *et al.*, 2006). In support of such low concentrations of NO representing physiological signals, studies using human embryonic kidney (HEK) cells transfected with a biosensor composed of the cGMP-binding domain of PKG fused to a circularly permuted enhanced green fluorescent protein have shown that even smaller concentrations of exogenous NO (1-3 pM) can be detected by NO-targeted guanylyl cyclase, even in the presence of a phosphodiesterase (PDE; a phosphohydrolase that degrades endogenous cGMP (see **1.4.4**); Batchelor *et al.*, 2010). Very recently, HEK cells containing this biosensor have been used to detect ~ 100-200 pM endogenous NO from overlying cerebellar and hippocampal slices upon stimulation with NMDA (Wood *et al.*, 2011). Consistent with such low amplitude physiological NO signals, only low nanomolar concentrations of NO have been recorded in cerebellar slices and hippocampal slice cultures following extreme stimuli, such as ischemia, maximal NMDA receptor activation and iNOS activation (reviewed by Hall and Garthwaite, 2009).

1.4.2 Spread of NO through tissues

NO is predicted to diffuse rapidly through tissues (tissue diffusion constant of 8.48 $\mu\text{m}^2/\text{s}$). At low nanomolar concentrations, the NO free radical is predicted to be relatively stable. For example, autoxidation of NO will be minimal. However, NO will react with lipid peroxyl radicals and haemoglobin in blood vessels, and it has been suggested that this will limit the half-life of NO in tissue to ~ 1 s (reviewed by Garthwaite, 2008). Further to this, the spread of NO in brain tissue appears to be hugely limited by an unknown means of NO inactivation. In cerebellar slices, this is predicted to limit the half-life of < 10 nM NO to ~ 10 ms. NO inactivation by brain tissue has been illustrated by a marked gradient of immunostaining for NO-induced

cGMP in cross-sections of 400 μm -thick cerebellar slices bathed in a solution containing exogenous NO (Hall and Garthwaite, 2006).

Using a high estimate of the rate of NO production by nNOS (20 molecules/s as measured using the purified enzyme) it has been predicted that, in a 400-nm-diameter PSD containing 50 NMDA receptors, each linked to one nNOS and all active simultaneously, ~ 2 nM NO would be generated, which, upon diffusion, would reduce to 1 nM NO on the other side of the synaptic cleft (60 nm away from the central source of NO), and 250 pM 1 μm away. Upon guanylyl cyclase activation, 250 pM NO would be capable of generating ~ 0.4 μM cGMP (Garthwaite, 2008), which is in excess of that needed to trigger downstream signalling, for example, by cGMP-dependent protein phosphorylation (Francis *et al.*, 2010).

Following lower NMDA receptor activation, the NO cloud would be predicted to become synapse specific, a property favouring the role of NO in input-specific synaptic plasticity. Considering continuous NO synthesis, such as by eNOS in blood vessels, it should be noted that, throughout the brain, brain cells are ≤ 25 μm (\sim a cell diameter) away from a capillary (Pawlik *et al.*, 1981), which are capable of tonic NO production (Mitchell and Tyml, 1996). Therefore, brain capillaries may be as well suited for bathing neurons in a low-level of NO as they are to delivering them O_2 (Garthwaite, 2008).

1.4.3 NO-induced cGMP signals

NO-targeted guanylyl cyclase is highly suited to the capture and transduction of low amplitude, brief NO signals. As discussed above (1.3.1), NO binds the prosthetic haem of the enzyme. Although unremarkable in structure, the haem, once incorporated into the NO-targeted guanylyl cyclase, has high affinity for NO (dissociation constant ~ 20 nM) and exhibits remarkable selectivity for it over NO^+ , NO^- and O_2 . This allows physiological NO signals to be detected in the presence of $> 10,000$ fold excess of O_2 . Unlike the binding of NO to other haem-containing proteins, such as haemoglobin, the binding of NO to NO-targeted guanylyl cyclase appears rapidly reversible (activity in cells decays with a half-time of ~ 200 ms upon

removal of NO). This endows the activation of the purified cyclase with a half-life of ~ 2-5 s following the addition of a NO scavenger. This half-life, coupled with almost instantaneous (within 20 ms) guanylyl cyclase activity upon NO binding, allows the faithful transduction of transient NO signals. It is interesting to note that NMDA receptor activation, which is thought to be the preferential means of stimulating nNOS *in vivo*, follows similar kinetics (reviewed by Bellamy and Garthwaite, 2002; Koesling *et al.*, 2004; Garthwaite, 2005; Garthwaite, 2008).

Surprisingly, physiological signals are predicted to be several 1000-fold lower than the EC₅₀ of NO-targeted guanylyl cyclase predicted using platelets and cerebellar cell suspensions (10 nM). Nevertheless, the remarkable sensitivity of NO-targeted guanylyl cyclase for picomolar concentrations of NO may be explained by a large receptor excess. This in turn explains why smooth muscles are capable of NO-induced relaxation despite the deletion of > 90 % of NO-targeted guanylyl cyclase (Mergia *et al.*, 2006). An excess of NO-targeted guanylyl cyclase is predicted to act as a sink for NO, which will create a gradient for the diffusion of NO into receptor pools, thereby promoting the diffusion of NO towards its targets (Batchelor *et al.*, 2010).

1.4.4 Termination of cGMP signals

Independent of the removal of NO and rapid deactivation of NO-targeted guanylyl cyclase, the declining phase of a cGMP signal is shaped by desensitisation of the cyclase and rapid (typically within 1 s) degradation of cGMP by PDEs. These mechanisms further enable the transduction of NO signals with high fidelity and may also prevent the generation of saturating concentrations of cGMP. Furthermore, diversity in the kinetics, sub-cellular location, tissue distribution and regulation of PDEs may allow NO signals to generate hugely diverse cGMP signals in different cells and within different intracellular compartments (see **Table 1.3** and Fischmeister *et al.*, 2005).

PDE's catalyse the hydrolysis of cyclic nucleotides to non-cyclised monophosphates (i.e. 3', 5'-cGMP to 5'-GMP) by degrading the 3' cyclic phosphate bond in the cyclic

nucleotide molecule (see **Figure 1.9B**). PDEs have been found to exist in all cell types tested. They are a superfamily comprising 11 distinct enzymes. The existence of multiple active subtypes of each enzyme and of splice variants has led to estimates that over 50 different PDEs exist in mammals. PDEs appear to exist as homodimers with a C-terminal catalytic domain and an N-terminal regulatory domain containing sites for interaction with proteins capable of influencing the enzyme's catalytic activity and subcellular location. Overall, PDEs appear to share less than 30 % homology in structure, and this is consistent with diversity in their sub-cellular location, tissue distribution and activity (see **Table 1.3**; reviewed by Bender and Beavo, 2006; Francis *et al.*, 2010).

Desensitisation of NO-targeted guanylyl cyclase has been demonstrated in cerebellar astrocytes, platelets and striatal neurons. In intact cerebellar cells, it occurs within seconds (or less), increases with NO concentration (EC_{50} 10-20 nM NO), and is slow to reverse (half-time of 16 min). Its mechanism is unclear, although desensitisation does not occur in cell lysates or to the purified enzyme, suggesting that some cellular factor(s) is required (Bellamy and Garthwaite, 2002; Garthwaite, 2008).

1.5 Major cGMP targets

1.5.1 cGMP-dependent protein kinase (PKG)

PKG is a serine/threonine kinase dependent upon cGMP binding for catalytic activity. Two isoforms of PKG, encoded by two genes, have been discovered: PKGI, of which there are two functional splice variants named α and β , and PKGII. All PKGs exist as homodimers, each subunit containing: a N-terminal domain responsible for dimerisation, interaction with regulatory proteins, autophosphorylation and autoinhibition; a regulatory domain with two homologous allosteric binding sites for cGMP; and a C-terminal catalytic domain with substrate- and ATP-binding sites (reviewed by Feil *et al.*, 2005a; see **Figure 1.8**). The N-terminal of PKGII, but not PKGI α or β , contains consensus sequences for myristoylation which allows the association of this isoform with plasma membranes (Vaandrager *et al.*, 1996). Additionally, PKGI α and β vary in the N-terminal region,

and this may confer each variant with differences in sensitivity, substrate specificity and localisation (reviewed by Francis *et al.*, 2010).

It is unclear exactly how cGMP binding to PKG causes an increase in phosphorylation. Currently, it is thought that, in the absence of cGMP, the catalytic domain of the kinase is covalently bound to and inhibited by the N-terminal. Binding of cGMP to the catalytic domain is hypothesised to cause a conformational change or elongation of PKG that distances the N-terminal from the catalytic domain, leading to the relief of autoinhibition and a three- to ten-fold increase in phosphotransferase activity. The binding of four cGMPs to PKG (two per monomer) is required for full activity (Feil *et al.*, 2005a). PKGI contains one high affinity and one low affinity cGMP site, whereas PKGII contains two low affinity sites. This may partly explain why the PKG isoforms are differentially sensitive to cGMP. Sensitivity to cGMP follows the order: PKGI α > PKGI β > PKGII (Gamm *et al.*, 1995). Gamm *et al.* (1995) report that the K_a values of recombinant PKGI α and PKGII purified from mouse brain and expressed in HEK 293 and Sf9 cells are 0.092 μ M and 0.80 μ M cGMP, respectively. The sensitivities of all the PKGs to cGMP may be increased by autophosphorylation at a site overlapping the autoinhibition domain in the N-terminal, leading to an increase in the enzymes activity at basal cGMP concentrations and prolonged activation (Francis *et al.*, 2010).

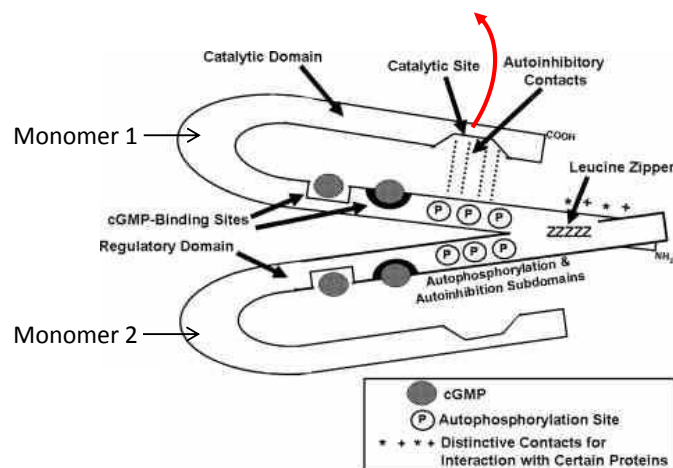


Figure 1.8 Predicted structure of PKGI. Monomers are labelled. The leucine zipper is the proposed site of homodimerisation. In the absence of cGMP, the catalytic site is inhibited by binding to the autoinhibitory subdomain. Binding of cGMP causes a conformational change that is proposed to

remove the catalytic site from autoinhibitory contacts (see red arrow). Adapted from Francis et al. (2010). Reproduced by kind permission of ASPET Journals.

Like NOS and NO-targeted guanylyl cyclase, PKG appears to be widely expressed in the mammalian body, and is predominant in brain, platelets and the cardiovascular system. Messenger RNA and protein for both PKG isoforms has been detected throughout the rodent brain, including in the cerebellum, olfactory bulbs, cortex and hippocampus. The distributions of each isoform appear to overlap (el-Husseini *et al.*, 1995; de Vente *et al.*, 2001; Feil *et al.*, 2005b). Using immunoblotting, it has also been shown that both the α and β PKG I splice variants are present, although to varying ratios in different brain regions (Feil *et al.*, 2005b).

Through the use of techniques such as ^{32}P -labelling, several potential PKG targets have been identified (**Table 1.2**), and PKG-mediated phosphorylation has been linked to multifarious processes, including synaptic plasticity, cytoskeletal dynamics and smooth muscle relaxation (Feil *et al.*, 2005a; Francis *et al.*, 2010). Given problems such as the lack of a known PKG phosphorylation consensus sequence, it is thought that many PKG substrates/effects of PKG-dependent phosphorylation are unknown. Nevertheless, the effects of PKG phosphorylation so far identified correlate well with the phenotype of PKG knock-out mice (Schlossmann *et al.*, 2005).

| Isoform | Substrate | Substrate location | Processes effected by phosphorylation | Reference |
|----------------------------------|----------------------------|-----------------------------------|--|-------------------------------|
| PKG 1 | G-substrate | Neurons | Synaptic plasticity (LTD ↑) | Detre <i>et al.</i> (1984) |
| | PDE 5 | Platelets | Multiple processes downstream of NO/cGMP signalling (↓↑) | Corbin <i>et al.</i> (2000) |
| | | Smooth muscle | | |
| | VASP | Platelets | Aggregation (↓) | Massberg <i>et al.</i> (1999) |
| | | Neurons | Structural plasticity (LTP ↑) | Wang <i>et al.</i> (1991) |
| IRAG/InsP ₃ receptors | Smooth muscle Platelets | Relaxation (↑) Aggregation (↓) | Schlossmann <i>et al.</i> (2000) | |
| PKG11 | GluR1 | Neurons | Synaptic plasticity (LTP ↑) | Serulle <i>et al.</i> (2007) |
| | CREB | Neurons | Gene expression (↑) | Gamm <i>et al.</i> (1995) |

Table 1.2 Potential PKG substrates. Some potential PKG substrates, their prime location and the processes that might be effected upon their phosphorylation by PKG are listed. CREB = cAMP response element-binding protein; GluR1 = AMPA receptor GluR1 subunit; InsP₃ = inositol 1,4,5-trisphosphate; IRAG = InsP₃R-associated cGMP Kinase Substrate; LTD = long-term depression; VASP = vasodilator-stimulated protein. Arrows indicate whether PKG phosphorylation is inhibitory (↓) or required/facilitatory (↑).

1.5.2 cGMP-regulated phosphodiesterases

Some PDEs are cGMP-regulated. This may occur via cGMP-mediated phosphorylation of PDEs, as exemplified by an increase in the catalytic activity of PDE 5 upon PKG-dependent phosphorylation (Thomas *et al.*, 1990; Corbin *et al.*, 2000), and/or by direct binding of cGMP to allosteric ‘GAF’ domains in PDE N-terminals, as in PDEs 2, 5, 6 and 10. A working model of cGMP-regulated, cGMP-hydrolysing PDE5 is shown in **Figure 1.9A**.

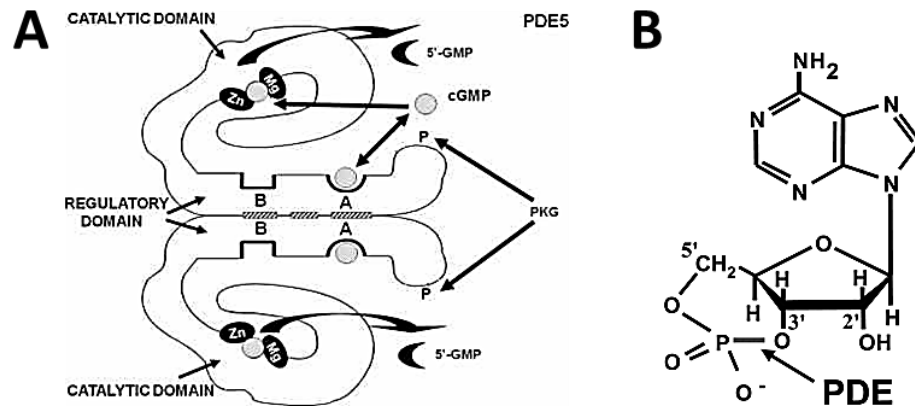


Figure 1.9 Predicted structure of PDE 5. A) PDE 5 is predicted to be a homodimer, each monomer comprising catalytic and regulatory domains. The catalytic site is found within the catalytic domain, close to a Zn^{2+} and another divalent metal ion (perhaps Mg^{2+} or Mn^{2+}) which facilitate the polarisation of a hydroxyl ion from water for breaking the cyclic phosphate ring. Catalysis can be enhanced by PKGI phosphorylation at serine-102 near the amino terminus, and/or by cGMP binding to GAF-A. B) PDEs degrade the 3' cyclic phosphate bond in cyclic nucleotides. Picture shows cAMP. Adapted from Francis et al. (2010) and Bender and Beavo (2006). Reproduced by kind permission of ASPET Journals.

'GAF' domains, named after an acronym of the first three classes of protein in which they were discovered (cGMP-regulated PDEs, cyanobacterial adenylyl cyclase and *Escherichia coli* transcription factor Fh1a), are common to proteins involved in cyclic nucleotide signalling. Two GAF domains (A and B) are found in the N-terminal of cGMP-regulated PDEs 2, 5, 6, and 10. In different PDEs, cGMP may selectively bind one or the other GAF domain, causing either an increase or decrease in cyclic nucleotide hydrolysis (see **Table 1.3**). It is unclear why cGMP preferentially binds one GAF domain over the other, and what the function(s) are of GAF domains that do not bind cGMP. PDE 11, which is found in skeletal muscle, prostate, kidney, liver, testes and pituitary glands, also contains GAF domains, although one is truncated and the PDE's activity is insensitive to cGMP (reviewed by Bender and Beavo, 2006).

PDE activity not only regulates the NO-cGMP pathway, but may also facilitate cross-talk between cAMP and cGMP-dependent signalling cascades. For example, it has been advanced that a rise in intracellular cGMP may lead to the competitive

inhibition of cAMP hydrolysis by PDEs that are not substrate-selective, for example PDE 1C. It has also been discovered that the hydrolysis of cAMP by PDE 3 is inhibited by a rise in cGMP, presumably because the enzyme has high affinity for cGMP but hydrolyses it slowly (Degerman *et al.*, 1997). In human cardiac myocytes, cGMP-mediated inhibition of PDE 3 is thought to occur downstream of NO, leading to cAMP accumulation, PKA activation and a phosphorylation-dependent increase in the activity of L-type VGCCs, which are critical to cardiac function (Kirstein *et al.*, 1995). The NO-cGMP-PDE 3 pathway has also been implicated in the regulation of other channels required for cardiac function, such as hyperpolarisation-activated, cyclic nucleotide-gated (HCN) channels, and is thought to act in concert with other cGMP-regulated PDEs, including cGMP-activated PDE 2 (Fischmeister *et al.*, 2005). Outside cardiac myocytes, a cGMP-induced increase in cAMP hydrolysis by PDE 2 has been implicated in platelet aggregation and hormone secretion from the adrenal gland (reviewed by Bender and Beavo, 2006). Other processes, including neurodevelopment and synaptic plasticity, might also be affected by PDE-mediated cAMP and cGMP cross-talk, since these nucleotides often act in parallel signalling pathways during these phenomena.

Given the above, the diversity in PDE tissue distribution, substrate selectivity and kinetics (summarised in **Table 1.3**), as well as the intracellular compartmentalisation of PDEs by their association with kinases and scaffolding proteins, PDE activity is likely to have huge consequences for the diversity of cGMP signals that could be elicited by one NO signal in one cell (reviewed by Fischmeister *et al.*, 2005; Bender and Beavo, 2006; Francis *et al.*, 2010).

| PDE | Location(s) | Cytosol/ Membrane | Substrate | ~K _m (μm) | | ~V _{max} (μmol/min/mg) | | cGMP | Notes |
|--------|---|--|--|----------------------|---------|------------------------------------|--------|------|---|
| | | | | cGMP | cAMP | cGMP | cAMP | | |
| 1A-C | Brain, smooth muscle, heart, lung, sperm, macrophages | C | <u>A-B</u> : cAMP < cGMP <u>C</u> : cAMP = cGMP | 1-6 | 1-100 | 30-300 | 10-150 | - | Activity enhanced by similar [Ca ²⁺ /CaM] required for nNOS. |
| 2A1-3 | Brain, adrenal gland, heart, platelets, endothelium | <u>A1</u> : C <u>A2-3</u> : M | cAMP = cGMP | 10 | 30 | 120 | 120 | ↑ | Major PDE in hippocampus. |
| 3A-B | Brain, heart, smooth muscle, kidney, sperm, oocytes | C and M | cAMP > cGMP | 0.1-0.2 | 0.2-0.4 | 0.3-2 | 3-9 | ↓ | |
| 5A | Brain, spine, platelets, smooth muscle, lung, heart, kidney | C | cGMP selective* | 3-6 | 300* | 1 | 1 | ↑ | Major PDE in hippocampus. |
| 6A-C | Retina, pineal gland only | <u>A-B</u> : M <u>C</u> : C | cGMP selective* | 15 | 650* | 2000 | - | ↓ | Most efficient PDE |
| 9A | All tissues tested, including brain, kidney, spleen, gut | C | cGMP selective* | 0.1 | 250* | 5 | - | - | Expression pattern similar to NO-targeted guanylyl cyclase |
| 10A2-3 | Brain, testes, heart, thyroid | <u>A1</u> , <u>A3</u> : C <u>A2</u> : M | cAMP < cGMP | 14 | 0.2-1 | 4 | 0.7 | - | cAMP-inhibited (by high cAMP affinity but slow cAMP hydrolysis) |

Table 1.3 cGMP-hydrolysing PDEs. The table lists all the known cGMP-hydrolysing PDEs, some of their main locations, their intracellular distribution, substrate selectivity, K_m and V_{max}. The column labelled 'cGMP' shows the effect of an increase in intracellular cGMP on PDE activity, where ↑ is facilitatory and ↓ is inhibitory. Information from Bender and Beavo (2006).

1.5.3 Cyclic nucleotide-gated channels

Cyclic nucleotide gated (CNG) channels were first discovered in rod cells in the retina (Fesenko *et al.*, 1985) as a result of research aimed at discovering the channel responsible for the cGMP-mediated 'dark current' (reviewed by Baylor, 1996). Soon after this they were also found in cone cells (Bonigk *et al.*, 1993) and olfactory sensory neurons (Dhallan *et al.*, 1990), in which they generate the main odorant-induced electrical signal (reviewed by Craven and Zagotta, 2006; Cukkeman *et al.*, 2011). Using techniques such as *in situ* hybridisation and Northern blotting, mRNA and protein for CNG channels has now been detected throughout the nervous system in brain areas including hippocampus and cerebellum, and in organs such as heart and kidney (reviewed by Kaupp and Seifert, 2002).

CNG channels are structurally related to voltage-gated K⁺ channels, although their activation by voltage is negligible. Rather, they open upon direct binding of cyclic

nucleotides to an intracellular domain within the C-terminal. Native channels are heterotetrameric, each subtype, of which three have been conclusively identified, typically comprising a combination of three α subunits (1-3) and a regulatory subunit ($\beta 1\alpha$, $\beta 1\beta$, $\beta 3$ or $\alpha 4$). The regulatory subunits influence ligand selectivity and sensitivity and bind regulatory factors like CaM. Different combinations of subunits appear to endow CNG channels in different tissues with unique properties. For example, CNG channels in rod cells, which contain three CNG $\alpha 1$ subunits and one CNG $\beta 1$ subunit, are highly selective for cGMP, whereas olfactory-type channels, which are hypothesised to contain two CNG $\alpha 2$, one CNG $\alpha 4$ and one CNG $\beta 1\beta$ subunit, respond equally well to cAMP and cGMP (Kaupp and Seifert, 2002).

All subunits share a common topology, comprising six transmembrane domains with a Ca²⁺-permeable, cation selective pore between the fifth and sixth. Each subunit contains a C-terminal domain for cyclic nucleotide binding (CNBD) which has been likened to the cGMP binding domain within PKG and is thought to be homologous with the CNBD of HCN channel subunits. Based on the recent crystallisation of the HCN2 subunit CNBD, it is thought that each CNG channel subunit CNBD binds one cyclic nucleotide. The dependence of channel activation on cyclic nucleotide concentration is very steep, therefore allowing a broad range of inputs to be transduced with high fidelity. Analysis of the concentration-response curve has led to the hypothesis that multiple, probably four, cyclic nucleotides are required for full channel opening. It is unclear how nucleotide binding causes channel opening, although it has been proposed that occupation of the CNBD causes a conformational change that is transferred to the sixth transmembrane domain by a C-linker (a stretch of ~ 80 amino acids that is essential for channel gating and promotes tetramerisation; see **Figure 1.10**). Unusually, CNG channels do not desensitise, but their sensitivity to cyclic nucleotides may be significantly inhibited by CaM binding, suggesting that the CNG channel Ca²⁺ current can affect negative feedback on CNG channel activity (see reviews by Kaupp and Seifert, 2002; Craven and Zagotta, 2006).

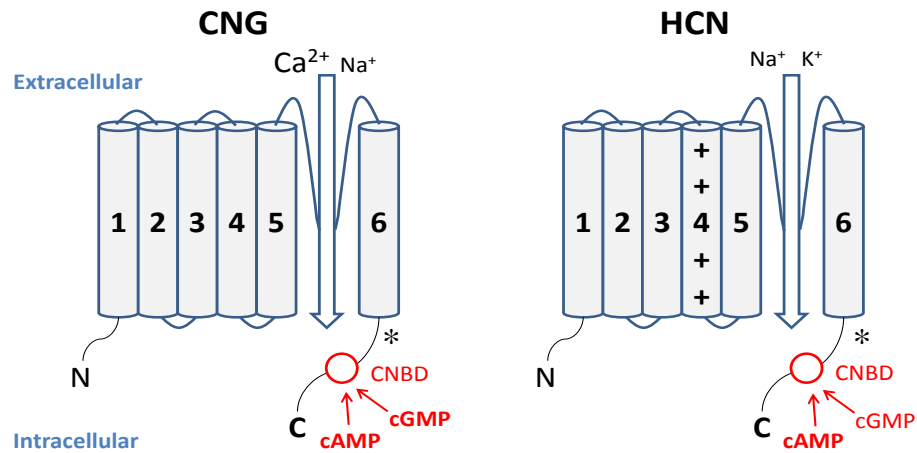


Figure 1.10 Predicted topology of CNG and HCN channel subunits. Each subunit constitutes six transmembrane domains (S1–6), a pore loop between S5–6, and a cyclic nucleotide-binding domain (CNBD) in the C-terminal connected to S6 by a C-linker (*). CNG channels conduct Ca^{2+} and Na^+ . HCN channels conduct Na^+ and K^+ . It is unclear whether they conduct Ca^{2+} . CNG channels are activated upon binding of either cAMP or cGMP to the CNBD, depending on the channel type. HCN channels are activated upon membrane hyperpolarisation which causes the movement of positively charged residues (+) in S4 and the opening of the pore. Binding of cAMP or cGMP to the CNBD causes a depolarising shift in voltage dependence.

The ability of CNG channels to directly translate NO/cGMP signals into rises in intracellular Ca^{2+} has generated intense interest in their physiology, although many aspects of CNG function remain unclear. Among the processes in which the NO/cGMP/CNG pathway has been implicated are axonal guidance in chick retina during development (Wu *et al.*, 1994), regulation of membrane potential (V_m) and activity-dependent conductance in frog and rat olfactory neurons (Schmachtenberg *et al.*, 2003), neurotransmitter release from lizard cones (Savchenko *et al.*, 1997) and synaptic plasticity (LTP) at CA1 synapses in mouse hippocampal slices (Parent *et al.*, 1998).

1.5.4 Hyperpolarisation-activated, cyclic nucleotide-regulated channels

HCN channels were first discovered in sinoatrial node cells in the heart and then in neurons, including hippocampal neurons, in the late 1970s and early 1980s. They have now been detected throughout the rodent central nervous system, including in brainstem, retina, olfactory bulbs, cerebellum and spinal cord (Notomi and

Shigemoto, 2004; Milligan *et al.*, 2006). They are closely phylogenetically related to CNG channels and are similar in structure, being tetramers comprised of varying (unknown) combinations of four different subunits (1-4), each including six transmembrane domains and an intracellular CNBD (**Figure 1.10**). Unlike CNG channels, they are primarily voltage-gated. As in voltage-gated K^+ channels, positively charged residues in the fourth transmembrane domain of each subunit serve as a voltage sensor which move inwards during hyperpolarisation. Unusually, this sensor, by some unknown downstream mechanism, elicits channel opening in response to hyperpolarisation (at potentials negative to -50 to -60 mV (resting V_m)). Channel opening leads to an inward Na^+ current known as I_h (hyperpolarisation), I_q (queer), or I_f (funny) and depolarisation of the membrane towards the action potential threshold. Consequently, HCN channels have been linked to the generation of oscillatory activity in excitable cells, most notably in sinoatrial node cells, which are pacemakers for heart rate, and thalamocortical neurons, which generate rhythmic 'burst' activity during non-rapid eye movement sleep (see **Figure 1.11**; reviewed by Craven and Zagotta, 2006).

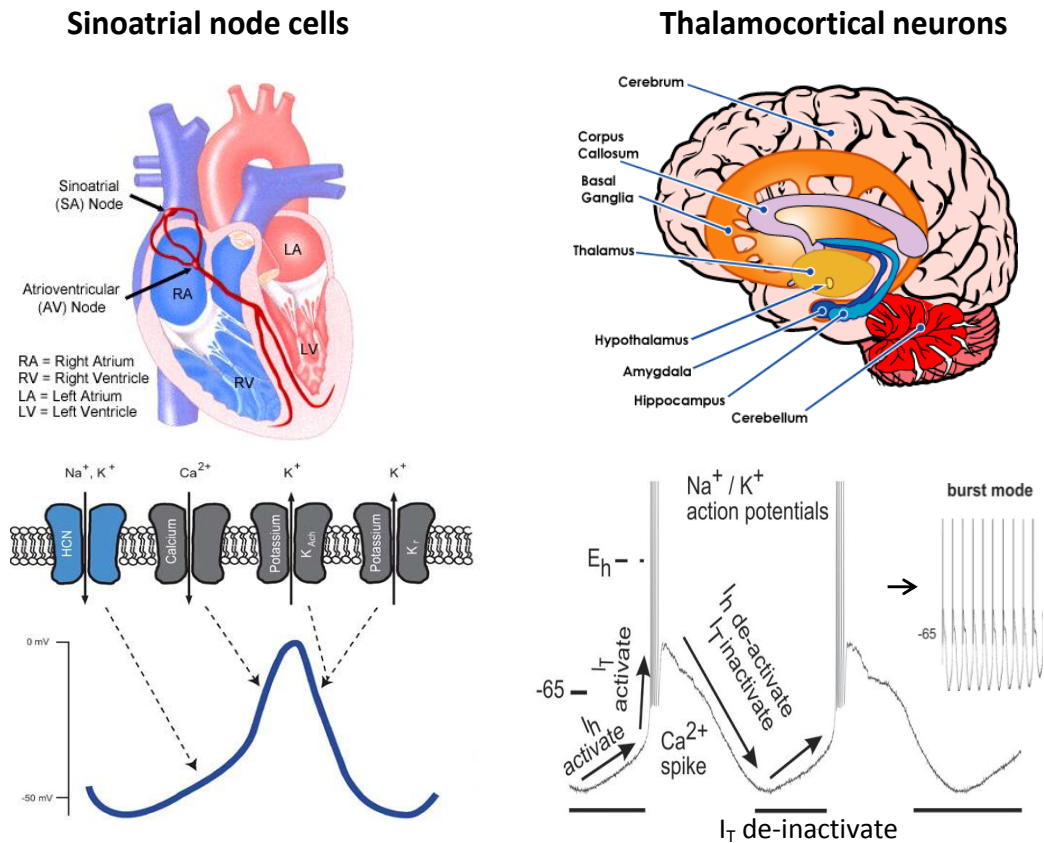


Figure 1.11 Role of HCN channel activity in oscillatory activities in excitable cells. HCN channel activation underpins the oscillatory activity of sinoatrial node cells in the heart and thalamocortical relay neurons in the brain (see locations in upper panels). The lower panels show the ionic currents responsible for each phase of each form of oscillation. I_T = low-voltage activated, T-type VGCC current. Figure compiled using images from www.texasheartinstitute.org (accessed 1/5/2012) and www.knol.google.com (accessed 22/09/11), Craven and Zagotta (2006) and Biel *et al.* (2009).

Binding of either cAMP or cGMP to the HCN channel CNBD causes a depolarising shift in HCN channel activation (by ~ 15 mV upon stimulation of recombinant homomeric HCN2 channels with saturating concentrations of cAMP), speeds up channel opening and increases the amplitude of I_h . Accordingly, cAMP binding to channels in sinoatrial node cells causes an increase in heart rate. Binding of cAMP and cGMP have similar effects on HCN channel activity, although recombinant and native channels are typically less sensitive to cGMP (by ~ 10 - 30 -fold compared to cAMP), which has led to doubt over whether cGMP is a natural ligand for HCN channels. Sensitivity to cyclic nucleotides, as well as activation kinetics and gating properties, appear to vary with subunit composition (reviews: Craven and Zagotta, 2006; Biel *et al.*, 2009).

The unusual properties of I_h have implicated HCN channels in the setting of resting V_m , which will be subject to a depolarising shift in the presence of HCN channels, and the regulation of resting membrane resistance, which will be lowered in the presence of I_h . Accordingly, Ohm's law dictates that an input current (either hyper- or depolarising) will evoke a smaller change in V_m when I_h is active. This will lead to the stabilisation of resting V_m under basal conditions and an increase in the amplitude attenuation of excitatory postsynaptic potentials (EPSPs) as they travel to the soma. Therefore, I_h is thought to be involved in dendritic integration and EPSP summation. Through the above processes, I_h has been found to regulate neurotransmission and synaptic plasticity in multiple areas of the nervous system, in particular the hippocampus (Biel *et al.*, 2009).

HCN channels have only recently been identified as potential targets of NO/cGMP. Some of the first research in support of this was performed in guinea pig and cat thalamocortical neurons. Pape and Mager (1992) found that the depolarisation of resting V_m via the NO/cGMP/HCN channel pathway causes a reduction in bursting by limiting the de-inactivation of T-type VGCCs and consequent rebound depolarisation. In this way, NO/cGMP has been hypothesised to regulate the switch in thalamocortical neurons from bursting behaviour during non-rapid eye movement sleep to 'single spike' mode which prevails during rapid eye movement sleep and wakefulness.

More recently, the NO/cGMP/HCN channel has been found to regulate the excitability of neurons in the spine (Kim *et al.*, 2005), optic nerve (Garthwaite *et al.*, 2006) and hippocampus (Neitz *et al.*, 2011). Depolarisation of spinal neurons by HCN channels has been postulated to underlie central sensitisation (Kim *et al.*, 2005), a process likened to LTP and a correlate of chronic pain (reviewed by Ji *et al.*, 2003). In the hippocampus, the modulation of HCN channels by endothelium-derived NO is thought to set a basal level of neurotransmitter release at CA1 synapses (Neitz *et al.*, 2011).

Several aspects of NO/cGMP/HCN signalling remain ambiguous and more work will be needed to elucidate its impact on physiology. Given the apparent insensitivity of

recombinant HCN channels to cGMP, it would be interesting to test whether the above effects of NO result from binding of cGMP to HCN channels directly, or through an indirect effect on cAMP-binding to channels, for example, by a reduction in PDE-induced hydrolysis of cAMP.

1.6 Pharmacology of NOS and NO-targeted guanylyl cyclase

Some of the major pharmacological tools available for the manipulation of NO/cGMP signalling are summarised in **Table 1.4**.

| Agent | Example compounds and notes |
|--|---|
| General NOS antagonists | NG-nitro-L-arginine (L-NNA) N-methyl-L-arginine (L-NMMA) NG-nitro-L-arginine methyl ester (L-NAME; L-NNA pro-drug) L-arginine analogues; low micromolar K_i 's; few secondary effects; actively transported into cells (reviewed by Alderton <i>et al.</i> , 2001). |
| Isoform selective NOS inhibitors | nNOS: N5-(1-Imino-3-butenyl)-L-ornithine (L-VNIO; Babu and Griffith, 1998) iNOS: [N-(3-aminoethyl)benzyl]-acetamidine (1400-W; Garvey <i>et al.</i> , 1997) The most potent, selective NOS inhibitors available; no eNOS inhibitors are available. |
| NO-targeted guanylyl cyclase inhibitors | 1H-[1,2, 4]oxadiazolo[4,3,-a]quinoxalin-1-one (ODQ; Garthwaite <i>et al.</i> , 1995) Prevents NO binding the cyclase by oxidising the haem prosthetic group (Schrammel <i>et al.</i> , 1996). Unlike other inhibitors such as methylene blue and LY83583, which inhibit secondary targets including NOS (Mayer <i>et al.</i> , 1993; Luo <i>et al.</i> , 1995) and CNG channels (Leinders-Zufall and Zufall, 1995), ODQ is highly selective at 10 μ M. |
| NO donors | 1-substituted diazen-1-ium-1,2-diolates (NONOates) A series of compounds that release NO at predictable rates (reviewed by Morley and Keefer, 1993). Other donors such as sodium nitroprusside and S-nitroso-N-acetylpenicillamine (SNAP) are widely used but release NO^+ , NO^- , cyanide ions and O^{2-} and decompose in an unpredictable manner (reviewed by Feelisch, 1998). |

Table 1.4 Major pharmacological tools used for the manipulation of NO/cGMP signalling.

1.7 Endogenous activators of NO-targeted guanylyl cyclase other than NO

Carbon monoxide (CO) has been postulated by several researchers to activate NO-targeted guanylyl cyclase. Like NO, CO is short-lived, freely-diffusible and endogenously produced. The enzyme responsible for its synthesis, haem oxygenase, is primarily responsible for degrading haem in old erythrocytes (Dawson and Snyder, 1994). *In situ* hybridisation has shown that mRNA for haem oxygenase is present throughout the CNS in a distribution complementary to that of NO-targeted guanylyl cyclase (Verma *et al.*, 1993).

Endogenous CO signalling has been implicated in various processes ranging from olfaction (Verma *et al.*, 1993), to LTP at hippocampal synapses (Zhuo *et al.*, 1993), to NANC transmission and smooth muscle relaxation (Xue *et al.*, 2000). Many studies, mostly performed on the enteric nervous system, suggest that CO and NO are co-transmitters.

However, unlike mice lacking NOS, mice deficient in haem oxygenase display no gross behavioural abnormalities and have normal whole brain cGMP levels (reviewed by Boehning and Snyder, 2003). Some of the specific effects of CO on physiology are also controversial. For example, it has been reported that LTP is normal in mice lacking haem oxygenase, and that supposed haem oxygenase inhibitors, though widely used, inhibit LTP in wild-type and haem oxygenase-deficient mice to a similar extent (Poss *et al.*, 1995). Furthermore, serious doubts over whether CO is a physiological activator of guanylyl cyclase have been raised by the finding that millimolar concentrations of CO yield only a four-fold increase in the activity of purified NO-targeted guanylyl cyclase (Brune and Ullrich, 1987). The poor sensitivity of NO-targeted guanylyl cyclase to CO may be explained by the finding that CO binding to the cyclase fails to break the bond between His-105 and the haem prosthetic group (Stone and Marletta, 1994). Additionally, doubts over the availability of the haem required for CO synthesis, and the apparent lack of regulation of haem oxygenase (reviewed by Boehning and Snyder, 2003) have led to

a general consensus that CO is not a physiologically relevant activator of NO-targeted guanylyl cyclase.

1.8 NO-targeted guanylyl cyclase-independent NO signal transduction

Some examples of presumed physiological NO signal transduction independent of NO-targeted guanylyl cyclase exist. For example, the heterosynaptic spread of LTP at synapses between rat cerebellar parallel fibres and Purkinje cells reported by Jacoby *et al.* (2001) was found to be prevented by NOS inhibition and NO scavenging but not by a concentration of the NO-targeted guanylyl cyclase antagonist, ODQ (5 μ M), that was effective in blocking cerebellar LTD.

It has been hypothesised that effects of NO independent of NO-targeted guanylyl cyclase might be transduced by the S-nitrosation of cysteine thiol (R-SH) groups. S-nitrosation can be evoked using high concentrations of NO that can react with oxygen to produce nitrosating species such as N_2O_3 . Changes in the function of proteins upon S-nitrosation are thought to result from changes in their tertiary structure, which is in part determined by the location of cysteine thiols (Dudzinski *et al.*, 2006). S-nitrosation was exemplified by the negative feedback of NO on synaptic NMDA receptors reported by Lipton *et al.* (2002), who proposed that it occurred via S-nitrosation of NMDA receptor cysteine residues. However, this was later found to be an artefact of un-caging supra-physiological concentrations of exogenous NO using UV light, which may have led to the spurious generation of nitrosating species (Hopper *et al.*, 2004). Perhaps in part because of the difficulty of studying nitrosated proteins, which are very unstable (Dudzinski *et al.*, 2006), there appear to be no unambiguous examples of physiological NO signalling via S-nitrosation, or by a related process called S-nitrosylation. Moreover, the requirement for high NO concentrations means that, *in vivo*, S-nitrosation and S-nitrosylation are likely to be restricted to certain pathological conditions involving raised NO concentrations, for example, following iNOS activation (Zhang and Hogg, 2005).

Mitochondrial cytochrome C oxidase, which is the last enzyme in the respiratory electron transport chain, has also been suggested as an alternative target for NO, leading to speculation that NO might, by competing with O₂ for binding, inhibit mitochondrial respiration (Erusalimsky and Moncada, 2007). An example of this in normal physiology is found in the firefly, in which phasic bursts of NO generated in the insect's lantern may transiently inhibit mitochondrial respiration, therefore allowing free oxygen to accumulate to a level necessary for the initiation of the biochemical cascade underlying the characteristic firefly flash (Dudzinski *et al.*, 2006). However, in mammals at physiological O₂ concentrations (20-30 μM), the EC₅₀ of cytochrome oxidase C for NO (~ 120 nM) is significantly greater than even generous estimates of physiological NO concentrations, which are probably within the low picomolar range (see 1.4.1). Furthermore, endogenous NO is unlikely to exceed a few nanomolar following even intense stimulation of NOS (reviewed by Hall and Garthwaite, 2009). Thus, mitochondrial inhibition by NO is also likely to be restricted to conditions involving supra-physiological concentrations of NO, and/or very low concentrations of O₂. As such, NO-targeted guanylyl cyclase is the only recognised physiological NO receptor.

1.9 NO signalling in brain

1.9.1 NO-mediated neurotransmission and modulation of cell excitability

NO acts as a neurotransmitter in the brain (Garthwaite, 2008). As in the PNS, anterograde neurotransmission may occur upon postsynaptic nNOS activation in response to action potential-dependent, intra-axonal Ca²⁺ influx via N-type VGCCs and/or other Ca²⁺ channels (reviewed by Vincent, 2010). Anterograde neurotransmission by NO has been exemplified at a synapse between two identifiable neurons of the buccal ganglia of the pond snail, *Lymnaea stagnalis*. The reliance of this synapse on NO as a neurotransmitter means that, when the participating neurons are co-cultured, depolarisation of one can cause an EPSP in the other, regardless of a physical connection (Park *et al.*, 1998).

Retrograde NO transmission may occur following the opening of postsynaptic NMDA receptors and has been exemplified by Arancio *et al.*. They have shown that, during LTP induction at synapses between dissociated hippocampal neurons, NMDA receptor activation leads to postsynaptic NO generation and a subsequent increase in neurotransmitter release through presynaptic NO-targeted guanylyl cyclase (Arancio *et al.*, 1995; Arancio *et al.*, 1996; Arancio *et al.*, 2001). The relevance of this to intact tissues remains unclear (see **Chapter 3**).

NO may also modulate neurotransmission by other molecules. Studies, predominantly of neurotransmitter efflux from tissue preparations *in vitro*, have implicated tonic and activity-dependent NO production in the regulation of the release of neurotransmitters including ACh, noradrenaline, dopamine, glutamate and GABA from brain areas as diverse as cortex, striatum, hypothalamus and hippocampus (see **Chapter 4** for examples). Interestingly, the release of one neurotransmitter may be both up- and down-regulated by NO depending on the concentration of NO involved and the tissue under study (reviewed by Prast and Philippu, 2001).

Most of these effects appear to be underpinned by NO-mediated changes in membrane excitability. Common targets for NO are K⁺ and Ca²⁺ channels (reviewed by Garthwaite, 2008). Other targets include, for example, GABA_A receptors, as illustrated in dissociated cerebellar granule cells by Robello *et al.* (1996), serotonin receptors, as illustrated using invertebrate neurons (Straub *et al.*, 2007), and the serotonin uptake transporter (reviewed by Garthwaite, 2007). Several effects appear to involve PKG-mediated phosphorylation. As well as an increase or decrease in cell excitability caused by NO, studies, for example, using hippocampal slices (Makara *et al.*, 2007) and in the hippocampus *in vivo* (Hada *et al.*, 2003), suggest that NO can cause the disinhibition of synaptic activity via a reduction of GABAergic transmission.

1.9.2 NO signalling between blood vessels and neurons

In the brain, NO may signal from central neurons to blood vessels, and this may link local synaptic activity with vasodilation. For example, application of NMDA to hippocampal slices has been reported to cause NO-dependent vasodilation of microvessels (Lovick *et al.*, 1999). Similar effects in other brain areas such as cerebellum and cortex (reviewed by Garthwaite, 2008) have been found to be sensitive to inhibition by the Na⁺ channel-inhibitor, tetrodotoxin (TTX), suggesting that the underlying mechanism is action potential-dependent.

Interestingly, NO also signals from blood vessels to neurons. Convincing evidence for vasculoneuronal NO transmission has been provided using optic nerves, which contain only blood vessels and axons and no nNOS. It has been found that a low-level NO tone produced by capillary eNOS causes tonic depolarisation of axons via a pathway involving HCN channels (Garthwaite *et al.*, 2006). A low-level (~ 0.1 nM), endothelium-derived NO tone has also been discovered in the hippocampus (Hopper and Garthwaite, 2006), and eNOS appears to be necessary for NO-dependent LTP at CA1 (Kantor *et al.*, 1996; Wilson *et al.*, 1999; Bon and Garthwaite, 2003; Hopper and Garthwaite, 2006) and mossy fibre (Doreulee *et al.*, 2001) synapses. Mice deficient in eNOS also exhibit impaired LTP in the neocortex (Haul *et al.*, 1999) and striatum (Doreulee *et al.*, 2003), suggesting that vasculoneuronal NO signals are active in multiple brain areas. *In vivo*, this form of NO signal may enable blood-borne agents to influence neuronal activity.

1.10 NO and synaptic plasticity in adults

1.10.1 Synaptic plasticity

The term synaptic plasticity was coined by Jerzy Konorski in 1948 to describe the ability of neurons to change the strength of their connections in response to activity. He, along with many scientists, assumed synaptic plasticity to be critical for information storage in the brain. This idea was first proposed by Santiago Ramon y

Cajal in 1894 but it was not until 1949, that this postulate was formalised into a hypothesis (see Andersen *et al.*, 2007 for a review). At this time, Donald Hebb proposed that if two connected neurons are simultaneously and repeatedly active, then the efficacy of the synapse involved will increase (Hebb, 1949).

1.10.2 Long-term potentiation

Hebb's hypothesis that 'neurons that fire together, wire together' attracted much attention as a putative explanation for learning and memory, but it was not until 1973 that Hebbian plasticity was first described. In a ground-breaking report, Tim Bliss and Terje Lomo (1973) demonstrated a persistent (lasting hours) enhancement in synaptic activity following a brief tetanus (100 or 15 Hz for 3-20 s) applied to hippocampal perforant path-granule cell synapses in anaesthetised rabbits. Consistent with Hebb's postulate, this long-lasting potentiation, later renamed LTP, was found to be specific to the pathway that was tetanised (Andersen *et al.*, 1977), to depend upon coincident pre- and postsynaptic depolarisation that exceeded a threshold for LTP induction (McNaughton *et al.*, 1978; Wigstrom *et al.*, 1986), and to persist over hours or days *in vitro* (Bliss and Gardner-Medwin, 1973) and up to a year *in vivo* (Abraham *et al.*, 2002). These properties of LTP have spurred its study at synapses throughout the brain, in areas such as the amygdala (Dityatev and Bolshakov, 2005) and cortex (Feldman, 2009), and in several species including humans (Cooke and Bliss, 2006). Now, the term 'LTP' has come to describe any long-lasting (> 1 hr), activity-dependent increase in the efficacy of a synapse. It is recognised that the potentiation can be composed of multiple pre- and postsynaptic expression mechanisms including, amongst others, increased neurotransmitter release, increased conductance via excitatory postsynaptic receptors, increased postsynaptic receptor density, a change in gene expression and/or the structural remodelling or growth of new synapses (Lynch, 2004; Malenka and Bear, 2004; Bliss *et al.*, 2007). The recruitment of specific expression mechanisms appears to depend upon the synapse under study, the animal used, and the conditions of the experiment, most notably the induction protocol used, of which there are multiple electrical and chemical procedures (reviewed by Bliss *et al.*, 2007).

It should be noted that the relationship between LTP, learning and memory is debatable (see **1.11**). Additionally, the study of LTP in certain areas of the nervous system has led to hypotheses that it represents a physiological correlate of various other phenomena, for example, chronic pain caused by the central sensitisation of nociceptive synapses in the spine (Ji *et al.*, 2003) and addiction caused by the potentiation of dopaminergic synapses in the ventral tegmental area (Wolf, 2003). Similarities between the mechanisms underpinning LTP and forms of activity-dependent synaptic plasticity thought to occur during the development and refinement of synapses have also been recognised (reviewed by Kandel and O'Dell, 1992; Contestabile, 2000).

In mammals, LTP is archetypal at hippocampal Schaffer-collateral/commissural CA1 synapses. The easy study of LTP at these synapses has been permitted by the use of transverse hippocampal slices. Slicing the hippocampus along the transverse plane reveals a laminar structure and allows for the preservation of all the major neural pathways which can be maintained *in vitro* for hours, easily manipulated and recorded from (reviewed by Teyler, 1999). At Schaffer-collateral/commissural-CA1 synapses, low frequency synaptic transmission is largely mediated by AMPA-type glutamate receptor activation (Davies and Collingridge, 1989). LTP is typically induced using high frequency stimulation (HFS; a 1 s, 100 Hz burst of stimuli or tetanus), although it has been reported following multiple other stimuli, as well as after some forms of learning (see **1.11.2**). In all cases tested, LTP has been found to depend upon postsynaptic Ca^{2+} (Lynch *et al.*, 1983; Malenka *et al.*, 1988) and with few exceptions (see **Chapter 5** for discussion), NMDA receptor activation (Collingridge *et al.*, 1983a; Collingridge *et al.*, 1983b; Malenka, 1991; Tsien *et al.*, 1996). NMDA receptor activation is glutamate- and voltage-dependent, the channel being blocked by Mg^{2+} close to the resting V_m . During HFS, depolarisation of the postsynaptic membrane, largely due to AMPA receptor activation, summates. The NMDA receptor channels are relieved of Mg^{2+} and permit Ca^{2+} influx which initiates LTP expression (**Figure 1.10**). In this way, NMDA-receptors act as molecular coincidence detectors for simultaneous presynaptic (glutamate release) and postsynaptic (depolarisation) activity, thus explaining why NMDA receptor-dependent LTP is input-specific and associative (reviewed by Bliss *et al.*, 2007). In

concurrency with NMDA receptor activation, multiple other means of raising the intracellular Ca^{2+} concentration may be necessary for LTP induction, including the activation of metabotropic glutamate receptors, VGCCs and intracellular Ca^{2+} stores (Lynch, 2004; Bliss *et al.*, 2007).

The rise in intracellular Ca^{2+} caused by the activation of NMDA receptors and other channels during LTP induction initiates multiple signalling cascades responsible for the persistent amplification of subsequent postsynaptic responses. Details of these cascades remain largely unclear, although two stages of LTP expression, early (early-LTP; > 1 hr post-induction) and late (late-LTP; usually > 4 hr post induction), have been distinguished by their dependency on new protein synthesis, with late-LTP relying on transcription and translation (Lynch, 2004; Malenka and Bear, 2004; Bliss *et al.*, 2007). It is also generally agreed that both sides of the synapse are involved in LTP expression, yet the conditions that dictate the extent that each side contributes and at what time point following induction remain ambiguous. Many recent studies have focused on the mechanisms responsible for increases in postsynaptic AMPA receptor density often observed following LTP induction (Nicoll, 2003; Malenka and Bear, 2004; Kerchner and Nicoll, 2008; Kessels and Malinow, 2009). In presynaptic neurons, increases in glutamate release have also been detected using quantal analysis (Dolphin *et al.*, 1982; Bekkers and Stevens, 1990) and, more recently, direct imaging techniques (Zakharenko *et al.*, 2001). Indeed, a recent study by Enoki *et al.* (2009) showed that LTP at Schaffer-collateral/commissural-CA1 synapses was, under their conditions, almost entirely presynaptically expressed.

Given that NMDA receptor-dependent LTP is induced postsynaptically, presynaptic LTP mechanisms necessitate a retrograde messenger, capable of relaying a signal for LTP expression from the postsynaptic induction site back to the presynaptic neuron. Several freely diffusible, as well as membrane spanning, molecules have been suggested as candidate retrograde messengers, including arachidonic acid (O'Dell *et al.*, 1991), carbon monoxide (Zhuo *et al.*, 1993) and cell adhesion molecules (Bliss *et al.*, 2007). However, NO has received the most attention.

1.10.3 LTP and NO

The first studies to implicate NO as an intercellular, possibly retrograde, transmitter in LTP showed a deficit in the maintenance of CA1 LTP in hippocampal slices following the application of non-selective NOS inhibitors or of the extracellular NO scavenger, haemoglobin, during LTP induction (Schuman and Madison, 1991; Bohme *et al.*, 1991). Subsequently guanylyl cyclase inhibitors were found to have similar effects on LTP (Boulton *et al.*, 1995; Lu *et al.*, 1999; Bon and Garthwaite, 2003). It is now generally accepted that NO/cGMP signalling may participate in LTP in several brain areas, possibly contributing to some forms of memory (see 1.11.3). It is also known that both a tonic (endothelial) and phasic (neuronal) NO signal are required for NO-dependent CA1 LTP (Bon and Garthwaite, 2003; Hopper and Garthwaite, 2006), consistent with reports that knock-out mice deficient in neuronal and endothelial NOS are incapable of wild-type LTP (Son *et al.*, 1996). Similarly, LTP in the visual cortex (Haghikia *et al.*, 2007) and hippocampus (Taqatqeh *et al.*, 2009) has also been shown to require both guanylyl cyclase isoforms, perhaps implying the existence of distinct NO/cGMP-mediated pathways that contribute to LTP. Numerous putative effectors of NO/cGMP-dependent LTP have been identified, including PKG (Arancio *et al.*, 2001; Serulle *et al.*, 2007), CaMKII (Ninan and Arancio, 2004), VASP (Wang *et al.*, 2005), CREB (Lu *et al.*, 1999), PDE2 (Boess *et al.*, 2004) and CNG channels (Parent *et al.*, 1998). However, there remain several unknowns regarding the precise role of NO/cGMP signalling in LTP.

Firstly, the conditions under which LTP becomes NO-dependent remain undefined. At Schaffer-collateral/commissural-CA1 synapses, for example, LTP has been found by several groups to be NO-independent *in vitro* (Cummings *et al.*, 1994; Phillips *et al.*, 2008) and *in vivo* (Bannerman *et al.*, 1994b). The involvement of NO in LTP may be determined by the experimental conditions used. Specific factors may be the LTP induction protocol used (Raymond, 2007), and/or the age or strain of animals (Williams *et al.*, 1993; Holscher, 2002). It should also be noted that the majority of studies that do show a role for NO in LTP also show a residual NO-independent component, consistent with the idea that LTP can be established by multiple, independent mechanisms.

Secondly, the specific cellular mechanisms underpinning the role of NO in plasticity, and, indeed the locus of NO-dependent potentiation, remain unclear. Postsynaptically, NMDA receptor/NO/cGMP/PKG signalling may play a role in the increased AMPA receptor density observed following LTP induction. Serulle *et al.* (2007) report that cGMP-activated PKGII can bind to the GluR1 AMPA receptor subunit C-terminal domain. This results in the phosphorylation of GluR1 at serine-845 and a subsequent increase in surface expression of AMPA receptors at extrasynaptic sites, presumably ready for insertion to synapses. The increased membrane expression of GluR1 correlated with changes in synaptic transmission that were also NO/cGMP/PKG-dependent and, it was found that LTP was reduced in hippocampal slices under PKGII antagonism (Serulle *et al.*, 2007). Lu *et al.* (1999) have also found that NO may effect changes in gene expression during late-LTP via a pathway involving PKG and CREB.

Presynaptic actions of NO have also been reported, consistent with putative retrograde NO transmission (reviewed in **Table 3.1**). Some of the most compelling evidence for this has been reported by Arancio *et al.*. Using pairs of dissociated hippocampal neurons, they have revealed that NO produced postsynaptically may, through presynaptic NO-targeted guanylyl cyclase, PKG and CaMKII, induce a LTP characterised by an increase in transmitter release (Arancio *et al.*, 1995; Arancio *et al.*, 1996; Arancio *et al.*, 2001; Ninan and Arancio, 2004). More recent studies also suggest a role for retrograde NO transmission in LTP, showing, for example, that mice lacking the AMPA receptor GluR1 subunit display a predominantly presynaptic LTP in the hippocampus and neocortex that is completely blocked by NOS antagonism (Hardingham and Fox, 2006; Phillips *et al.*, 2008). Some immunohistochemical evidence is also consistent with retrograde NO transmission (see **1.12.5**), as are reports that the remodelling of presynaptic varicosities often observed in culture following LTP can be induced in hippocampal slices cultures upon the application of NO donors (Nikonenko *et al.*, 2003). Nevertheless, there remains little evidence in functional neural pathways that LTP requires retrograde NO transmission (see **Chapter 3**).

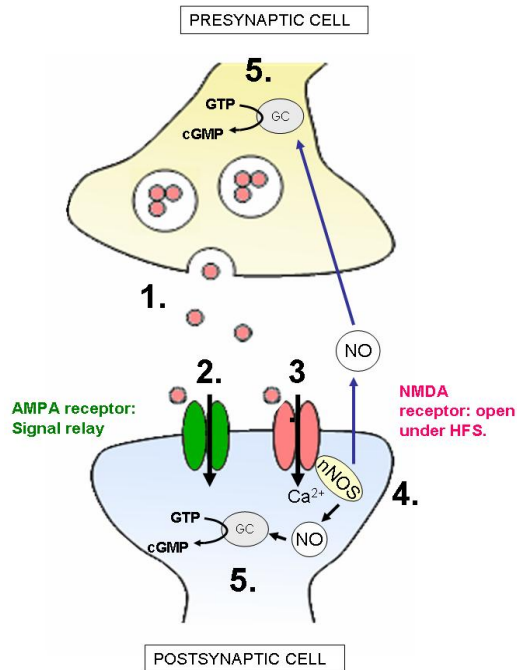


Figure 1.12 NMDA receptor-dependent LTP induction and possible expression through NO. **1.** Glutamate released from the presynaptic terminal. **2.** Postsynaptic AMPA receptors activate, depolarising the cell. **3.** Depolarisation summates sufficiently to relieve NMDA receptor channels of Mg²⁺. **4.** NMDA receptors permit Ca²⁺ influx which activates nNOS and NO synthesis. **5.** NO may contribute to postsynaptic and/or presynaptic LTP mechanisms by activation of guanylyl cyclase and cGMP accumulation. Presynaptic mechanisms require retrograde NO transmission (blue arrows).

1.10.4 Long-term depression and NO

Reciprocal in nature to LTP is LTD, a persistent decrease in synaptic efficacy that can be induced by low frequency stimulation (for example, 100 stimuli at 1 Hz). NMDA receptor-dependent LTD has been described in the hippocampus at CA1 synapses (Bliss *et al.*, 2007), but this form of plasticity has been best characterised at Purkinje cell synapses in the cerebellum. At these synapses, LTD is induced by the repeated, low frequency activation of climbing fibre inputs, just after parallel fibre inputs. It is hypothesised that the climbing fibre input acts as an error signal and attenuates inappropriate parallel fibre input to Purkinje cells (Ito, 2001).

Interestingly, NO, produced in parallel fibres or interneurons upon NMDA receptor activity, appears to play a critical role in cerebellar LTD (reviewed by Garthwaite, 2008). Studies have shown that NO causes an increase in cGMP in Purkinje cells,

leading to PKG-mediated phosphorylation of the phosphatase inhibitor, G-substrate. This, in combination with protein kinase C activity, leads to a pattern of AMPA receptor phosphorylation which favours AMPA receptor endocytosis, a mechanism of LTD expression that may also be active following the induction of this form of plasticity at CA1 hippocampal synapses (Bliss *et al.*, 2007).

1.10.5 Other forms of synaptic plasticity

Multiple forms of short-term synaptic plasticity have also been characterised, including facilitation (discussed in **Chapters 3-4**) and post-tetanic potentiation (PTP): a transient plasticity that is underpinned by multiple mechanisms and is usually observed in the first 1-2 min after LTP induction (Zucker and Regehr, 2002). In addition, Abraham and Bear (1996) have coined the term ‘metaplasticity’ to describe the hypothesis that synaptic plasticity may be influenced by past events at a synapse. Metaplasticity may influence the threshold level for the induction of LTP and LTD, as well as the direction of plasticity following synaptic stimulation. As such, metaplasticity may be intimately linked to the homeostasis of synaptic activity, preventing, for example, the saturation of efficacy at active synapses, as would be predicted to occur at a purely Hebbian synapse (Abraham, 2008).

1.11 LTP, NO and learning and memory

1.11.1 Types of memory

Based mainly on studies of memory in humans with brain damage and on animal models of memory loss, different forms of memory have been delineated by several researchers (see **Figure 1.13**), most famously Endel Tulving. It is also recognised that long-term memory occurs in phases, for example, acquisition, consolidation and retrieval, each of which may rely on different physiological processes in different brain areas.

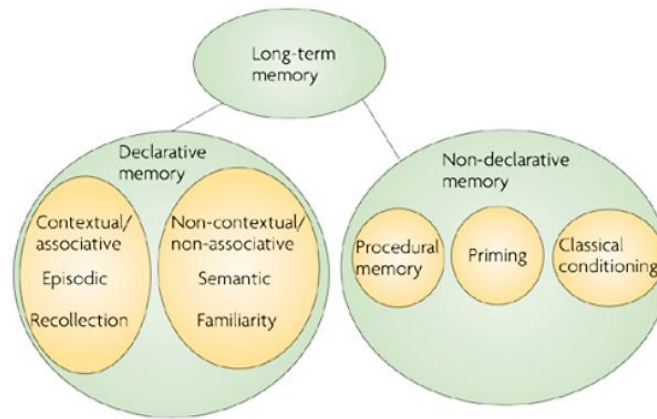


Figure 1.13 Current taxonomy of memory. Declarative memory is conscious. Non-declarative memory is non-conscious. Episodic memory refers to memory for events. Semantic memory refers to memory for facts. Taken from Bird and Burgess (2008). Adapted by kind permission of Nature Publishing Group.

1.11.2 LTP and memory

The initial report of LTP by Bliss and Lomo (1973), coupled with studies showing that it was input-specific, associative and persistent, provided the first demonstration of a Hebbian synaptic plasticity. The Hebbian characteristics of LTP have led many researchers to view LTP as a correlate of learning and memory, although this is highly debated.

In 2000, Martin *et al.* formalised the ‘synaptic plasticity and memory’ (SPM) hypothesis. This proposes that activity dependent synaptic plasticity occurs during normal brain activity at synapses necessary for learning and memory, and is necessary and sufficient for the storage of information. Martin *et al.* (2000) described four criteria that must be met of a synaptic plasticity sufficient to explain memory. Based on these criteria, Bliss *et al.* (2007) have posed four main questions that must be answered to test whether LTP is a correlate of learning and memory: 1) are the mechanisms underlying LTP correlated with those underlying learning and memory?; 2) does learning induce LTP?; 3) do changes in synaptic weights subsequent to learning cause forgetting?; 4) does LTP induction generate a memory without animals having gone through learning?

A wealth of studies have been directed to answering the first question, and suggest that, in general, the mechanisms underlying LTP of synapses are correlated with those underlying learning and memory in tasks dependent on the same brain area. Early studies showed that factors such as ageing and stress impact LTP and learning and memory in a similar manner (reviewed by Lynch, 2004). Manipulations that attenuate or augment LTP were also shown to similarly affect the ability of animals to learn and remember some behavioural tasks. For example, Morris *et al.* (1986) found that the NMDA antagonist, D/L-AP5, inhibited LTP at perforant path-granule cell synapses *in vivo* and learning in the Morris water maze, a task that is hippocampus-dependent (Morris *et al.*, 1982). Morris *et al.*'s findings have since been supported by numerous studies (for example, Tsien *et al.*, 1996; Tang *et al.*, 1999). Additionally, other LTP 'players' appear to be required for learning and memory (reviewed by Lynch, 2004). For example, Giese *et al.* (1998) have found that, in accordance with multiple other reports (for example Silva *et al.*, 1992a; Silva *et al.*, 1992b), mice lacking functional α CaMKII, a kinase heavily associated with LTP (Lisman *et al.*, 2002), display impaired hippocampal LTP and Morris water maze learning. It should also be noted that a positive correlation between LTP and learning and memory has been observed outside the hippocampus (reviewed by Lynch, 2004). For example, in the amygdala, manipulations, including the blockade of the NMDA/NO/cGMP pathway, that have been found to inhibit LTP at synapses between the lateral amygdala and auditory thalamus have also been found to attenuate auditory fear conditioning (for example, Bauer *et al.*, 2002; Ota *et al.*, 2008), an amygdala-dependent task (Goosens and Maren, 2001)

In further support of the SPM hypothesis, and consistent with the second question (is learning associated with the induction of LTP?), stimuli that enhance subsequent learning, such as environmental enrichment and training in behavioural tasks, have been found to enhance field EPSPs (fEPSPs), neurotransmitter release and cause various biochemical changes associated with LTP, such as increased AMPA receptor density at synapses, in brain areas including the visual cortex, motor cortex and amygdala (reviewed by Lynch, 2004; Bliss *et al.*, 2007). In the hippocampus, two key studies have been performed by Gruart *et al.* (2006) and Whitlock *et al.* (2006) who used arrays of electrodes implanted in area CA1 to measure synaptic efficacy

during learning. Gruart *et al.* (2006) found that, in mice during trace eye blink conditioning, the amplitude of evoked fEPSPs steadily increased in a manner that was NMDA receptor-dependent. Whitlock *et al.* (2006) found that at a minority of electrodes, fEPSPs were significantly and persistently increased in rats following one-trial inhibitory avoidance learning. Strikingly, this increase occluded subsequent LTP.

Accordant with the third question (do changes in synaptic plasticity caused by LTP induction cause forgetting, i.e. by altering synaptic weights?), Brun *et al.* (2001) have found that high frequency stimulation applied to the dentate gyrus of rats through implanted electrodes blocked prior memory for the Morris water maze (i.e. induced retrograde amnesia). Interestingly, high frequency stimulation had no effect when applied in the presence of a NMDA antagonist, 3-(2-carboxypiperazin-4-yl)propyl-1-phosphonic acid, suggesting that the retrograde amnesia may have been caused by a NMDA receptor-dependent change in synaptic weights.

These data are broadly in favour of the SPM hypothesis, although it should be noted that there are several pieces of evidence that are inconsistent with the theory. For example, whereas most forms of LTP are NMDA receptor-dependent, the NMDA antagonist, D/L-AP5 seems only to attenuate spatial learning in task-naïve animals, suggesting that the relationship between LTP and learning is not direct (Bannerman *et al.*, 1995; although see **Chapter 5** for examples of NMDA receptor-independent LTP). Additionally, some, but not all (Moser *et al.*, 1998), studies have found no effect of manipulations designed to saturate LTP on subsequent learning (Bliss and Richter-Levin, 1993). These inconsistencies perhaps reflect the possibility that learning and memory require the activity of multiple neural pathways involved in networks spanning several brain areas. Indeed many researchers agree that the view that ‘LTP equals memory’ is too simplistic (reviewed by Lynch *et al.*, 1983; Bliss *et al.*, 2007).

The use of LTP induction protocols that are unlikely to represent natural patterns of neuronal activity have also raised doubts over the relevance of the mechanisms underlying LTP to learning, although induction protocols patterned after the theta

rhythm, which can be observed in the hippocampus using electroencephalography during exploratory behaviour, or involving ‘primed bursts’ are efficient in generating LTP (for example, Morgan and Teyler, 2001). The idea that synaptic plasticity, as modelled by LTP, is involved in memory is further complicated by the fact that it has not been possible to link LTP-like synaptic plasticity to a certain stage or type of memory. The role of other forms of plasticity such as depotentiation and LTD are also unclear, and a major outstanding question is whether synaptic plasticity in the hippocampus must persist for as long as a memory.

Finally, it should be noted that synaptic plasticity has been proposed to better model physiological processes that are related to, but distinct from learning and memory, such as attention (Shors and Matzel, 1997), and that there have been no direct-tests of fourth prediction of the SPM hypothesis (does LTP induction generate a memory without animals having gone through learning?). Furthermore, it is unclear how plasticity at an individual synapse might affect the activity of a network. Nevertheless, studies, for example, those by Whitlock *et al.* (2006) and Gruart *et al.* (2006) are compelling. Therefore, while it cannot be said that ‘LTP equals memory’, or that LTP in the form induced in the laboratory exists naturally, the mechanisms underlying LTP appear to be the best molecular correlates of learning and memory currently amenable to study in the laboratory. Additionally, an appreciation of LTP mechanisms could have wide implications for our understanding of all basic principles of plastic synaptic transmission, especially if neurons make use of all the means of synaptic plasticity available to them (Bliss *et al.*, 2007).

1.11.3 NO and learning and memory

If LTP is a correlate of learning, and NO is required for some forms of LTP, then it is predicted that NO is necessary for at least some forms of learning. In support of this prediction, several studies suggest that a role for NO in learning and memory has been evolutionarily conserved. In invertebrates such as the sea slug, *Aplysia californica*, the pond snail, *Lymnaea stagnalis*, and honey bee, *Apis mellifera*, for example, NO appears to be required for associational learning during classical conditioning. In particular, tasks involving olfactory or appetitive cues seem

particularly sensitive to NOS inhibition (reviewed by Susswein *et al.*, 2004). For example, application of the NOS inhibitor, L-NAME, during and after aversive appetitive conditioning in *Aplysia* has been found to block short- and long-term memory for the conditioned stimulus. In contrast, L-NAME had no effect on spontaneous feeding, and no effect when applied one min after training. The authors therefore concluded that NO was required during the acquisition but not consolidation of the memory (Katzoff *et al.*, 2002).

In mammals, NOS and NO-targeted guanylyl cyclase inhibition has also been found to attenuate learning during hippocampus-dependent tasks. For example, intraperitoneal injection of the NOS inhibitor, L-NNA, was found by Bohme *et al.* (1993) to block the ability of rats to learn in a radial arm maze (which is hippocampus-associated) and a social recognition test involving olfactory memory. CA1 LTP was blocked in slices from rats that received injections of the NOS inhibitor. Similarly, Majlessi *et al.* (2008) have found that rats treated with L-NAME via a cannula implanted near the CA1 region of the hippocampus were impaired in the Morris water maze. Specifically, escape latency and travelled distance were increased whereas the number of entries into the quadrant containing the platform decreased. No effects on motivation or sensorimotor coordination were observed and the inhibition could be reversed by the co-application of L-arginine, which may have outcompeted L-NAME for binding to NOS, as has been shown to occur in hippocampal slices (East and Garthwaite, 1991). In addition, 3-(5-hydroxymethyl-2-furyl)-1-benzyl-indazole, a compound that sensitises NO-targeted guanylyl cyclase to NO (Ko *et al.*, 1994) and also blocks PDEs (Galle *et al.*, 1999), has been found to enhance CA1 LTP via a mechanism involving the NO/cGMP/PKG pathway and shorten the escape latency of mice from the Morris water maze (Chien *et al.*, 2003; Chien *et al.*, 2005).

It should be noted that some forms of learning and memory in tasks associated with other brain areas also appear to be NOS-dependent, for example, NOS inhibition has been found to impair cerebellum-dependent eye blink conditioning in rabbits (Chapman *et al.*, 1992) and amygdala-dependent place conditioning (Zarrindast *et al.*, 2002). ‘Natural’ forms of learning, such as olfactory learning of a ewe for her

lamb, have also been found to require NO/cGMP signalling (reviewed by Susswein *et al.*, 2004).

As with the role of NO in LTP, more work is necessary to elucidate the contribution of NO to learning and memory. Reported effects of NO on learning and memory phenomena are so diverse that NO has not been associated with a particular stage or form of memory (reviewed by Susswein *et al.*, 2004). Additionally, and consistent with the role of NO in LTP, several groups have found no effect of NO on learning in tasks which other groups have found to be NOS-dependent, for example, the Morris water maze (Bannerman *et al.*, 1994a; Blokland *et al.*, 1999). The species and strain of the animal under study, the behaviour being tested and crucially the training paradigm may dictate whether NO is required. These factors also appear to regulate the requirement of learning and memory during behavioural tasks for other LTP 'players'. For example, the requirement of mice for functional α CaMKII to learn an inhibitory avoidance task appears to be dependent on the number of training trials given (Irvine *et al.*, 2005).

1.11.4 The hippocampus and memory

As discussed above, the archetype of LTP occurs in the hippocampus. If LTP is a correlate of learning and memory, then the SPM hypothesis dictates that the hippocampus should be required for these phenomena. Consistent with this, theories of hippocampal function have moved away from early hypotheses suggesting that it is involved in olfaction, attention or emotion and towards a role in memory (Andersen *et al.*, 2007).

Probably the best known evidence for a role of the hippocampus in memory came from a case study of a patient, named HM, by William Scoville and Brenda Milner (1957). HM had ~ two thirds of his hippocampus, as well as other areas of the hippocampal formation, removed in a surgery aimed to treat his epilepsy. The operation successfully alleviated his condition, but at the expense of his ability to form new long-term declarative memories. In accordance with the current taxonomy of memory (**Figure 1.11**), HM's short-term and non-declarative (for example procedural or skills) memory remained intact (reviewed by Corkin, 2002).

Since Scoville and Milner's study, multidisciplinary evidence has combined to assert the consensus that the hippocampus is required for declarative memory. Several theories of the specific role of the hippocampus have been developed. One of the first, named 'the declarative theory', proposes that, in concert with other areas of the medial temporal lobe, the hippocampus is required for the acquisition of all declarative memory but that, after some period, these are consolidated to the neocortex, explaining why old memories are often spared following hippocampal damage (as in HM). More elaborate theories suggest that the hippocampus is also the site for the long-term storage of episodic memories, and/or that the hippocampus is involved in the acquisition of episodic, but not semantic, memory. Another set of theories, for example, 'the relational theory', propose that, during acquisition and recollection, the hippocampus allows the association of information, such as the contextual details of an event, that are initially processed and later stored in different neocortical areas.

An extension of the relational theory is 'the cognitive-map theory', which proposes that the major role of the hippocampus is to construct and store an allocentric representation of an environment in order to enable navigation through it. It is thought that the cognitive map may arise via the acquisition, and subsequent retrieval of spatiotemporal associations (reviewed by Lynch, 2004; Bird and Burgess, 2008). This theory was borne of findings that humans and animals with hippocampal damage have problems in navigation, for example during the Morris water maze (for example, Morris *et al.*, 1982), and from the discovery by O'Keefe and Dostrovsky in 1971 that pyramidal neurons are place cells- cells which fire when an animal is in or imagining to be in a specific location in an environment (reviewed by O'Keefe, 2007).

1.12 The hippocampus

The hippocampus (Greek for sea horse) was first named by Aranzi (1587) because of its resemblance to the fish. The laminar structure of the hippocampus (see **1.12.2**) facilitates the study of neurons and synaptic connections within it using extracellular

and intracellular electrophysiological recording *in vivo* and *in vitro*. As such, many basic aspects of neurotransmission, neuropharmacology and neurophysiology have been elucidated by studies of the hippocampus and its principal cells, pyramidal neurons (reviewed by Teyler, 1999; Andersen *et al.*, 2007).

1.12.1 Location of the hippocampus

The hippocampus proper (sometimes called ‘Ammon’s horn’ or ‘Cornu Ammonis’ because of its resemblance to the rams horn of the Egyptian God, Amun) is part of the hippocampal formation, which also comprises the dentate gyrus (a structure interlocked with the hippocampus proper), the subiculum, presubiculum, parasubiculum, and the entorhinal cortex. The location of the hippocampus in human and rodent brain is shown in **Figure 1.14**. The hippocampal formation is part of the limbic system, an elaboration of the cerebral cortex in the temporal lobe that also contains the amygdala, mammillary bodies and entorhinal cortex, amongst other structures. The limbic system is not considered to have a unified function (reviewed by Amaral and Lavenex, 2007).

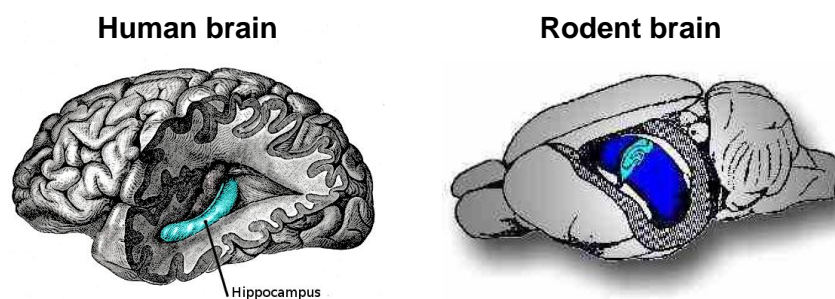


Figure 1.14 Location of the hippocampus in human and rodent brain. Hippocampus shown in blue. Light blue image in the rodent brain shows a transverse hippocampal slice. Images from www.en.wikipedia.org and www.ucl.ac.uk.

1.12.2 Anatomy of the dentate gyrus and hippocampus

The components of the limbic system generally have fewer layers than the neocortex and the hippocampus and dentate gyrus are no exceptions. The dentate gyrus consists of three layers or strata: the principal, granule cell layer (stratum granulare), the

molecular layer (stratum moleculare), and the polymorphic layer (stratum polymorph or hilus; see **Figure 1.15A**). The stratum granulare is ~ 4-8 cells thick and densely packed. There are ~ 1.2×10^6 granule cells in one rat dentate gyrus. Their dendrites form a conical tree and extend perpendicularly into the molecular layer where they form synapses with axons of several pathways (**Figure 1.15B**).

In 1934, Lorente de Nó subdivided the hippocampus into three regions named Cornu Ammonis (CA) 1-3 (see **Figure 1.15A**). The polymorphic layer of the dentate gyrus was also ascribed CA4. The principal layer of the hippocampus is called the pyramidal cell layer, or stratum pyramidale. Within it, pyramidal neurons are arranged 3-6 cells thick. They are characterised by a triangular soma (~ 20 μm in diameter) and extensive dendritic trees that extend perpendicularly from the stratum pyramidale in both directions: the basal dendritic arbour, which contains multiple primary dendrites, extends into the stratum oriens; the longer, apical dendrites extend into the strata lucidum (in CA3), radiatum and lacunosum moleculare (in CA2-1; see **Figure 1.15B**). As the stratum pyramidale extends from CA3 to CA1 and into the subiculum, pyramidal cells become smaller and the connections that they make change. On average, a single pyramidal neuron may receive 30000 excitatory and 1700 inhibitory inputs. Excitatory synapses form on dendritic spines, whereas inhibitory synapses form on dendritic shafts, soma and axons. Pyramidal and granule neurons are predominantly glutamatergic (reviewed by Amaral and Lavenex, 2007).

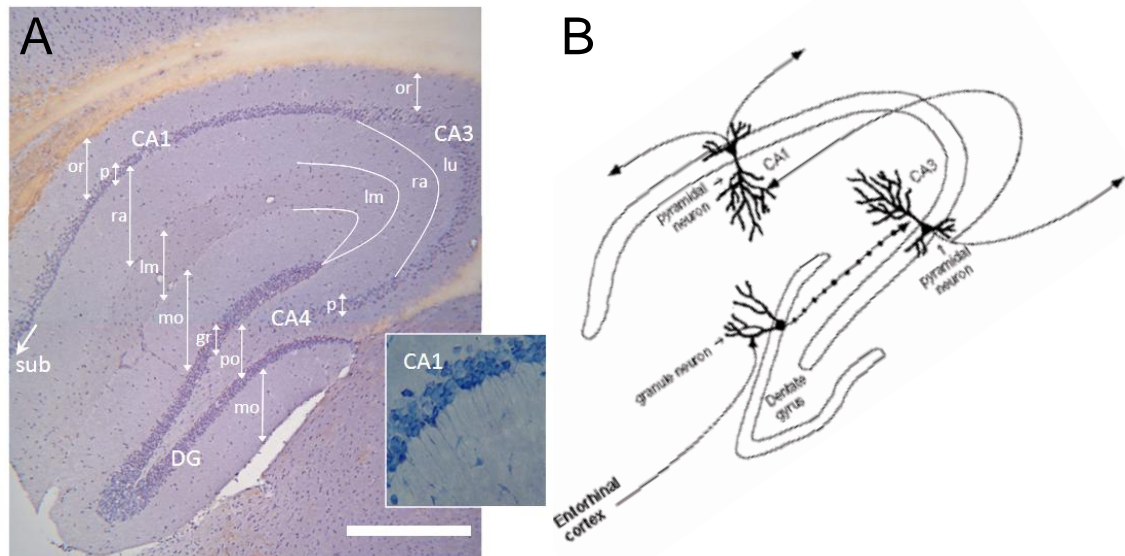


Figure 1.15 Strata of the hippocampus. **A)** Image is a 10 μm -thick transverse section of adult mouse hippocampus stained with Mayer's hemalum (scale = 500 μm). Key: dg = dentate gyrus; gr = stratum granulare; lm = lacunosum moleculare; lu = stratum lucidum; mo = stratum moleculare; or = stratum oriens; p = stratum pyramidale; po = stratum polymorph; ra = stratum radiatum; sub = subiculum. Inset shows a magnified section of CA1 stained with toluidine blue (see **Chapter 7** for methods of staining). The stratum pyramidale is shown and the proximal apical dendrites of pyramidal neurons are visible. Scale is 100 μm . Orientation is as in main image. **B)** Line drawing showing the orientation of pyramidal neuron and granule cell dendrites. The directions of their spread are illustrated by arrows (see **1.12.4** for discussion of pathways). Image adjusted from www.cyberounds.com.

1.12.3 Hippocampal interneurons

GABAergic interneurons exist throughout all strata of the hippocampus and dentate gyrus, and although they are outnumbered by principal cells (pyramidal and granule cells), all principal cells are thought to be contacted by interneurons. The interactions between principal cells and interneurons are complex. For example, hundreds of pyramidal cells may contact one interneuron which in turn may synapse with thousands of pyramidal neurons. Additionally, interneurons are a major target of pathways entering the hippocampus from other brain areas, such as the septum and raphe nucleus. Interneurons are thought to effect feedback and feed-forward on principal neurons, and may play a critical role in the generation of behaviourally-

cued oscillatory activity in the hippocampus, such as theta rhythm (reviewed by Freund and Buzsaki, 1996).

Multiple subtypes of hippocampal interneuron have been discovered. Each have different locations within the hippocampus, morphology, connections, electrophysiology, pharmacology and immunocytochemistry. This diversity has been illustrated by the finding that, in area CA1 alone, at least 16 types of interneuron have been delineated (Parra *et al.*, 1998). Interneurons with cell bodies in the pyramidal cell layer have been classified into four groups on the basis of their synaptic targets. These are: 1) axo-axonic or chandelier cells, which each contact the axon initial segment of over 1000 pyramidal cells and regulate action potential initiation; 2) basket cells, which innervate and receive excitatory input from as many as 1000-plus pyramidal cells; 3) bistratified cells, which synapse onto apical and basal pyramidal cell dendrites; 4) radial trilaminar cells, which span the entire radius of pyramidal cell dendrites. Interneuron specific interneurons also occur throughout all hippocampal strata. Their axons terminate only on other interneurons (reviewed by Freund and Buzsaki, 1996; Amaral and Lavenex, 2007).

1.12.4 Connections in the hippocampus

The major input to the hippocampus is from the entorhinal cortex. This brain area forms an interface between the hippocampus and neocortex. It receives, and is thought to integrate, highly processed, multimodal sensory information from multiple areas of the cortex, especially the associational, perirhinal and parahippocampal cortices, as well as other brain areas such as the thalamus. It is thought to be required for declarative memory, in particular spatial memory, and grid and head direction cells, which may be required for spatial memory, have been found within it (reviewed by Bird and Burgess, 2008).

A major input to the hippocampus from the entorhinal cortex occurs from pyramidal neurons in layer II via the perforant path, which perforates the subiculum and forms connections with granule cell dendrites (**Figure 1.16**). The perforant path may also contact GABA-positive interneurons in the molecular layer and apical dendrites of

CA3 pyramidal neurons. Additionally, neurons from layer III of the entorhinal cortex project to CA1 neurons and the subiculum via the temporoammonic pathway.

Within the hippocampus, a trisynaptic circuit exists which is thought to conduct a unidirectional flow of information from CA3 to CA1 and the subiculum (**Figure 1.16**). First, the granule cells give rise to distinctive unmyelinated axons, named mossy fibres because they display varicosities (called mossy fibre expansions) along their entire length. These extend into the polymorphic cell layer, where they synapse with GABAergic interneurons, and then enter the stratum lucidum in CA3, where they make large glutamatergic synapses with CA3 pyramidal neurons. A single mossy fibre may contact a dozen pyramidal neurons, and make ~ 30 contacts with each of them. Each CA3 pyramidal neuron may receive input from more than 50 granule cells. From CA3 and CA2 pyramidal neurons, information may then be passed to CA1 via the Schaffer collaterals residing in the strata radiatum and oriens. Each CA3 pyramidal neuron may contact multiple CA1 neurons. Each CA1 neuron might be innervated by over 5000 CA3 cells.

From CA1 pyramidal cells, connections extend into the oriens and alveus and on to the deep layers of the entorhinal cortex via the subiculum. The deep layers of the entorhinal cortex then send outputs back to the cortex. Through this pattern of connections, it is thought that relatively unprocessed information entering the entorhinal cortex from multiple cortical areas traverses the entire hippocampus, may be processed and perhaps associated somehow, and then returned back to the cortex, perhaps for long-term storage (reviewed by Bird and Burgess, 2008; Neves *et al.*, 2008).

Finally, it should be noted that there are also multiple connections between areas of the hippocampus other than those noted above. Within CA3 and CA2 (but not CA1), for example, there are multiple recurrent (associational) connections, as well as connections from the contralateral CA3 and CA2 (commissural connections). Modifications of recurrent connections in area CA3 during the acquisition of information are central to a key computational mode of hippocampal function proposed by Marr (1971). Additionally, Marr suggests that the reactivation of some

recurrent connections in CA3 and subsequent hippocampal pathways by an incomplete cue may induce the reactivation of multiple other pathways in CA1 and subsequently throughout the cortex, eventually leading to the reinstatement of the full memory of an event by pattern completion (see Bird and Burgess, 2008 for a review). This model has since been supported by findings that mice lacking NMDA receptors in area CA3 are impaired in the Morris water maze when only partial spatial cues are present (Nakazawa *et al.*, 2002).

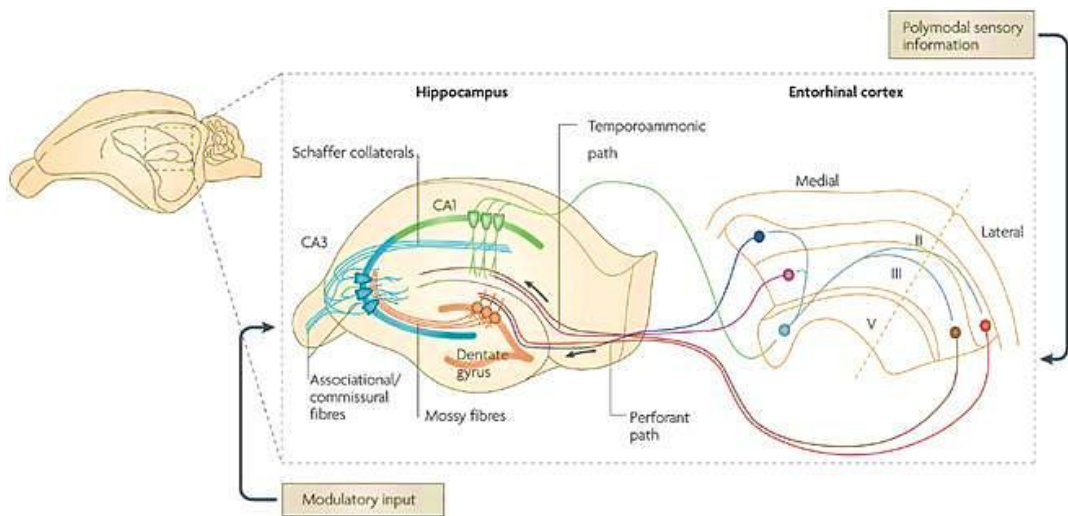


Figure 1.16 Major connections of the hippocampal formation. Taken from Neves *et al.* (2008).
Reproduced by kind permission of Nature Publishing Group.

1.12.5 Location of NOS and NO-targeted guanylyl cyclase in the hippocampus

At CA1-CA3 synapses, functional/pharmacological evidence detailing a role for NO in NMDA receptor-dependent LTP and other processes has implied the presence of e- and nNOS (Hopper and Garthwaite, 2006), as well as all three functionally relevant guanylyl cyclase subunits ($\alpha 1$, $\alpha 2$ and $\beta 1$; Taqatqeh *et al.*, 2009), and this has been corroborated by histological data showing the presence of these proteins in relevant structures.

Initial histological studies found nNOS to be primarily located in the stratum granulare of the dentate gyrus, in the neuropil of the dentate molecular layer and stratum radiatum of Ammon's horn, as well as in scattered cells, presumably interneurons, throughout CA1 (see **Figure 1.15** for key to anatomy; Brecht *et al.*, 1991a; Vincent and Kimura, 1992; Valtschanoff *et al.*, 1993; Dun *et al.*, 1994; Lin and Totterdell, 1998). Since then, immunostaining and electron microscopy following relatively weak fixation of tissues (0.5- 1 % paraformaldehyde; PFA) has also revealed nNOS protein in the cytoplasm of pyramidal cell soma and at synapses throughout the stratum radiatum where it may contribute to synaptic transmission and/or plasticity (Wendland *et al.*, 1994; Gonzalez-Hernandez *et al.*, 1996; Burette *et al.*, 2002). This distribution of nNOS has since been confirmed by the isolation of nNOS mRNA from dissociated CA1 pyramidal neurons (Chiang *et al.*, 1994). The increase in stained structures following immunohistochemistry for nNOS using relatively weakly fixed tissue may reflect better preservation of nNOS epitopes or improved access of the antibody to the protein due to a reduction in aldehyde cross-linking of proteins, for example, in the PSD.

Unsurprisingly, eNOS is found throughout the hippocampal vasculature (Blackshaw *et al.*, 2003). As mentioned above (**1.2.2**), some groups have also reported eNOS staining in pyramidal neurons in rodent (Dinerman *et al.*, 1994; O'Dell *et al.*, 1994) and human (Doyle and Slater, 1997) hippocampus, although attempts to replicate these results have failed. Rather, several studies (for example Chiang *et al.*, 1994) support the current consensus that eNOS expression is restricted to blood vessels.

An initial study of the location of guanylyl cyclase in hippocampus using *in situ* hybridisation showed message for the protein throughout the strata pyramidale and granulare (Matsuoka *et al.*, 1992). Later, mRNA for all three functionally-relevant subunits of the NO-targeted guanylyl cyclase, $\alpha 1$, $\alpha 2$ and $\beta 1$, was shown to be present in the developing and adult rat hippocampus (Gibb and Garthwaite, 2001; Mergia *et al.*, 2003). In contrast to other brain areas in which the amount of mRNA for each of the α subunits is approximately equal, Mergia *et al.* (2003) have found that, in the hippocampus, mRNA for the $\alpha 2$ subunit is significantly more abundant than message for the $\alpha 1$ subunit. Using *in situ* hybridisation, Gibb and Garthwaite

(2001) detected an abundance of mRNA for the $\alpha 2$ and $\beta 1$ subunits in the stratum pyramidale, but it was unclear whether the $\alpha 1$ subunit was also present in pyramidal cells or in the surrounding strata radiatum and oriens (Gibb and Garthwaite, 2001).

At CA3-CA1 synapses, functional evidence detailing both post- (for example, Serulle *et al.*, 2007) and presynaptic (for example, Phillips *et al.*, 2008) effects of NO following the induction of LTP has been corroborated by a complimentary distribution of guanylyl cyclase and nNOS either side of the synapse (Burette *et al.*, 2002). Using immunohistochemistry optimised to detect synaptic proteins, Burette *et al.* (2002) have shown that nNOS and the guanylyl cyclase $\beta 1$ subunit preferentially associate with each other at a subpopulation of synapses (< 10 %) within CA1. In support of putative retrograde NO transmission, post-embedding immunogold electron microscopy revealed nNOS within the PSD of asymmetric axospinous synapses and in close spatial proximity to presynaptic guanylyl cyclase $\beta 1$ located within axon terminals. Additionally, Burette *et al.* (2002) imply that a minority of postsynaptic densities were positive for guanylyl cyclase $\beta 1$ and presynaptic varicosities positive for nNOS, suggesting that anterograde and/or intracellular NO transmission may occur. The location of the NO-targeted guanylyl cyclase α subunits is the topic of **Chapter 5**.

1.13 General Aim

Interest in the role of NO in LTP is largely rooted in the hypothesis that NO, synthesised by nNOS upon NMDA receptor channel opening, acts as a retrograde messenger during NMDA receptor-dependent LTP (reviewed by Feil and Kleppisch, 2008). In this way, NO might account for presynaptic effects of LTP. Although evidence for a presynaptic effect of NO during LTP has been yielded from studies of synapses between dissociated hippocampal pyramidal neurons (Arancio *et al.*, 1995; Arancio *et al.*, 1996; Arancio *et al.*, 2001), and many researchers describe NO as a retrograde messenger, there is little unambiguous evidence for retrograde NO transmission or a presynaptic effect of NO following LTP induction at synapses in intact tissues (reviewed in **Table 3.1**). The first aim of the project was therefore to isolate the NO-dependent component of NMDA receptor-dependent LTP at CA3-

CA1 synapses in intact tissues (transverse hippocampal slices) and to test whether it was characterised by a persistent increase in neurotransmitter release using changes in the magnitude of PPF of CA1 fEPSPs as an indicator of presynaptic efficacy (see **Chapter 3**).

Related to this, the second aim was to investigate the effect of NO on neurotransmitter release at CA1 synapses under basal stimulation (i.e. stimulation causing no observable persistent plasticity; see **Chapter 4**). The major reason was that mice lacking the NO-targeted guanylyl cyclase $\alpha 1$ subunit had recently been found to exhibit reduced CA1 PPF under basal conditions, consistent with tonic facilitation of neurotransmitter release at wild-type CA1 synapses (Taqatqeh *et al.*, 2009). We hypothesised that if NO was found to regulate neurotransmitter release at CA1 synapses under basal conditions, then the isoform responsible might be eNOS, because a low-level, activity-dependent, endothelium-derived NO tone exists in the hippocampus (Chetkovich *et al.*, 1993; Hopper and Garthwaite, 2006).

A third aim related to whether the role of NO in CA1 LTP is strictly NMDA receptor-dependent (see **Chapter 5**). Although nNOS is thought to be preferentially activated by NMDA receptor opening, we noticed that the properties of a NMDA receptor-independent CA1 LTP (reviewed by Teyler *et al.*, 1994) were similar to NO-dependent LTP. Therefore, we tested the involvement of NO in the NMDA receptor-independent CA1 LTP.

Finally, we wanted to investigate the location of the NO-targeted guanylyl cyclase in the hippocampus. Of specific interest was the location of the cyclases' α subunits (**Chapter 7**), because it had been recently suggested that the $\alpha 1\beta 1$ and $\alpha 2\beta 1$ isoforms of the cyclase have distinct roles in LTP (Taqatqeh *et al.*, 2009).

Chapter 2:
General materials and methods

2.1 Materials

2.1.1 Pharmacological compounds

The pharmacological compounds/ peptides that were used are listed in **Table 2.1**. Unless otherwise stated, compounds were prepared such that the final concentration of the solvent applied *in vitro* was no more than 1:100, or 1:1000 for DMSO. See **2.5 Key to Suppliers** for supplier details.

| Compound/ Peptide | Chemical name and primary reason for use* | Solvent | Supplier |
|-------------------------------------|---|------------------|----------|
| Acetylcholine chloride (ACh) | 2-acetyloxyethyl(trimethyl)azanium chloride (Cholinergic agonist) | H ₂ O | Sigma |
| ω-Agatoxin IVA | - (P/Q-type VGCC inhibitor) | H ₂ O | Alomone |
| D-AP5 | (2R)-2-amino-5-phosphonopentanoic acid (NMDA antagonist) | NaOH | Tocris |
| L-Arginine | (2S)-2-amino-5- (diaminomethylideneamino)pentanoic acid (NOS substrate) | aCSF | Sigma |
| BAY 60-7550 | 2-[(3,4-dimethoxyphenyl)methyl]-7-[(1R)-1- hydroxyethyl]-4-phenylbutyl]-5-methyl-imidazo[5,1- f][1,2,4]triazin-4(1H)-one (PDE 2 inhibitor) | DMSO | Cayman |
| Cadmium sulphate | cadmium trisulphate octahydrate (VGCC antagonist (non-selective)) | H ₂ O | Sigma |
| 2-Chloroadenosine | (2R,3R,4S,5R)-2-(6-amino-2-chloropurin-9-yl)-5- (hydroxymethyl)oxolane-3,4-diol (Adenosine receptor agonist) | aCSF | Sigma |
| CNQX disodium | disodium 6-cyano-7-nitroquinoxaline-2,3-diolate (AMPA/kainate receptor inhibitor) | DMSO | Tocris |
| ω-Conotoxin GVIA | - (N-type VGCC inhibitor) | H ₂ O | Sigma |
| EGTA | 2-[2-[2-[2- [bis(carboxymethyl)amino]ethoxy]ethoxy]ethyl- (carboxymethyl)amino]acetic acid | NaOH | Sigma |

| | | | |
|----------------------------------|--|------------------|-------------------------------|
| | (Ca ²⁺ chelator) | | |
| Forskolin | [(3R,4aR,5S,6S,6aS,10S,10aR,10bS)-3-ethenyl-6,10,10b-trihydroxy-3,4a,7,7,10a-pentamethyl-1-oxo-5,6,6a,8,9,10-hexahydro-2H-benzo[f]chromen-5-yl]acetate (Adenylyl cyclase agonist) | DMSO | Tocris |
| FPL 64176 | methyl 4-(2-benzylbenzoyl)-2,5-dimethyl-1H-pyrrole-3-carboxylate (L-type VGCC current enhancer) | DMSO | Tocris |
| FX-4053.3HCl | 6-[[[(3R,4R)-4-(2-{[2,2-difluoro-2-(3-fluorophenyl)ethyl]amino}ethoxy)pyrrolidin-3-yl]methyl]-4-methylpyridin-2-amine trihydrochloride (nNOS inhibitor) | DMSO | Prof. Richard Silverman |
| Gadolinium (III) chloride | Trichlorogadolinium hexahydrate (Transient receptor potential channel antagonist) | DMSO | Sigma |
| IBMX | 1-methyl-3-(2-methylpropyl)-7H-purine-2,6-dione (PDE inhibitor (non-selective)) | DMSO | Sigma |
| JK-5.3HCl | 6-[[[(3R,4R)-4-(2-{[2-(3-chloro-5-fluorophenyl)-2,2-difluoroethyl]amino}ethoxy)pyrrolidin-3-yl]methyl]-4-methylpyridin-2-amine trihydrochloride (Proposed nNOS inhibitor) | DMSO | Prof. Richard Silverman |
| S-MCPG | 4-[(2S)-2-amino-1-hydroxy-1-oxopropan-2-yl]benzoic acid (Metabotropic glutamate receptor inhibitor) | NaOH | Tocris |
| (+)-MK-801 maleate | (+)-5-methyl-10,11-dihydro-5H-dibenzo[a,d]cyclohepten-5,10-imine maleate (NMDA receptor open channel blocker) | H ₂ O | Tocris |
| NBQX disodium | 2,3-Dioxo-6-nitro-1,2,3,4-tetrahydrobenzo[f]quinoxaline-7-sulfonamide disodium (AMPA/kainate receptor inhibitor) | DMSO | Tocris |
| Nifedipine | dimethyl 2,6-dimethyl-4-(2-nitrophenyl)-1,4-dihydropyridine-3,5-dicarboxylate (L-type VGCC inhibitor) | DMSO | Tocris |
| NMDA | (2R)-2-(methylamino)butanedioic acid (NMDA receptor agonist) | NaOH | Tocris |
| L-NNA | 2-amino-5-[[amino(nitramido)methylidene]amino]pentanoic acid (NOS inhibitor (non-selective)) | HCl | Tocris |

| | | | |
|----------------------------|--|--|---------|
| LY 341495 | 2-[(1 <i>S</i> ,2 <i>S</i>)-2-carboxycyclopropyl]-3-(9 <i>H</i> -xanthen-9-yl)-D-alanine (Metabotropic glutamate receptor inhibitor) | NaOH | Tocris |
| Nickel(II) chloride | Dichloronickel (T/R-type VGCC inhibitor) | H ₂ O | Sigma |
| ODQ | [1,2,4]oxadiazolo[4,3- <i>a</i>]quinoxalin-1-one (NO-targeted guanylyl cyclase antagonist) | DMSO | Sigma |
| PAPA/ NONOate | N-[3-aminopropyl(propyl)amino]-N-hydroxynitrous amide (NO donor) | NaOH | Enzo |
| Thapsigargin | (3 <i>S</i> ,3 <i>aR</i> ,4 <i>S</i> ,6 <i>S</i> ,6 <i>aR</i> ,7 <i>S</i> ,8 <i>S</i> ,9 <i>bS</i>)-6-(acetyloxy)-4-(butyryloxy)-3,3 <i>a</i> -dihydroxy-3,6,9-trimethyl-8--2-oxo-2,3,3 <i>a</i> ,4,5,6,6 <i>a</i> ,7,8,9 <i>b</i> -decahydroazuleno[4,5- <i>b</i>]furan-7-yl octanoate (Sarco/endoplasmic reticulum Ca ²⁺ ATPase inhibitor) | DMSO | VWR |
| TTX (citrate free) | (4 <i>R</i> ,4 <i>aR</i> ,5 <i>R</i> ,6 <i>S</i> ,7 <i>S</i> ,8 <i>S</i> ,8 <i>aR</i> ,10 <i>S</i> ,12 <i>S</i>)-2-azaniumylidene-4,6,8,12-tetrahydroxy-6-(hydroximethyl)-2,3,4,4 <i>a</i> ,5,6,7,8-octahydro-1 <i>H</i> -8 <i>a</i> ,10-methano-5,7-(epoxymethanoxy)quinazolin-10-olate (Na ²⁺ channel blocker) | C ₂ H ₄ O ₂ | Latoxan |
| L-VNIO.HCl | N5-(1-imino-3-butenyl)-L-ornithine, monohydrochloride (nNOS inhibitor) | DMSO | Enzo |
| 1400-W.2HCl | N ¹ -[[3 (aminomethyl)phenyl]methyl]ethanimidamide dihydrochloride (i/nNOS inhibitor) | H ₂ O | Enzo |

Table 2.1 Pharmacological compounds used. *Secondary actions of each compound are discussed in the text where appropriate.

2.1.2 Antibodies

The antibodies that were employed are listed in **Table 2.2**.

| Primary antibodies | | | |
|---|-------------|--|---|
| Antigen | Host | Concentration used | Catalogue number and/or supplier |
| Actin 1-19 | Goat | 1:500 | SC-1616; Santa Cruz Biotechnology |
| cGMP | Rabbit | 1:560 | Made by Dr Giti Garthwaite |
| Guanylyl cyclase α 1 subunit | Rabbit | 1:400 immunoperoxidase staining; 1:500 Western blot analysis | G4280; Sigma |
| Guanylyl cyclase β 1 subunit | Rabbit | 1:250 | CAY-160897-1; Cayman Chemical |
| | Rabbit | 1:600 | Prof. Soenke Behrends (see van Staveren <i>et al.</i> , 2004) |
| nNOS | Rabbit | 1:700 | 61-7000; Invitrogen (Zymed) |
| Biotinylated secondary antibodies (Immunoperoxidase staining) | | | |
| Antigen | Host | Concentration used | Catalogue number and supplier |
| Rabbit | Donkey | 1:200 | AP182B; Chemicon |
| Horseradish peroxidase-conjugated secondary antibodies (Western blot analysis) | | | |
| Antigen | Host | Concentration used | Catalogue number and supplier |
| Rabbit | Goat | 1:15000 | 31460; Perbio, Fisher |
| Goat | Donkey | 1:20000 | SC-2020; Santa Cruz Biotechnology |

Table 2.2 Antibodies used.

2.1.3 PCR primers

Where used, transgenic mice were genotyped by PCR and gel electrophoresis. The primers that were employed are detailed in **Table 2.3**. Stocks of primers were prepared in double-distilled H₂O.

| Genotyping of CaMKII^{T286A} mice | | |
|--|-------------------------------|-----------------|
| Primer | Sequence (5'-3') | Supplier |
| Lox 1 | CTG TAC CAG CAG ATC AAA GC | Invitrogen |
| Lox 2 | ATC ACT AGC ACC ATG TGG TC | Invitrogen |
| Genotyping of eNOS^{-/-} mice | | |
| Primer | Sequence (5'-3') | Supplier |
| eNOS forward | GGT GTT TGG CTG CCG ATG C | Sigma |
| eNOS reverse | GCA CAG CAC ACG GTG AAC C | Sigma |
| NEO forward | GCA TAC GCT TGA TCC GGC TAC C | Sigma |
| NEO reverse | GAA GGC GAT GCG CTG CGA ATC | Sigma |

Table 2.3 Primers used for PCR.

2.1.4 Other special materials

The other special materials that were used, including assay kits and enzymes, are listed in **Table 2.4**. Standard chemicals that have not been listed were purchased from VWR International.

| Reagent/ enzyme | Abbreviation | Supplier |
|--|-----------------------|------------------------|
| Agar, noble | - | DIFCO |
| Agarose gel | - | BioLine |
| Bicinchoninic acid protein assay kit | BCA protein assay kit | Fisher |
| Bovine serum albumin (fraction V) | BSA | Sigma |
| 100 base pairs DNA ladder | - | Promega |
| Bromophenol blue | - | Sigma |
| Chromium potassium sulfate dodecahydrate | Chrome alum | Sigma |
| ColourPlus prestained protein ladder | - | New England BioLabs |
| Cyclic guanosine monophosphate (sodium salt) | cGMP | Sigma |
| Deoxyribonucleotide triphosphates | dNTPs | Takara |
| 3,3'-Diaminobenzidine | DAB | Sigma |
| threo-1,4-Dimercapto-2,3-butanediol | DTT | Sigma |
| Dimethyl sulfoxide | DMSO | Sigma |
| Di-n-butylphthalate in xylene | DPX | Agar Sci. |

| | | |
|---|-------------------------------|---------------|
| Disodium ethylenediaminetetraacetate dehydrate | EDTA | Sigma |
| Donkey serum | - | Millipore |
| Ethidium bromide | - | Sigma |
| Gelatine | - | Sigma |
| Glycerol | - | Sigma |
| GoTaq hot start DNA polymerase | - | Promega |
| Halt protease inhibitor cocktail | - | Fisher |
| High performance chemiluminescence film | - | GE Healthcare |
| Hydrogen peroxide in H₂O | H ₂ O ₂ | Sigma |
| Hyperladder 1 | - | BioLine |
| Mayer's hemalum | - | Merck |
| Sodium hydroxide | NaOH | Sigma |
| Optimal cutting temperature embedding medium | OCT | Fisher |
| Paraformaldehyde | PFA | Sigma |
| PCR buffer (10 x) | - | Invitrogen |
| Peroxidase suppressor | - | Fisher |
| Phosphate buffered saline | PBS | Sigma |
| Pico Fluor 40 scintillant | - | PerkinElmer |
| Polyvinylidene fluoride membrane | PVDF membrane | Millipore |
| Polyvinylpyrrolidone | PVP | Sigma |
| Potassium methyl sulphate | KMeSO ₄ | Fisher |
| Proteinase K from <i>Tritirachium album</i> | - | Sigma |
| Ready gels | - | Bio-Rad |
| Restore Western blot stripping buffer | - | Fisher |
| Sodium azide | - | Sigma |
| Sodium dodecyl sulphate | SDS | Sigma |
| SuperSignal west pico chemiluminescent substrate | - | Fisher |
| Taq DNA polymerase (recombinant) | - | Invitrogen |
| Toluidine blue | - | Sigma |
| Tris base, acetic acid and EDTA buffer | TAE | Sigma |
| Trisma base | Tris | Sigma |
| Tritium-labelled cGMP | [³ H]-cGMP | GE Healthcare |
| Triton X-100 | - | Sigma |
| Tween 20 | - | Sigma |
| Vectastain avidin biotin complex | ABC | Vector |

*Table 2.4 Special chemicals, reagents and enzymes used.***2.1.5 Key to suppliers**

| | |
|---------------------------------|--|
| Agar Sci. | Agar Scientific Ltd., Essex, UK. |
| Alomone | Alomone Labs Ltd., Jerusalem, Israel. |
| BioLine | BioLine Ltd., London, UK. |
| Bio-Rad | Bio-Rad Laboratories Ltd., Hertfordshire, UK. |
| Cayman | IDS Ltd. (Cayman Chemical), Tyne and Wear, UK. |
| Chemicon | Chemicon Europe Ltd., Hampshire, UK. |
| DIFCO | BD, Oxford, UK. |
| Dr Giti Garthwaite | Dr Giti Garthwaite, UCL, London, UK. |
| Enzo | Enzo Life Sciences Ltd., Exeter, UK. |
| Fisher | Fisher Scientific, Leicestershire, UK. |
| GE Healthcare | GE Healthcare, Bucks, UK. |
| Invitrogen | Invitrogen Ltd., Paisley, UK. |
| Latoxan | Latoxan Laboratories, Valence, France. |
| Merck | MSD, Hertfordshire, UK. |
| Millipore | Millipore (UK) Ltd., Watford, UK |
| New England BioLabs | New England BioLabs (UK) Ltd., Herts, UK. |
| PerkinElmer | PerkinElmer, Cambridge, UK. |
| Prof. Richard Silverman | Prof. Richard Silverman, Northwestern University, Chicago, USA. |
| Prof. Soenke Behrends | Prof. Soenke Behrends, Technische Universität Braunschweig, Braunschweig, Germany. |
| Promega | Promega Corporation UK, Southampton, UK. |
| Santa Cruz Biotechnology | Santa Cruz Biotechnology, Inc., Heidelberg, Germany |
| Sigma | Sigma-Aldrich Company Ltd., Dorset, UK. |
| Takara | Takara Bio. Inc., Shiga, Japan. |
| Tocris | Tocris Cookson Ltd., Bristol, UK. |
| Vector | Vector Labs Ltd., Peterborough, UK. |
| VWR | VWR International Ltd., Leicestershire, UK. |

Table 2.5 Suppliers of materials

2.1.6 NO donors

In various experiments, the NO donor, PAPA/NONOate, was used. The NONOates offer several advantages over other commercially available NO donors such as nitroprussides, since they release the authentic NO radical at predictable rates when $\text{pH} < 8$ (Keefer *et al.*, 1996). **Figure 2.1** shows a generalised NONOate structure.

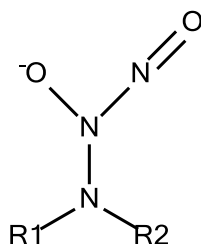


Figure 2.1 General NONOate structure. $R1$ and $R2$ = alkyl groups.

Table 2.6 details the structure and properties of PAPA/NONOate in comparison with DEA/NONOate.

| NONOate | Structure | $\sim E_{\text{NO}}$ | $\sim t_{1/2}$ (pH 7.4) |
|--------------|-----------|----------------------|-------------------------------|
| DEA/NONOate | | 1.5 | 16 at 22-25 °C 2 at 37 °C |
| PAPA/NONOate | | 1.5 | 77 at 22-25 °C 15 at 37 °C |

Table 2.6 Structure and properties of PAPA/NONOate. E_{NO} = efficiency of NO release (mol NO/ mol NO donor); $t_{1/2}$ (pH7.4) = half-life at pH 7.4 (min). Structures and values from Enzo (see **2.5 Key to Suppliers**). Details for DEA/NONOate are included for comparison.

PAPA/NONOate was used since it was predicted to release NO over a time course well-suited to the experiments, causing rapid (~ 2 min) accumulation of NO in oxygenated buffer to a concentration that would remain ~ stable for several minutes under the prevailing conditions (pH 7.4, 30 ± 1 °C; **Figure 2.2**).

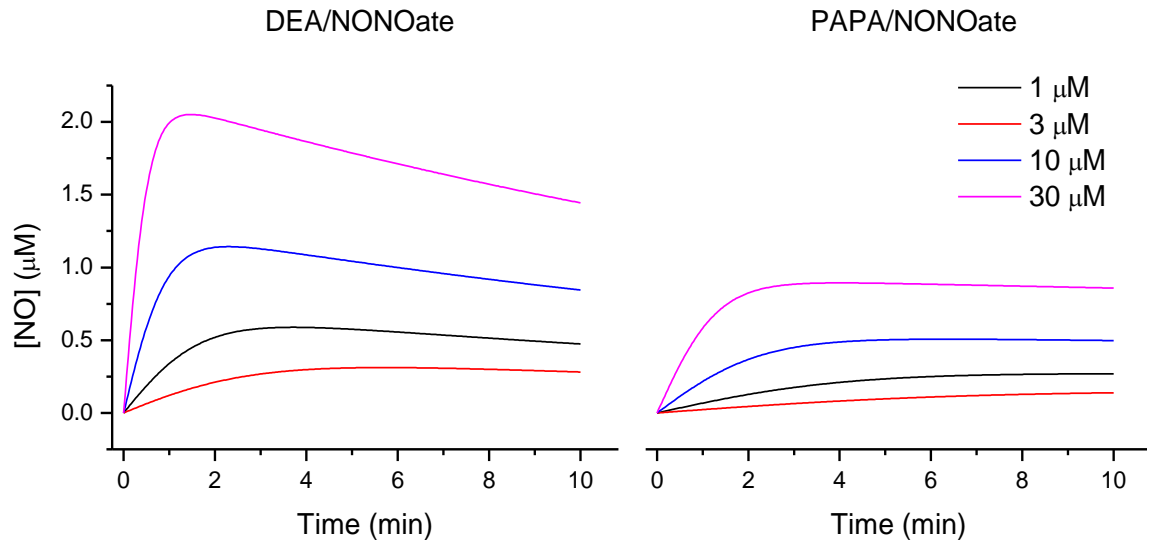


Figure 2.2 Predicted profile of NO release from two NONOates at 30 °C, pH 7.4. $t_{1/2} = 8$ min for DEA/NONOate; 45 min for PAPA/NONOate. PAPA/NONOate is predicted to release NO slower than DEA/NONOate, resulting in a smaller accumulation of NO that remains roughly stable over 10 min.

See below for details on how to calculate the release profile.

To prevent decomposition prior to application *in vitro*, PAPA/NONOate was prepared freshly on the day of each experiment as a 10 mM stock in 10 mM NaOH (pH > 12) and kept on ice until immediately before use. It should be noted that during the application of PAPA/NONOate to tissues, there will undoubtedly be uncontrolled losses of NO that have not been accounted for in calculating the above profile of NO release. These losses will occur due to evaporation from *in vitro* solutions and through diffusion out of tubing used in tissue perfusion systems (unpublished observations made in the laboratory). Precise estimates of the concentration of NO in a bath that will permeate a tissue are also not possible, partly because the proportion of PAPA/NONOate that will release NO within a tissue, as opposed to in the bathing solution, is unknown.

Calculating NO release from a NONOate at a given time

The NO release profiles shown in **Figure 2.2** were calculated using a $\sim t^{1/2}$ at 30 °C of 8 and 45 min for DEA/NONOate and PAPA/NONOate respectively and an accepted model of NO release from a NONOate (Schmidt *et al.*, 1997). The model assumes that in oxygenated solution at pH 7.4: 1) NONOates decay exponentially; 2) the primary route of removal of the resulting NO is via autoxidation. Therefore, the concentration of NO released by a NONOate (C_{NO}) at a given time (t) in oxygenated solution at pH 7.4 can be calculated as the difference in the rate of NONOate decay and the autoxidation of NO:

$$\frac{d}{dt} c_{NO}(t) = k_1 c_D(t) e_{NO} - k_2 O_2 c_{NO}(t)^2$$

where initial conditions are:

$$c_D(0) = c_0 \text{ and } c_{NO}(0) = 0$$

and:

$$\frac{dc_D(t)}{dt} = -k_1 c_D(t)$$

and:

t = time (s)

$c_{NO}(t)$ = concentration of NO at time t (M)

$c_D(t)$ = concentration of donor at time t (M)

c_0 = initial concentration of donor (M)

e_{NO} = mol of NO per mol donor

O_2 = concentration of oxygen (M); estimated at 1 mM in carbogenated aCSF

k_1 = rate constant for donor decomposition (s^{-1})

k_2 = rate constant for NO oxidation ($M^{-2}s^{-1}$); estimated at 13.6×10^6

2.1.1 General solutions

aCSF was composed of (in mM) 120 NaCl, 2.5 KCl, 1.3 MgCl₂, 1 NaH₂PO₄, 26 NaHCO₃, 10 D-glucose, 2 CaCl₂, equilibrated with 95% O₂/5% CO₂ to pH 7.4 at 30 °C.

Inactivation buffer comprised (in mM) 50 tris-HCl, 4 EDTA adjusted to pH 7.4.

2.2 General methods

2.2.1 Animals

All experiments were performed in accordance with British Home Office regulations on laboratory animal use and welfare. With the exception of those that employed transgenic mice, experiments were conducted using 6-8 week-old, male C57Bl/6 mice or 8-9 day-old, male Sprague Dawley rats (Charles River, Kent, UK).

2.2.2 Preparation of transverse hippocampal slices

Mice were euthanised by cervical dislocation and decapitated. The brains were removed and the hippocampi were swiftly dissected out into ice-cold aCSF and mounted on an agar (4 % in 1 % saline) block. Transverse slices (400 μm thick) were cut from the middle of the hippocampi (as shown in **Figure 2.3**) using a vibratome (Series 100 Sectioning System, Technical Products International Inc., St Louis, MO, USA). As a precaution against NMDA receptor-dependent, glutamate excitotoxicity, buffer in which the hippocampi were sliced contained 6 mM MgCl_2 . After slicing, tissues were placed on a nylon net submerged in aCSF constantly bubbled with oxygenated aCSF and were allowed to recover at room temperature for at least 1 hr.

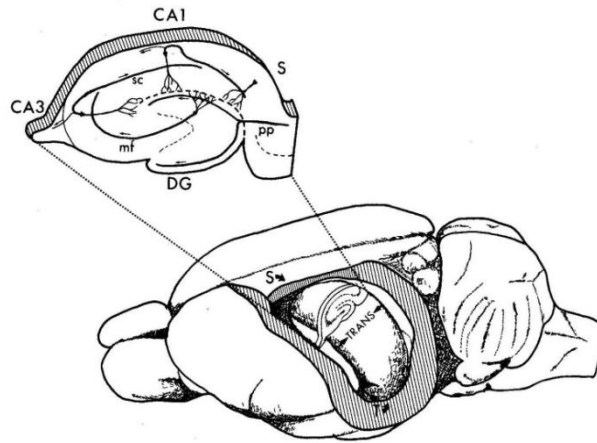


Figure 2.3 The location of the hippocampus within the rodent brain and the orientation of transverse slices. CA- = corpus ammonis -; DG = dentate gyrus; mf = mossy fibre; pp = perforant path; s (slice) = subiculum; s (brain) = septal nuclei; sc = Schaffer collateral; t = temporal cortex; TRANS = transverse plane. Adapted from Amaral and Witter (1989). Reproduced by kind permission of Elsevier.

2.2.3 Extracellular electrophysiological recordings at hippocampal CA3-CA1 synapses

After recovery, slices were transferred to a submerged recording chamber under a dissecting microscope (Carl Zeiss Ltd., Hertfordshire, UK) and superfused with oxygenated aCSF at a rate of 1-1.5 ml/min at 30 ± 1 °C. Field EPSPs were recorded from the stratum radiatum of CA1 following stimulation of the Schaffer-collateral/commissural pathway at 0.033 Hz (**Figure 2.4A**). Recording electrodes were pulled from borosilicate glass capillaries and filled with aCSF (1-3 M Ω resistance). A concentric bipolar stimulating electrode was used (SNEX: 100x, David Kopf Instruments supplied by Bilaney Consultants Ltd., Kent, UK). Field EPSPs were amplified using an Axoclamp-2B (Axon Instruments supplied by Molecular Devices, Sunnyvale, CA, USA), filtered at 1 kHz, and sampled using Clampex 10.2 (Molecular Devices).

Synaptic efficacy was quantified using the initial slope (20-50 % of the peak amplitude) of the fEPSP. The initial slope is a reliable indicator of synaptic efficacy and is less vulnerable to contamination by population spikes than the peak amplitude (**Figure 2.4B-C**). Once the initial slope had stabilised, input-output curves were

measured. The stimulus intensity was then set to 40-50 % of that necessary to produce a population spike. After slices acclimatised to the conditions of the recording chamber, a baseline of responses was recorded for at least 30 min prior to the beginning of the experiment. In a minority of cases, responses recorded over this time were unstable. The fEPSP initial slope either steadily decreased from the start of the recording or was consistently too variable from the average ($\pm > 20\%$). These slices were rejected.

LTP was induced using a 1-s, 100-Hz tetanus (i.e. 100 pulses; high frequency stimulation; HFS) or a 200-ms, 200-Hz train (i.e. 40 pulses) delivered 10 times at 5-s intervals at a stimulus intensity that evoked a 0.5-1 mV population spike in the stratum pyramidale adjacent to the recording electrode (high frequency burst stimulation). Drugs were delivered through the perfusion system and took ~ 20 s to reach the recording chamber, as determined in a separate experiment using a coloured indicator. Experiments were interleaved or run simultaneously with controls.

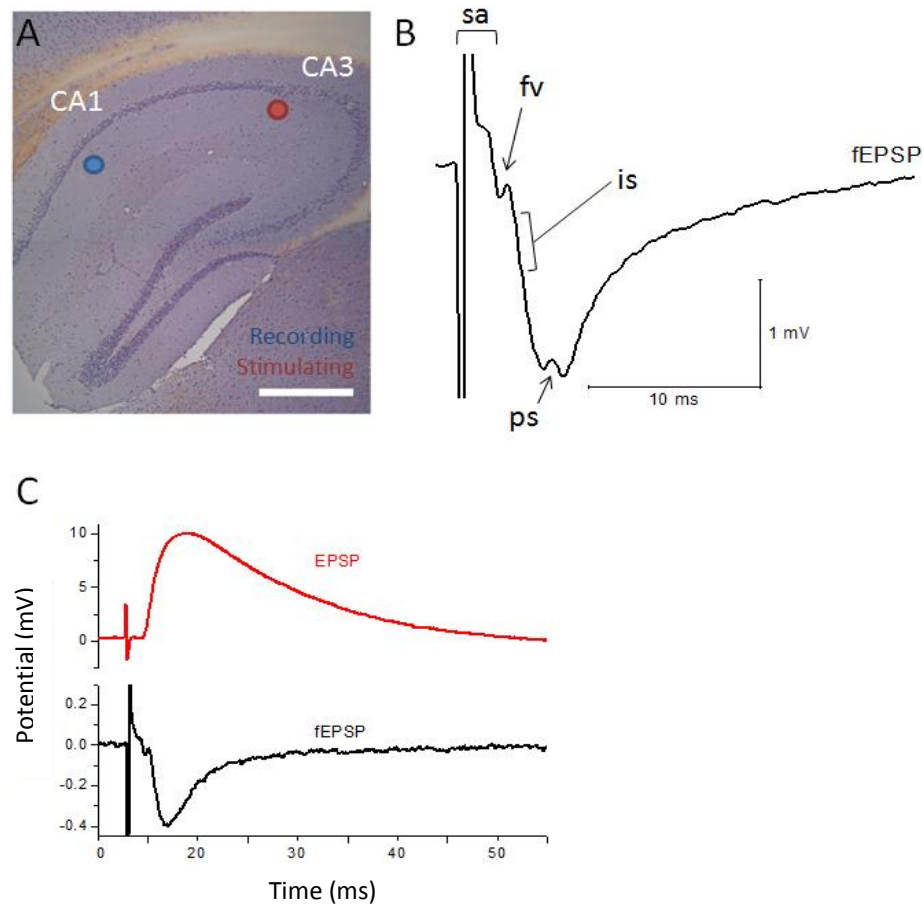


Figure 2.4 Stimulating and recording from Schaffer collateral-CA1 synapses in transverse hippocampal slices. **A)** The target sites of the stimulating (red) and recording (blue) electrode during a typical experiment are illustrated using an image of a 10 μm -thick transverse section of the hippocampus stained with Mayer's hemalum (methods for sectioning and staining tissue are detailed in **Chapter 7**). Scale = 500 μm . **B)** A representative fEPSP recorded at high stimulus amplitude to show a population spike (ps). fv = fibre volley; is = initial slope; sa = stimulus artefact (truncated). **C)** Comparison of a fEPSP (black) recorded in the stratum radiatum with an EPSP (red) simultaneously recorded in a pyramidal neuron (identified by its electrophysiology) in an adjacent section of the stratum pyramidale using a sharp electrode filled with KMeSO_4 (120 $M\Omega$). Note the relationship between the fEPSP and EPSP initial slopes. Responses are an average of 10 consecutive traces. Methods for intracellular recording are detailed in **Appendix 1**.

2.2.4 Protein measurement

Intact tissues were individually sonicated in inactivation buffer. The protein content of the resulting homogenates, or of lysates prepared for Western blot analysis, was measured using the bicinchoninic acid (BCA) method and a series of bovine serum albumin (BSA) standards (0-100 $\mu\text{g/ml}$ inactivation buffer). 10 μl of each sample or BSA standard were dispensed in triplicate into a 96-well plate. 200 μl BCA reagent was added to each well and the plates were incubated for 30 min at 37 $^{\circ}\text{C}$ to allow for the assay reaction to occur. The assay reaction comprises two steps: 1) Cu^{2+} is reduced to Cu^{+} by protein in the sample/standard; 2) Cu^{+} chelates the BCA to form a purple, water soluble complex that exhibits a strong absorbance at 562 nm. After this, the plates were allowed to cool to room temperature and absorbance was measured at 562 nm using a Spectra Max 250 spectrometer (Molecular Devices, California, USA). As shown in **Figure 2.5**, the magnitude of the absorbance was dependent on the concentration of the starting protein and, over the concentration range of the BSA standards, was linear. From this, the protein content of each sample was quantified.

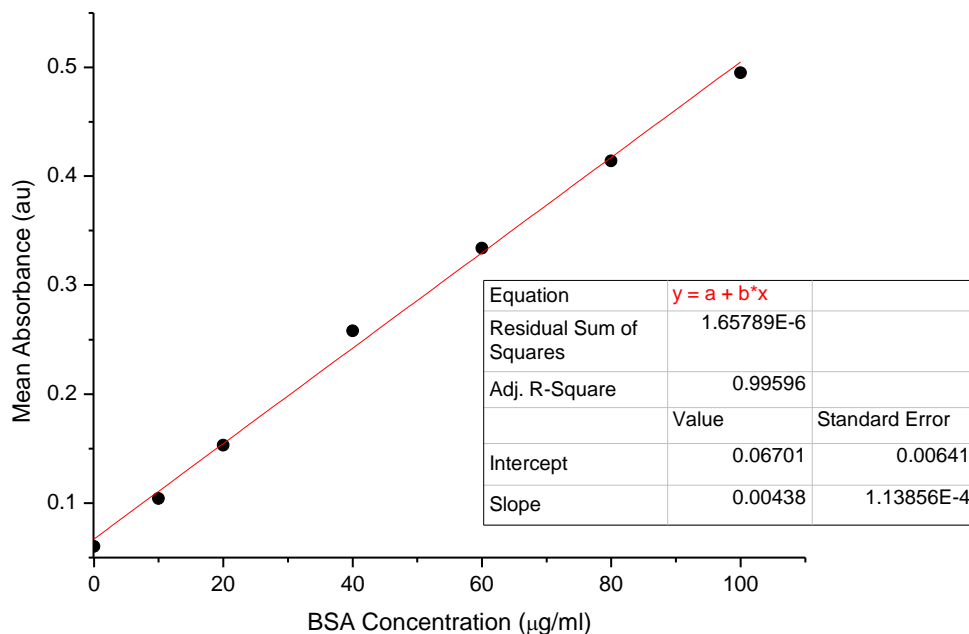


Figure 2.5 An example of absorbance at 562 nm by a series of BSA standards (0-100 $\mu\text{g/ml}$ inactivation buffer) following the BCA protein assay. Data are means of triplicate measurements \pm SE. The inset shows the linear function used to fit the data, where a = intercept, b = slope. The

goodness of fit was verified by the residual sum of squares and the adjusted R^2 statistic showed that the fit could be used to quantify the unknown protein content of the samples.

2.2.5 Measurement of endogenous cGMP

Following protein measurement (see 2.2.4), the remainder of each sample was centrifuged at 12500 rpm for 1 min at room temperature. The resulting pellet was discarded and the cGMP in the supernatant was measured using radioimmunoassay (performed by Kathryn Harris) and a series of standards containing a known concentration of cGMP.

Radioimmunoassay (first described by Wood and Marks (1978)) is highly sensitive and selective for cGMP over other nucleotides, such as cAMP (observations in the laboratory). Briefly, 100 μ l of each sample supernatant or standard comprising 0-10 μ M cGMP sodium salt in inactivation buffer were added to 50 μ l inactivation buffer containing [3 H]-cGMP (8×10^{-4} μ Ci) and 50 μ l of a solution of cGMP antibody and left on ice to allow the cGMP species to compete for binding to the antibody. After 2-18 hr, 1 ml of an ice-cold, 60 % saturated solution of ammonium sulphate (2.95 M in double-distilled H₂O) was then added in order to precipitate the antibody-cGMP complex. After 5 min, the solution was centrifuged (12500 rpm; 5 min; 4 °C) to pellet the complex and the supernatant containing unbound cGMP was discarded. 1 ml double-distilled H₂O was added and the pellet was left for 30 min to dissolve. Subsequently, 0.95 ml of the resulting suspension was added to 5 ml Pico Fluor 40 scintillant. After mixing well, the radioactivity of the solution was measured in disintegrations per min (dpm; the number of atoms in a quantity of radioactivity that decay per min) for 5 min using a scintillation counter (LS6500 model, Beckman Coulter Ltd., High Wycombe, UK).

A lower radioactivity count is indicative of a higher concentration of cGMP in the sample, since it has displaced more [3 H]-cGMP from binding to the cGMP antibody. **Figure 2.6** shows an example standard curve obtained after radioimmunoassay from which the endogenous cGMP in each experimental sample was determined.

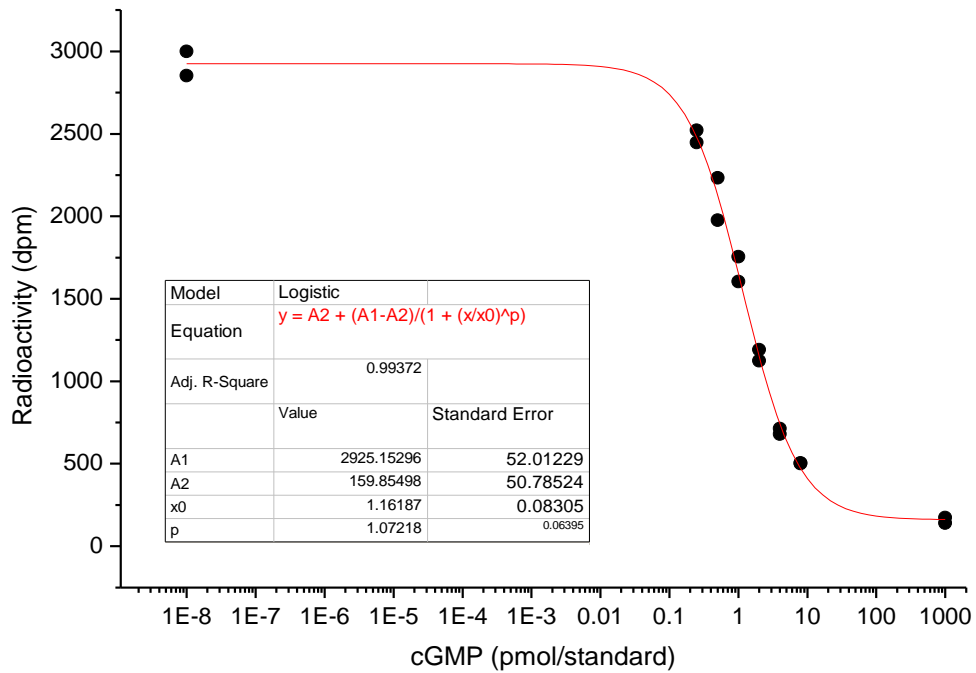


Figure 2.6 An example standard curve obtained by radioimmunoassay. The inset shows the equation used to fit the data where $y = \text{dpm}$, $A1$ and $A2 = \text{minimum and maximum dpm}$, $p = \text{slope}$, $x = \text{pmol cGMP/standard}$, $x_0 = \text{pmol cGMP at which half the displacement has occurred}$. Note that the first data point on the abscissa is actually zero. The adjusted R^2 statistic showed that the fit was good and could be used to quantify the endogenous cGMP in each experimental sample processed at the same time.

2.2.6 Genotyping by PCR and agarose gel electrophoresis

DNA extraction

Approximately 5 mm of tail or 0.2 mm² ear were removed from each mouse and added to 100 μl of tail lysis buffer which contained 10 mM tris (pH 8), 100 mM NaCl, 10 mM EDTA (pH 8), 1 mM Ca²⁺ acetate (pH 7.5) and 100 $\mu\text{g/ml}$ proteinase K (~ 0.5-1.3 units) prepared in 50 % glycerol, 0.5 % SDS. This was then warmed to 55 °C to provide optimal conditions for enzymatic digestion. After at least 24 hr the lysates were vortexed to destroy any hard tissue and then diluted 1/10 with double-distilled H₂O.

PCR

DNA from each lysate was amplified for electrophoresis using hot-start PCR. Unless otherwise stated, 25 µl reactions were set up in 200 µl PCR tubes which contained: 0.2 µM primers, 200 µM deoxyribonucleotides, 0.5 U recombinant *Taq* DNA polymerase (Invitrogen, Paisley, UK) and 1 µl of genomic DNA lysate (obtained as above) in 1 x PCR buffer (Invitrogen).

PCR reactions were carried out in a MWG-Biotech Primus 96 plus (Ebersberg, Germany). Samples were denatured at 93 °C for 2 min. 35 PCR cycles were then performed, each composed of: 30 s at 93 °C, during which samples are denatured, 30 s at 58 °C, in which primers anneal to the sample, and 30 s at 72 °C for DNA extension. Samples were then left at 72 °C for 10 min to allow for the completion of DNA extension. Each PCR included a negative control, in which the DNA sample was replaced with double-distilled H₂O, and a positive control including DNA of a known genotype. PCR products were stored at 4 °C until further use.

Agarose gel electrophoresis

After PCR, the products were mixed with 5 µl loading buffer containing ficol and dyed with bromophenol. Unless otherwise stated, 5 µl of each product were then electrophoresed in 2 % agarose gel in a tank containing 1 x TAE and 5 µg/ml ethidium bromide for a minimum of 45 min at 80 V. DNA bands were visualised under UV light using a Chemi-imager 4400 v 5.1 (Alpha Innotech, California, USA).

2.2.7 Statistics and data analysis

Statistics were performed using GraphPad InStat 3 software (GraphPad Software Inc., California, USA). The significance level was 0.05. Where necessary, data were fit with a logistic or exponential decay model using Origin Pro 8.1 (OriginLab Corporation, Massachusetts, USA). The equations used are given below.

$$y = \frac{A_1 - A_2}{1 + \left(\frac{x}{x_0}\right)^p} + A_2 \quad \text{Logistic equation}$$

where:

A_1 = initial predicted value of y

A_2 = final predicted value of y

x_0 = value of x at which y is half-maximal

p = slope

$$y = y_0 + Ae^{-x/t} \quad \text{Exponential equation}$$

where:

y_0 = the offset of y

A = initial predicted value of y

e = exponential constant, ~ 2.718281828

t = decay constant or τ

Chapter 3:

NO-induced, long-lasting potentiation at hippocampal CA1 synapses

3.1 Introduction

LTP is a long-lasting (> 1 hr), activity-dependent increase in the efficacy of a synapse, typically with Hebbian characteristics and therefore, intensely studied as a correlate of information processing and storage in the nervous system (see **Chapter 1**). Since Bliss and Lomo (1973) reported a persistent (up to 10 hr) enhancement in synaptic activity following brief tetanic stimulation of hippocampal perforant path-granule cell synapses in anaesthetised rabbits, LTP has been studied throughout the mammalian nervous system, and in several species, including humans (Cooke and Bliss, 2006).

The archetype of LTP occurs at Schaffer-collateral/commissural-CA1 synapses in the hippocampus. Often, this is induced using high frequency stimulation (HFS; 1-s, 100-Hz tetanus), although it has been generated by multitude other electrical and chemical stimuli *in vitro* and *in vivo* (Bliss *et al.*, 2007), and by learning in rodents (Whitlock *et al.*, 2006). Its induction is dependent upon postsynaptic Ca^{2+} influx (Lynch *et al.*, 1983; Malenka *et al.*, 1988) and, typically, NMDA receptor activation (Collingridge *et al.*, 1983a; Collingridge *et al.*, 1983b; Malenka, 1991), thereby explaining why LTP is associative and input specific. Its expression is thought to rely upon multiple, pre- and postsynaptic mechanisms (Malenka and Bear, 2004; Bliss *et al.*, 2007). However, the details of these expression mechanisms and the conditions under which they are recruited are, to varying extents, unclear. In particular, the retrograde messenger presumably required to reconcile the postsynaptic induction with presynaptic expression of NMDA receptor-dependent CA1 LTP, is, despite intense and long-lasting interest, yet to be conclusively identified.

Amongst several candidate retrograde messengers, such as CO and arachidonic acid (reviewed by Tao and Poo, 2001), NO has, arguably, received the most attention since there appears to be a particularly good match between the properties of NO signals necessary for LTP and the requirements of a retrograde messenger (see **Table 3.1** and **Chapter 1** for general discussion of the role of NO in LTP).

| Requirements of a retrograde transmitter active in LTP | Evidence consistent with retrograde NO transmission in NMDA receptor-dependent CA1 LTP |
|--|--|
| The machinery for synthesis/release of the transmitter is located postsynaptically | Immunohistochemistry with electron microscopy on hippocampal sections has shown that nNOS is expressed post- (and pre-) synaptically (Burette <i>et al.</i> , 2002; Szabadits <i>et al.</i> , 2007). |
| LTP-inducing stimuli elicit synthesis of the transmitter | NMDA has been found to induce NO synthesis in hippocampal slices (see Chapter 5) and <i>in vivo</i> (Luo and Vincent, 1994). Tetanic stimulation (three, 1-s, 100-Hz trains) sufficient for LTP has been shown to elicit NO synthesis in slices (Chetkovich <i>et al.</i> , 1993). |
| Postsynaptic injection of inhibitors that block the synthesis of the transmitter inhibit LTP | <p>In dissociated hippocampal neurons: post- but not presynaptic injections of the NOS inhibitor, L-NMMA, found to block tetanus (three 50-Hz, 2-s trains at 20 s intervals, Mg²⁺-free solution)-evoked LTP (Arancio <i>et al.</i>, 1996).</p> <p>In slices: postsynaptic L-NMMA and L-NNA shown to block pairing-induced LTP (Schuman and Madison, 1991; O'Dell <i>et al.</i>, 1991).</p> |
| Extracellular scavengers of the transmitter inhibit presynaptic LTP | <p>In dissociated hippocampal neurons: oxymyoglobin, an extracellular NO scavenger, blocked potentiation evoked by a weak tetanus paired with photolysis of caged NO in the postsynaptic neuron, but had no effect on potentiation when caged NO was presynaptic (Arancio <i>et al.</i>, 1996).</p> <p>In slices: haemoglobin blocked pairing-induced, NO-dependent LTP (Schuman and Madison, 1991; O'Dell <i>et al.</i>, 1991).</p> |
| The transmitter affects a presynaptic target | Immunohistochemistry with electron microscopy on hippocampal sections indicates that NO-targeted guanylyl cyclase is expressed pre- (and post-) synaptically (Burette <i>et al.</i> , 2002; Szabadits <i>et al.</i> , 2007). |
| Presynaptic injections of inhibitors of the presynaptic target inhibit LTP. | Not-tested. |
| The retrograde transmitter and its presynaptic target cause an increase in the probability of neurotransmitter release and/or number of active release sites | <p>In dissociated hippocampal neurons:</p> <ul style="list-style-type: none"> • exogenous NO (5-10 nM) or 8-Br-cGMP (50-100 μM) found to elicit a persistent increase in the frequency, independent of the amplitude, of miniature excitatory postsynaptic currents (O'Dell <i>et al.</i>, 1991; EPSCs; Arancio <i>et al.</i>, 1995). • activation of the NMDA receptor/NO/cGMP pathway shown to |

| | |
|--|---|
| | <p>enhance neurotransmitter vesicle recycling (Micheva <i>et al.</i>, 2001; Micheva <i>et al.</i>, 2003).</p> <ul style="list-style-type: none"> • LTP found to cause a rapid increase in presynaptic protein clusters via the NMDA receptor/NO/cGMP pathway (Ninan and Arancio, 2004; Wang <i>et al.</i>, 2005). <p>In slices:</p> <ul style="list-style-type: none"> • the NO donors, hydroxylamine and sodium nitroprusside, caused an increase in the efflux of noradrenaline and ACh from un-stimulated hippocampal slices (Lonart <i>et al.</i>, 1992). • theta burst stimulation-induced LTP in slices from mice lacking the AMPA receptor GluR1 subunit found to be presynaptic (as assessed using PPF) and abolished by NOS antagonism (Phillips <i>et al.</i>, 2008). • a decrease in PPF (consistent with an increase in neurotransmitter release) measured 2 min after HFS-induced LTP was observed in wild-type slices but not in slices from mice lacking the NO-targeted guanylyl cyclase $\alpha 1$ subunit (Taqatqeh <i>et al.</i>, 2009). • endogenous NO was necessary for the rapid 10-30 min NMDA receptor-dependent remodelling of presynaptic varicosities in area CA1 of hippocampal slice cultures following theta burst stimulation (Nikonenko <i>et al.</i>, 2003). |
| <p>Exogenous retrograde transmitter induces or facilitates presynaptic LTP</p> | <p>In dissociated hippocampal neurons:</p> <ul style="list-style-type: none"> • NO (< 60 s, 10 nM) paired with a weak tetanus (50-Hz, 0.5-s) during NMDA receptor blockade produced a persistent potentiation that was blocked by pre- but not postsynaptic injection of oxymyoglobin (Arancio <i>et al.</i>, 1996). • pre- but not postsynaptic cGMP or PKG I paired with a weak tetanus produced a similar potentiation (Arancio <i>et al.</i>, 1995; Arancio <i>et al.</i>, 2001). <p>In hippocampal slices: see discussion below.</p> |

Table 3.1 Evidence consistent with retrograde NO transmission during NMDA receptor-dependent LTP at CA1 synapses. The table summarises some of the main requirements of a retrograde transmitter responsible for facilitating neurotransmitter release during NMDA receptor-dependent LTP in area CA1, and some of the key NO research consistent with each requirement. The list of requirements has been adapted from Bliss *et al.* (2007).

Given the above, NO has become widely described as a retrograde messenger during LTP (for example, Feil and Kleppisch, 2008). However, three aspects of research on the role of NO in LTP should not be overlooked when considering putative retrograde NO transmission during synaptic plasticity. First, the results of some studies of the role of NO in LTP are discordant with retrograde NO transmission. Most notably, several groups have observed NO-independent LTP at CA1 synapses (for example, Cummings *et al.*, 1994; Bannerman *et al.*, 1994b; Phillips *et al.*, 2008, and see the discussion in **Chapter 5**).

Second, some of the evidence consistent with retrograde NO transmission is also consistent with a postsynaptic effect of NO in LTP. For example, the blockade of pairing-induced LTP by postsynaptic injection of NOS inhibitors reported by Schuman and Madison (1991) and O'Dell *et al.* (1991) could have resulted if NO acts as an intracellular transmitter. Evidence consistent with intracellular NO transmission shows that NOS and NO-targeted guanylyl cyclase co-localise in some CA1 dendrites (Burette *et al.*, 2002). The inhibition of the LTP described by Schuman and Madison (1991) and O'Dell *et al.* (1991) by extracellular NO scavengers is also consistent with intracellular NO signalling because an efficient extracellular scavenger will draw NO out of a cell by keeping the NO concentration gradient across the membrane steep (Garthwaite, 2008).

Third, most evidence in favour of a presynaptic effect of NO following long-lasting plasticity has been generated using pairs of dissociated hippocampal pyramidal neurons (as shown in **Table 3.1**). The use of dissociated hippocampal neurons offers several advantages over using intact tissues, such as transverse slices, in which presynaptic terminals are inaccessible. Some of the most compelling research has been performed by Arancio *et al.* who have reported that NO produced postsynaptically is, through presynaptic cGMP and PKG I, critical for NMDA receptor-dependent LTP (Arancio *et al.*, 1995; Arancio *et al.*, 1996; Arancio *et al.*, 2001). In accordance with these findings, NO/cGMP signalling at synapses between dissociated hippocampal neurons has been positively linked to neurotransmitter release (see **Table 3.1**). However, the relevance of these data to the role of NO in LTP at synapses in intact tissues is unclear. It has, for example, been speculated that

differences in the developmental stage of neurons maintained in slice preparations versus dissociated cultures may cause differences in LTP expression (Enoki *et al.*, 2009). Additionally, eNOS, which is expressed only in blood vessels (Stanarius *et al.*, 1997; Blackshaw *et al.*, 2003; Chan *et al.*, 2004) and, therefore, was unlikely to be present in the neuronal cultures used by Arancio *et al.*, has recently been positively linked to neurotransmitter release at CA1 synapses under conditions of basal stimulation (**Chapter 4** and Neitz *et al.*, 2011) and is required for some forms of CA1 LTP (Hopper and Garthwaite, 2006). Therefore, it is possible that the presynaptic effect of NO during LTP at synapses between dissociated neurons was favoured because: 1) the NO necessary for the potentiation had compensated for a lack of eNOS; 2) the probability of neurotransmitter release and/or number of active release sites present at synapses between the dissociated neurons was unnaturally low during baseline recording. Indeed, it has been reported that an increase in the probability of neurotransmitter release and/or number of active release sites at CA1 synapses following LTP is more likely if the initial probability and/or number are low (Schulz *et al.*, 1994).

In more intact tissues, some evidence consistent with a positive link between NO and neurotransmitter release during LTP at CA1 synapses has been reported. For example, if NO acts as a retrograde messenger to cause presynaptic changes following NMDA receptor-dependent LTP induction, one prediction is that exogenous NO should partially overcome the inhibitory effect of NMDA receptor blockade on potentiation and induce a presynaptic component of LTP (the last requirement in **Table 3.1**). Using hippocampal slices, three different groups have provided evidence consistent with part of this prediction (Zhuo *et al.*, 1993; Malen and Chapman, 1997; Bon and Garthwaite, 2003). They have shown that a sub-threshold induction protocol (for example, 0.1-s, 50-Hz), unable to produce LTP alone, could, when delivered in the presence of exogenous NO, produce a significant and long-lasting potentiation that was independent of NMDA-receptor activation. Zhuo *et al.* (1993) showed that this potentiation was pathway specific and, consistent with a subsequent study by Bon and Garthwaite (2003), that it was also activity-dependent, insensitive to NMDA receptor-antagonism and occluded tetanus-induced LTP. Later it was also reported that a potentiation with similar properties, which also

occluded subsequent LTP, could be induced at CA1 synapses by pairing of one of two cGMP analogues with a weak, sub-threshold tetanus (Zhuo *et al.*, 1994).

These data are consistent with a presynaptic effect of NO and are regarded as the major evidence in favour of NO as a retrograde messenger at CA1 synapses in intact tissues (for example, Hawkins *et al.*, 1994). They also concur with the data collected from dissociated cells by Arancio *et al.* (see above) and with more recent work on CA1 LTP in slices from transgenic mice (see penultimate row of **Table 3.1**). However, the data presented by Bon and Garthwaite (2003), Malen and Chapman (1997) and Zhuo *et al.* (1993) are also consistent with a postsynaptic NO-induced potentiation, and tests of this possibility are missing in the literature. Furthermore, the potentiations observed by Zhuo *et al.* (1993) and Bon and Garthwaite (2003) could only be induced when exogenous NO was paired with simultaneous synaptic activity. Indeed, there are no examples of potentiation by exogenous NO under physiological conditions in the absence of high frequency synaptic stimulation. This suggests that simultaneous synaptic activity is required for the NO-dependent component of LTP. Since the potentiations observed by Zhuo *et al.* (1993), Malen and Chapman (1997) and Bon and Garthwaite (2003) were induced using a sub-threshold induction protocol, a different complement of LTP mechanisms may have been activated from those recruited by the induction protocols typically used in studies of hippocampal LTP and perhaps by natural stimuli causing synaptic potentiation *in vivo*. Surprisingly, given the proposed role of NO in NMDA receptor-dependent LTP, tests of the prediction that exogenous NO, paired with a standard induction protocol, should restore the NO-dependent component of LTP when NMDA receptors are blocked have not been reported.

3.2 Aim

Initial characterisation of LTP at Schaffer-collateral/commissural-CA1 synapses in hippocampal slices under our conditions found it to be NMDA receptor- and NO-dependent (data shown below). Given the above, we therefore aimed to test the prediction that exogenous NO paired with a standard LTP induction protocol (a 1-s, 100-Hz tetanus or high frequency stimulation; HFS) during NMDA receptor

blockade would restore a persistent NO-dependent component of LTP. In this way we sought to isolate the long-lasting, NO-dependent component of LTP from other mechanisms of LTP expression and to test its locus (pre and/or postsynaptic) at synapses in functional neural pathways.

3.3 Methods

3.3.1 Animals

Experiments were conducted using 6-8 week-old male C57Bl/6 mice (Charles River, Margate, UK). Transgenic mice incapable of α CaMKII autophosphorylation (α CaMKII^{T286A}; Giese *et al.*, 1998) were obtained as heterozygotes in a 129sv/C57Bl/6 background and bred. Siblings were not mated with each other. In preparation for experiments, pups were genotyped, heterozygotes were euthanised and an appropriate number of male wild-type and homozygote mice were kept. On the day of each experiment, a second person selected either a homozygote or wild-type mouse for use. The experimenter was left blind to genotype until after all experiments and data analysis were completed. Mice were used at 6-9-weeks old.

3.3.2 Transverse hippocampal slice preparation and extracellular electrophysiology

Transverse hippocampal slices were prepared and extracellular electrophysiological recordings of activity at CA3-CA1 synapses were made as described in **Chapter 2.2.2-3**. LTP was induced using high-frequency stimulation (HFS; a 1-s, 100-Hz tetanus). PPF (reviewed by Zucker and Regehr, 2002; Bliss *et al.*, 2007) was induced at 0.033 Hz using pairs of stimuli separated by various intervals (called the inter-stimulus interval (ISI)), which ranged from 10 to 400 ms. The magnitude of PPF was measured using the mean paired-pulse ratio (PPR; calculated by the initial slope of the second fEPSP/the initial slope of the first fEPSP) of ~ 10 consecutive pairs of fEPSPs.

In experiments using the NO donor, PAPA/NONOate, the optimum concentration for use was determined by a concentration-response curve. Under the conditions prevailing in **Figures 3.6-9, 3.12 and 3.14-16**, the optimum PAPA/NONOate concentration was found to be 3 μM (data shown in **Figure 3.6**). Subsequent to these experiments, the effect on synaptic efficacy of 3 μM PAPA/NONOate was found to be diminished. This was most likely because the introduction of a drop chamber into the perfusion system, which was done in order to minimise electrical noise, enhanced NO loss from the aCSF prior to its entry into the recording chamber. To compensate for this, 10 μM , rather than 3 μM PAPA/NONOate was used in subsequent experiments (**Figures 3.10-11, 3.13 and 3.19**). With the altered perfusion system, 10 μM PAPA/NONOate produced a similar effect on synaptic plasticity as had previously been observed using 3 μM (see **Figure 3.13 and 3.19**).

3.3.3 Genotyping of $\alpha\text{CaMKII}^{\text{T286A}}$ mice

The $\alpha\text{CaMKII}^{\text{T286A}}$ mice (described in Giese *et al.*, 1998) were genotyped using PCR and gel electrophoresis, as described in **Chapter 2.2.6**. For PCR, primers flanking loxP sites present only in the transgenic DNA were used (Giese *et al.*, 1998; see **Table 3.2** for primer sequences).

| Primer | Sequence 5'-3' | Stock Concentration |
|--------|----------------------------|---------------------|
| loxP 1 | CTG TAC CAG CAG ATC AAA GC | 5 μM |
| loxP 2 | ATC ACT AGC ACC ATG TGG TC | 5 μM |

Table 3.2 LoxP primers used for PCR of $\alpha\text{CaMKII}^{\text{T286A}}$ mouse DNA.

Each PCR included a negative control, in which the DNA sample was replaced with double-distilled H_2O , and a positive control including DNA of a known genotype.

After PCR, the products were electrophoresed and DNA bands were visualised under UV light. In accordance with the inclusion of Lox P sites in transgenic DNA only (Giese *et al.*, 1998), distinct wild type and homozygous bands separated by ~ 80 base pairs (\sim the length of two loxP sites) were observed. Heterozygote lysates showed

both bands. Each gel included a DNA ladder (Hyperladder 1, Invitrogen; 1 μ l), positive and negative control (**Figure 3.1**).

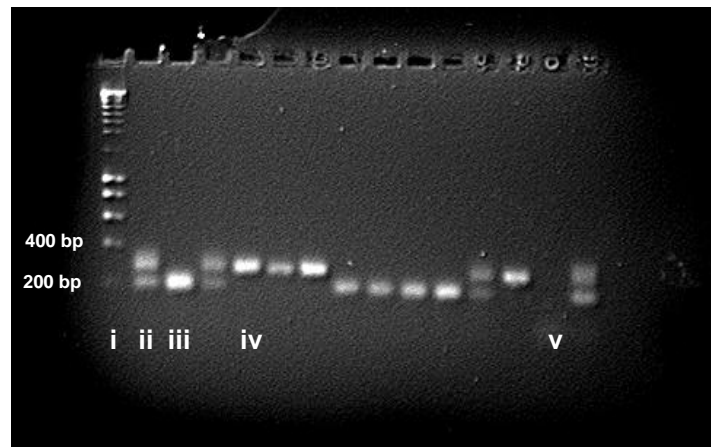


Figure 3.1 Genotyping wild-type and α CaMKII^{T286A} mice. PCR products were electrophoresed and visualised under UV light. The labelled columns show: (i) the DNA ladder (relevant bands are indicated); (ii) heterozygote bands; (iii) a wild-type band; (iv) a homozygote band ~ 80 base pairs (bp) longer; (v) a negative control containing no DNA.

3.3.4 Analysis and Statistics

In each figure, fEPSP slopes have been normalised to the first 10 min of baseline recording (in the absence of any drug). Unless otherwise stated, values of LTP quoted in the text are mean values \pm standard error of the mean (SEM) measured 55-60 min post HFS. In each figure, HFS was applied at the arrow and inset traces represent the mean fEPSP recorded at the time indicated by the numbered bars. For clarity, the stimulus artefacts of the representative fEPSPs have been truncated. Two-tailed *t*-tests and ANOVA with an appropriate multiple comparisons test were used to assess statistical significance between data sets.

3.4 Results

3.4.1 Initial characterisation of HFS-induced LTP

In accordance with several previous reports, HFS (1-s, 100-Hz tetanus) applied to Schaffer collateral/commissural fibres in area CA3 yielded a transient PTP followed by a stable LTP in area CA1 that lasted longer than 1 hr (**Figure 3.2A**). As is typical, LTP was accompanied by a leftward shift in input-output and stimulus-response curves (**Figure 3.2B-C**). Consistent with the LTP constituting a synaptic change, rather than a change in presynaptic excitability, there was no effect of LTP on the relationship between stimulus and fibre volley amplitude (see half-max. values, **Figure 3.2D**).

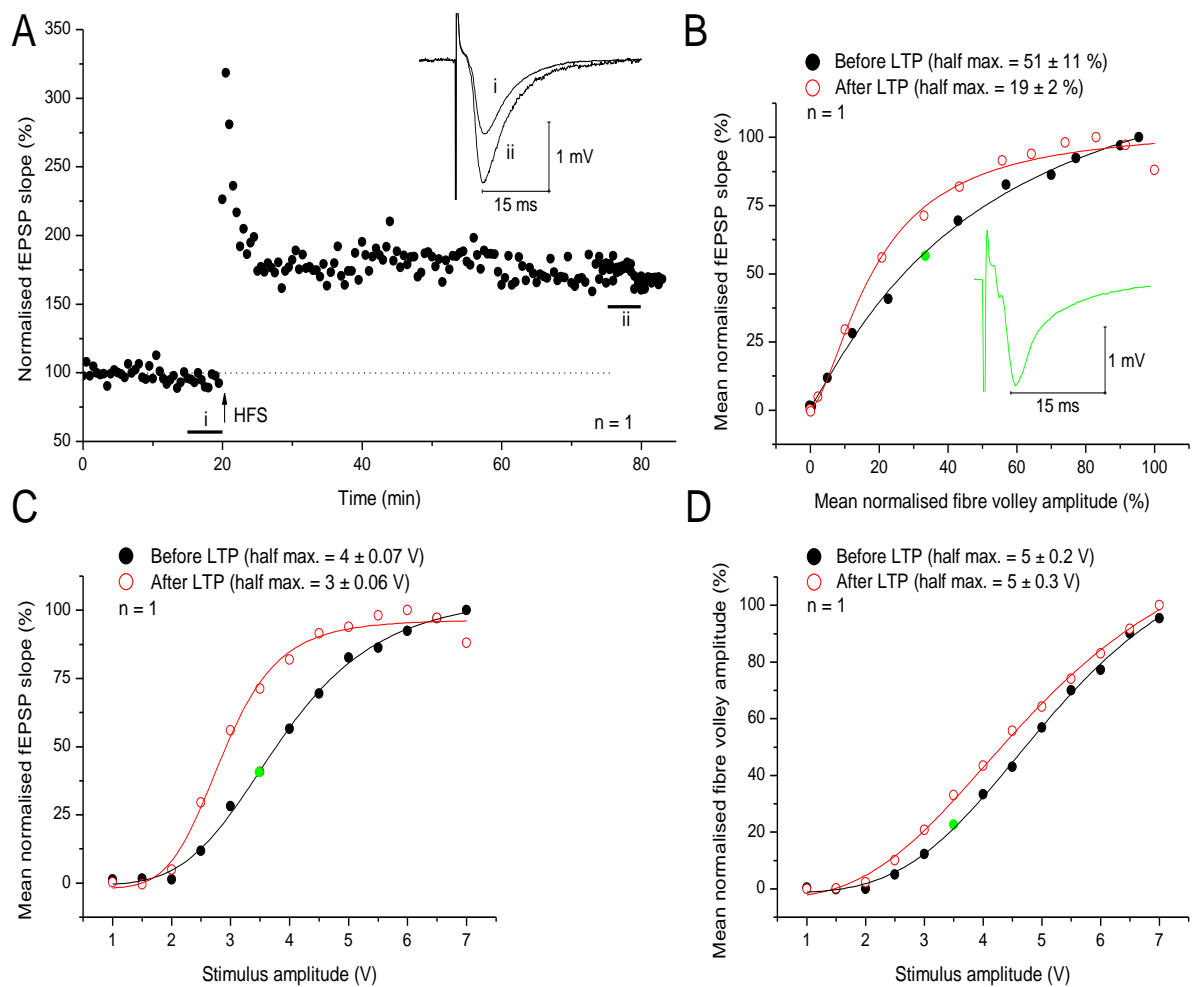


Figure 3.2 Characterisation of HFS-induced LTP. **A**) A typical example of LTP ($n = 1$ of > 20). **B-D**) LTP was accompanied by a leftward shift in the input-output (**B**) and stimulus-response curves (**C**) but

*there was no effect of LTP on the relationship between stimulus amplitude and mean normalised fibre volley amplitude (see half-max. values). Data were recorded 20 min prior to, and 60 min after HFS. Each point is a mean of 5-10 consecutive fEPSPs measured from one typical slice. In B-C, data has been normalised to the maximum mean value in each data set. In D, data have been normalised to the maximum value recorded after LTP. The half-max. values were determined using the logistic fits shown (adjusted $R^2 > 0.99$; see **Chapter 2** for logistic equation). The data coloured in green were measured from the mean fEPSP shown in B. The fibre volley amplitude was measured as the negative peak relative to the baseline.*

Under certain conditions, LTP at CA1 synapses can be NMDA receptor- (Grover and Teyler, 1990) and NO-independent (Cummings *et al.*, 1994; Phillips *et al.*, 2008). Therefore, we tested the involvement of NMDA receptors and NO in LTP under our conditions.

In agreement with the majority of previous findings at CA3-CA1 synapses (for example, Collingridge *et al.*, 1983a; Collingridge *et al.*, 1983b; Malenka, 1991), the NMDA antagonist, D-AP5 (50 μM , applied 10 min prior to and 5 min after HFS), reversibly blocked HFS-induced LTP: following HFS in the presence of D-AP5, the initial fEPSP was unchanged compared to the last 5 min of baseline recording, although a second HFS, delivered ~ 1 hr after washing the antagonist, yielded significant LTP (**Figure 3.3A**). There was no significant effect of D-AP5 on baseline transmission (**Figure 3.3A** and **Figure 3.3B**).

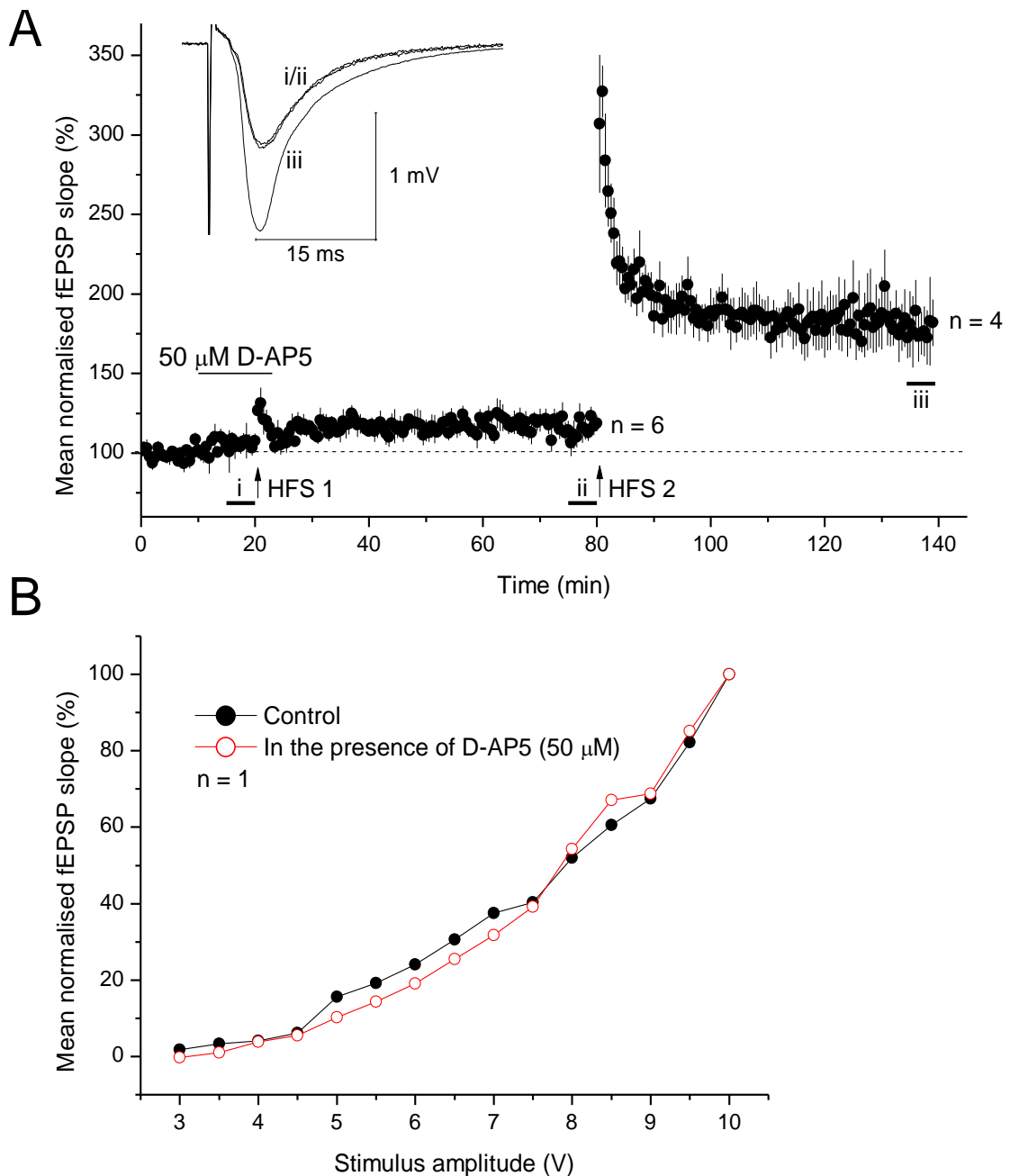


Figure 3.3 Requirement of LTP for NMDA receptor channel opening. **A**) Following the establishment of a stable baseline of responses, HFS was delivered in the presence of the competitive NMDA antagonist, D-AP5 (50 μ M). Compared to the last 5 min of baseline, this had no effect on synaptic efficacy (55-60 min post HFS in the presence of D-AP5: 115 ± 5 %; paired *t*-test, $p = 0.287$; 0.5-60 min post HFS in the presence of D-AP5: 117 ± 6 %; paired *t*-test, $p = 0.112$ compared to the last 5 min of baseline). However, HFS delivered after washing D-AP5 for ~ 1 hr yielded significant LTP (174 ± 15 %; $p = 0.0375$ compared to fEPSP slope measured 5 min prior to HFS). There was no effect of D-AP5 on baseline transmission (first vs. last 5 min of baseline, paired *t*-test, $p = 0.183$). **B**) Analysis of stimulus response curves measured prior to and 30 min after constant perfusion of D-AP5 (50 μ M) showed no effect of the antagonist on baseline transmission. Data are 5-10 consecutive

fEPSPs measured from one slice and are normalised to the maximum mean value recorded in each data set.

The involvement of endogenous NO in HFS-induced LTP was tested using the non-selective NOS antagonist, L-NNA (100 μ M, applied 30 min prior to, and at least 30 min after HFS). Consistent with previous reports (for example, Hopper and Garthwaite, 2006; Taqatqeh *et al.*, 2009), HFS in the presence of L-NNA resulted in a steadily declining potentiation. One hr after HFS, this potentiation was significantly smaller than the LTP generated in un-treated, interleaved controls, although the initial slope was significantly augmented from the baseline. There was no effect of L-NNA on baseline transmission (**Figure 3.4A** and **Figure 3.4B**).

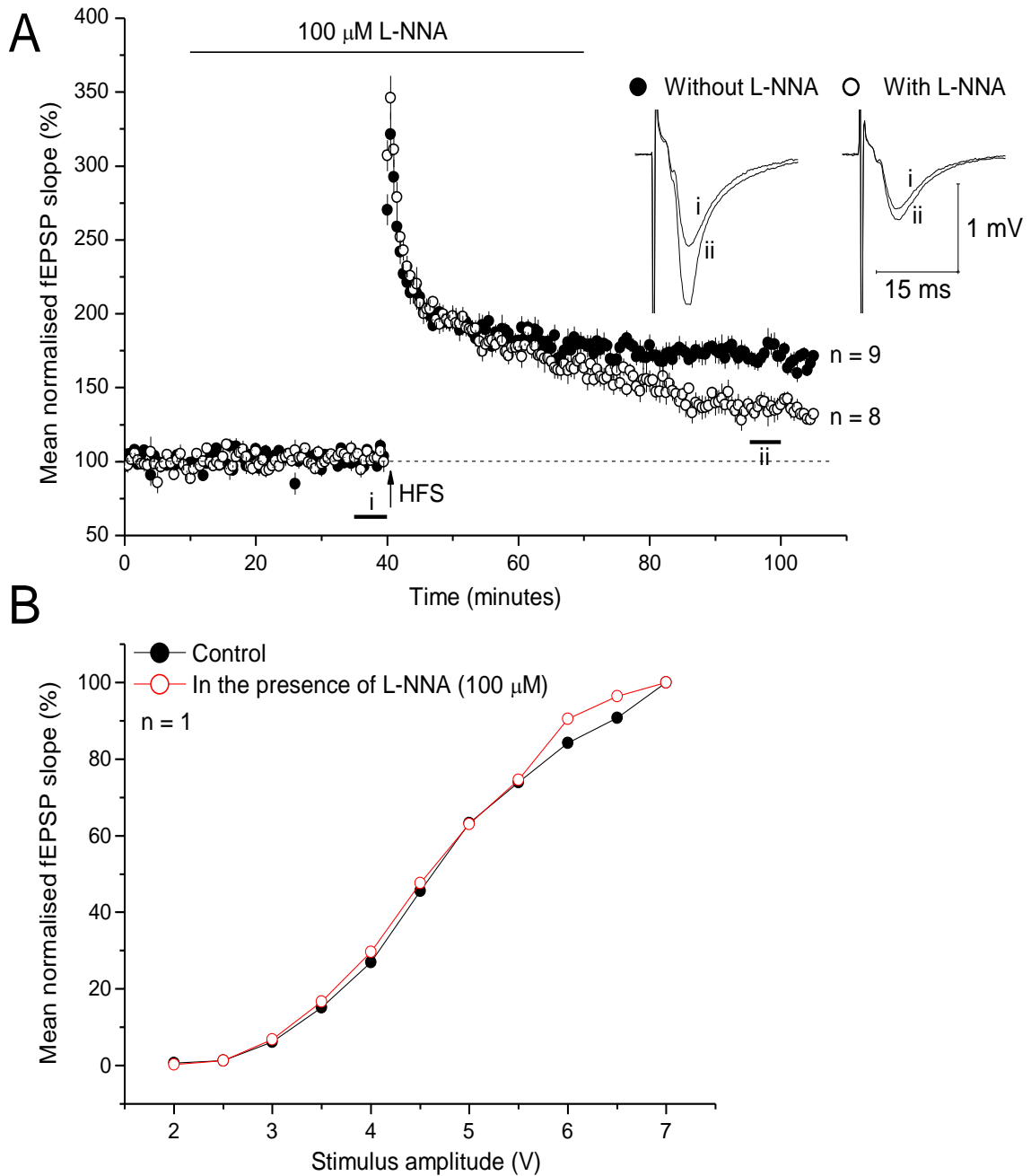


Figure 3.4 Involvement of NOS in LTP. **A**) HFS was delivered in the presence or absence of the non-selective NOS antagonist, L-NNA ($100 \mu\text{M}$). In the absence of L-NNA, a stable LTP was induced (black). In the presence of L-NNA, HFS elicited a slowly declining potentiation. 55-60 min post HFS, this potentiation was significantly smaller than the LTP elicited in interleaved, untreated controls ($137 \pm 9\%$ vs. $173 \pm 7\%$; unpaired *t*-test, $p = 0.0021$), although the initial slope was significantly different from baseline (paired *t*-test, $p = 0.0033$ compared to the last 5 min of baseline). There was no effect of L-NNA on baseline transmission (first vs. last 5 min of baseline, paired *t*-test, $p = 0.259$). **B**) Analysis of stimulus-response curves measured before and 30 min after constant perfusion of $100 \mu\text{M}$ L-NNA showed no effect of the inhibitor on baseline transmission. Data are means of 5-10 consecutive fEPSPs recorded in one slice and are normalised to the maximum mean value in each data set.

The effect of the NOS substrate, L-arginine, on LTP was also investigated. L-arginine is present in the cerebrospinal fluid of adult rats (50-80 μM ; Takasugi *et al.*, 2003) and humans (20 μM ; Martens-Lobenhoffer *et al.*, 2007). However, the amino acid is not normally added to solutions used *in vitro*, raising the possibility that the concentration of L-arginine might limit NO synthesis and therefore NO-mediated plasticity in hippocampal slices. Previously it has been reported that NMDA-induced cGMP accumulation is augmented in rat hippocampal and cerebellar slices pre-incubated with L-arginine (Garthwaite *et al.*, 1989; East and Garthwaite, 1991), but there are no reports of the effect of L-arginine on NO-dependent LTP *in vitro*.

To test the effect of L-arginine on our LTP, the amino acid (50 μM) was applied 30 min before HFS and remained present for the duration of the experiment. Compared to un-treated interleaved controls, there was no significant effect of L-arginine on the magnitude of LTP or on baseline transmission (**Figure 3.5**).

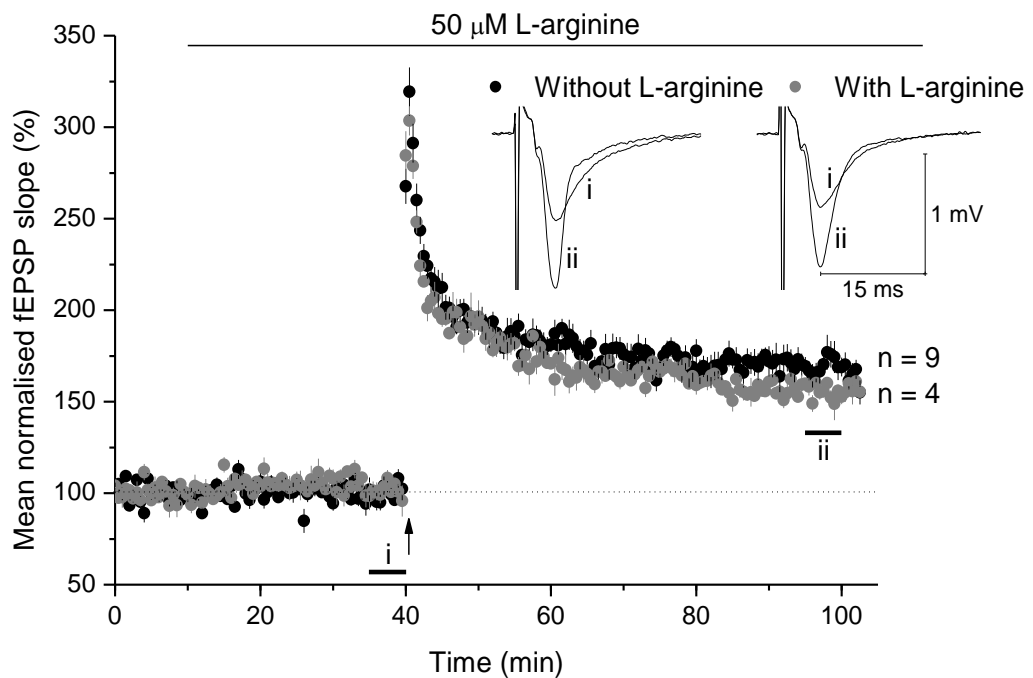


Figure 3.5 Dependency of LTP on extracellular L-arginine. L-arginine (50 μM) was applied 30 min prior to HFS and for the remainder of the experiment. Compared to the LTP induced in interleaved, untreated controls, the magnitude of LTP induced in slices perfused with L-arginine was not significantly altered (with L-arginine (grey): $155 \pm 4\%$; without L-arginine (black): $170 \pm 7\%$;

*unpaired t-test, $p = 0.109$). There was also no significant effect of L-arginine on baseline transmission (mean fEPSP slope over the first vs. last 5 min of baseline transmission = $101 \pm 0.7\%$ vs. $101 \pm 4\%$; paired t-test, $p = 0.871$). Note that control data is the same as that shown in **Figure 3.4** but has been shown again for ease of comparison.*

3.4.2 Effect of pairing exogenous NO with HFS during NMDA receptor blockade

Under our conditions, LTP was NMDA receptor- (**Figure 3.3**) and NO-dependent (**Figure 3.4**). Therefore the hypothesis that pairing exogenous NO with HFS during NMDA receptor blockade should restore the NO-dependent component of LTP was valid and could be tested.

For this purpose, the NO donor, PAPA/NONOate was used. As previously described (see **Chapter 2.1.6**), PAPA/NONOate releases NO in a predictable manner ($t_{1/2} = 15$ min at $37\text{ }^{\circ}\text{C}$ in oxygenated aCSF, pH 7.4; Keefer *et al.*, 1996). Since the concentration of NO generated at a synapse during LTP is unknown, the effects of different concentrations of PAPA/NONOate, co-applied with the D-AP5 during HFS, were investigated. Tests of each concentration were interleaved with each other and with control experiments in which: 1) HFS was delivered alone (as a positive control for LTP induction and expression); 2) HFS was delivered in the presence of D-AP5 only (to control for the NMDA receptor-dependency of LTP; data have been shown in **Figure 3.3** and are shown again for ease of comparison).

As above, HFS delivered alone yielded a significant LTP (data shown in grey in **Figure 3.6**). As shown previously (**Figure 3.3**), and again here for ease of comparison, LTP was blocked by the NMDA antagonist, D-AP5 (data shown in black in **Figure 3.6**). Consistent with our prediction, application of $3\text{ }\mu\text{M}$ PAPA/NONOate in the presence of $50\text{ }\mu\text{M}$ D-AP5 and HFS yielded a long-lasting potentiation (data shown in blue **Figure 3.6A**). This ‘NO-induced potentiation’ was slow to develop (half-maximal value = 18 ± 2 min; red line in **Figure 3.6A**) but reached a magnitude comparable to that observed in control slices that received HFS alone (compare blue and grey in **Figure 3.6A**).

The magnitude of the NO-induced potentiation was dependent on the concentration of PAPA/NONOate. Concentrations lower than 3 μM failed to give rise to a significant potentiation in fEPSP slope, as did concentrations above 3 μM (ANOVA with one factor Dunnett's test, $p < 0.05$ compared to the fEPSP slope measured after HFS in the presence of D-AP5 alone; **Figure 3.6B-G**).

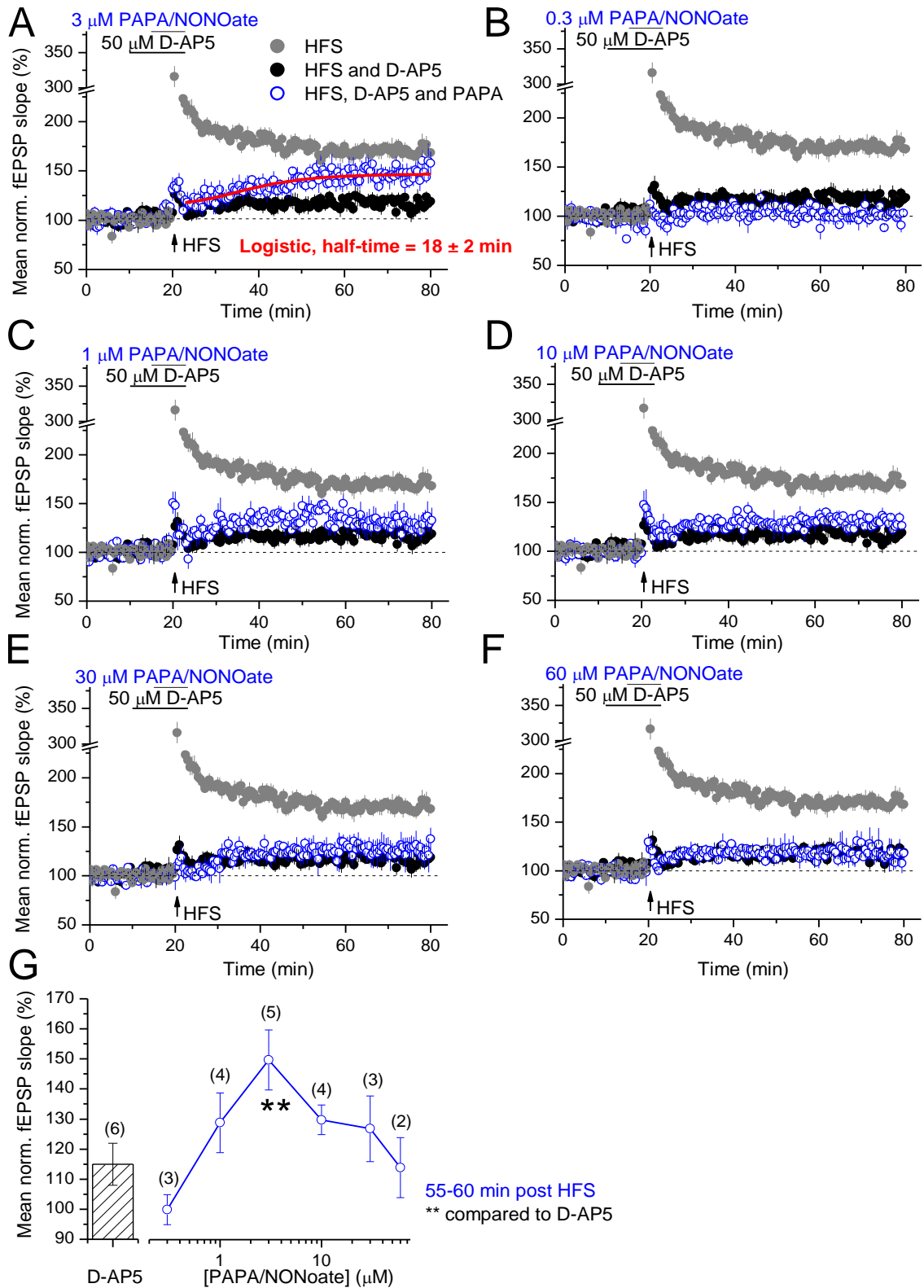


Figure 3.6 Effect of PAPA/NONOate application during HFS and NMDA receptor blockade on synaptic efficacy. **A)** HFS yielded a significant LTP (grey; $170 \pm 5\%$; paired t -test = 4.50×10^{-6} compared to the last 5 min of baseline; $n = 8$) that was blocked by the NMDA antagonist, D-AP5 (50

μM ; black; $115 \pm 5\%$; paired *t*-test, $p = 0.287$ compared to the last 5 min of baseline recording; $n = 6$; note that these data have been previously shown in **Figure 3.3**). Application of $3 \mu\text{M}$ PAPA/NONOate during HFS in the presence of D-AP5 led to a significant, long-lasting potentiation in fEPSP slope (blue; $150 \pm 8\%$; one factor ANOVA with Dunnett's test, $p < 0.01$ compared to the fEPSP slope measured following HFS in the presence of D-AP5 alone (black)). This was slowly-rising (red; half-maximal value = 18 ± 2 min as estimated using a logistic fit of the data 3 min after HFS; adjusted $R^2 = 0.664$; see **Chapter 2** for fit details) but reached a magnitude comparable to control HFS-induced LTP (grey; unpaired *t*-test; $p = 0.0545$). **B-F**) Pairing of HFS and D-AP5 with lower ($0.3\text{-}1 \mu\text{M}$; B-C) or higher ($10\text{-}30 \mu\text{M}$; D-F) concentrations of PAPA/NONOate had no significant effect on synaptic efficacy (one factor ANOVA with Dunnett's test, $p > 0.05$ compared to the fEPSP following HFS in the presence of D-AP5 alone). Black and grey data are the same as in panel A but have been shown repeatedly for ease of comparison. **G**) Summary showing the magnitude of NO-induced potentiation 55-60 min following HFS as a function of [PAPA/NONOate]. Numbers above points are *n* values; ** = one factor ANOVA with Dunnett's test, $p < 0.01$ compared to HFS in the presence of D-AP5 alone.

3.4.3 Characterisation of NO-induced potentiation

The NO-induced potentiation (generated using $3 \mu\text{M}$ PAPA/NONOate) was consistent with the possibility that exogenous NO had bypassed the requirement for NMDA receptor activity during LTP induction and prompted the expression of the NO-dependent component of HFS-induced LTP. To test this and begin to characterise the NO-induced potentiation, we investigated the relationship between the NO-induced potentiation and standard HFS-induced LTP.

Interaction between the NO-induced potentiation and HFS-induced LTP

It was hypothesised that, if the NO-induced potentiation relied upon the same mechanisms as the NO-dependent component of HFS-induced LTP, then these forms of plasticity would be non-additive. To test this postulate, a second HFS was delivered to slices at the end of the experiments shown in **Figure 3.6** (i.e. 1 hr after pre-treatment with D-AP5, PAPA/NONOate and HFS). After pre-treatment with $3 \mu\text{M}$ PAPA/NONOate, which generated significant NO-induced potentiation (see **Figure 3.6A** and **3.7A**), a second HFS (labelled HFS 2 in **Figure 3.7A**) generated significant LTP, of an apparently remarkably high magnitude ($255 \pm 11\%$; **Figure**

3.7A). The magnitude of the HFS-induced LTP appeared to be related to the magnitude of the preceding NO-induced potentiation (**Figure 3.7B-D**).

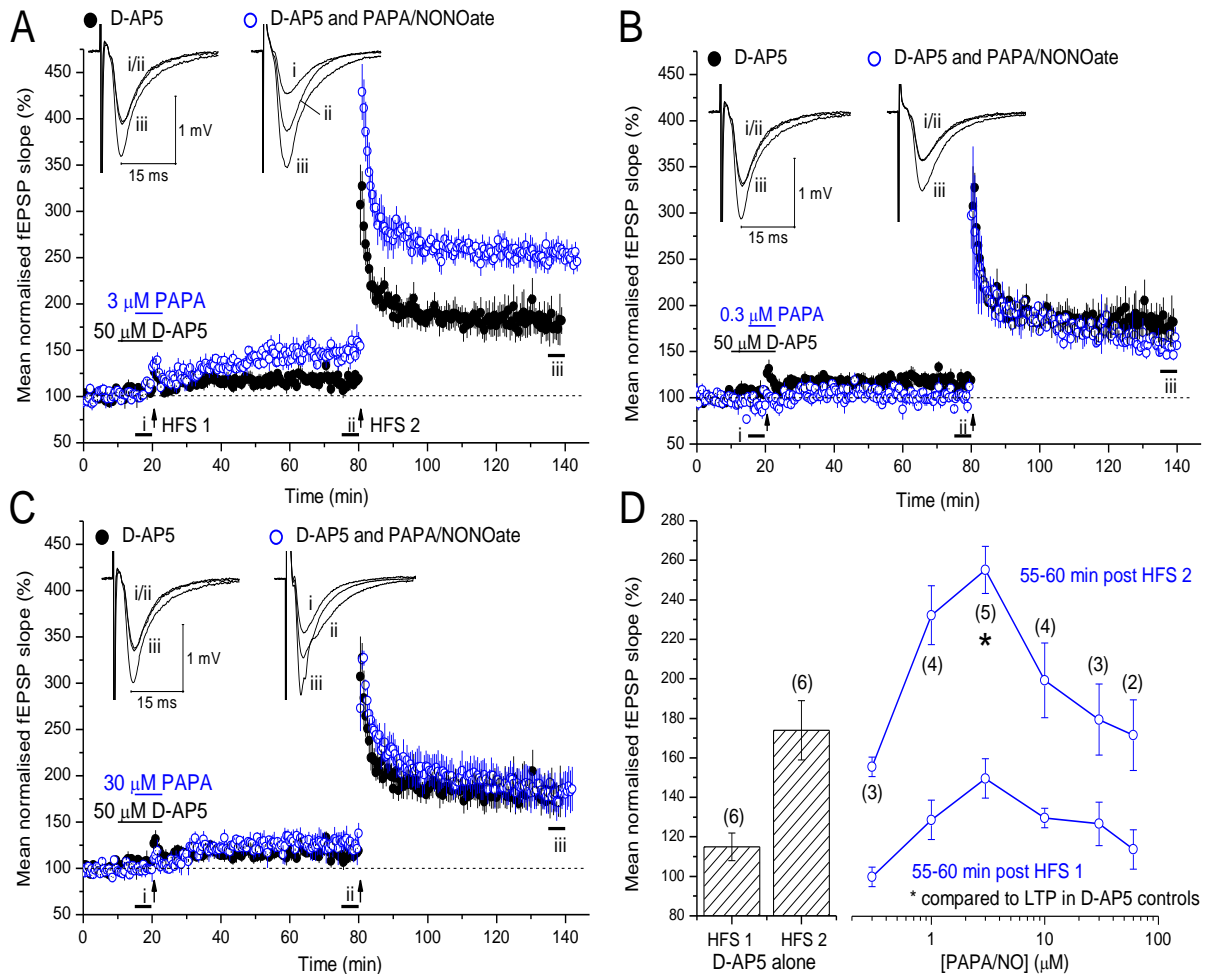


Figure 3.7 Impact of the NO-induced potentiation on subsequent HFS-induced LTP. **A)** Slices received HFS in the presence of D-AP5 alone (black) or HFS in the presence of D-AP5 and 3 μM PAPA/NONOate, which generated a significant NO-induced potentiation (blue; same data as in **Figure 3.6A**). One hr later, all slices received a second HFS (labelled HFS 2). In both conditions, this resulted in significant LTP (paired *t*-tests, $p < 0.05$ compared to the initial slope measured 5 min prior to HFS). In slices that had undergone NO-induced potentiation, the LTP was of a remarkably high magnitude (unpaired *t*-test, $p = 0.0162$ compared to LTP in control slices after D-AP5 wash-out (black)). **B- C)** Subsequent to treatment with HFS, D-AP5 and lower (0.3 μM ; **B**) or higher (30 μM ; **C**) concentrations of PAPA/NONOate, HFS-induced LTP was not significantly different to that observed in control slices after D-AP5 wash-out (one factor ANOVA with Dunnett's test, $p > 0.05$). **D)** The magnitude of the NO-induced potentiation (measured 55-60 min post HFS 1) and the magnitude of subsequent HFS-induced LTP (measured 55-60 min post HFS 2) were similarly dependent on

*[PAPA/NONOate]. Numbers by points are n; * = one factor ANOVA with Dunnett's test, $p < 0.05$ compared to the magnitude of HFS-induced LTP in control slices after D-AP5 wash-out (see black bar).*

Relative to the initial slope measured 5 min prior to HFS 2, the amount of LTP yielded by HFS subsequent to the NO-induced potentiation (generated using 3 μ M PAPA/NONOate) was not significantly different from the amount yielded by HFS subsequent to pre-treatment with D-AP5 alone (unpaired t-test, $p = 0.0516$; see **Figure 3.7A**). This suggested that the NO-induced potentiation was additive with subsequent HFS-induced LTP.

Further analysis of the relationship between the magnitude of the NO-induced potentiation generated using 3 μ M PAPA/NONOate and subsequent HFS-induced LTP was also consistent with a purely additive interaction: the magnitude of the NO-induced potentiation (generated using 3 μ M PAPA/NONOate) was significantly positively correlated with the magnitude of subsequent HFS-induced LTP (**Figure 3.8**, red); there was no significant correlation between the NO-induced potentiation and subsequent LTP when the latter was normalised to the former (blue); the mean magnitude of HFS-induced LTP, once normalised to the magnitude of the NO-induced potentiation, was not significantly different from the magnitude of control, HFS-induced LTP (grey bar vs. blue mean).

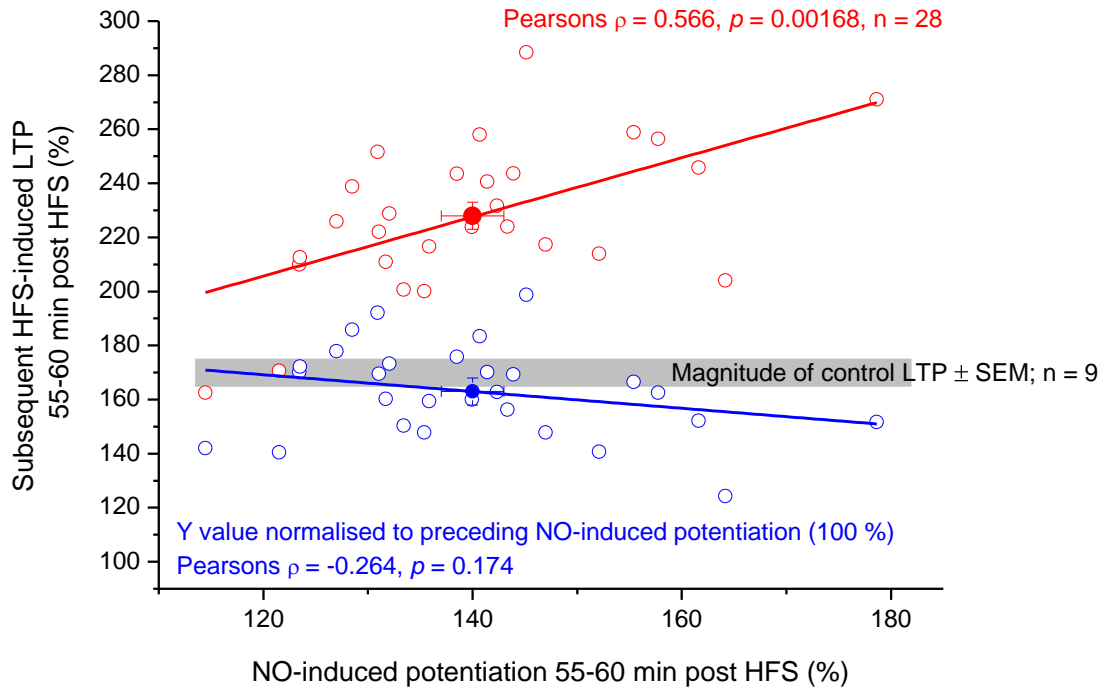


Figure 3.8 Correlation between the magnitude of the NO-induced potentiation and subsequent HFS-induced LTP. NO-induced potentiation was generated using 3 μ M PAPA/NONOate and 1 hr later, LTP was induced by HFS. Red: the magnitude of the NO-induced potentiation was positively correlated with that of the HFS-induced LTP (Pearson's $\rho = 0.566, p = 0.00168$). Spearman's correlation coefficient was similar (0.523, $p = 0.00432$) suggesting that the trend over this data range was linear. Blue: when the magnitude of HFS-induced LTP was normalised to the magnitude of the preceding NO-induced potentiation, the data were not correlated (Spearman's $\rho = -0.264, p = 0.174$). Grey: The grey bar shows the mean magnitude of the control LTP shown in **Figure 3.6** \pm SEM. There was no significant difference between the mean grey and blue value (unpaired t -test, $p = 0.478$).

Filled points are means. Fits are linear.

There were *at least* two possible reasons why the NO-induced potentiation and subsequent HFS-induced LTP were additive: 1) the potentiations shared common mechanisms, but one HFS did not saturate them; 2) the NO-induced potentiation was mechanistically distinct from HFS-induced LTP. To address these possibilities and determine in which context the NO-induced potentiation should be interpreted, experiments were designed to assess: 1) the number of HFS needed to saturate HFS-induced LTP; 2) the effect of the NO-induced potentiation on the maximum possible magnitude of HFS-induced LTP.

HFS was paired with D-AP5 and 3 μ M PAPA/NONOate, or D-AP5 alone. As above, pairing of HFS with D-AP5 and PAPA/NONOate resulted in a significant potentiation, although pairing of HFS with D-AP5 alone did not. Thirty min later, one HFS was delivered every 30 min until no difference in the magnitude of LTP generated by consecutive tetani was observed (**Figure 3.9A**).

Using repeated measures ANOVA with Dunnett's test to compare the fEPSP slope 25-30 min after each HFS (labelled 1-4 in **Figure 3.9**) to that measured after the last HFS (labelled 5), it was determined that, regardless of previous NO-induced potentiation, the magnitude of LTP was not saturated by one HFS. It was reasoned that, if the NO-induced potentiation was representative of a NO-dependent component of LTP, then LTP subsequent to it would saturate one HFS earlier than the LTP subsequent to pre-treatment with D-AP5 alone. However, LTP saturated after HFS 3 in both groups (see **Figure 3.9C**). It was also hypothesised that, if the NO-induced potentiation was representative of a NO-dependent component of LTP, then LTP subsequent to the NO-induced potentiation would saturate at the same magnitude as LTP subsequent to pre-treatment with D-AP5 alone. However, the magnitude of LTP 25-30 min after each HFS was consistently and significantly higher in slices that had previously undergone NO-induced potentiation than in slices that were pre-treated with D-AP5 alone (**Figure 3.9B**). This effect was not observable when the data within each condition was normalised to the fEPSP slope 25-30 min after HFS1 (see **Figure 3.9B** inset), implying that the NO-induced potentiation had no effect on the magnitude of LTP generated by each HFS, compared to controls.

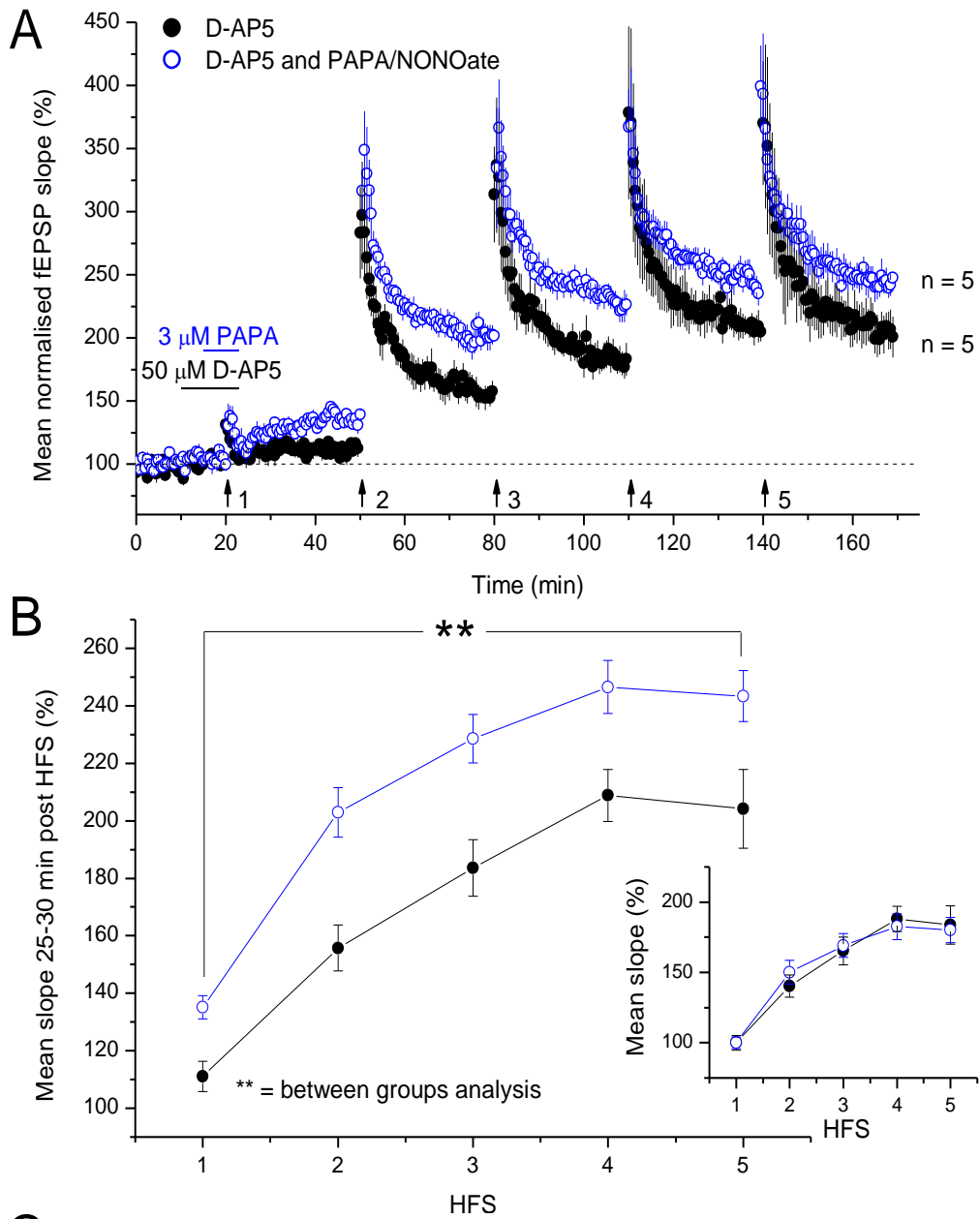


Figure 3.9 LTP saturation subsequent to NO-induced potentiation. **A)** In experiments separate from those shown in **Figure 3.6-7**, HFS was paired with D-AP5 and PAPA/NONOate, thereby generating significant NO-induced potentiation (measuring $135 \pm 4\%$ 25-30 min after HFS; paired *t*-test, *p* =

0.00401 compared to the last 5 min of baseline), or D-AP5 alone, which had no significant effect on the fEPSP slope ($111 \pm 5\%$ 25-30 min after HFS; $p = 0.103$ compared to the last 5 min of baseline). 30 min later a series of HFS were delivered to slices (one every 30 min; HFS 2-5) until the magnitude of LTP was saturated (see comparison 4 vs. 5 in C). **B**) The mean fEPSP slope recorded 25-30 min following each HFS (1-5) is plotted. ** = the magnitude of LTP measured 25-30 min after each HFS was significantly higher in slices that had undergone NO-induced potentiation than in slices pre-treated with D-AP5 alone (two factor ANOVA with repeated measures across HFS, $p = 0.0007$). Inset: within each group, the data have been normalised to the value recorded after HFS 1. **C**) Within each group, the magnitude of LTP yielded after each HFS is compared to that after the last HFS (HFS 5) using repeated measures ANOVA with Dunnett's test. Within both groups, LTP was saturated after HFS 3.

The above results were discordant with the possibility that the NO-induced potentiation and subsequent LTP were additive because one HFS was not saturating LTP. Rather, they were consistent with the possibility that the NO-induced potentiation and subsequent LTP were mechanistically distinct. To test this, a series of HFS were delivered to slices (one every 30 min; see HFS 1-5 in **Figure 3.10A**) until there was no observable effect of consecutive tetani on the magnitude of LTP. As above, repeated measures ANOVA with Dunnett's test used to compare the magnitude of LTP 25-30 min following each HFS (labelled 1-4) to that recorded after the final tetanus (labelled 5) showed that 3 tetani were required to saturate the magnitude of LTP (see **Figure 3.10B**). Subsequently, HFS was delivered in the presence of PAPA/NONOate (see HFS 6 in **Figure 3.10**). If the NO-induced potentiation was mechanistically distinct from HFS-induced LTP, then pairing of exogenous NO with HFS was predicted to further increase the fEPSP slope. However, there was no significant effect of pairing HFS with PAPA/NONOate (**Figure 3.10B**).

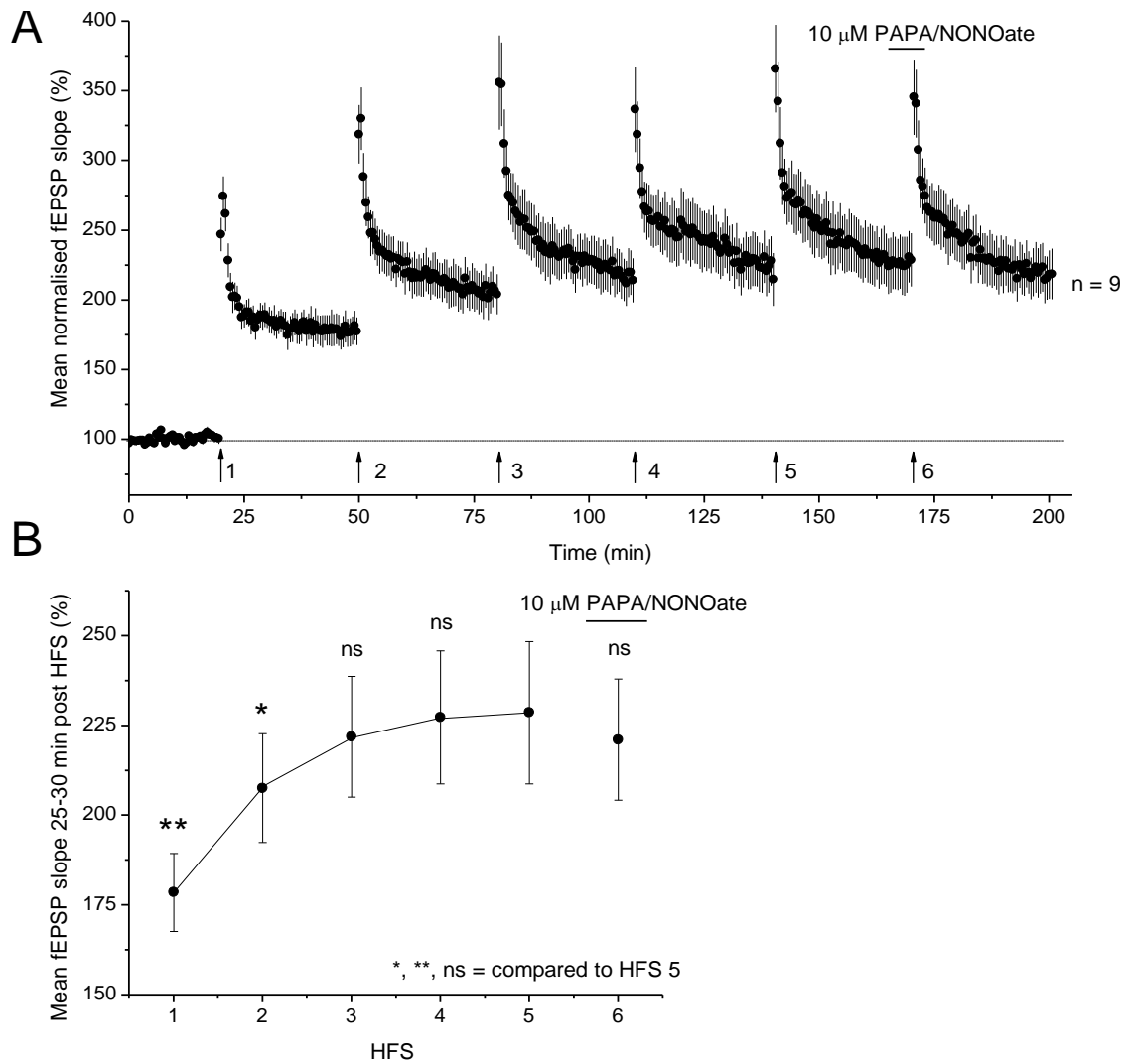


Figure 3.10 The number of HFS required to saturate LTP and the effect of exogenous NO on saturated LTP. **A**) One HFS was delivered to slices every 30 min until there was no observable difference between the magnitudes of LTP yielded by consecutive tetani. Subsequently, PAPA/NONOate was paired with HFS (HFS 6). **B**) The mean fEPSP slope recorded 25-30 min following each HFS (1-6) is plotted and compared to that after HFS 5 (the last HFS prior to NO) using repeated measures ANOVA with Dunnett's test; ** = $p < 0.01$; * = $p < 0.05$; ns = $p > 0.05$.

Note that 10 μ M PAPA/NONOate was used due to the reasons outlined in 3.3.2.

Further investigation revealed that there was also no effect of exogenous NO paired with HFS on the magnitude of LTP in slices that had not undergone any previous long-lasting potentiation (**Figure 3.11**).

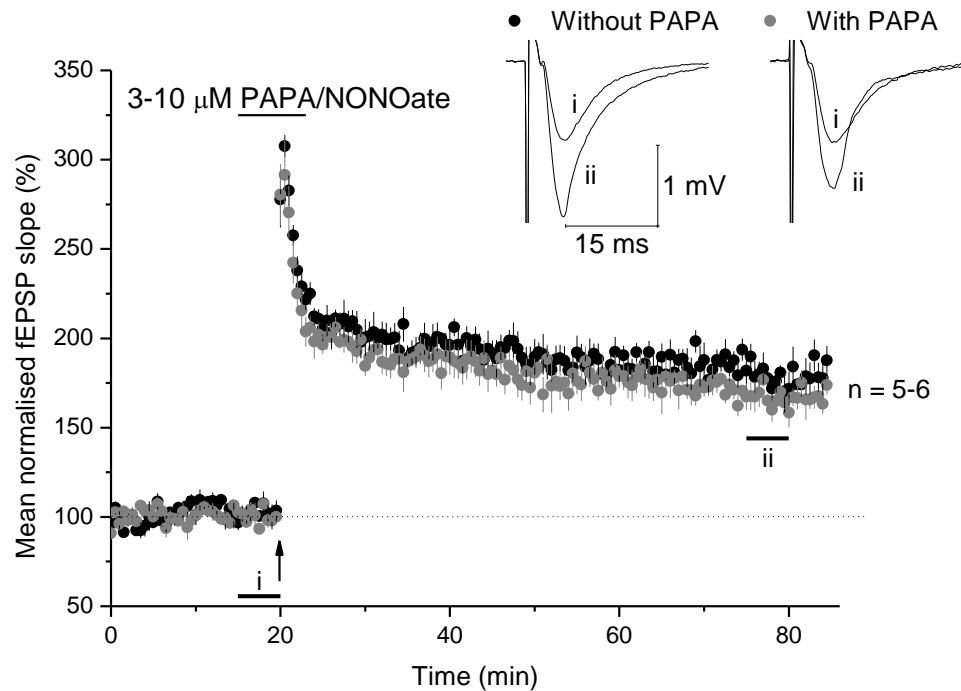


Figure 3.11 Effect of exogenous NO on control LTP. Slices received HFS, or HFS in the presence of PAPA/NONOate. PAPA/NONOate had no significant effect on the magnitude of the resulting LTP (HFS alone = $178 \pm 8\%$; HFS and PAPA/NONOate = $166 \pm 6\%$; unpaired *t* test, $p = 0.199$). Two concentrations of PAPA/NONOate were tested due to the reasons discussed in 3.3.2.

Mechanisms underlying the NO-induced potentiation

The NO-induced potentiation was additive with subsequent HFS-induced LTP (**Figure 3.7-9**) and this could not be explained by the inability of one HFS to saturate LTP (**Figure 3.9**). These findings were discordant with the hypothesis that exogenous NO paired with a standard LTP induction protocol during NMDA receptor blockade would restore a persistent NO-dependent component of LTP and suggested that the NO-induced potentiation was mechanistically distinct from LTP. However, exogenous NO paired with HFS had no significant effect on the magnitude of the resulting potentiation (**Figure 3.10-11**). Possible explanations for this are detailed below (see **3.5 Discussion**). To further investigate whether the NO-induced potentiation was dependent upon similar mechanisms as NMDA receptor- and NO-dependent LTP, key properties of the NO-induced potentiation were investigated.

Firstly, we sought to test whether the NO-induced potentiation was dependent on HFS. Activity-dependence is a hallmark characteristic of LTP and associative synaptic plasticity. In the present study, it was found that HFS (labelled HFS 1 in **Figure 3.12**) was critical for the generation of NO-induced potentiation and subsequent high-magnitude HFS-induced LTP. Regardless of whether HFS 1 was delivered, there was no significant difference in the amount of LTP generated by subsequent HFS (labelled HFS 2 in **Figure 3.12**). This was consistent with the results shown in **Figure 3.8** and the conclusions drawn from **Figure 3.9**.

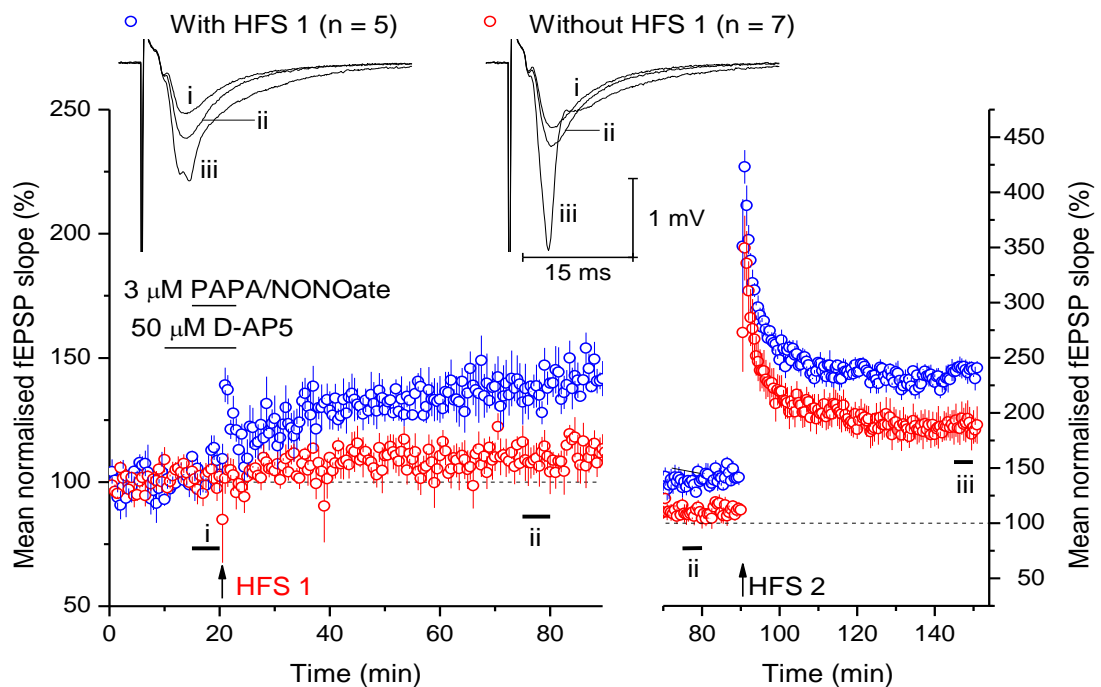


Figure 3.12 Activity-dependence of NO-induced potentiation. PAPA/NONOate and D-AP5 were applied to slices and this application was either paired or not with HFS (HFS 1). HFS 1 was critical for NO-induced potentiation (without HFS 1: $109 \pm 7\%$; paired *t*-test, $p = 0.158$ compared to baseline; with HFS 1: $137 \pm 6\%$; paired *t*-test, $p = 0.0039$ compared to baseline; without HFS 1 vs. with HFS 1: unpaired *t*-test, $p = 0.00479$; left panel) and subsequent high-magnitude, HFS-induced LTP (without HFS 1: $189 \pm 15\%$; with HFS 1: $239 \pm 8\%$; unpaired *t*-test, $p = 0.0172$; without HFS 1 vs. with HFS 1: unpaired *t*-test, $p = 0.0147$). Measured from the fEPSP slope 10 min prior to HFS 2, the magnitude of LTP in each condition was not significantly different (unpaired *t*-test, $p = 0.155$).

Note that the two parts of this experiment have been illustrated on different scales.

Classically, the requirement of LTP for HFS is explained by its requirement for NMDA receptor activity. However, the NO-induced potentiation was insensitive to a

high concentration of the NMDA antagonist, D-AP5 (50 μ M), raising the question: what does HFS contribute to the NO-induced potentiation?

Following high frequency (200 Hz) burst stimulation or long-lasting theta burst stimulation, several groups have observed a NMDA receptor-independent, L-type VGCC (L-VGCC)-dependent LTP at CA1 synapses that may rely on distinct expression mechanisms from those involved in NMDA receptor-dependent LTP (Grover and Teyler, 1990; Cavus and Teyler, 1996; Morgan and Teyler, 1999; Bayazitov *et al.*, 2007). Like the NO-induced potentiation, this L-VGCC-dependent LTP was slowly rising and measured \sim 150 % (Grover and Teyler, 1990). Furthermore, it has been hypothesised that L-VGCCs could become active during 100 Hz HFS (Cavus and Teyler, 1996), although, to our knowledge, this has not been tested. Therefore, to determine whether the NO-induced potentiation was related to NMDA receptor-independent, L-VGCC-dependent LTP, and whether a requirement for L-VGCC opening accounted for the activity-dependence of the NO-induced potentiation, the L-VGCC antagonist, nifedipine (30 μ M) was employed.

As shown in **Figure 3.13**, there was no effect of nifedipine on the magnitude of the NO-induced potentiation and no effect of nifedipine pre-treatment on subsequent HFS-induced LTP. Note that, under our conditions, the same concentration of nifedipine was effective in blocking a NMDA receptor-independent, L-VGCC-dependent LTP at CA1 synapses (see **Chapter 5**).

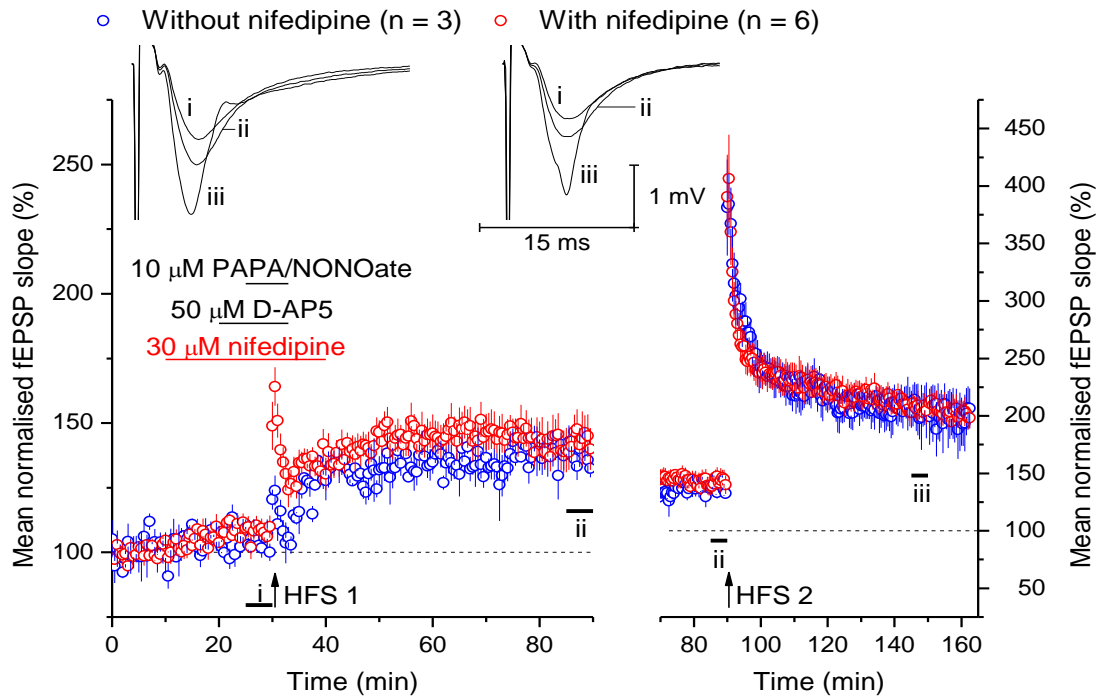


Figure 3.13 Impact of L-VGCC inhibition on NO-induced potentiation. The selective L-VGCC antagonist, nifedipine (30 μ M; applied 20 min prior to HFS), had no significant effect on the NO-induced potentiation (with nifedipine: $143 \pm 7\%$; without nifedipine: $139 \pm 5\%$; unpaired t-test, $p = 0.668$) and there was no effect of nifedipine pre-treatment on subsequent HFS-induced LTP (with nifedipine: $208 \pm 10\%$; without nifedipine: $204 \pm 27\%$; unpaired t-test, $p = 0.794$). Control experiments were separate from those shown in **Figure 3.12**.

It has been previously reported that HFS-induced LTP at CA1 synapses requires both eNOS and nNOS activity. The former is thought to provide a tonic, activity-independent NO signal (Hopper and Garthwaite, 2006) that is D-AP5-insensitive (Bartus, 2009). The latter is hypothesised to provide a phasic, activity-dependent NO signal (Hopper and Garthwaite, 2006) and is thought to be preferentially elicited upon NMDA receptor activity (Garthwaite, 2008). Therefore, to test the involvement of D-AP5-insensitive, endogenous NO in the NO-induced potentiation the non-selective NOS inhibitor, L-NNA (100 μ M) was used. In common with its effect on HFS-induced LTP (**Figure 3.4**), L-NNA caused a steady decline in the NO-induced potentiation such that, 55-60 min post HFS, the potentiation was significantly reduced compared to that observed in un-treated controls. In slices pre-treated with L-NNA, subsequent HFS-induced LTP was also reduced compared to

that observed in un-treated controls (**Figure 3.14**). It is unclear whether this was a consequence of reduced NO-induced potentiation, or incomplete L-NNA wash-out.

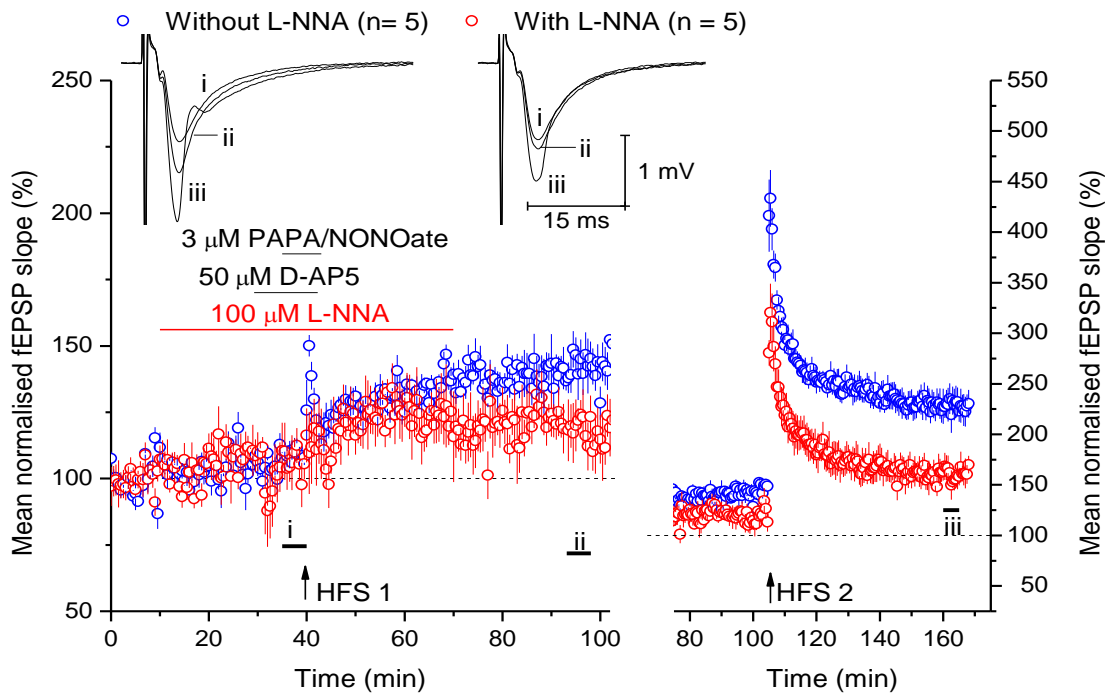


Figure 3.14 Requirement of NO-induced potentiation for NOS. The non-selective NOS inhibitor, L-NNA ($100 \mu\text{M}$), was applied to slices 30 min prior to and after HFS. This caused a steady decline in the NO-induced potentiation such that, 55–60 min post HFS it was significantly reduced compared to interleaved, un-treated controls ($118 \pm 8\%$ vs. $148 \pm 11\%$; unpaired *t*-test, $p = 0.0383$). In slices pre-treated with L-NNA, subsequent HFS-induced LTP was also significantly reduced compared to that in un-treated controls ($160 \pm 11\%$ vs. $238 \pm 19\%$; $p = 0.0049$).

Physiological NO signal transduction is thought to occur via guanylyl cyclase activation and cGMP accumulation (Garthwaite, 2008). Consistent with this mechanism, NO-dependent CA1 LTP has been found to be significantly inhibited by the NO-targeted guanylyl cyclase antagonist, ODQ (for example, Boulton *et al.*, 1995; Lu *et al.*, 1999; Bon and Garthwaite, 2003). Accordingly, we sought to test the requirement of the NO-induced potentiation for NO-targeted guanylyl cyclase activity. In common with the effect of L-NNA, ODQ ($10 \mu\text{M}$) caused a significant decline in the expression of the NO-induced potentiation, and in slices pre-treated with ODQ, the magnitude of subsequent HFS-induced LTP was also significantly

reduced compared to un-treated controls (**Figure 3.15**). As above, this could be explained by reduced NO-induced potentiation or incomplete ODQ wash-out.

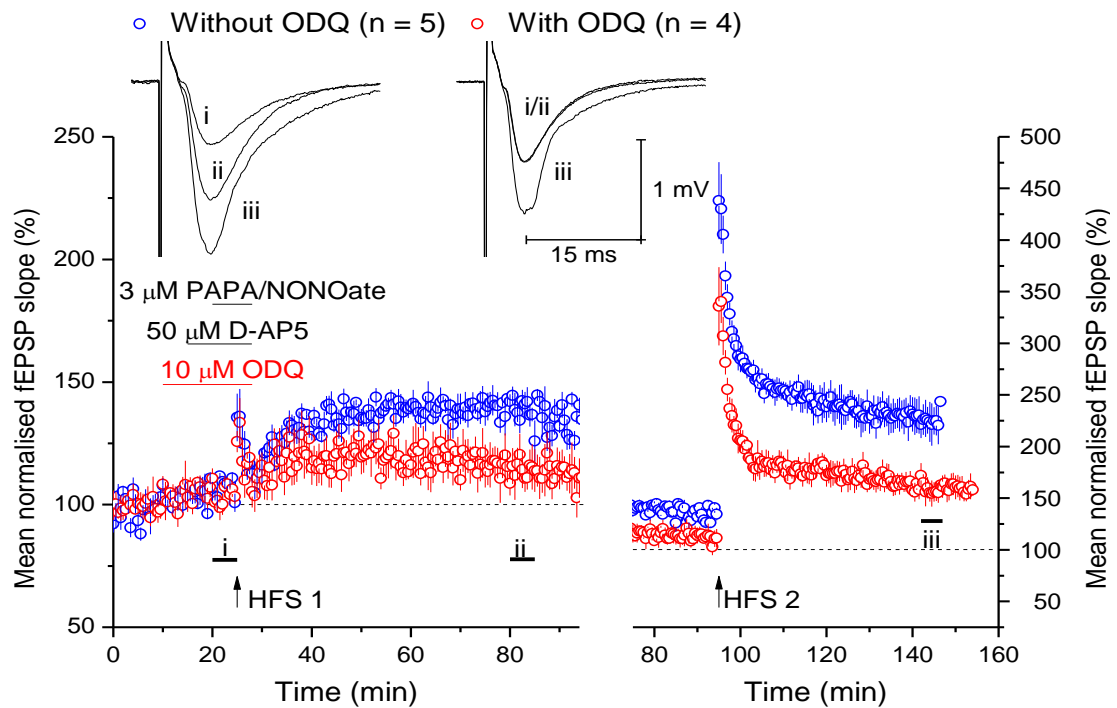


Figure 3.15 Dependence of NO-induced potentiation on NO-targeted guanylyl cyclase activity. The NO-targeted guanylyl cyclase antagonist, ODQ (10 μ M), was applied to slices 20 min prior to and 5 min after HFS. This caused a significant decline in the NO-induced potentiation, such that, 55-60 min post HFS, it was significantly reduced compared to interleaved, untreated controls ($115 \pm 8\%$ vs. $138 \pm 5\%$; unpaired *t*-test, $p = 0.0341$). Subsequent HFS-induced LTP was also significantly reduced in slices pre-treated with ODQ compared to that recorded in untreated controls ($159 \pm 10\%$ vs. $228 \pm 14\%$; unpaired *t*-test, $p = 0.0064$).

Finally, the involvement of α CaMKII in the NO-induced potentiation was tested. This kinase is viewed as a general effector of LTP at mature CA1 synapses (Lisman *et al.*, 2002) and is required for NO/cGMP-dependent LTP between pairs of dissociated hippocampal neurons (Ninan and Arancio, 2004). Although α CaMKII is Ca^{2+} -activated, autophosphorylation at threonine-286 (T286) allows it to maintain activity hours after the dissociation of CaM. Replacement of T286 with alanine (T286A) renders autophosphorylation of the kinase impossible and has been reported to block LTP at CA1 synapses and learning of hippocampus-dependent tasks (Logue *et al.*, 1997; Giese *et al.*, 1998). Therefore, to test the requirement of the NO-induced potentiation for α CaMKII, we attempted to generate NO-induced potentiation in

slices prepared from $\alpha\text{CaMKII}^{\text{T286A}}$ homozygote and wild-type mice (described by Giese *et al.*, 1998).

At CA1 synapses in slices prepared from wild-type littermates, significant NO-induced potentiation was observed. However, at synapses in slices from $\alpha\text{CaMKII}^{\text{T286A}}$ homozygote mice, neither the NO-induced potentiation nor subsequent HFS-induced LTP could be induced (**Figure 3.16A**).

Compared to the magnitude typically observed in C57Bl/6 mice, a relative decrease in the magnitude of the NO-induced potentiation and subsequent HFS-induced LTP was apparent in the wild-type mice (NO-induced potentiation in wild-type data set: $130 \pm 4 \%$; subsequent LTP: $183 \pm 10 \%$; $n = 5$). However, the magnitude of NO-induced potentiation was identical to the degree of HFS-induced LTP observed in a pilot experiment using 1 wild-type littermate (130% ; **Figure 3.16B**). The relative decrease may, therefore, be inherent to these mice and caused, perhaps, by their background.

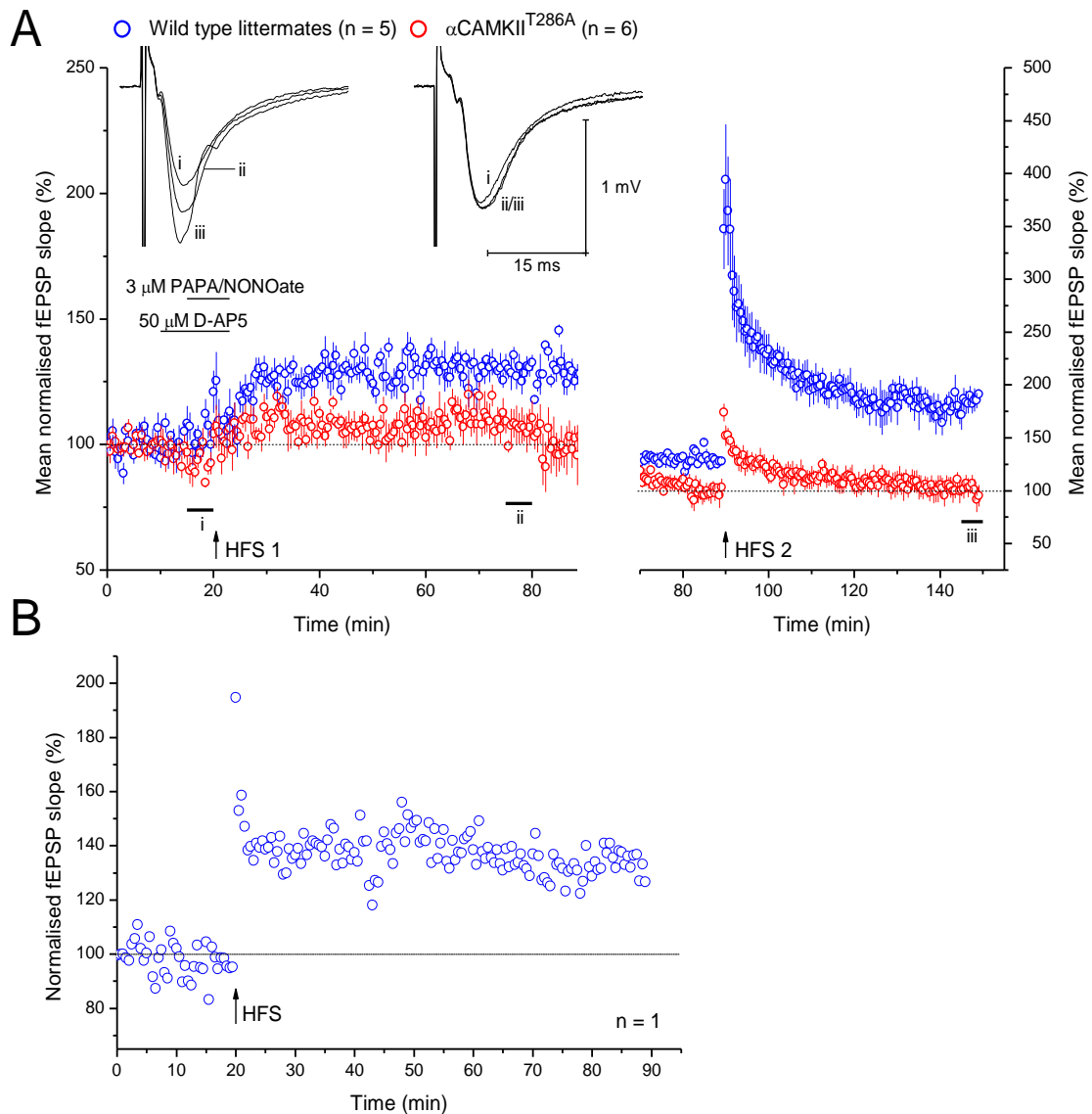


Figure 3.16 Involvement of α CaMKII in NO-induced potentiation. **A**) Neither the NO-induced potentiation, nor subsequent HFS-induced LTP could be induced in α CaMKII^{T286A} homozygote mice (NO-induced potentiation: $99 \pm 8\%$; paired *t*-test, $p = 0.461$ compared to baseline; subsequent HFS-induced LTP: $101 \pm 9\%$; $p = 0.367$ compared to baseline). However, both forms of potentiation could be observed in wild-type littermates (NO-induced potentiation: $130 \pm 4\%$; paired *t*-test, $p = 0.0006$ compared to baseline; HFS-induced LTP: $183 \pm 10\%$; paired *t*-test, $p = 0.0247$ compared to the last 5 min of the NO-induced potentiation). **B**) HFS-induced LTP in a wild-type littermate (130 %).

3.4.4 Synaptic locus of the NO-induced potentiation

Although the precise relationship between the NO-induced potentiation and HFS-induced LTP was unclear (**Figure 3.8-11**), initial characterisation of the NO-induced

potentiation showed that it had properties in common with at least some forms of LTP. For example, the NO-induced potentiation required HFS (**Figure 3.12**), endogenous NO (**Figure 3.14**), NO-targeted guanylyl-cyclase activity (**Figure 3.15**), and functional α CaMKII (**Figure 3.16**). Given the hypothesis that the NO acts as a retrograde messenger during LTP (see **3.1 Introduction**), we therefore sought to test the synaptic locus (pre- or postsynaptic) of the NO-induced potentiation.

To this end, the effect of the NO-induced potentiation on PPF, at CA1 synapses was investigated. PPF, which can be elicited when a pair of stimuli are delivered to synapses in quick succession (typically with an ISI < 500 ms), is characterised by a transient increase in synaptic efficacy (for example, see **Figure 3.17**). Although some doubts exist over the synaptic locus of PPF (reviewed by Bliss *et al.*, 2007), the facilitation can be explained by a change in presynaptic efficacy caused, for example, by residual Ca^{2+} in the axon bouton (Wu and Saggau, 1994b) or a related mechanism, such as the saturation of a presynaptic Ca^{2+} buffer (Rozov *et al.*, 2001). Therefore changes in PPF are often used to diagnose a presynaptic change in efficacy following LTP induction. Specifically, an increase in the probability of neurotransmitter release following LTP is thought to reduce the scope for a subsequent increase during PPF and, therefore, cause a decrease in the magnitude of PPF (measured using the PPR; the initial slope of the second fEPSP/the initial slope of the first fEPSP; Zucker and Regehr, 2002; Bliss *et al.*, 2007).

Initial characterisation of PPF

Before testing the effect of the NO-induced potentiation on the magnitude of PPF at CA1 synapses, we sought to characterise PPF under our conditions and determine whether statistically significant, evoked changes in the PPR could be detected. In accordance with previous reports (Creager *et al.*, 1980), initial studies showed that PPF of CA1 fEPSPs could be consistently generated using ISIs of 10-400 ms (**Figure 3.17**). The magnitude of PPF (determined using the PPR) was dependent on the ISI used, and the relationship was remarkably similar to that previously described at CA1 synapses in rat hippocampal slices (Creager *et al.*, 1980; Dunwiddie and Haas, 1985) and in awake C57/B16 mice (Fontinha *et al.*, 2009).

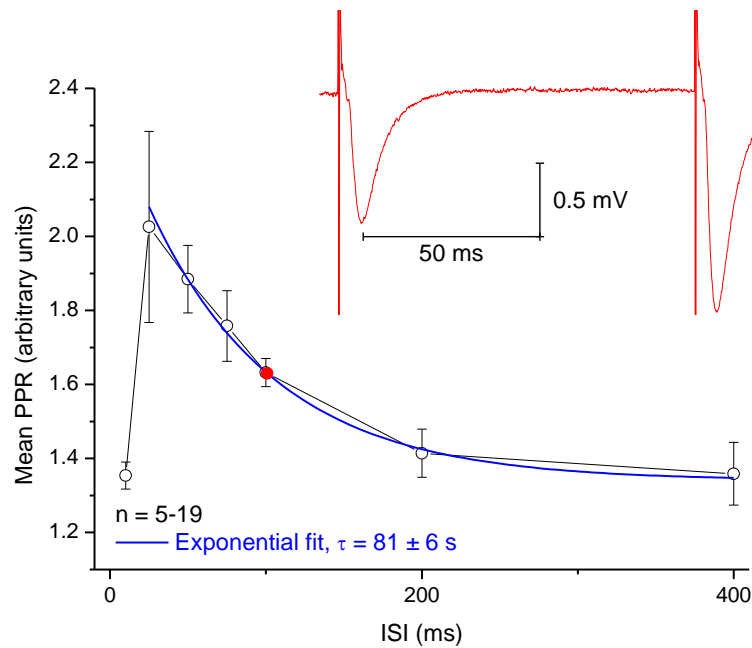


Figure 3.17 PPF of CA1 fEPSPs. PPF of CA1 fEPSPs could be consistently elicited by stimulating the Schaffer collateral/commissural fibres twice in quick succession (ISI = 10-400 ms). The magnitude of PPF (determined using the PPR) was dependent on the ISI: the PPR increased from 10 ms to peak at 25 ms and then decreased exponentially over the range of 25-400 ms. The PPR was half-maximal at 81 ± 6 s (see τ ; see **Chapter 2** for exponential equation; adjusted $R^2 = 0.993$). In individual experiments, PPRs were measured from the mean of 10 consecutive pairs of fEPSPs (an example is inset).

To determine whether, at a given ISI, statistically significant, evoked changes in PPF could be detected under our conditions, we measured alterations in the PPR in response to 2 compounds, 2-Cl-adenosine and forskolin, known to have opposite effects on the magnitude of PPF at CA1 synapses. To avoid ceiling effects on any changes in the PPR, the ISI was set to 100 ms, since this ISI was found to elicit ~ half-maximal PPF in initial experiments (see τ in **Figure 3.17**).

In accordance with previous studies of the effect of adenosine on PPF at CA1 synapses in adult rat hippocampal slices (Dunwiddie and Haas, 1985; Dumas and Foster, 1998), bath application of 2-Cl-adenosine (0.5 μ M) elicited a depression of fEPSP 1 and, to a lesser extent, fEPSP 2 (**Figure 3.18A**), causing a significant increase of the mean PPR from baseline (**Figure 3.18C**). As shown in **Figure 3.18B**, the increase in PPR was observed in all the slices tested.

After washing of 2-Cl-adenosine and re-establishing a steady baseline, 0.5 μM forskolin was applied. As has been previously observed at CA1 synapses in rat hippocampal slices (Dumas and Foster, 1998; Lu and Gean, 1999; Wu *et al.*, 1999), forskolin caused a potentiation of fEPSP 1 and, to a lesser extent, fEPSP 2 (**Figure 3.18A**), resulting in a significant decrease of the mean PPR from baseline (**Figure 3.18C**). This decrease was observed in the majority of slices tested, although two of seven showed an increase (see **Figure 3.18B**).

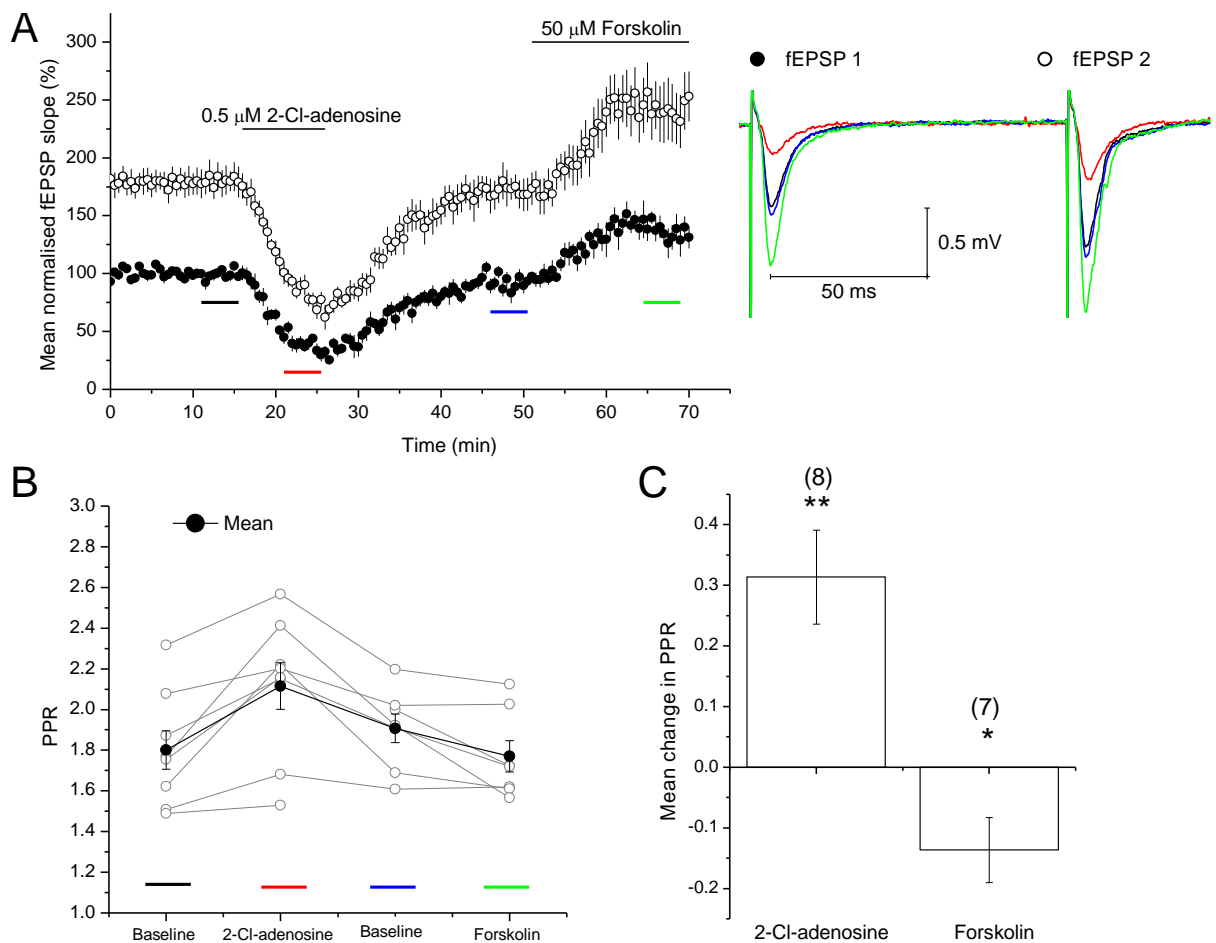


Figure 3.18 Effect of 2-Cl-adenosine and forskolin on PPF. **A**) Paired pulses ($\text{ISI} = 100 \text{ ms}$) were delivered to CA1 synapses every 30 s. 2-Cl-adenosine ($0.5 \mu\text{M}$) and forskolin ($50 \mu\text{M}$) were applied at the times indicated and their effects on the mean initial slopes of fEPSP 1 and 2 were recorded. **B**) Summary showing the mean PPR recorded at the colour coded bars in **A** in each experiment (grey) and on average (black). **C**) Summary of the mean change in PPR from the preceding baseline caused by 2-Cl-adenosine and forskolin. 2-Cl-Adenosine caused a significant increase in the mean PPR

(mean change (red minus black in A and B): 0.31 ± 0.08 ; ** one factor t-test, $p = 0.00482$ compared to zero). Forskolin induced a significant decrease in the mean PPR (mean change (green minus blue in A and B): 0.14 ± 0.05 ; * one factor t-test, $p = 0.0436$ compared to zero change). Numbers above bars are n.

Effect of HFS-induced LTP and the NO-induced potentiation on the magnitude of PPF

The above results suggested that significant bidirectional changes in PPF could be detected under our conditions. Therefore, the effects of the NO-induced potentiation and subsequent HFS-induced LTP on PPF were determined. For the reasons outlined in **3.3.2**, 10 μ M PAPA/NONOate was used to generate a significant NO-induced potentiation, which measured 138 ± 5 %. Subsequent LTP was 222 ± 11 %. Additionally, experiments were performed to control for the effect of HFS paired with D-AP5 on PPF. In these experiments, HFS in the presence of D-AP5 alone had no significant effect on fEPSP slope, although HFS subsequent to D-AP5 wash-out generated significant LTP (**Figure 3.19A**). PPF was induced at the coloured bars shown in **Figure 3.19A**. As above, the ISI was set to 100 ms.

As shown in grey in **Figure 3.19B**, the effects of all treatments on PPF varied between experiments. On average, there was no significant change in the mean PPR from baseline after pairing D-AP5 with HFS, or after LTP induced subsequent to D-AP5 wash-out. Compared to the change in PPR following HFS in the presence of D-AP5 alone, there was no significant effect of the NO-induced potentiation on PPR. Compared to the change in PPR following LTP in slices pre-treated with D-AP5 alone, LTP subsequent to the NO-induced potentiation also had no effect on mean PPR (**Figure 3.19C**).

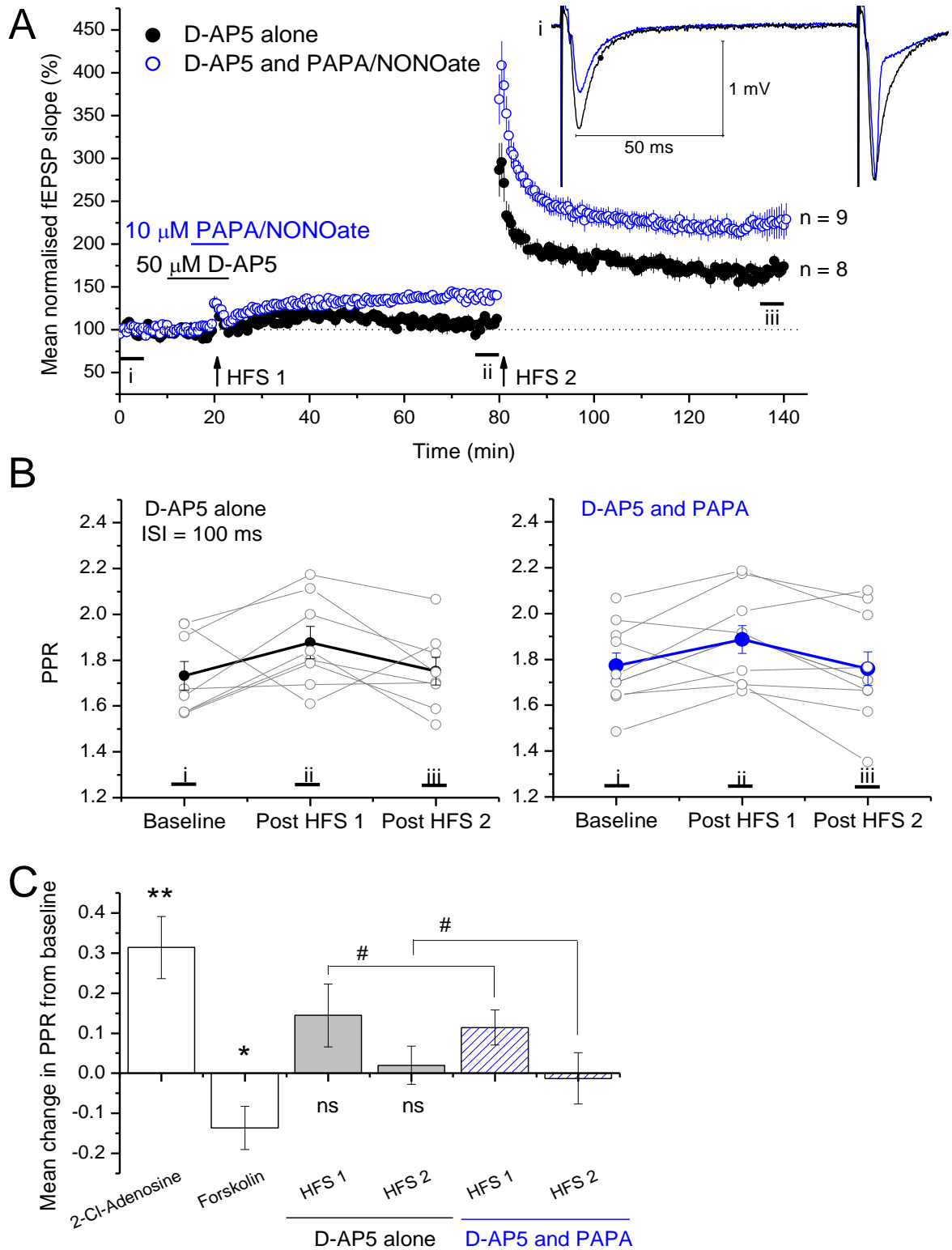


Figure 3.19 Changes in PPF subsequent to the NO-induced potentiation. **A)** Pairing of PAPA/NONOate and HFS in the presence of D-AP5 generated significant NO-induced potentiation ($138 \pm 5\%$; paired *t*-test, $p = 8.56 \times 10^{-5}$ compared to the last 5 min of baseline) and 1 hr later, delivery of a second HFS yielded significant LTP ($222 \pm 11\%$; paired *t*-test, $p = 5.94 \times 10^{-6}$

compared to the last 5 min of NO-induced potentiation). HFS in the presence of D-AP5 alone generated no significant potentiation ($107 \pm 5\%$; paired *t*-test, $p = 0.312$ compared to the last 5 min of baseline), although after washing D-AP5, a significant LTP was generated ($163 \pm 8\%$; paired *t*-test, $p = 7.08 \times 10^{-6}$ compared to fEPSP slope 5 min prior to HFS). Paired stimuli (ISI = 100 ms) were delivered at the bars number i-iii. **B)** The magnitudes of the PPF elicited at the time points indicated by the numbered bars in A in individual experiments (grey) and on average (black or blue) are plotted. **C)** Summary showing the average change in PPR following HFS 1 or 2 (see panel A) in slices treated with D-AP5 or D-AP5 and PAPA/NONOate compared to baseline. The average changes in PPR following treatment with $0.5 \mu\text{M}$ 2-Cl-adenosine or $50 \mu\text{M}$ forskolin (ISI = 100 ms; see **Figure 3.17**) are shown again for comparison. Statistics: one factor *t*-tests compared to zero change: ** = $p < 0.01$, * = $p < 0.05$, ns = $p > 0.05$ compared to zero; #: unpaired *t*-test, $p > 0.05$.

Finally, to place the above results into context, the effect of HFS-induced LTP on PPF was evaluated. In these experiments, LTP measured $179 \pm 6\%$ (**Figure 3.20A**). As shown in **Figure 3.20B**, the effect of HFS-induced LTP on PPF when the ISI was 100 ms was very variable (PPR increased in 4 slices and decreased in 6 slices) and on average, there was no significant change. Similar results were obtained when the ISI was 25 or 200 ms (**Figure 3.20C**).

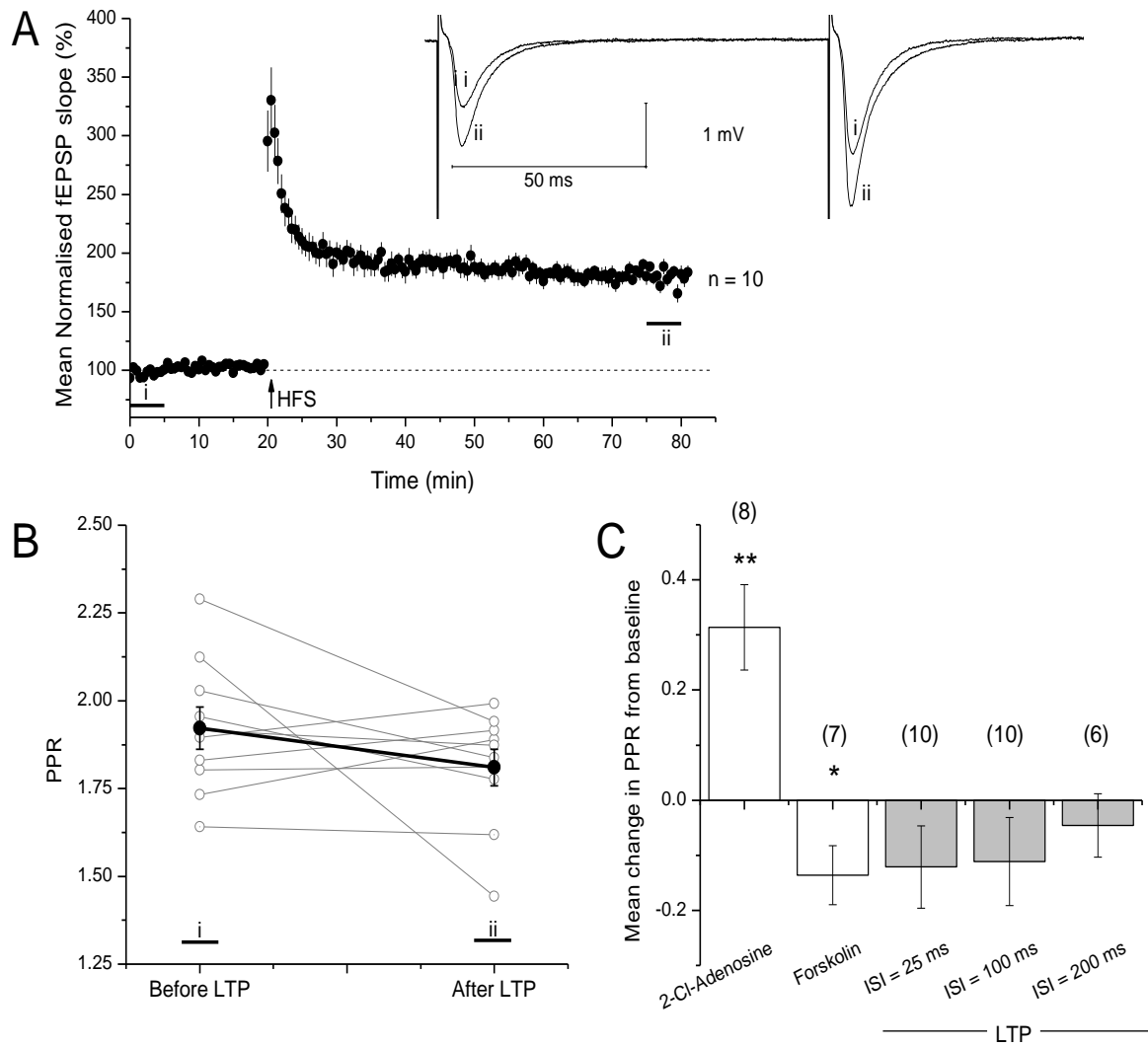


Figure 3.20 Control HFS-induced LTP and PPF. **A**) Paired-stimuli (various ISIs) were delivered before (bar labelled i) and after (bar labelled ii) HFS-induced LTP (LTP measured $179 \pm 6\%$; paired *t*-test, $p = 1.04 \times 10^{-6}$ compared to last 5 min of baseline; $n = 10$). **B**) The mean PPRs (ISI = 100 ms) measured before and after LTP are shown for individual experiments (grey) and on average across all experiments (black). Four slices showed a decrease in PPF and 6 an increase. **C**) Summary showing the average change in PPR following LTP when ISI = 25, 100 or 200 ms. None of the changes were statistically significant (one factor *t*-test, $p > 0.05$ compared to 0). The mean changes in PPR following treatment with $0.5 \mu\text{M}$ 2-Cl-adenosine and $50 \mu\text{M}$ forskolin (ISI = 100 ms; see **Figure 3.17** for full details) are shown for comparison. **: one factor *t*-test, $p < 0.01$ compared to zero change; *: one factor *t*-test, $p < 0.05$ compared to zero.

3.5 Discussion

Under our experimental conditions, LTP at CA1 synapses in hippocampal slices was, in accordance with several previous reports (Collingridge *et al.*, 1983a; Collingridge *et al.*, 1983b; Schuman and Madison, 1991; Bohme *et al.*, 1991; Malenka, 1991; Son *et al.*, 1996; Hopper and Garthwaite, 2006), NMDA receptor- (**Figure 3.3**) and NO-dependent (**Figure 3.4**). The aim of this study was to test the prediction that exogenous NO, paired with a standard LTP induction protocol during NMDA receptor blockade would restore a persistent NO-dependent component of NMDA receptor-dependent LTP. In this way, we sought to isolate the long-lasting NO-dependent component of LTP from other LTP expression mechanisms (such as those observed > 1 hr post HFS in the presence of L-NNA; **Figure 3.4**) and test its locus (pre and/or postsynaptic).

3.5.1 NO-induced potentiation

We report that pairing of the NO donor, PAPA/NONOate, with HFS of Schaffer collateral/commissural fibres in the presence of a NMDA receptor antagonist yielded a long-lasting potentiation of CA1 fEPSPs that we have called ‘NO-induced potentiation’. Surprisingly, given the proposed role of NO in NMDA receptor-dependent LTP, tests of the effect of pairing NO with a standard LTP induction protocol on synaptic efficacy have not been previously reported. Multiple groups have, reported a long-lasting potentiation of activity at CA1 synapses after a sub-threshold tetanus was paired with exogenous NO (Zhuo *et al.*, 1993; Malen and Chapman, 1997; Bon and Garthwaite, 2003). In common with this potentiation, and consistent with the effect of the NOS inhibitor, L-NNA, on HFS-induced LTP (**Figure 3.4**), the NO-induced potentiation that we observed was slowly rising (half-max. ~ 18 min) and, could reach a magnitude similar to HFS-induced LTP (**Figure 3.6**).

Characterisation of the NO-induced potentiation revealed that it shared other properties with the potentiation induced by Bon and Garthwaite (2003) and Zhuo *et al.* (1993), as well as with NO-dependent LTP in general. Firstly, it was found that

the NO-induced potentiation was HFS-dependent and presumably, therefore, pathway-specific (**Figure 3.12**). This would serve to restrict the effects of the exogenous NO to synapses that are active at the same time, thereby allowing NO to participate in Hebbian signalling, rather than as a simple volume transmitter. The dependence of the NO-induced potentiation on HFS suggests that it is dependent upon NMDA receptor-independent, as well as NMDA receptor-dependent mechanisms. Activity presumably provides a pre- and/or postsynaptic signal that primes or tags synapses for potentiation, perhaps by activating a signalling cascade convergent with the NO-cGMP pathway. The signalling cascade that converges with the NO-cGMP pathway might involve CaMKII (**Figure 3.16**), or alternatively, CaMKII may be downstream of NO-cGMP during NO-induced potentiation, as has been suggested by Ninan and Arancio (2004). The signal provided by the HFS appears to be independent of L-VGCC activation (**Figure 3.13**), suggesting that the NO-induced potentiation is distinct from the slowly-rising, NMDA receptor-independent, L-VGCC-dependent LTP that has been described at CA1 synapses (reviewed by Teyler *et al.*, 1995). Other possible sources of Ca²⁺ that may be required for the signal include other VGCCs, metabotropic glutamate receptors and/or intracellular Ca²⁺ stores, all of which have been implicated in LTP (reviewed by Bliss *et al.*, 2007).

Secondly, the NO-induced potentiation was attenuated by NOS antagonism (**Figure 3.14**). This finding was consistent with LTP at CA1 synapses requiring a phasic, neuronal, and tonic, NMDA receptor-independent, endothelial NO signal (Hopper and Garthwaite, 2006; Bartus, 2009).

Third, the NO-induced potentiation was inhibited by NO-targeted guanylyl cyclase-inhibition (**Figure 3.15**). This finding was consistent with the current consensus that physiological NO signal transduction is achieved by NO-targeted guanylyl cyclase activation (reviewed by, Garthwaite, 2008) and with previous reports that NO-dependent LTP is transduced through NO-targeted guanylyl cyclase (for example, Boulton *et al.*, 1995; Lu *et al.*, 1999; Bon and Garthwaite, 2003).

Fourth, the NO-induced potentiation and subsequent HFS-induced LTP were abolished in α CaMKII^{T286A} mice (**Figure 3.16**). This kinase constitutes ~ 1-2 % of total brain protein and co-localises with NMDA receptors at CA1 synapses. Although the kinase is Ca²⁺-activated, autophosphorylation at threonine-286 allows it to maintain activity hours after the dissociation of CaM. The ability of the kinase for autophosphorylation has led to the hypothesis that α CaMKII may play multiple roles in LTP, firstly as a transducer for the Ca²⁺ signal required during LTP induction and secondly as a persistent mechanism for LTP expression (Lisman *et al.*, 2002). Replacement of threonine-286 with alanine (T286A) renders autophosphorylation of the kinase impossible, blocks LTP at CA1 synapses (Giese *et al.*, 1998; Cooke *et al.*, 2006) and delays hippocampus-dependent maze learning (Jarrard, 1993; Giese *et al.*, 1998; Irvine *et al.*, 2005), even though the enzyme's CaM-dependent activity remains intact (Giese *et al.*, 1998). In combination with other evidence (reviewed by Lisman *et al.*, 2002), these findings have led to the view that α CaMKII is a critical for NMDA receptor-dependent LTP. It should be noted that some exceptions to this apply (Cooke *et al.*, 2006), and it could be argued that the deficit in LTP observed in α CaMKII^{T286A} mice is due to secondary effects of the point mutation, since the nervous system has developed without the functional protein. Indeed α CaMKII is required for developmental processes including dendrite morphogenesis and stabilisation (Lisman *et al.*, 2002). Nevertheless, the original characterisation of the α CaMKII^{T286A} mice argues against a major effect on synaptic transmission in CA1 (Giese *et al.*, 1998). Therefore, the lack of NO-induced potentiation in slices from α CaMKII^{T286A} mice suggests that the plasticity is dependent on signalling pathways typically required for 'classical' NMDA receptor-dependent LTP. Interestingly, a study performed using dissociated neurons has suggested that CaMKII may act downstream of NO-cGMP during LTP (Ninan and Arancio, 2004).

The data discussed above are consistent with the hypothesis that pairing of exogenous NO with HFS during NMDA receptor-antagonism should restore the NO-dependent component of LTP, and suggest that the NO-induced potentiation is a useful model for the NO-dependent component of LTP, in isolation of other LTP expression mechanisms. Importantly, the data conflict with (but do not rule out) the possibility that the NO-induced potentiation represents a general change in neuronal

excitability. However, in stark contrast with the potentiation yielded by Zhou *et al.* (1993) and Bon and Garthwaite (2003) after pairing exogenous NO with a sub-threshold tetanus, the NO-induced potentiation that we observed did not occlude subsequent LTP (**Figure 3.7-9**), raising the possibility that the NO-induced potentiation was distinct from the NO-dependent component of LTP, and that pairing of exogenous NO with HFS during NMDA receptor blockade had resulted in more than a simple rescue of the NO-dependent component of LTP.

3.5.2 Relationship between the NO-induced potentiation and HFS-induced LTP

The magnitude of the NO-induced potentiation and of subsequent HFS-induced LTP showed a similar biphasic pattern of dependence upon the concentration of PAPA/NONOate (**Figure 3.7**). A diffusion-inactivation model suggests that application of 3 μM PAPA/NONOate would, under the conditions used, give a concentration in the recording bath of $\sim 0.4 \mu\text{M}$ NO 5 min following application (i.e. during HFS) that would remain stable until wash-out began at 8 min (see **Figure 2.2**). Studies in cerebellar slices estimate that this would give rise to $\sim 1 \text{ nM}$ NO on average in the slice (Hall and Garthwaite, 2006), close to the hypothesised physiological NO concentration at active synapses (Garthwaite, 2008) and in excess of that necessary to cause a physiologically relevant rise in cGMP (see **Chapter 1: General introduction**). Considering that the NO-induced potentiation generated using 3 μM PAPA/NONOate was blocked by ODQ, the increase in magnitude from 0.3 to 3 μM PAPA/NONOate likely reflects increasing NO-targeted guanylyl cyclase stimulation. The decrease in the NO-induced potentiation following the application of higher concentrations (from 3 to 60 μM) could reflect several factors, including guanylyl cyclase de-sensitisation or an increase in PDE 2 or 5 activity through cGMP feedback (Garthwaite, 2008). It could be argued that the decrease in magnitude might reflect a pathological effect of high NO concentrations, for example on mitochondrial respiration, as NO competes with O_2 for cytochrome C oxidase. However, contrary to expectations if metabolism were being inhibited, there was no effect of any NO concentration applied on baseline transmission and it is unlikely

that the concentration of NO generated would be able to compete with physiological O₂ concentrations for binding to cytochrome oxidase C (Bellamy *et al.*, 2002).

Analysis of the relationship between the NO-induced potentiation and subsequent HFS-induced LTP showed that the phenomena were additive (**Figure 3.8**). As discussed in the results section, two main explanations for this effect arose: 1) HFS was not saturating for LTP; 2) the NO/HFS-induced potentiation was mechanistically distinct from HFS-induced LTP. Upon testing of these possibilities, it was found that multiple HFS were necessary to saturate LTP under our conditions (**Figure 3.9**). However, this result could not account for the failure of the NO-induced potentiation to occlude subsequent LTP, since the NO-induced potentiation had no significant effect on the number of HFS required to saturate subsequent LTP. Furthermore, the NO-induced potentiation offset the ceiling magnitude of subsequent HFS-induced LTP (**Figure 3.9**). Rather, the data presented in **Figure 3.9** were consistent with the phenomena being mechanistically distinct.

If the NO-induced potentiation and LTP were mechanistically distinct, it was predicted that pairing of exogenous NO with HFS would result in a potentiation higher in magnitude than control, HFS-induced LTP. However, tests of this possibility revealed no such effect (**Figure 3.10-11**). These results were hard to unite with the finding that the NO-induced potentiation was additive with subsequent LTP, and with the conclusion that the NO-induced potentiation was distinct from LTP. Precedent for such a relationship between a slowly rising potentiation and LTP has previously been reported at CA1 synapses *in vivo* (Li *et al.*, 2007). In this case, a slowly rising potentiation elicited by metabotropic acetylcholine antagonists was found to be additive with subsequent LTP, but occluded if LTP was induced first. The antagonist-induced potentiation was later found to rely upon PKA and PKM ζ (Hayes *et al.*, 2008), but, an explanation for its relationship with tetanus-evoked LTP was not provided.

Several possible reasons for the relationship between the NO-induced potentiation and LTP were considered. A working scheme for HFS-induced LTP that

accommodates all the data is illustrated in **Figure 3.21**. Consistent with current views of LTP expression (Lynch, 2004; Malenka and Bear, 2004; Bliss *et al.*, 2007), the scheme relies upon the assumption that HFS activates multiple signalling cascades that act in concert to generate ‘classical’ LTP. Within the scheme, rapid onset LTP is unstable and decays to baseline over time. Rapid onset LTP is NO-independent but NMDA receptor-dependent. In accordance with the typical effect of NOS inhibition on LTP (for example see **Figure 3.4**), the NO-dependent component of LTP is proposed to be slowly-rising, becoming maximal > 40 min post HFS. This time-course matches that of the NO-induced potentiation, which within the boundaries of this scheme, can be interpreted as representative of the NO-dependent component of HFS-induced LTP. Consistent with results found on pairing of a LTP induction protocol with exogenous NO during NMDA receptor-blockade, the NO-induced potentiation would be generated by activating part of the pathway labelled ‘c’ and all of pathway labelled ‘d’ (and ‘a’) in **Figure 3.21**. The results of our tests of the properties of the NO-induced potentiation (**Figures 3.12-16**) support the possibility that the NO-induced potentiation is representative of the NO-dependent component of LTP.

The expression of both the rapid onset and slowly-rising phases of LTP shown in the scheme rely upon HFS-induced, NMDA receptor-independent signals. This reliance potentially explains why inhibitors of certain NMDA receptor-independent mechanisms inhibit LTP in a manner similar to NMDA antagonists (reviewed by Bliss *et al.*, 2007), and why the NO-induced potentiation necessitates HFS (**Figure 3.12**). Importantly, the pathways contributing to the rapid onset phase of LTP (labelled ‘a’ and ‘b’ in **Figure 3.20**) would determine the amplitude generated by one HFS, as well as the maximum ceiling. This hypothesis accommodates an additive interaction between the NO-induced potentiation and subsequent LTP (**Figure 3.9**), because induction of the NO-induced potentiation would not involve the expression of rapid onset LTP. The hypothesis also explains why exogenous NO paired with HFS fails to effect the magnitude of the resulting LTP (because rapid onset LTP dictates the LTP amplitude; **Figure 3.10-11**).

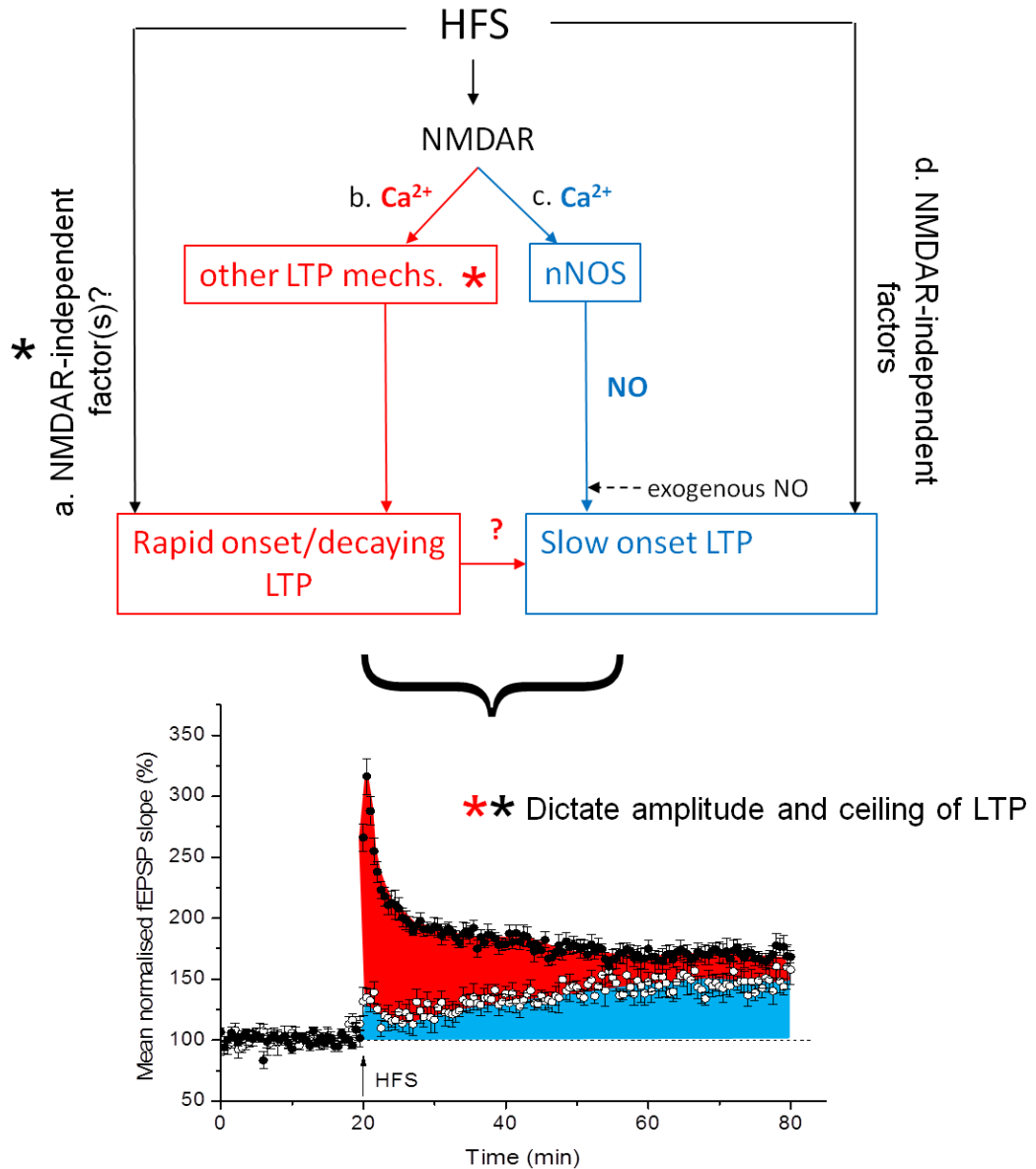


Figure 3.21 Working scheme for the involvement of NO in NMDA receptor-dependent LTP. HFS activates a, b, c and d, and this results in the expression of classical LTP. Both a and b are required for the expression of rapid onset LTP, which is decaying. Both c and d are required for the expression of slow onset, slowly rising LTP. During the induction of the NO-induced potentiation, a, part of c and d are activated, yielding a slowly-rising, NO-dependent component of LTP. Pathways a and b limit the amount of potentiation that can be yielded by one HFS, and dictate the ceiling magnitude of LTP.

NMDAR = NMDA receptor.

An outstanding issue relates to why the NO-induced potentiation we observed did not occlude subsequent LTP, whereas the potentiation induced by pairing a sub-threshold tetanus (ST) with exogenous NO did (Zhuo *et al.*, 1993; Bon and

Garthwaite, 2003). On this point, it is worth noting that even if the NO-induced potentiation characterised in the present study were representative of the NO-dependent component of HFS-induced LTP, we would not expect it to occlude further HFS-induced LTP, because one HFS was not saturating of LTP under our conditions (**Figure 3.9-10**). Given the scheme presented in **Figure 3.21**, a tentative explanation for the results obtained using the ST is that this stimulus failed to activate pathway 'a'. Pathway 'a' could act like a switch for subsequent HFS-induced LTP and determine the magnitude of LTP generated by one HFS. HFS subsequent to pairing exogenous NO with the sub-threshold tetanus would activate pathway 'a' for the first time, enabling the expression of rapid onset LTP. This rapid onset LTP would be equal in magnitude to the potentiation induced by the ST and exogenous NO. Since rapid onset LTP would determine the magnitude of potentiation that can be yielded by one HFS, no further slow onset LTP would be induced, giving the appearance that the potentiation induced by the weak threshold paired with exogenous NO had occluded subsequent HFS-induced LTP.

It should be noted that the scheme outlined in **Figure 3.21** is one of several possible explanations for our data. However, with the exception of a role for eNOS in LTP, the scheme does accommodate all of the data presented in this chapter and in the key literature on the role of NO in NMDA receptor-dependent LTP. Therefore, it may be a useful guide for further tests of the role of NO in the NO-induced potentiation and LTP.

3.5.3 Synaptic locus of the NO-induced potentiation

Given that NO is a putative retrograde messenger during LTP, but that there is little evidence for this at wild-type synapses in intact tissues (see **Table 3.1**), we sought to test the locus (pre- or postsynaptic) of the NO-induced potentiation, a presynaptic effect being consistent with retrograde NO transmission. To do this, the effect of the NO-induced potentiation on PPF, a standard indicator of presynaptic efficacy, was determined. Initially, we sought to measure changes in the PPF of pyramidal neuron EPSCs, using intracellular sharp electrodes, as well as CA1 fEPSPs, because: 1) it was unclear whether significant changes in fEPSP PPF would be detectable; 2)

intracellular recordings are more amenable than extracellular recordings to other measurements of presynaptic efficacy, such as changes in the coefficient of variation of postsynaptic responses (discussed by Korn and Faber, 1991). However, ~ 50 % of intracellular recordings were too short-lasting to allow for experiments to be completed (< 20 min), and although LTP was consistently observed using adjacent field electrodes, ~ 50 % of recorded neurons were incapable of LTP (induction and expression; see **Appendix 1**). One explanation for the lack of LTP in this proportion of cells was that not all pyramidal neurons contribute to the LTP of nearby fEPSPs, and therefore, we conducted experiments using field electrodes only.

To determine whether statistically significant evoked changes in the magnitude of fEPSP PPF could be detected under our conditions, control experiments using 2-Cl-adenosine or the adenylyl cyclase agonist, forskolin, were conducted. Each compound was found to cause a statistically significant change in fEPSP PPF (ISI = 100 ms; **Figure 3.18**). The directions of the changes were consistent with previous findings of the effects of adenosine and forskolin on PPF at CA1 (Dunwiddie and Haas, 1985; Dumas and Foster, 1998; Lu and Gean, 1999; Wu *et al.*, 1999) and other synapses (Kahle and Cotman, 1993; Chen and Regehr, 1997; Chen and Roper, 2003), and on other measures of presynaptic efficacy such as mEPSC frequency (Wu and Saggau, 1994a; Sokolova *et al.*, 2006; Bender *et al.*, 2009). The changes in PPF that were under observed our conditions were accompanied by changes in the slope of the first fEPSP that were similar in magnitude to the NO-induced potentiation. Therefore, it was reasoned that the locus of the NO-induced potentiation could be investigated by its effect on fEPSP PPF.

Contrary to predictions based on work using dissociated hippocampal neurons, which has shown a primarily presynaptic effect of NO following LTP (Arancio *et al.*, 1995; Arancio *et al.*, 1996; Arancio *et al.*, 2001), we observed no significant change in PPF following the NO-induced potentiation (**Figure 3.19**). Considering the results of our control experiments, which showed that a significant change in PPF could be detected under our conditions following ~ 50 % changes in fEPSP initial slope (**Figure 3.18**), there were two different explanations for the lack of a significant change in PPF following the NO-induced potentiation: 1) the potentiation was

primarily postsynaptic (see **Chapter 1: General introduction** for examples of postsynaptic NO-dependent plasticity); 2) the NO-induced potentiation relied upon coordinated pre- and postsynaptic effects which yielded no net observable change in the probability of presynaptic neurotransmitter release and/or number of release sites. Given current estimates of the spread of NO through tissues (see **Chapter 1: General introduction**), NO is well-placed to affect plasticity at both sides of the synapse, and could do so almost simultaneously. Consistent with NO acting on both sides of the synapse, studies of LTP at synapses between dissociated hippocampal neurons have shown that the activation of the NO/cGMP/PKG pathway elicits a rapid (within 1-10 min) increase in pre- and postsynaptic clusters (Antonova *et al.*, 2001; Wang *et al.*, 2005). Nikonenko *et al.* (2003) also report that theta burst stimulation of Schaffer collateral/commissural fibres in hippocampal slice cultures yields NO-dependent synaptogenesis in area CA1 with a time-course similar to that of the NO-induced potentiation (occurring within 10-30 min).

It should also be noted that our PPF analysis raises the issue that the role of NO in LTP at synapses between dissociated neurons may not be directly applicable to the role of NO in LTP at synapses in intact tissues. As discussed in **3.1 Introduction**, a lack of eNOS in neuronal cultures may give rise to differences in NO-dependent synaptic plasticity at synapses between dissociated cells, compared to plasticity at cells in intact tissues.

Finally, the lack of a significant change in PPF following HFS-induced LTP (**Figure 3.20**), though consistent with some other studies of the effect of CA1 LTP on PPF (Schulz *et al.*, 1994), and suggestive of the NO-induced potentiation being representative of the NO-dependent component of LTP, is discordant with the effect of NO-dependent CA1 LTP on PPF reported by some groups (Taqatqeh *et al.*, 2009). The difference between our results and those of other groups could arise from subtly different experimental conditions or from the use of different protocols to induce LTP (HFS vs. TBS). Indeed, the induction protocols used to generate LTP are known to affect the expression mechanisms recruited (Raymond, 2007). Alternatively, the difference could reflect the different time points relative to LTP induction at which PPF is sampled. Taqatqeh *et al.* (2009) sampled PPF 2 min post TBS, whereas we

tested for persistent presynaptic effects by measuring PPF 55-60 post HFS. On this point, it should be noted that the after-effects of PTP, which is distinct from LTP (Zucker and Regehr, 2002) and lasted ~ 2 min under Taqatqeh *et al.*'s conditions, may have confounded their PPF analysis.

3.6 Conclusion

Consistent with the proposed role for NO in NMDA receptor-dependent LTP, pairing of exogenous NO with HFS in the presence of D-AP5 was found to elicit an enduring potentiation of activity at CA1 synapses. This NO-induced potentiation shared several properties with classical, control LTP and with a potentiation yielded at CA1 synapses by pairing a sub-threshold tetanus with exogenous NO (Bon and Garthwaite, 2003; Zhuo *et al.* 1993). However, in contrast with the plasticity observed by Bon and Garthwaite (2003) and Zhuo *et al.* (1993), the NO-induced potentiation that we observed was additive with LTP. This raised the possibility that the NO-induced potentiation might be distinct from the NO-dependent component of LTP. Unfortunately, our data leave this possibility open. However, our data led to the generation of a scheme (**Figure 3.21**) for NO-dependent, HFS-induced LTP that accommodates the current literature on the role of NO in LTP, and may be a useful guide for the generation of further testable hypotheses. The scheme assumes that the NO-induced potentiation is representative of the NO-dependent component of LTP, and if correct, this implies that the NO-induced potentiation is a useful correlate for persistent NO-dependent potentiation in isolation of other LTP expression mechanisms.

The mechanisms underlying the NO-induced potentiation, and the NO-dependent component of LTP, require further investigation. The slow rise time of the NO-induced potentiation, as well as other forms of NO-dependent plasticity (for example, Bon and Garthwaite, 2003; Phillips *et al.*, 2008), and the slow effect of NOS inhibition on HFS-induced LTP, are consistent with an expression mechanism that is slow to take effect. As outlined above, one reported outcome of NO-dependent plasticity that has an appropriate time-course is the synthesis of new synapses. This,

or a combination of changes on both sides of the synapse, could explain the lack of effect of the NO-induced potentiation, and HFS-induced LTP, on PPF.

Chapter 4:

Modulation of basal synaptic efficacy by NO in area CA1 of the hippocampus

4.1 Introduction

NO signalling has been linked to the expression of activity-dependent synaptic plasticity (see **Chapter 3**). Most research has focused on the role of NO in NMDA receptor-dependent LTP at CA1 synapses in the hippocampus, a plasticity that is usually induced by high frequency (100 Hz) or theta burst stimulation (Bliss *et al.*, 2007). In contrast, the potential for endogenous NO to modulate the efficacy of 'naive' synapses (i.e. where no attempt has been made to induce long-lasting plasticity) undergoing 'basal' stimulation (i.e. that causes no observable change in synaptic efficacy) has received little attention.

Recently, it was reported by Taqatqeh *et al.* (2009) that the magnitude of PPF (ISI = 20-50 ms) of EPSCs at 'naive' CA1 synapses undergoing 'basal' stimulation (0.033 Hz) is larger in hippocampal slices from mice lacking the NO-targeted guanylyl cyclase $\alpha 1$ subunit than in slices from wild-type mice. As discussed in the previous chapter, PPF can be explained by an increase in the probability of neurotransmitter release (reviewed by Zucker and Regehr, 2002; Bliss *et al.*, 2007) caused by residual axonal Ca^{2+} (Wu and Saggau, 1994b) or a related mechanism, such as the saturation of a Ca^{2+} buffer (Rozov *et al.*, 2001). Therefore, one interpretation of the finding made by Taqatqeh *et al.* (2007) is that, at wild-type synapses under basal conditions, there is less scope for an increase in the probability of neurotransmitter release during PPF because neurotransmitter release is tonically facilitated by a NO/ $\alpha 1$ -containing NO targeted guanylyl cyclase/cGMP pathway.

Consistent with this, direct measurements of the efflux of various neurotransmitters, such as glutamate, GABA and dopamine, from brain areas including the hypothalamus and corpus striatum have been reported to be subject to increase or decrease by exogenous NO or NOS inhibitors, respectively (reviewed by Prast and Philippu, 2001). Regarding the hippocampus, the NO donors, sodium nitroprusside (10-30 mM) and hydroxylamine (1-300 μM), have been found to increase the basal efflux of radiolabelled noradrenaline and ACh from slices (Lonart *et al.*, 1992). Brief applications of more physiological concentrations of exogenous NO (5-10 nM; O'Dell *et al.*, 1991) or a cGMP analogue (50-100 μM 8-Br-cGMP; Arancio *et al.*,

1995) to dissociated hippocampal neurons have been also been found to cause an increase in the frequency, independent of the amplitude, of miniature EPSCs, consistent with an increase in the efficacy of neurotransmitter release (Bliss *et al.*, 2007).

The mechanisms underlying NO-dependent or -induced increases in neurotransmitter release are unclear. However, some research links NO to the modulation of resting neuronal excitability in brain areas including the visual cortex and hypothalamus by the modulation of targets such as voltage-gated K^+ , HCN and CNG channels. This may shape the presynaptic action potential and thereby effect neurotransmitter release (reviewed by Garthwaite, 2008; Steinert *et al.*, 2010). Long-term regulation of basal neurotransmitter release by NO might also occur via the regulation of the number of functional release sites, since it has also been reported that application of an NO donor (150 μ M DETA/NOONOate, 2 days) or cGMP analogue, 8-Br-cGMP (5 mM, 2 days), to hippocampal slice cultures causes an increase in the proportion of multiply-innervated spines in area CA1. Conversely, chronic NOS inhibition (using 200 μ M L-NAME, 2 days) was found to reduce synapse density (Nikonenko *et al.*, 2008). Alternatively, the mechanisms may be similar to those underlying NO-dependent, activity-dependent increases in neurotransmitter release (see previous chapter, **Table 3.1**).

The notion that basal synaptic efficacy might be facilitated by endogenous NO raises questions over the isoform(s) of NOS involved. It is unclear whether nNOS, which is thought to be preferentially activated by NMDA receptor opening (Garthwaite, 2008), is spontaneously active at synapses or whether it can become activated during basal stimulation such as that used by Taqatqeh *et al.* (2009; 0.033 Hz). However, it is well-known that eNOS can become Ca^{2+} - and consequently activity-independent upon phosphorylation by kinases, most notably protein kinase Akt (Fulton *et al.*, 2001). Although endothelial NOS is expressed solely in blood vessels (Stanarius *et al.*, 1997; Blackshaw *et al.*, 2003; Chan *et al.*, 2004), it is estimated that central neurons are $\sim 25 \mu$ m (equivalent to \sim one cell diameter) at most from a capillary (Pawlik *et al.*, 1981). Early work on the physiology of endothelium-derived NO was focused on its synthesis in endothelial cells upon innervations by cholinergic nerves

and subsequent diffusion to smooth muscle to affect vasodilation (Furchgott and Martin, 1985). However, a study using optic nerve has now set a precedent for NO signalling from blood vessels to nerves in the CNS (Garthwaite *et al.*, 2006), the effect being the tonic depolarisation of axons. Moreover, an activity-independent, eNOS-dependent low-level NO tone has been discovered in the hippocampus and found to influence the expression of LTP in area CA1. These findings have generated the hypothesis that eNOS may prime synapses for activity-induced plasticity (Hopper and Garthwaite, 2006), perhaps, we speculate, by providing a prerequisite level of synaptic efficacy.

4.1 Aim

The possibility that endogenous NO might regulate the basal efficacy of CA1 synapses is by itself intriguing and may also have far-reaching implications for our understanding of the role of NO in activity-dependent plasticity. Nevertheless, adequate tests of the effect of endogenous NO on basal synaptic efficacy in the hippocampus are lacking. Musleh *et al.* (1993) have reported that the non-selective NOS inhibitor, N-methyl-L-arginine (L-NMA; 125 μ M), has no effect on the magnitude of PPF at CA1 synapses in adult rat hippocampal slices. Yet it is known that L-NMA can become hydroxylated *in situ* and metabolised by NOS, resulting in the formation of amino acid products, including L-arginine, several of which are capable of activating NOS (Olken and Marletta, 1993).

Given the above, we investigated whether endogenous NO could modulate the efficacy of basal neurotransmission at CA1 synapses in intact tissues (containing both e- and nNOS), and, if so, aimed to test the potential involvement of each NOS isoform present.

4.2 Methods

4.2.1 Animals

Unless otherwise stated, 6-8-week-old male C57Bl/6 mice were used (Charles River, Margate, UK). Male, 6-9-week-old, 129sv/C57Bl/6 transgenic mice lacking functional eNOS (eNOS^{-/-}; Huang *et al.*, 1995) were kindly provided by Dr Adrian Hobbs (UCL, London, UK).

4.2.2 Transverse hippocampal slice preparation and electrophysiology

Transverse hippocampal slices were prepared as detailed in **Chapter 2.2.2**. Electrophysiological activity at Schaffer collateral/commissural-CA1 synapses was recorded extracellularly using the methods described in **Chapter 2.2.3**. Pairs of stimuli were delivered to Schaffer collateral/commissural fibres at 0.033 Hz at a stimulus intensity set to 40-50 % of that required to elicit a population spike. The ISI was 10 or 100 ms. PPF of CA1 fEPSPs was measured using the PPR (the initial slope of fEPSP 2/the initial slope of fEPSP 1; **Figure 4.1**). Drugs were delivered through the perfusion system. In all figures, fEPSP slopes have been normalised to the mean slope of fEPSP 1 during the first 10 min of baseline recording shown (in the absence of any drugs). In each experiment, baseline measurements of PPR were made over 5 min immediately prior to the application of drugs. To avoid sample bias, PPR in the presence of L-NNA, ODQ and D-AP5 was measured 30-35, 15-20 and 10-15 min respectively following their application. These times were chosen based on the duration that each drug was applied to slices prior to HFS in the experiments shown in the previous chapter.

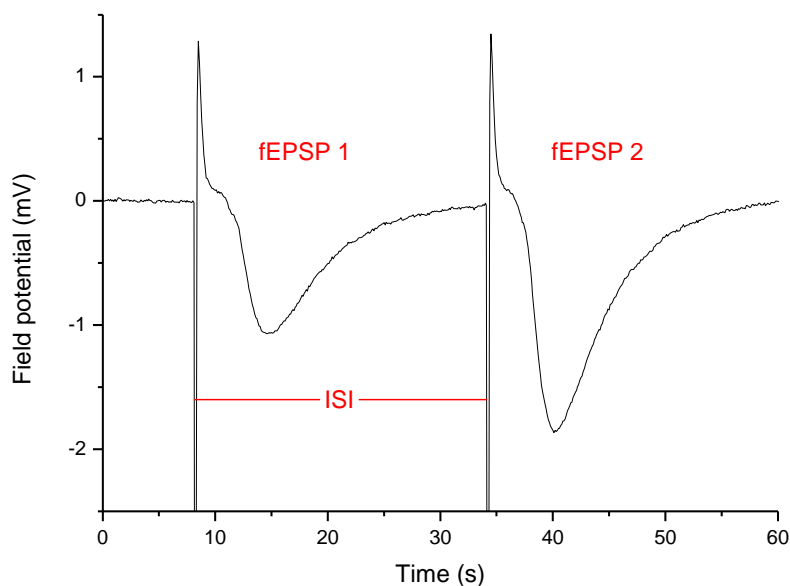


Figure 4.1 A typical example of PPF. CA1 synapses were stimulated twice in quick succession (ISI = 25 ms in this example). This resulted in the temporary facilitation of the second fEPSP (fEPSP 2).

4.3.3 Genotyping of eNOS^{-/-} mice

Mice lacking functional eNOS due to the insertion of a neomycin (NEO) cassette in the eNOS gene (eNOS^{-/-}; see Huang *et al.*, 1995) were genotyped by PCR and gel electrophoresis. Briefly, lysates were prepared from samples of mouse tail using proteinase K (see **Chapter 2.2.6** for further detail). Hot-start PCR was performed using ‘GoTaq Hot Start polymerase’ (Promega) and primers for wild-type eNOS and a NEO cassette (**Table 4.1**).

| Primer | Sequence 5'-3' | Stock Concentration (pmol/μl) |
|--------------|-------------------------------|-------------------------------|
| eNOS forward | GGT GTT TGG CTG CCG ATG C | 2 |
| eNOS reverse | GCA CAG CAC ACG GTG AAC C | 2 |
| NEO forward | GCA TAC GCT TGA TCC GGC TAC C | 1.5 |
| NEO reverse | GAA GGC GAT GCG CTG CGA ATC | 1.5 |

Table 4.1 PCR primers used for genotyping eNOS^{-/-} mice.

Each PCR and gel included a negative control, in which the DNA sample was replaced with double-distilled H₂O, and a positive control containing DNA from an

age-, sex- and strain-matched wild-type mouse (obtained from Harlan, Wyton, UK) prepared under identical conditions as the transgenic samples. A DNA ladder (1 μ l, 100 base pairs ladder, Promega) was also run on each gel. DNA for a NEO cassette, but not for wild-type eNOS could be detected in PCR products of eNOS^{-/-} lysates. DNA for wild-type eNOS but not for a NEO cassette could be detected in PCR products of wild-type lysates (**Figure 4.2**).

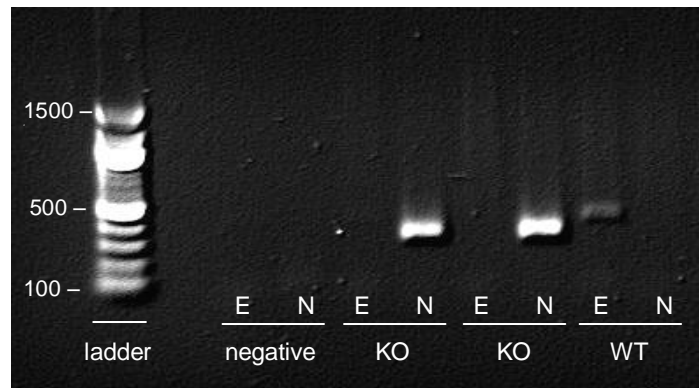


Figure 4.2 Genotyping wild-type and eNOS^{-/-} mice. PCR products were electrophoresed in a 2 % agarose gel and visualised under UV light. A typical gel is shown in which the lanes were filled with PCR products of a negative control containing no DNA (negative), eNOS^{-/-} lysates (KO) and a wild-type lysate (WT) amplified using eNOS (E) and NEO cassette (N) primers. Bands of the ladder are labelled in base pairs. Note that the first lane after the ladder was empty.

4.3.4 Analysis and Statistics

Unless otherwise stated, values quoted in the text are means \pm SEM. In each figure, inset traces represent the mean fEPSPs recorded at the time indicated by the colour coded bars. For clarity, the stimulus artefacts of the representative fEPSPs have been truncated. Two-tailed t-tests were used to assess whether differences between data sets were statistically significant.

Results

4.4.1 Effect of endogenous NO on PPF at naive CA1 synapses

To test the hypothesis that NO modulates the efficacy of naive CA1 synapses during basal stimulation, we investigated the effect of endogenous NO on the magnitude of PPF of CA1 fEPSPs in hippocampal slices. It is predicted that, following any manipulation of synaptic efficacy that results in an increase in the probability of neurotransmitter release, the scope for further increase during PPF will be reduced, and, therefore, a decrease in the magnitude of PPF will be observed (measured using the PPR; the initial slope of the second fEPSP/ the initial slope of the first fEPSP; Zucker and Regehr, 2002; Bliss *et al.*, 2007). The results of previous experiments showed that statistically significant, evoked changes in PPF could be detected under our conditions (see experiments using 2-Cl-adenosine and forskolin, **Figure 3.18**).

Pairs of stimuli were delivered to slices at 0.033 Hz and the effect of the non-selective NOS inhibitor, L-NNA (100 μ M, 30 min), on the magnitude of the resulting PPF (measured using the PPR) was tested (see **Figure 4.3A** for the time course of experiments). In order to determine whether any changes in the PPR were consistent when PPF was induced using different ISIs, and because the magnitude of basal PPF reported in mice lacking the α 1 NO-targeted guanylyl cyclase subunit deviated most from wild-type PPF at short ISIs (< 50 ms; Taqatqeh *et al.* 2010), experiments were conducted using an ISI of 100 ms (as in the experiments detailed in **Figure 3.18**) and 10 ms.

When PPF was continuously elicited at 0.033 Hz, the PPR was stable and there was no effect on the initial slope of fEPSP 1 (see baseline in **Figure 4.3A**). Application of the non-selective NOS inhibitor, L-NNA, caused a significant increase in the mean PPR (measured 30-35 min after the application of L-NNA) relative from that measured over the last 5 min of baseline prior to L-NNA application (**Figure 4.3B-D**). This was observed whether the ISI was 100 or 10 ms (change in PPF when ISI was 10 ms: 0.19 ± 0.04 ; one factor t-test, $p = 0.00144$ compared to zero change; $n = 10$; change in PPF when ISI was 100 ms: 0.12 ± 0.05 ; one factor t-test, $p = 0.0487$

compared to zero change; $n = 10$). This increase in PPR was observed in the majority of individual experiments, although a decrease was observed in 1 of 10 slices when the ISI was 10 ms (**Figure 4.3B**), and two of ten slices when the ISI was 100 ms (**Figure 4.3C**).

To assess whether the effect of L-NNA could be reversed by exogenous NO, the NO donor, PAPA/NONOate (10 μ M, 10 min) was co-applied with L-NNA. On average, the PPR measured in the presence of PAPA/NONOate and L-NNA was not significantly different from that measured in the presence of L-NNA alone (**Figure 4.3B-D**; ISI = 10 ms: paired t-test, $p = 0.708$; ISI = 100 ms: paired t-test, $p = 0.537$).

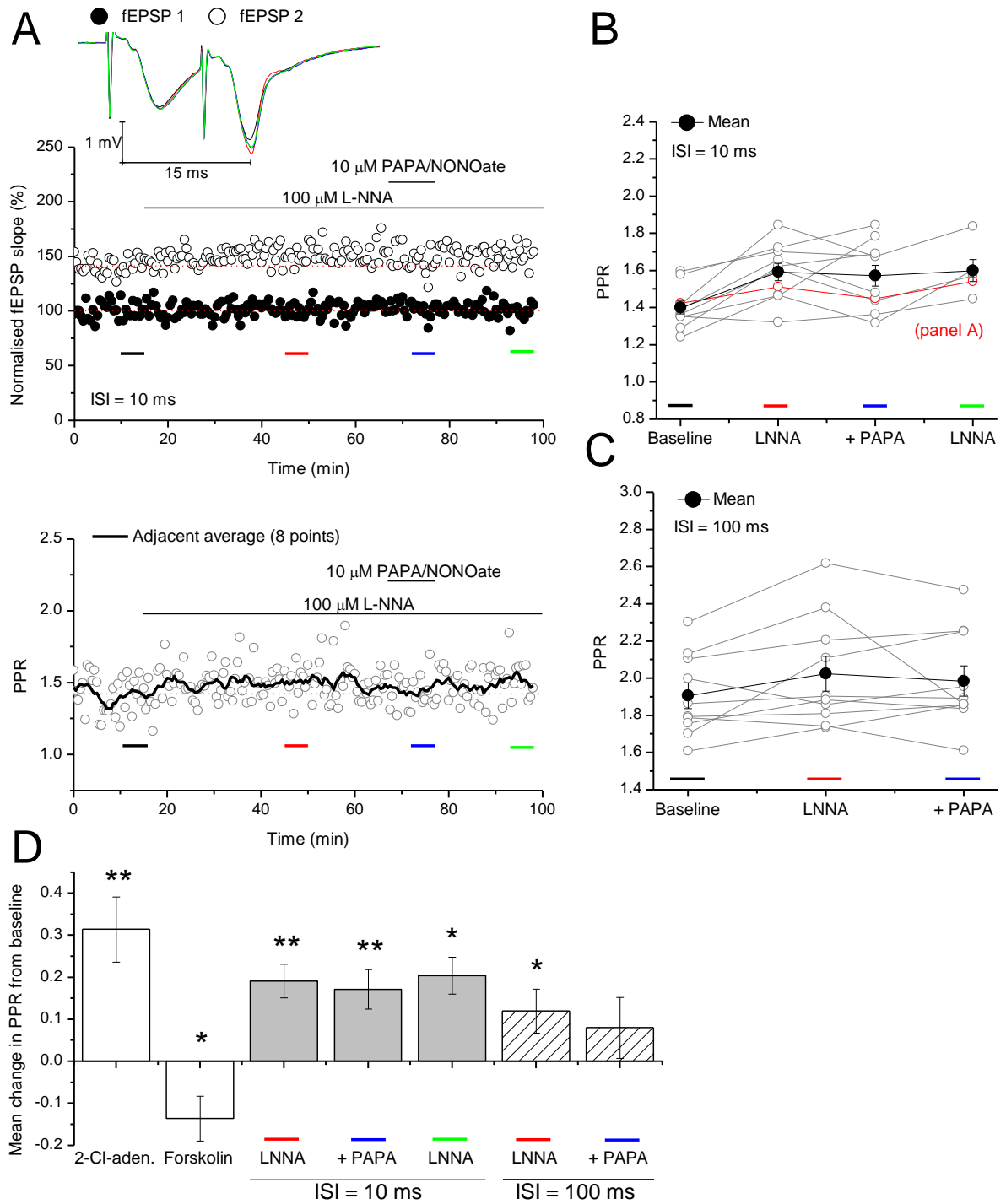


Figure 4.3 Involvement of endogenous NO in basal PPF. **A**) The time-course of a typical experiment is illustrated. Pairs of stimuli (ISI = 10 or 100 ms) were delivered to slices every 30 s and the initial slopes of fEPSP 1 and 2 (upper panel) and the PPR (lower panel) were continuously monitored. The general NOS inhibitor, L-NNA (100 μ M), and the NO donor, PAPA/NONOate (10 μ M) were applied at the times indicated. The red dashed lines in each figure show the mean fEPSP slope or PPR recorded prior to L-NNA application. **B-C**) The mean PPRs recorded at the times indicated by the colour-coded bars in A during individual experiments (grey) and on average (black) are plotted (B:

*ISI = 10 ms; C; ISI = 100 ms; n = 10). The data drawn in red in B were collected from the experiment shown in A. D) The mean changes in the PPR from baseline (black bar in A-C) measured during the application of L-NNA (red bar A-C), L-NNA and PAPA/NONOate (blue bar A-C), and where tested, after PAPA/NONOate wash-off (green bar A-B; n = 5) are illustrated. The effects of 0.5 μ l 2-Cl-adenosine and 50 μ l forskolin on mean PPR (ISI = 100 ms) are shown for comparison (see **Figure 3.18** for full details of the experiments using these compounds). One factor t-test, $p = ** < 0.01$, $* < 0.05$ compared to zero change.*

4.4.2 Effect of NO-targeted guanylyl cyclase activity on PPF at naive CA1 synapses

The effect of L-NNA on the magnitude of PPF was consistent with the hypothesis that endogenous NO facilitates basal synaptic activity at CA1 synapses. Since physiological NO transduction is thought to be NO-targeted guanylyl cyclase- and cGMP-dependent (reviewed by Garthwaite, 2008), we next sought to determine whether the effect of L-NNA could be mimicked by the NO-targeted guanylyl cyclase antagonist, ODQ (10 μ M).

Figure 4.4A illustrates the time-course of a typical experiment. As in experiments using L-NNA, CA1 synapses received paired stimuli (ISI = 10 or 100 ms) at 0.033 Hz. Following the establishment of a stable baseline of responses, ODQ (10 μ M) was applied. The PPR was measured 15-20 min later and compared to the baseline PPR measured over the last 5 min of baseline prior to ODQ application.

In accordance with the effect of L-NNA on PPF, and regardless of the ISI used, ODQ caused a significant increase in the mean PPR from baseline (ISI = 10 ms: 0.08 ± 0.02 ; one factor t-test, $p = 0.0097$ compared to zero change; $n = 10$; ISI = 100 ms: 0.07 ± 0.03 ; one factor t-test, $p = 0.0225$ compared to zero change; $n = 11$; **Figure 4.4D**). This increase was observed in the majority of the slices tested; however some slices did not follow this trend. When the ISI was 10 ms, PPR increased in 9 slices but decreased in 1 slice (**Figure 4.4B**). When the ISI was 100 ms PPR increased in 9 slices and decreased in 2 slices (**Figure 4.4C**).

It should be noted that the increase in mean PPR from baseline caused by ODQ was smaller than that caused by L-NNA (**Figures 4.4D**), and, when the ISI was 10 ms, this trend was statistically significant (ISI = 10 ms: unpaired t-test, $p = 0.0303$; $n = 10$; ISI = 100 ms: unpaired t-test, $p = 0.375$; $n = 10-11$).

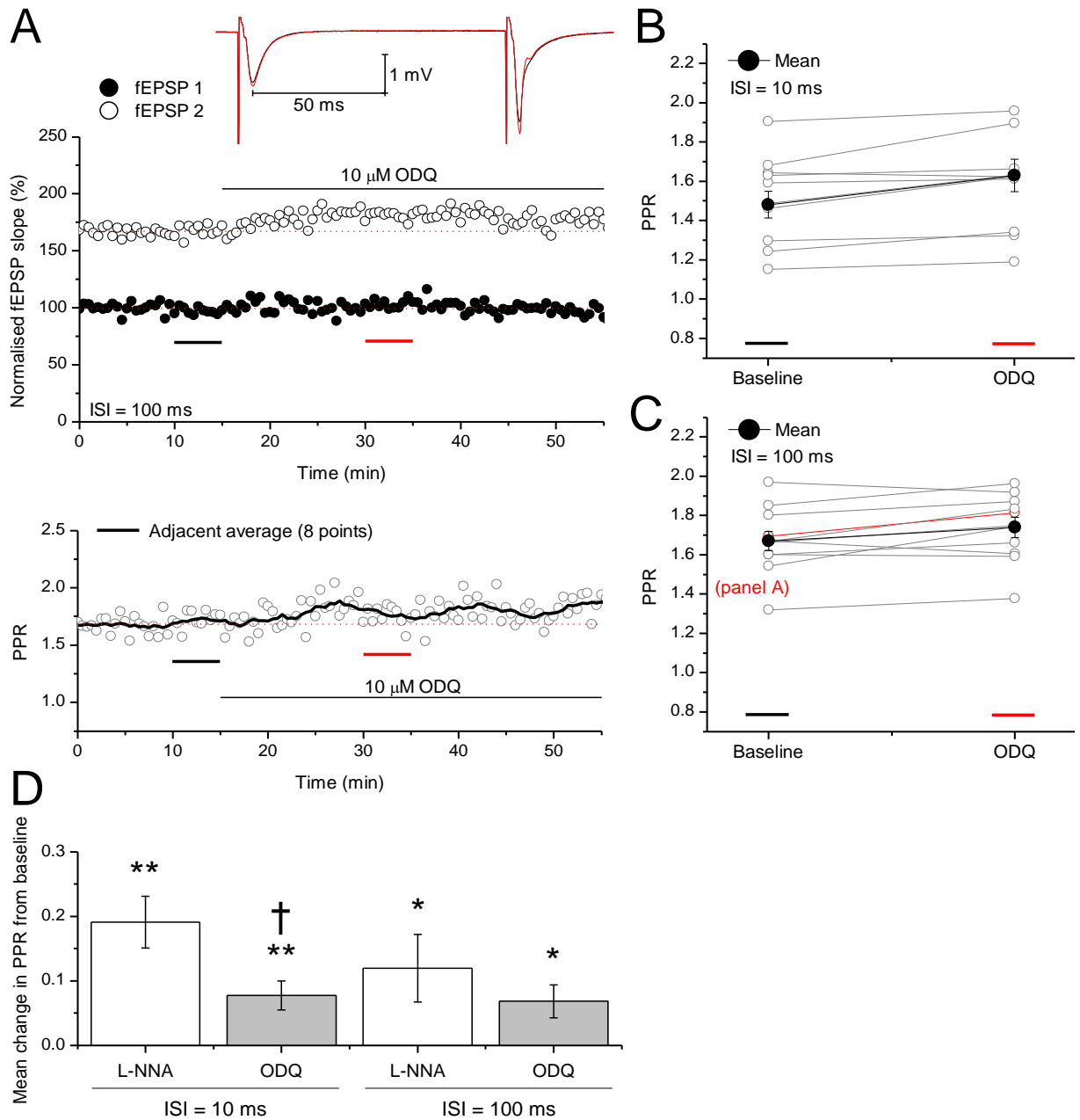


Figure 4.4 Contribution of NO-targeted guanylyl cyclase to basal PPF. **A**) The time-course of a typical experiment is shown. Paired stimuli (ISI = 10 or 100 ms) were delivered to slices every 30 s and the initial slopes of fEPSP 1 and 2 (upper panel) and the PPR (lower panel) were continuously recorded. The NO-targeted guanylyl cyclase antagonist, ODQ (10 μ M) was applied at the time

indicated. The red dashed lines in each figure show the mean fEPSP slope or PPR recorded prior to ODQ application. **B-C**) The mean PPRs recorded at the times indicated by the colour-coded bars in A during individual experiments (grey) and on average (black) are plotted. The red data in C correspond to the experiment in A. **D**) Summary of the mean change in PPR from baseline (black bar in A-C) caused by ODQ (red bar; A-C; $n = 10-11$). The effect of L-NNA on the mean PPR is shown for comparison (see **Figure 4.3** for full details). One factor t-test, $p = ** < 0.01$, $* < 0.05$ compared to zero change. Unpaired t-test, $p = † < 0.05$ compared to the mean change in PPR from baseline caused by L-NNA in experiments using the same ISI.

4.4.3 Isoform of NOS involved in the regulation of PPF by endogenous NO

Like the NOS inhibitor, L-NNA (**Figure 4.3**), the NO-targeted guanylyl cyclase antagonist, ODQ, caused a significant increase in the magnitude of PPF at naive CA1 synapses (**Figure 4.4**). As previously discussed (see **Chapter 1**), two constitutively expressed isoforms of NOS, endothelial and neuronal, are present in the hippocampus. Both are thought to be required for the expression of NO-dependent LTP at CA1 synapses, although they may provide distinct activity-dependent, phasic (neuronal) and activity-independent, tonic (endothelial) NO signals (Hopper and Garthwaite, 2006).

To elucidate the NOS isoform(s) underlying the effect of L-NNA and ODQ on PPF at naive synapses, and therefore characterise the nature of the NO signal involved, the experiment illustrated in **Figure 4.3** (using L-NNA) was repeated using slices prepared from eNOS^{-/-} mice (see **Figure 4.5A**). In contrast to the effect of L-NNA on PPF at wild-type synapses (**Figure 4.3**), L-NNA had no significant effect on the average magnitude of PPF at eNOS^{-/-} synapses. The mean change in PPR from baseline following L-NNA application was 0.02 ± 0.04 (one factor t-test, $p = 0.665$ compared to zero change; $n = 9$; **Figure 4.B**) when the ISI was 10 ms and 0.05 ± 0.04 (one factor t-test, $p = 0.536$ compared to zero change; $n = 9$; **Figure 4.5D**) when the ISI was 100 ms. Accordingly, the mean change in PPR from baseline evoked by L-NNA was smaller in transgenic compared to wild-type slices, and when the ISI was 10 ms (though not 100 ms), this was statistically significant (ISI = 10 ms:

unpaired t-test, $p = 0.00897$; $n = 9-10$; ISI = 100 ms: unpaired t-test, $p = 0.0993$; $n = 9-10$; **Figure 4.5D**).

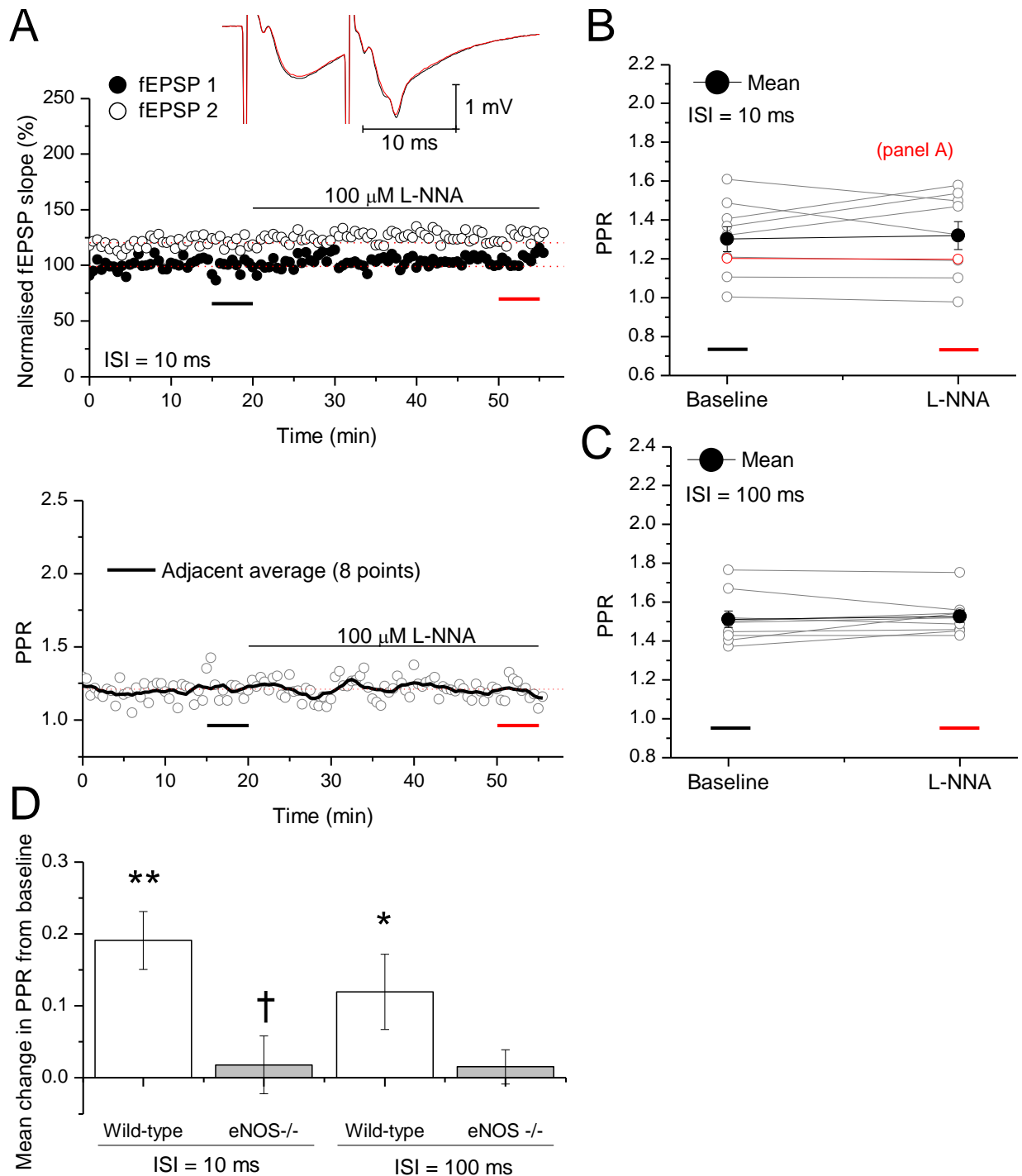


Figure 4.5 Effect of NOS inhibition on the magnitude of PPF in slices from $eNOS^{-/-}$ mice. A) The time-course of a typical experiment is shown. Paired stimuli (ISI = 10 or 100 ms) were delivered to slices every 30 s and the initial slopes of fEPSP 1 and 2 (upper panel) and the PPR (lower panel) were continuously monitored. The general NOS inhibitor, L-NNA (10 μ M) was applied at the time

indicated. The red dashed lines in each figure show the mean fEPSP slope or PPR recorded prior to L-NNA wash-on. B-C) The mean PPRs recorded at the times indicated by the colour-coded bars in A during individual experiments (grey) and on average (black) are plotted. The red data in B were collected during the experiment shown in A. D) Summary of the mean change in PPR from baseline (black bar in A-C) caused by L-NNA (red bar; A-C; $n = 9$) in $eNOS^{-/-}$ mice, and, for comparison, wild-type C57Bl/6 mice (see **Figure 4.3**). One factor t -test, $p = ** < 0.01$, $* < 0.05$ compared to zero change. Unpaired t -test, $p = † < 0.01$ compared to the change in wild-type mice in experiments using the same ISI.

The above findings were consistent with eNOS providing the entire NO responsible for the regulation of basal PPF at naive CA1 synapses. However, it should be noted that, in contrast with the proposed role of eNOS in regulating basal PPF, the mean basal (baseline) PPR was significantly lower in slices from $eNOS^{-/-}$ compared to wild-type mice when the ISI was 100 ms (baseline PPR in $eNOS^{-/-}$ mice vs. baseline PPR shown in **Figure 4.3-4**: unpaired t test, $p = 0.0042$), although not when the ISI was 10 ms (unpaired t -test, $p = 0.140$). This could be explained by natural variation, or if a compensatory mechanism also responsible for the regulation of basal PPF were acting at synapses in slices from $eNOS^{-/-}$ mice. Alternatively the discrepancy in PPF between slices might be explained by strain differences between the $eNOS^{-/-}$ and wild-type mice. Unfortunately, the prevailing lack of eNOS inhibitors (Alderton *et al.*, 2001) meant that the role of eNOS could not be directly tested in wild-type mice. Likewise, no reliable means of testing the effect of nNOS on PPF are available because the best characterised nNOS-deficient mice express active splice variants in the hippocampus (Eliasson *et al.*, 1997), and our recent results show that supposed nNOS inhibitors are inadequately selective to be of use diagnostically (**Chapter 6**). Therefore, based on the assumption that, in brain, nNOS is preferentially stimulated by NMDA receptor activity (Garthwaite, 2008), we used the NMDA receptor antagonist, D-AP5, to test the involvement of the NMDA receptor-nNOS pathway in modulating basal neurotransmitter PPF (see **Figure 4.6A**).

As shown in **Figure 4.6**, D-AP5 (50 μ M; pre-applied for 10 min) had no significant effect on the average magnitude of PPF when the ISI was 10 ms (-0.07 ± 0.09 ; one factor t -test, $p = 0.928$ compared to zero change; $n = 9$; **Figure 4.6D**) or 100 ms (0.12 ± 0.10 ; one factor t -test, $p = 0.264$ compared to zero; $n = 8$; **Figure 4.6D**).

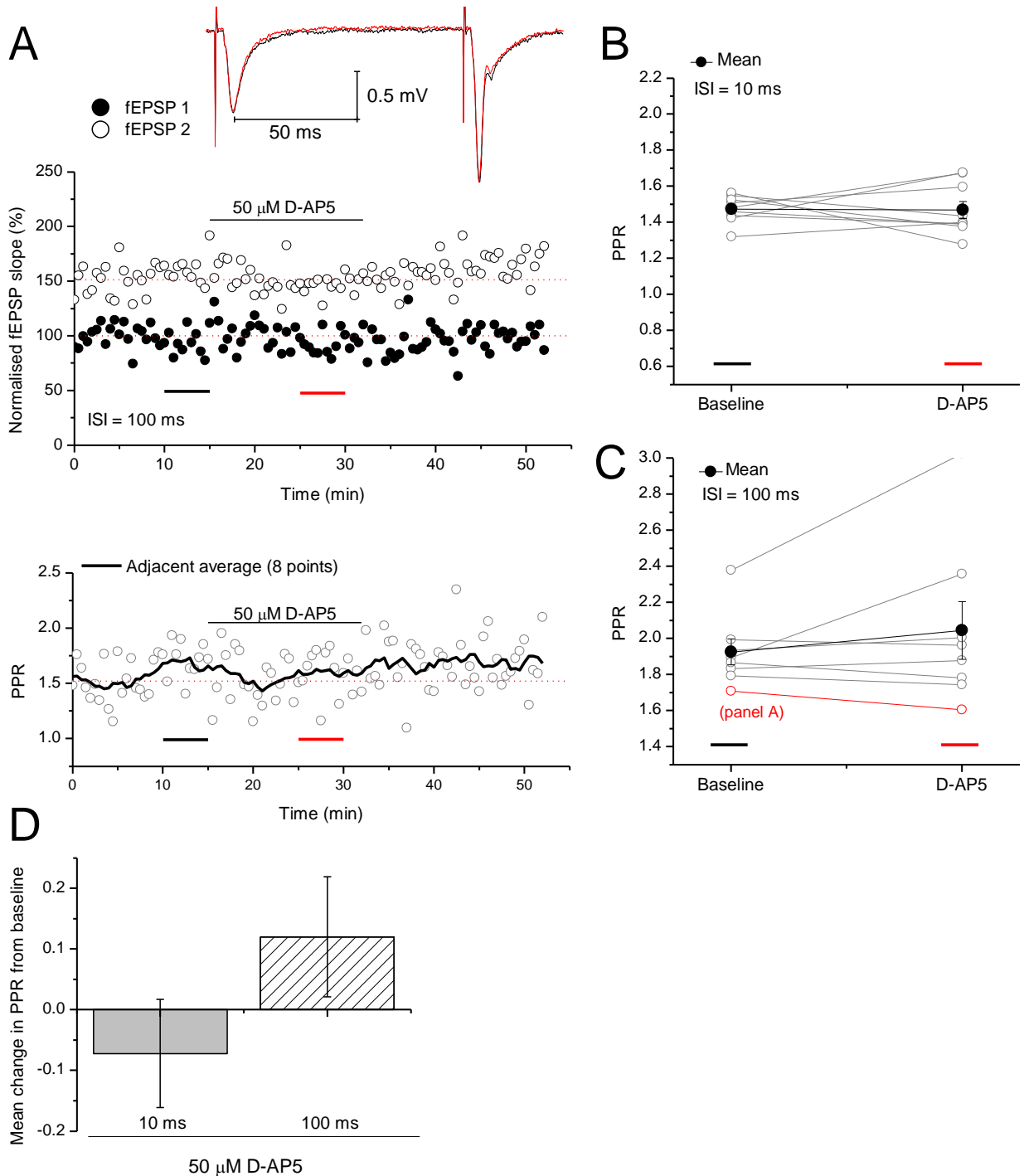


Figure 4.6 NMDA receptor-dependency of basal PPF in wild-type mice. **A**) The time-course of a typical experiment is shown. Paired stimuli ($ISI = 10$ or 100 ms) were delivered to slices every 30 s and the initial slopes of fEPSP 1 and 2 (upper panel) and the PPR (lower panel) were continuously recorded. The NMDA receptor antagonist, D-AP5 ($50 \mu\text{M}$) was applied at the time indicated. The red dashed lines in each figure show the mean fEPSP slope or PPR recorded prior to perfusion with D-AP5. **B-C**) The mean PPRs recorded at the times indicated by the colour-coded bars in A during individual experiments (grey) and on average (black) are plotted. The red data in C are from the

experiment in A. D) Summary of the mean change in PPR from baseline (black bar in A-C) caused by D-AP5 (red bar in A-C; n =8- 9).

4.3 Discussion

Under many, though not all conditions, NO is required for the expression of long-lasting, activity-dependent plasticity, in particular NMDA receptor-dependent LTP at CA1 synapses (Garthwaite, 2008). Some studies of the effect of exogenous NO or NO-targeted guanylyl cyclase $\alpha 1$ subunit knock-out on neurotransmitter release from hippocampal neurons have also suggested that endogenous NO, via cGMP, might regulate the basal efficacy of CA1 synapses, through the up-regulation of neurotransmitter release (O'Dell *et al.*, 1991; Lonart *et al.*, 1992; Arancio *et al.*, 1995; Taqatqeh *et al.*, 2009).

Here, we report that superfusion of hippocampal slices with the NOS or NO-targeted guanylyl cyclase antagonists, L-NNA (100 μ M) or ODQ (10 μ M), caused a significant increase in PPF of fEPSPs in area CA1 (**Figure 4.3-4**). The increase in PPF could not be mimicked by inhibition of NMDA receptors, suggesting that the NMDA receptor-nNOS pathway (**Figure 4.6**) was not involved in the basal regulation of PPF. However, the effect of L-NNA was abolished in slices lacking functional eNOS (**Figure 4.5**). This finding was against the possibility that the rise in PPF observed in experiments using L-NNA and ODQ was the effect of a general increase in basal PPF over time (for example, caused by baseline drift).

These findings are in accordance with the facilitation of neurotransmitter release at naive CA1 synapses under basal conditions by endogenous NO/cGMP and, although tests of the involvement of each NOS isoform present were limited, with the conclusion that eNOS provides all the NO necessary for the regulation of basal synaptic efficacy. (Note that our data cannot exclude the influence of NMDA receptor-independent nNOS activity). It was found that L-NNA and ODQ caused an increase in PPF in C57/Bl6 mice when the ISI was both short (10 ms) and long (100 ms; **Figure 4.3-4**). Because the duration of inhibitory postsynaptic potentials (IPSPs) measured at CA1 synapses under our conditions using sharp intracellular electrodes

was < 100 ms (for an example trace see **Appendix 1**), it seems unlikely that the changes in PPF caused by L-NNA and ODQ were the result of changes in the inhibitory input to pyramidal neurons. However, GABAergic transmission was not blocked in these studies and therefore, endogenous NO might have been acting at inhibitory and/or excitatory synapses on pyramidal cells to regulate neurotransmitter release under basal conditions. It should be noted that at CA1 synapses in slices from mice lacking the NO-targeted guanylyl cyclase $\alpha 1$ subunit, PPF was significantly increased from that recorded in slices from wild-type mice only when the ISI was < 50 ms (Taqatqeh *et al.*, 2009). However, an insignificant increase in PPF was observed by Taqatqeh *et al.* when the ISI was 100 ms and it is possible that if paired statistical analysis were permitted, this would become a significant increase.

At the time of this investigation, Neitz *et al.* (2011) published the results of a series of experiments also aimed at determining the effect of endogenous NO on basal synaptic efficacy at naive CA1 synapses in hippocampal slices. They also focused on the potential presynaptic effects of NO. In accordance with the effects of L-NNA and ODQ on the magnitude of PPF observed in the present study, Neitz *et al.* (2011) found that the frequency, but not the amplitude, of AMPA receptor-mediated miniature EPSCs was reduced in area CA1 of mice lacking the NO-targeted guanylyl cyclase $\alpha 1$ subunit. The reduction in frequency was reversed by application of the cGMP analogue, 8-Br-PET-cGMP (100 μ M), and replicated in slices from wild-type mice upon L-NNA or ODQ application. Concordant effects of NO-targeted guanylyl cyclase $\alpha 1$ subunit knock-out and ODQ on the frequency of minimally evoked EPSCs and magnitude of EPSC PPF were also found. The effects on miniature EPSC frequency were replicated by the HCN channel blocker, ZD7288 (10 μ M), suggesting that NO, via cGMP and the regulation of I_h might facilitate neurotransmitter release by enhancing axon depolarisation, as in the optic nerve (Garthwaite *et al.*, 2006).

To address the question of which NOS isoform was responsible for maintaining a reduced PPF at synapses in slices from wild-type mice, Neitz *et al.* (2011) used the supposedly isoform selective nNOS inhibitor, L-VNIO (0.1 μ M). They found no effect of 0.1 μ M L-VNIO on miniature EPSC frequency and therefore, concluded

that eNOS, but not nNOS, was responsible for the modulation of basal synaptic efficacy in area CA1. While our data support this conclusion, our recent findings strongly suggest that L-VNIO was completely ineffective in inhibiting NOS at the concentration used by Neitz *et al.* (**Chapter 6**).

Apart from the experiments using L-VNIO, the results of Neitz *et al.* (2011) clearly add strength to the conclusions that can be drawn from our study, in which the effect of endogenous NO on only one indicator of synaptic efficacy was assessed. Nevertheless, there are at least three points that need to be addressed to clarify the effect of endogenous NO on basal synaptic efficacy at naive CA1 synapses.

Firstly, in our study, the mean change in PPR from baseline caused by ODQ was significantly smaller than that caused by L-NNA when the ISI was 10 ms, and therefore experiments are necessary to elucidate the source of this difference (**Figure 4.4**). It is unlikely that this reflects a difference between the potencies of L-NNA and ODQ, since the concentrations of each inhibitor that were used (100 μ M and 10 μ M, respectively) are considered to be supra-maximal for enzyme inhibition. Furthermore, we have found that both inhibitors abolish cGMP accumulation in our hippocampal slices in response to maximal doses of NMDA (see **Chapter 5**). It also seems unlikely that the difference reflects the involvement of guanylyl-cyclase-independent NO signalling, since almost all physiological NO signals are transduced by cGMP (Garthwaite, 2008). Rather, the most parsimonious explanation is natural variation, especially considering that Neitz *et al.* (2011) report that the effects of L-NNA and ODQ on miniature EPSC frequency were comparable and that, as is typical of evoked changes in PPR (for example Schulz *et al.*, 1995), the amplitude of the change in PPF that we observed was small and highly variable. This may also explain why eNOS knock-out caused a significant change in PPR compared to wild-type PPR when the ISI was 10, but not 100 ms (**Figure 4.3**).

Secondly, the finding that the NO donor, PAPA/NONOate (10 μ M, applied for 10 min), could not reverse the effect of L-NNA on PPF (**Figure 4.3**) is seemingly at odds with the facilitation of basal synaptic activity by endogenous NO. It seems unlikely that the effect of L-NNA on PPF can be attributed by an effect other than

NOS inhibition, since no secondary targets of L-NNA are known (Alderton *et al.*, 2001) and, consistent with the effect of ODQ on PPF, NMDA-induced cGMP accumulation in hippocampal slices treated with L-NNA can be reconstituted by exogenous NO (Bartus, 2009). Therefore, investigations are necessary to determine whether a longer application and/or different concentration of exogenous NO is required to reverse the effect of L-NNA on PPF. Regarding this possibility, it is interesting to note that the NO-induced potentiation described in the previous chapter was induced during NMDA receptor (and therefore presumably nNOS) antagonism but was inhibited by L-NNA and ODQ (see **Figures 3.6** and **3.13-14**), suggesting that the exogenous NO used to induce it (3 or 10 μ M PAPA/NONOate, applied for 8 min in total) was not sufficient to mimic completely the endogenous NO profile.

Finally, it should be also be noted that as with most parameters used to define the locus of changes in synaptic efficacy, including those used by Neitz *et al.* (2011), evidence provided by PPF analysis is suggestive rather than conclusive. Typically, changes in the magnitude of PPF are explained by changes in the probability of presynaptic release and/or number of release sites (reviewed by Zucker and Regehr, 2002; Bliss *et al.*, 2007), and all the data presented in this study, as well as the studies discussed above, are consistent with NO acting on a presynaptic target to effect the modulation of basal synaptic efficacy. Furthermore, immunohistochemistry and *in situ* hybridisation studies suggest that the α 1 NO-targeted guanylyl cyclase subunit is presynaptic in area CA1 (Szabadits *et al.*, 2007; although see **Chapter 7**). However, a change in postsynaptic efficacy could account for our results, as well as those of the above studies, if, for example, NOS inhibition caused the internalisation of postsynaptic receptors and this was favoured at synapses with a high probability of release, as during LTD at CA1 synapses (Bliss *et al.*, 2007). On this point, it should be noted that HCN channels appear to be predominantly postsynaptic in area CA1 (Notomi and Shigemoto, 2004).

4.4 Conclusion

Clearly, further experiments are necessary to clarify the effect of endogenous NO on the efficacy of naïve CA1 synapses, especially because effect sizes yielded from PPF

analysis are typically small and highly variable. Certain caveats of the data also limit the strength of the conclusions that can be drawn from our study, for example, the inability of exogenous NO to reverse the effect of L-NNA on PPR. However, the potential role of eNOS and NO in the modulation of basal synaptic efficacy in area CA1 does extend the finding that NO derived from blood vessels influences axons in the optic nerve (Garthwaite *et al.*, 2006), and suggests a novel role for the eNOS-derived NO tone discovered in the hippocampus (Chetkovich *et al.*, 1993; Hopper and Garthwaite, 2006). As discussed above, it has been hypothesised that eNOS primes CA1 synapses for LTP (Hopper and Garthwaite, 2006) and it is conceivable that this could occur via the setting of a prerequisite, basal level of neurotransmitter release (or postsynaptic quantal amplitude). Indeed, homeostatic mechanisms are thought to be critical in maintaining the ability of synapses and networks to be both up- and down-regulated in response to varying stimuli (Pozo and Goda, 2010), and the potential involvement of eNOS in this links NO to metaplasticity (reviewed by Abraham, 2008).

The requirement of basal synaptic efficacy and LTP expression for eNOS in area CA1 complicates the interpretation of NO-dependent LTP between dissociated pyramidal neurons, since blood vessels are unlikely to be present in neuron cultures. This lack of eNOS could explain why Arancio *et al.* (1995; 1996; 2001) found that NO-dependent LTP at synapses between pairs of dissociated neurons was presynaptic, whereas the NO-induced potentiation described in the previous chapter was not accompanied by a persistent decrease in PPF. For example, it is possible that the increase in transmitter release that was observed by Arancio *et al.* was caused because the NO necessary for the LTP had compensated for a lack of eNOS, or because the baseline probability of neurotransmitter release was unnaturally low. Indeed, it is well-known that the magnitudes of PPF recorded under basal conditions and following LTP are inversely correlated (Schulz *et al.*, 1995). Accordingly, Serulle *et al.* (2007) have found that neither NOS nor NO-targeted guanylyl cyclase antagonism alters the magnitude of PPF in dissociated hippocampal neurons.

Finally, it should be noted that endothelium-derived NO is unlikely to be the only mechanism capable of regulating PPF at CA1 synapses, since baseline PPF (in the

absence of any drugs) was not significantly increased in eNOS^{-/-} slices (**Figure 4.5**). In fact, baseline PPF was significantly decreased in slices from eNOS^{-/-} compared to wild-type mice when the ISI was 100 ms. If eNOS is truly responsible for the regulation of basal synaptic efficacy at CA1 synapses, it is also likely to affect synaptic transmission at other synapses, since eNOS and guanylyl cyclase are expressed throughout the brain (; eNOS: Seidel *et al.*, 1997; Stanarius *et al.*, 1997; Topel *et al.*, 1998; Demas *et al.*, 1999; NO-targeted guanylyl cyclase: Matsuoka *et al.*, 1992; Gibb and Garthwaite, 2001; Ding *et al.*, 2004). It is tempting to speculate that, in a situation where NO derived from blood vessels influences neurons and vice versa (reviewed by Garthwaite, 2008), changes in blood flow, basal neuronal efficacy and the probability of plasticity might be coordinated. As well as the physiological implications of this, it is conceivable that disordered NO signalling might contribute to pathologies characterised by anomalous network or synaptic efficacy, such as hippocampal epileptogenesis, which may result from the increase in neuronal excitability of CA3 neurons capable of generating recurrent bursts of activity (Walker *et al.*, 2007), or central sensitisation (a processes likened to LTP) of noiceceptive synapses in the spine (Ji *et al.*, 2003).

Chapter 5:

**NO and NMDA receptor-independent, L-type voltage-gated
Ca²⁺ channel-dependent LTP**

5.1 Introduction

Ca^{2+} influx to cells via NMDA receptors plays a central role in the induction of LTP, and this has been particularly well-studied in the hippocampus at CA1 synapses (see **Chapter 3**). However, LTP cannot be entirely explained by NMDA receptor-dependent mechanisms. In fact, forms of NMDA receptor-independent LTP have been discovered throughout the nervous system (for example, see Nicoll and Schmitz, 2005), including at CA1 synapses (Grover and Teyler, 1990). If, as is currently thought, a rise in intracellular Ca^{2+} is an absolute requirement for LTP (Lynch *et al.*, 1983; Malenka *et al.*, 1988; Grover and Teyler, 1990), then an NMDA receptor-independent mechanism of increasing intracellular Ca^{2+} is necessary to explain some types of long-lasting synaptic plasticity.

5.1.1 L-type Voltage Gated Ca^{2+} Channels

L-type voltage-gated Ca^{2+} channels (L-VGCCs) may represent one mechanism for increasing intracellular Ca^{2+} during NMDA receptor-independent LTP. L-VGCCs are high-voltage activated (typically half-maximally activated between ~ -20 to 10 mV), heteropentameric transmembrane channels (see **Figure 5.1**), that can be delineated from other VGCCs (named N, P/Q, R and T) by their slow inactivation kinetics ($\tau \sim 5$ to 30 ms) and inhibition by dihydropyridines, phenylalkylamines and benzothiazepines (Catterall *et al.*, 2009).

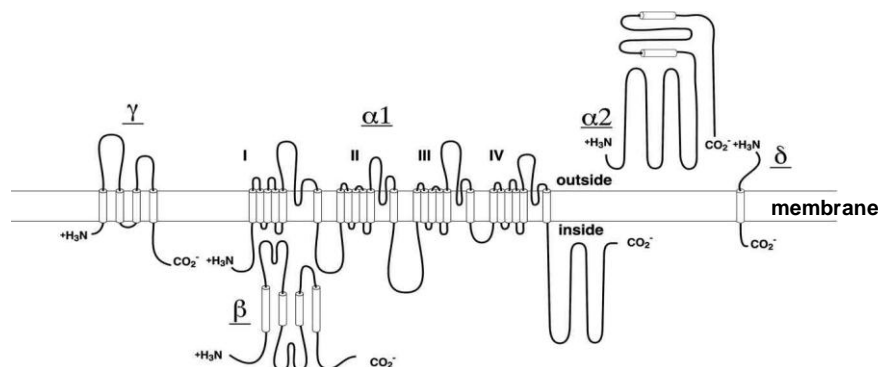


Figure 5.1 Predicted subunit structure and composition of L-VGCCs based on channels purified from skeletal muscle. The γ subunit may only be present in skeletal muscle (Catterall, 2000). The cylinders

depict predicted α -helices and lengths of lines approximate lengths of polypeptide segments. Diagram taken from Catterall et al. (2005). Reproduced by kind permission of ASPET journals.

The $\alpha 1$ L-VGCC subunit forms the pore of the channel and contains the voltage sensor, the selectivity filter and antagonist binding sites. On its own, the $\alpha 1$ subunit is capable of forming a functional channel (Perez-Reyes *et al.*, 1989; Striessnig, 1999), although other subunits (see **Figure 5.1**) may influence its cell surface targeting, electrophysiological properties and stability of the channel.

So far, four subtypes of the $\alpha 1$ subunit have been discovered (Ca_v1.1-1.4; **Table 5.1**). These subtypes vary in their electrophysiological properties (kinetics and voltage-dependency of activation and inactivation and channel conductance), tissue distribution and physiology. This diversity is reflected in the myriad physiological processes and pathologies that L-VGCCs have been implicated in, which range from smooth muscle contraction, blood pressure regulation and hypertension (Ozawa *et al.*, 2006) to neurotransmitter release and the modulation of neuronal excitability (Lacinova *et al.*, 2008), pain sensitisation (Park and Luo, 2010), psychiatric disorders (Casamassima *et al.*, 2010), Alzheimer's disease (Anekonda *et al.*, 2011) and epilepsy (N'Gouemo *et al.*, 2010).

| Class | Antagonists | Subtype | Subtype localisation | Subtype function(s) |
|--------------|---|---------------------|---|---|
| L | Dihydropyridines; phenylalkylamines; benzothiazepines | Ca _v 1.1 | Skeletal muscle | Muscle contraction |
| | | Ca _v 1.2 | Cardiac and smooth muscle; endocrine cells; neurons (soma and dendrites) | Muscle contraction, hormone secretion, neurotransmission, gene transcription, synaptic plasticity, learning, memory |
| | | Ca _v 1.3 | Cardiac muscle; pacemaker cells; endocrine cells; cochlear hair cells; neurons (soma and dendrites) | Smooth muscle contraction, hormone secretion, neurotransmission |
| | | Ca _v 1.4 | Retinal rod and bipolar cells; mast cells; adrenal gland | Neurotransmission |
| N | ω-conotoxins | Ca _v 2.2 | Neurons (axons and dendrites); neuroendocrine cells | Neurotransmission, hormone release |
| P/Q | ω-agatoxins | Ca _v 2.1 | Neurons (axons and dendrites); neuroendocrine cells | Neurotransmission, hormone release |
| R | SNX-482 | Ca _v 2.3 | Neurons (soma and dendrites) | Neurotransmission |
| T | Ni ²⁺ Flunarizine Mibefradil Ethosuximide | Ca _v 3.1 | Neurons (soma and dendrites); cardiac and smooth muscle | Pacemaking, repetitive firing. |
| | | Ca _v 3.2 | Neurons (soma and dendrites); cardiac and smooth muscle | Pacemaking, repetitive firing. |
| | | Ca _v 3.3 | Neurons (soma and dendrites) | Pacemaking, repetitive firing. |

Table 5.1 Summary of the pharmacological properties, tissue distribution and function of L-VGCC subtypes. Different subtypes contain different $\alpha 1$ subunits. Information for N-, P/Q-, R- and T-type VGCCs are given for comparison. Like L-VGCCs, N-, P/Q- and R-VGCCs are high voltage activated. T-type VGCCs are low voltage activated. Adapted from Catterall *et al.* (2009).

In the hippocampus, where radioligand binding has shown the Ca_v1.2 subtype to predominate (Clark *et al.*, 2003), L-VGCC subunits appear to be densely expressed

in the membrane of pyramidal cell soma and at the base of apical dendrites. Subunits have also been detected histologically in granule cells, interneurons and at synapses in more distal dendrites of pyramidal neurons, particularly in area CA3 (Ahlijanian *et al.*, 1990; Westenbroek *et al.*, 1990; Hell *et al.*, 1993). They may be activated by back-propagating somatic action potentials and/or EPSPs (Mermelstein *et al.*, 2000), and, like NMDA receptors, have been demonstrated to cause significant intradendritic Ca^{2+} influx to pyramidal neurons. Fura-2 measurements in hippocampal slices, for example, show that L-VGCCs contribute ~ 30 % of the whole-cell Ca^{2+} current during spiking (Regehr and Tank, 1992; Christie *et al.*, 1995) and this is in agreement with estimates made using electrophysiological recordings from dissociated pyramidal neurons (Mermelstein *et al.*, 2000). Following step depolarisations to negative voltages (-30 mV) designed to approximate the effect of an EPSP, the contribution of L-VGCCs to the total Ca^{2+} current was found to increase to ~ 50 % (Mermelstein *et al.*, 2000). L-VGCC activity is also thought to contribute to the resting intracellular Ca^{2+} concentration of pyramidal neurons (Magee *et al.*, 1996), neuronal excitability in response to depolarising pulses (Lacinova *et al.*, 2008), and has been implicated in hippocampal synaptic plasticity, learning and memory (see below).

5.1.2 L-VGCC-dependent LTP at CA1 synapses

Following 200 Hz- or prolonged theta burst stimulation of hippocampal Schaffer collaterals *in vitro*, a high magnitude ‘compound’ LTP has been observed at CA1 synapses that is composed of two pharmacologically-separable components: one blocked by NMDA receptor-antagonism, the other independent of NMDA receptor blockade but attenuated by L-VGCC inhibitors (Grover and Teyler, 1990; Grover and Teyler, 1994; Cavus and Teyler, 1996; Morgan and Teyler, 2001). Similar findings have been made *in vivo* (Morgan and Teyler, 1999), and L-VGCC inhibitors have also been reported to attenuate spike timing-dependent potentiation (Fuenzalida *et al.*, 2010), as well as CA1 LTP induced by various other stimuli (Aniksztejn and Ben-Ari, 1991; Kato *et al.*, 1993; Huang and Malenka, 1993; Impey *et al.*, 1996).

Like NMDA receptor-dependent LTP, L-VGCC-dependent LTP has been reported to be input-specific, blocked by Ca^{2+} chelators (Grover and Teyler, 1992), induced postsynaptically and yet expressed on both sides of the synapse (Grover, 1998; Bayazitov *et al.*, 2007). While some studies indicate that the expression mechanisms underlying L-VGCC-dependent LTP may be shared with NMDA receptor-dependent LTP (for example, Little *et al.*, 1995), several indicate that L-VGCC- and NMDA receptor-dependent LTP are, at least in part, mechanistically distinct. For example, using synapto-pHlourin to continuously monitor presynaptic vesicle recycling in area CA1, it was found by Bayazitov *et al.* (2007) that the L-VGCC-dependent component of compound LTP induced using 200 Hz burst stimulation was slow to start ($t_{1/2} \sim 35$ min), partly presynaptic and long-lasting (of \sim maximal magnitude at least 3 hr post induction). Conversely, the NMDA receptor-dependent component was found to be almost immediate, largely postsynaptic and, although clearly evident 3 hr post-induction, was not of maximal magnitude over this time.

The difference in the onset of NMDA receptor- and L-VGCC-dependent LTP has also been observed electrophysiologically (for example, Grover and Teyler, 1990) and the distinction between their synaptic loci is supported by studies using FM-143 to monitor presynaptic plasticity (Zakharenko *et al.*, 2001; Zakharenko *et al.*, 2003). Using a spatially-restricted brain-derived neurotrophic factor (BDNF) knock-out mouse, Zakharenko *et al.* (2003) also identified BDNF release from CA3 neurons as critical for L-VGCC-dependent, but not NMDA receptor-dependent LTP at CA1 synapses. This was in accordance with a previous report showing that the expression of the BDNF receptor, tyrosine kinase B (TrkB), is up-regulated following L-VGCC, but not NMDA receptor-dependent LTP (Teyler *et al.*, 1994), and has since been supported by evidence that TrkB is necessary for 200 Hz burst stimulation-induced LTP (Gruart *et al.*, 2007).

The persistent expression of L-VGCC-dependent but not NMDA-receptor dependent LTP noted by Bayazitov *et al.* (2007) also accords with other data showing that L-VGCCs, but not NMDA receptors, are necessary for CA1 late-LTP and cAMP response element (CRE)-mediated β -galactosidase expression induced by multiple 100-Hz tetani in hippocampal slices (Impey *et al.*, 1996). L-VGCC activation has

also been reported to be critical for activity-dependent gene expression in cortical neurons (Murphy *et al.*, 1991) and glutamate-induced, CRE-regulated transcription in hippocampal neurons (Bading *et al.*, 1993). Indeed, several authors have hypothesised that the dense expression of L-type channels at the base of dendrites makes them likely candidates for the transduction of distal dendritic activity to the soma where alterations in gene expression may occur (for example, Westenbroek *et al.*, 1990). Further, the requirement of late-LTP for L-VGCC's may explain why more stringent induction protocols than those needed for NMDA receptor-dependent early-LTP are necessary for its induction and expression.

5.1.3 Physiological relevance of L-VGCC-dependent LTP

In the past, it has been suggested that, because L-VGCCs are typically high voltage-activated (Catterall *et al.*, 2009), the natural occurrence of L-VGCC-dependent long-lasting plasticity may be restricted to pathological conditions such as epileptogenesis during which cell excitability may become supra-physiological (Huang and Malenka, 1993). Since then, however, L-VGCCs have been shown to account for a significant proportion (30-50 %) of the whole cell Ca^{2+} current of pyramidal neurons following stimulation designed to mimic dendritic EPSPs, as well as spikes (Regehr and Tank, 1992; Christie *et al.*, 1995; Mermelstein *et al.*, 2000) and it has been ventured by Morgan and Teyler (1999) that the activation requirements for L-VGCC-dependent long-lasting plasticity *in vitro* may be met in nature by short, aperiodic, high-frequency (200 Hz), high-magnitude (1-3 mV) sharp waves (population EPSPs) produced by Schaffer collaterals that project onto CA1 neurons and interneurons. Furthermore, pharmacological, electrophysiological and behavioural evidence has combined to show that L-VGCC and NMDA receptor dependent plasticity may have distinct functions, modulating different aspects of memory. For example, it has been reported that, while systemic injection of the NMDA receptor antagonist, MK-801, inhibits rats' ability to acquire memory of an eight-arm radial maze, which is a hippocampus-dependent task (Jarrard, 1993), the L-VGCC inhibitor, verapamil, and not MK-801, inhibits long term (7-10 days) retention of the memory (Borroni *et al.*, 2000; Woodside *et al.*, 2004). Injection with both drugs during the task training blocks all acquisition and retention.

It should be noted that other studies in the hippocampus have failed to find an effect of L-VGCC inhibition on memory retention/consolidation, and that some research has found L-VGCC inhibition to enhance spatial memory formation, although these effects are most common when learning and memory is already compromised (reviewed by Casamassima *et al.*, 2010). Research surrounding the issue of whether fear extinction in amygdala is L-VGCC dependent has also highlighted the problems of interpreting data following systemic injection of L-VGCC inhibitors, which can have multiple indirect effects on learning and memory through, for example, actions on locomotor activity and cerebral blood flow (Schafe, 2008). Nevertheless, temporally-restricted knock-out of Ca_v1.2 in the hippocampus and neocortex has been reported to result in a selective loss of NMDA receptor-independent LTP at Schaffer collateral/commissural-CA1 synapses and a gross impairment in performance of spatial learning (maze) tasks (Kleppisch *et al.*, 2004; Moosmang *et al.*, 2005a; Moosmang *et al.*, 2005b). Deletion of Ca_v1.3, which accounts for ~ 20 % of L-VGCCs present in the hippocampus, has not been found to effect NMDA receptor-independent LTP at CA1 synapses (Clark *et al.*, 2003), although it has been reported to attenuate LTP in the lateral amygdala and to severely limit the consolidation of fear conditioning (McKinney and Murphy, 2006; McKinney *et al.*, 2009).

5.1.4 NO and L-VGCC-dependent LTP

Previously, it was noted that L-VGCC-dependent LTP follows a similar time course to HFS-dependent, NO-induced potentiation (see **Chapter 3**) and to other slowly-rising forms of NO-dependent LTP observed at CA1 synapses. Using nifedipine (30 μM), it was found that the HFS-dependent, NO-induced potentiation did not rely on L-VGCCs, either for induction or expression. However, the involvement of NO in L-VGCC-dependent LTP at CA1 synapses remained untested.

As a freely diffusible and putative retrograde transmitter, the involvement of NO in L-VGCC-dependent LTP could reconcile previous results showing that L-VGCC-dependent LTP is postsynaptically induced (Grover, 1998), yet, at least in part, presynaptically expressed (Bayazitov *et al.*, 2007). Indeed it has been previously

hypothesised that a retrograde messenger must be necessary for L-VGCC-dependent LTP (Bayazitov *et al.*, 2007). Furthermore, NO-dependent LTP has been shown to rely on similar mechanisms to L-VGCC-dependent LTP. For example, NO/cGMP is also necessary for late-LTP and activity-induced CREB phosphorylation at CA1 synapses (Lu *et al.*, 1999). Evidence that NO- and BDNF-dependent LTP rely on common mechanisms has also recently been reported (Lessmann *et al.*, 2011).

5.2 Aim

Given the above, we sought to determine whether NO is necessary for L-VGCC-dependent LTP, with the aim to better understand NO- and L-VGCC-dependent synaptic plasticity.

5.3 Methods

5.3.1 Animals

Unless otherwise stated, 6-9-week-old, male, C57Bl/6 mice were used (Charles River, Margate, UK). In some experiments, male, 6-9 week-old, 129sv/C57Bl/6 mice lacking a functional eNOS gene (eNOS^{-/-}; Huang *et al.*, 1995) were used. These were kindly provided by Dr Adrian Hobbs (UCL, London, UK). Age-, sex- and strain-matched wild-type mice obtained from Harlan (Wyton, UK) were used as controls. It was requested from the supplier that these animals were not part of the subpopulation of Harlan C57Bl/6 mice known to lack α -synuclein (Specht and Schoepfer, 2001), which is necessary for efficient transmitter release in several brain areas and for some forms of LTP (Abeliovich *et al.*, 2000; Liu *et al.*, 2004; Liu *et al.*, 2007).

5.3.2 Transverse hippocampal slice preparation and extracellular electrophysiology

As has been detailed in **Chapter 2.2.2-2.2.3**, transverse hippocampal slices were cut using a vibratome and fEPSPs were recorded from the stratum radiatum of CA1

following stimulation of the Schaffer-collateral/commissural pathway. LTP was induced using high frequency (200 Hz) burst stimulation according to the protocol described by Cavus and Teyler (1996): a train of 40 stimuli were delivered at 200 Hz at a stimulus intensity that evoked a 0.5-1 mV population spike in the adjacent stratum pyramidale (**Figure 5.2**). This train was repeated 10 times every 5 s.

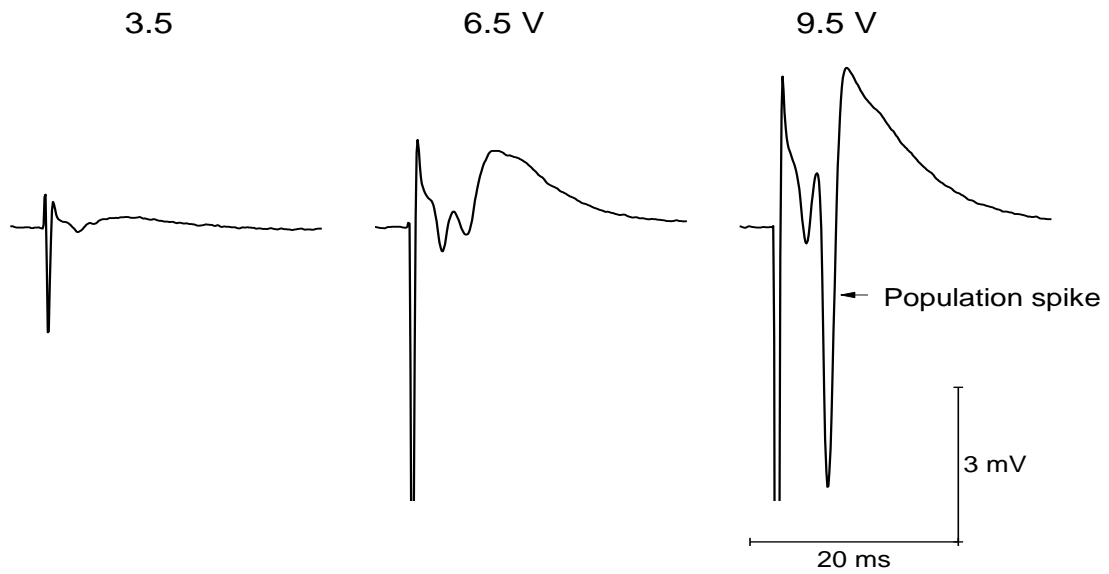


Figure 5.2 Example extracellular recordings of synaptic activity made in one area of the stratum pyramidale. Single stimuli were applied to area CA3 at the amplitude indicated above each trace and synaptic activity was recorded from an area of the stratum pyramidale in CA1. Population spikes were measured as the difference between peak and anti-peak amplitude in the response. Traces are an average of 8 consecutive responses. Stimulus artefacts have been truncated.

Field EPSP initial slopes were normalised to the first 10 min of recording shown in each figure. Drugs were delivered through the perfusion system and took ~ 20 s to reach the recording chamber (as measured in a separate experiment using a coloured indicator). Nifedipine, which is light-sensitive, was prepared freshly on the day of each experiment and was applied to slices in the dark. Experiments were interleaved with, or run simultaneously with, controls.

5.3.3 Measuring cGMP production in hippocampal slices

Hippocampal slices from multiple animals were randomly assigned to flasks of oxygenated aCSF (30 °C) held in a shaking water-bath. NOS dependent-cGMP production was stimulated by submerging the slices in high K^+ (30-122.5 mM) aCSF for 5 min. Standard aCSF contained 2.5 mM K^+ (see **Chapter 2**). The concentration of Na^+ in high K^+ aCSF was lowered to maintain osmolarity. After stimulation, slices were individually inactivated by submersion in 200 μ l boiling buffer containing 50 mM tris-HCl and 4 mM EDTA (pH 7.4) for ~ 30 min and then sonicated. The cGMP content of the resulting solution was measured by radioimmunoassay and protein using the BCA method (see **Chapter 2** for methods).

In order that endogenous cGMP generation could be detected, all slices were incubated with an inhibitor of PDE 2 (BAY 60-7500, 1 μ M, 30 min), which is the main PDE responsible for cGMP breakdown in the hippocampus (van Staveren *et al.*, 2001; Suvarna and O'Donnell, 2002; van Staveren *et al.*, 2003), prior to submersion in high K^+ , low Na^+ aCSF. TTX (1 μ M, 35 min) was also pre-applied to prevent network activity upon stimulation, and D-AP5 (100 μ M, 35 min) to isolate the NMDA receptor-independent response. In every experiment, un-stimulated/basal and NMDA-induced cGMP levels were measured so that the consistency of cGMP accumulation could be monitored. NMDA was applied for 2 min at 100 μ M in the absence of D-AP5.

5.3.4 Estimating membrane potential (V_m) as a function of extracellular K^+ concentration

The effect of extracellular K^+ concentration ($[K^+]_o$) on V_m was estimated using the Goldman-Hodgkin-Katz equation:

$$V_m = \frac{RT}{F} \ln \left(\frac{p_k [K]_o + p_{Na} [Na]_o + p_{Cl} [Cl]_i}{p_k [K]_i + p_{Na} [Na]_i + p_{Cl} [Cl]_o} \right)$$

where:

V_m = membrane potential (V)

R = universal gas constant (8.314 J.K⁻¹.mol⁻¹)

T = absolute temperature (303.15 K in these experiments)

F = Faraday's constant (96485 C mol⁻¹)

p_x = relative membrane permeability of ion x. Estimated values were $p_k = 1$, $p_{Na} = 0.05$ and $p_{Cl} = 0.45$ (Trezise *et al.*, 2010; www.physiologyweb.com).

$[x]_o$ = extracellular concentration of ion x (mM). Under basal conditions (standard aCSF) $[K^+]_o = 2.5$ mM and $[Na^+]_o = 147$ mM. $[Cl^-]_o = 127.8$ mM.

$[x]_i$ = intracellular concentration of ion x (mM). Estimated values were $[K^+]_i = 140$ mM, $[Na^+]_i = 15$ mM, $[Cl^-]_i = 10$ mM (Trezise *et al.*, 2010; www.physiologyweb.com).

The relationship between $[K^+]_o$ and the K⁺ equilibrium potential (E_k) is given by the Nernst equation:

$$E_k = \frac{RT}{zF} \ln \left(\frac{[K]_o}{[K]_i} \right)$$

5.3.5 Genotyping of eNOS^{-/-} mice

Mice lacking functional eNOS due to the inclusion of a NEO cassette in the eNOS gene (eNOS^{-/-}; see Huang *et al.*, 1995) were obtained from Dr Adrian Hobbs (UCL, UK) and genotyped according to the protocol described in **Chapter 4**.

5.3.6 Analysis and Statistics

Analysis of LTP

Unless otherwise stated, values of LTP quoted in the text are means \pm SEM 55-60 min post HFS. In each figure, HFS was applied at the arrow and insets represent the mean fEPSP recorded at the time indicated by the numbered bars. In all sample fEPSPs, the stimulus artefact has been truncated. Two-tailed *t*-tests or repeated

measures, one-factor ANOVA with Bonferroni test were used to assess statistical significance between data sets 55-60 min post HFS.

Analysis of NOS activity assays

Values in the text are means \pm SEM. Statistical significance was assessed using one-factor ANOVA with Dunnett's test or unpaired t-tests.

5.4 Results

5.4.1 Characterisation of LTP induced by high frequency (200 Hz) burst stimulation

As was found originally by Grover and Teyler (1990), LTP could be reliably induced at CA1 synapses by 200 Hz burst stimulation (**Figure 5.3**). Consistent with the original observation, the LTP was of high magnitude (200 ± 13 %; $n = 3$). As expected of a compound LTP, no further significant potentiation could be yielded by subsequent 200 Hz burst stimulation or HFS (100-Hz, 1-s), suggesting that the limiting factor(s) for the magnitude of this plasticity was saturated.

Unlike LTP induced by HFS, or the LTP originally observed by Grover and Teyler (1990) and Cavus and Teyler (1996) using 200 Hz burst stimulation, the LTP induced by 200 Hz burst stimulation was not preceded by PTP. Rather, a short-lasting (1-2 min) post-tetanic depression of the initial slope measuring ~ 50 % from baseline was consistently observed (**Figure 5.3-4**). Consequently, the potentiation was more reminiscent of the slow onset (10-15 min to maximum slope) LTP induced by 200 Hz burst stimulation *in vivo* by Morgan and Teyler (1999). Since it is known that high frequency burst stimulation can induce a transient (lasting ~ 5 min) heterosynaptic depression of synaptic activity in area CA1 (Grover and Teyler, 1992), it is conceivable that in this study, small methodological differences led to the induction of a stronger depression than that induced by Grover and Teyler (1990) and that this masked PTP. This would explain the biphasic shape of the potentiation

shown in **Figure 5.3** and more clearly in **Figure 5.4** over the first 15 min post tetanus.

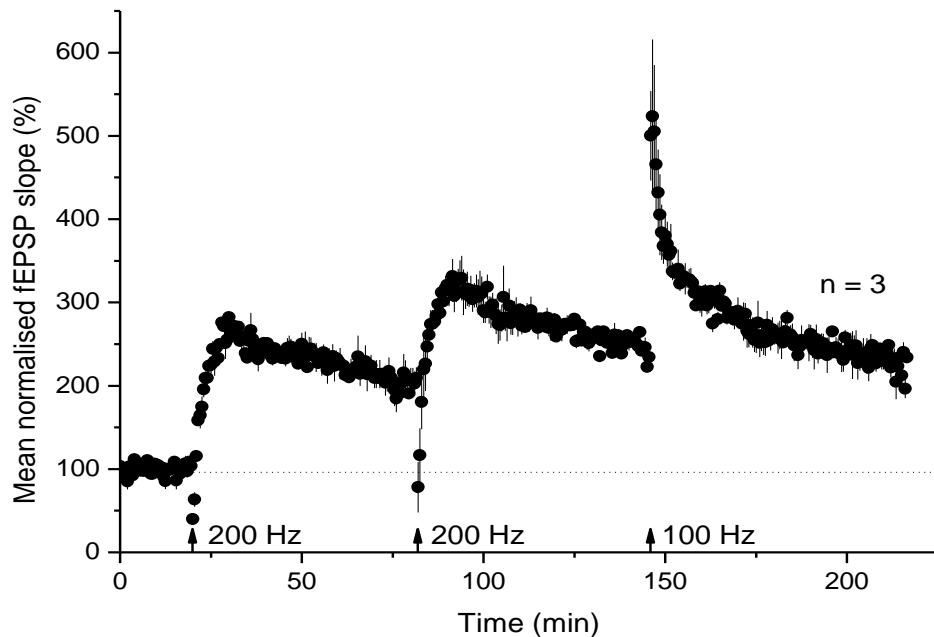


Figure 5.3 LTP induced by high frequency (200 Hz) burst stimulation. Following an initial depression in fEPSP slope, 200 Hz burst stimulation yielded a persistent LTP of high magnitude ($200 \pm 12\%$). This potentiation prevented further LTP by subsequent 200 Hz burst stimulation ($252 \pm 5\%$; $p > 0.05$) and 100-Hz HFS ($p > 0.05$). Statistics are repeated measures ANOVA with Bonferroni post-test.

To test whether the LTP was composed of separable NMDA receptor- and L-VGCC-mediated components, the NMDA receptor inhibitor, D-AP5, and the L-VGCC antagonist, nifedipine, were employed. To ensure effective NMDA receptor inhibition, slices were pre-incubated with 50 or 100 μM D-AP5 for 20 min prior to 200 Hz burst stimulation. These concentrations of D-AP5 were 2 and 4 times higher than that shown previously to maximally block NMDA receptor-mediated depolarization in hippocampal slices in response to 200-Hz burst stimulation (Grover and Teyler, 1990; Grover and Teyler, 1994).

In accordance with previous findings (Grover and Teyler, 1990; Cavus and Teyler, 1996), 200 Hz burst stimulation in the presence of 50 or 100 μM D-AP5 generated a stable LTP. This LTP was significantly reduced compared to that observed in interleaved controls not treated with D-AP5; however its magnitude was significantly different from baseline (**Figure 5.4A**).

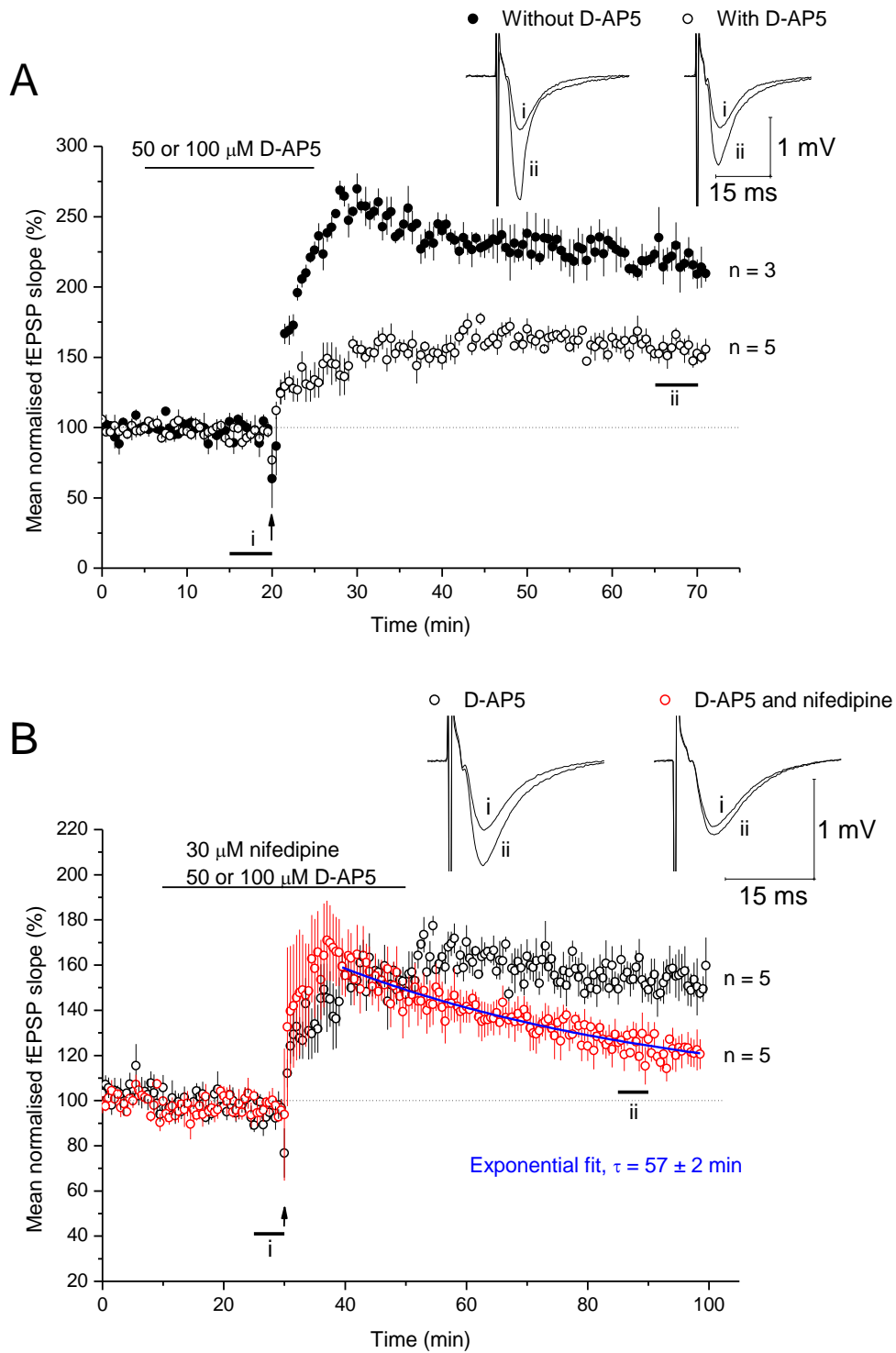


Figure 5.4 Effect of NMDA receptor and L-VGCC inhibition on LTP induced by 200 Hz burst stimulation. **A)** In the presence of the NMDA receptor antagonist, D-AP5 (50 or 100 μM), 200 Hz burst stimulation produced a stable, but significantly reduced LTP (unfilled circles) compared to interleaved untreated controls (50 μM D-AP5: $149 \pm 5\%$; $n = 3$; 100 μM D-AP5: $166 \pm 7\%$; $n = 2$; no D-AP5: $200 \pm 13\%$; unpaired t -test, 50 and 100 μM D-AP5 (which were not significantly different from each other: unpaired t -test, $p = 0.137$), vs. no D-AP5, $p = 0.009$). This potentiation was significantly different from baseline, however (paired t -test, $p = 1.91 \times 10^{-4}$ compared to the last 5

*min of baseline) B) The D-AP5 insensitive LTP was significantly attenuated when induced in the presence of nifedipine ($155 \pm 6\%$ vs. $125 \pm 5\%$; unpaired *t*-test, $p = 0.004$), although it was significantly different from baseline 55-60 min post HFS (paired *t*-test, $p = 0.00469$ compared to the last 5 min of baseline). The decay constant (τ) of the potentiation induced in the presence of nifedipine was 57 ± 2 min (calculated using an exponential fit (blue line) of the data 10 min after burst stimulation; adjusted $R^2 = 0.843$; offset set to 100; see **Chapter 2** for exponential equation). No effect of nifedipine on baseline transmission was observed (paired *t*-test between the first and last 5 min of baseline transmission, $p = 0.455$). All conditions were interleaved. The D-AP5 insensitive LTP shown in A has been shown again in B for ease of comparison.*

In interleaved experiments, co-application of nifedipine (30 μ M) with D-AP5 resulted in a gradually declining potentiation. This potentiation was significantly smaller than the D-AP5-insensitive LTP 55-60 min post HFS, although it was significantly different from baseline (**Figure 5.4B**).

Nifedipine is a member of the 1,4-dihydropyridines, which are thought to alter L-VGCC open/closed state probabilities by binding to an allosteric site in the $\alpha 1$ subunit, causing the stability of the selectivity filter in conducting/non-conducting configurations to change (Catterall and Striessnig, 1992; Hockerman *et al.*, 1997; Striessnig, 1999). Dihydropyridines are widely regarded to be selective for L-VGCCs over other types of VGCCs, but it should be noted that effects of nifedipine other than on L-VGCCs have been reported. For example, the compound has been shown to inhibit cAMP- and, to a lesser extent, cGMP-hydrolysing PDE's purified from bovine heart and porcine smooth muscle cells (Norman *et al.*, 1983; Kishi *et al.*, 1995). Nevertheless, 2 different concentrations of nifedipine (10 μ M, Grover and Teyler, 1990; 30 μ M, Cavus and Teyler, 1996), another dihydropyridine, nitrendipine (20 μ M; Bayazitov *et al.*, 2007), and a non-dihydropyridine-based L-VGCC inhibitor, verapamil (10 mg/kg; Morgan and Teyler, 1999) have all been shown to inhibit 200 Hz burst stimulation induced LTP at CA1 synapses over a similar magnitude and time-course to that shown in **Figure 5.4B**. In support of a direct effect of these compounds on L-VGCCs, it has also been reported that CA1 LTP induced in the presence of D/L-AP5 by 200 Hz burst stimulation is significantly inhibited in hippocampal slices lacking $Ca_v1.2$ (Moosmang *et al.*, 2005a). Against any major effect of 30 μ M nifedipine on synaptic transmission, we report that it did not alter the baseline fEPSP slope (paired *t*-test between the first and last 5 min of

baseline recording, $p = 0.455$; $n = 5$). Therefore, it was concluded that LTP induced by 200 Hz burst stimulation could be dissociated into a NMDA receptor-dependent and a NMDA receptor-independent, L-VGCC-dependent component, and the role of NO in the latter could be tested.

5.4.2 Contribution of NO to NMDA receptor-independent, L-VGCC-dependent LTP

To test whether NO was required for the L-VGCC-dependent, NMDA receptor-independent LTP, the non-selective NOS inhibitor, L-NNA (100 μM), was used (**Figure 5.5**). Compared to the LTP observed following 200 Hz burst stimulation in the presence of D-AP5, the potentiation induced in the presence of L-NNA and D-AP5 was unstable and significantly reduced 55-60 min following induction. Although it was significantly different from baseline 55-60 min post HFS, it appeared to be declining further.

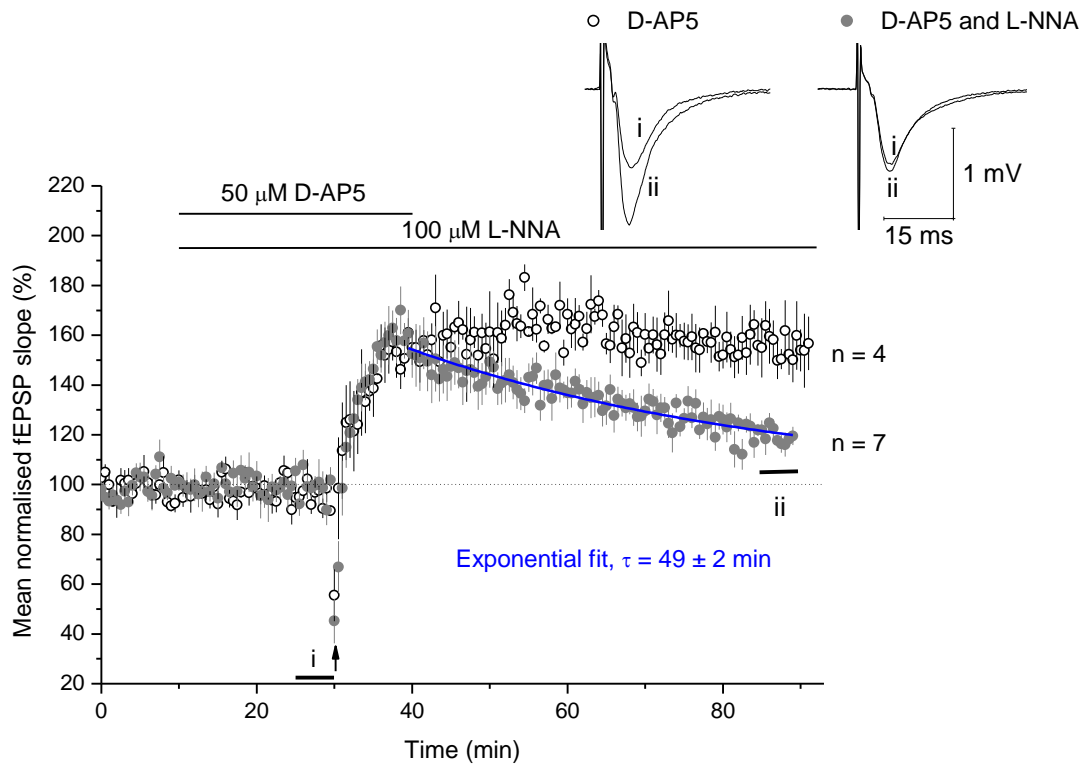


Figure 5.5 Involvement of NOS in NMDA receptor-independent, L-VGCC-dependent LTP. Compared to the stable LTP produced by 200 Hz burst stimulation in the presence of D-AP5 (unfilled circles; $156 \pm 9\%$), LTP induced during application of D-AP5 and the non-selective NOS inhibitor, L-NNA ($100 \mu\text{M}$), was significantly reduced (grey; $120 \pm 4\%$; unpaired *t*-test, $p = 0.008$). The potentiation was significantly different from the last 5 min of baseline (paired *t* test, $p = 0.0108$), however it appeared to be declining further. The decay constant of the LTP induced in the presence of L-NNA was 49 ± 2 min (calculated as in **Figure 5.4**; adjusted $R^2 = 0.861$; offset set to 100).

5.4.3 Role of NO-targeted guanylyl cyclase in NMDA receptor-independent, L-VGCC-dependent LTP

To test for the involvement of NO-targeted guanylyl cyclase in the L-VGCC-dependent component of LTP, ODQ ($10 \mu\text{M}$) was applied to slices 20 min prior to tetanus. This resulted in a significant inhibition of the L-VGCC-dependent LTP compared to controls. As above, the potentiation was significantly different from baseline 55-60 min post HFS, but it appeared to be declining further (**Figure 5.6**). The decay constant of the potentiation (60 ± 3 min) was remarkably similar to that observed following HFS in the presence of nifedipine (57 ± 2 min; **Figure 5.4B**) and L-NNA (49 ± 2 min; **Figure 5.5**).

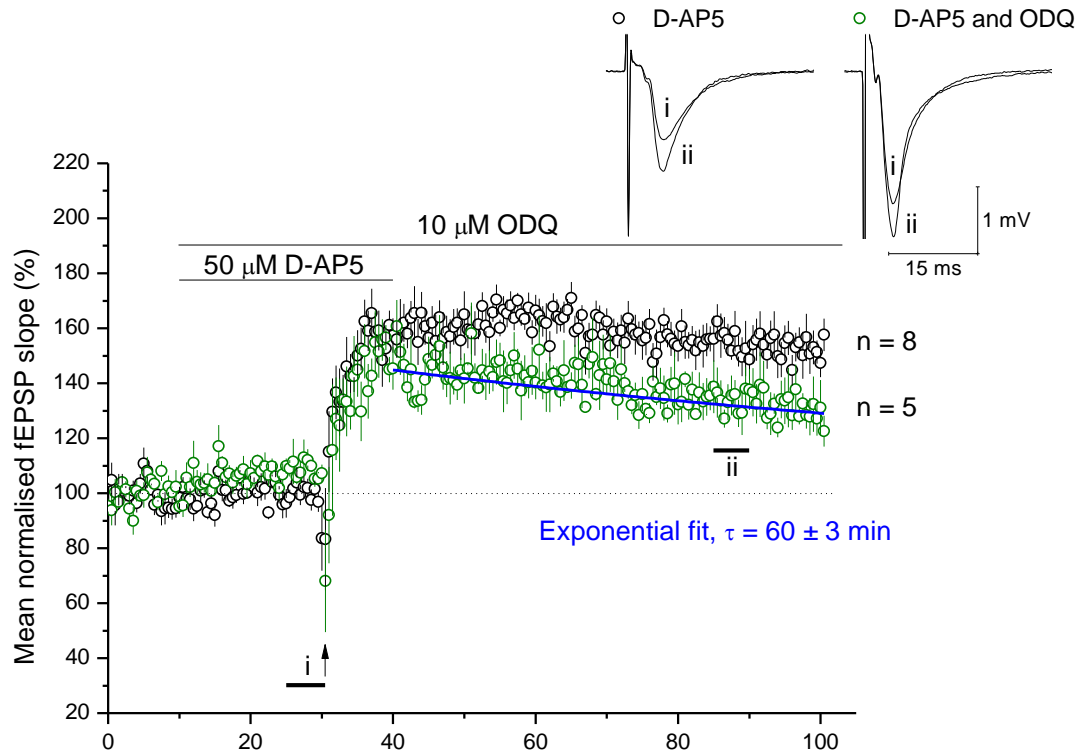


Figure 5.6 Requirement of L-VGCC-dependent, NMDA receptor-independent LTP for NO-targeted guanylyl cyclase. Compared to the stable LTP produced by 200 Hz burst stimulation in the presence of D-AP5 (black; $155 \pm 7\%$), LTP induced during application of D-AP5 and the NO-targeted guanylyl cyclase antagonist, ODQ ($10 \mu\text{M}$), was significantly reduced 55–60 min following tetanus (green; $134 \pm 7\%$; unpaired *t*-test, $p = 0.031$). Measured 55–60 min post HFS, this potentiation was significantly different from the last 5 min of baseline (paired *t*-test, $p = 0.00304$), however it appeared to be declining further. The decay constant of the LTP induced in the presence of ODQ was 60 ± 3 min (calculated as in **Figure 5.4**; adjusted $R^2 = 0.450$; offset set to 100). Note that control data was pooled with that shown in **Figure 5.5**.

5.4.4 NOS isoform involved in NMDA receptor-independent, L-VGCC-dependent LTP

L-NNA and ODQ inhibited the NMDA receptor-independent, L-VGCC-dependent component of the LTP induced by 200 Hz burst stimulation (**Figure 5.5-6**). As previously discussed, both eNOS and nNOS are thought to be required for NO-dependent LTP at CA1 synapses induced by a 1-s, 100-Hz tetanus (HFS). The former isozyme is thought to provide a basal NO tone, the latter to generate an activity-dependent, phasic NO signal (Hopper and Garthwaite, 2006).

To elucidate the NOS isoform(s) required for NMDA receptor-independent, L-VGCC-dependent LTP, and therefore begin to characterise the nature of the NO signal involved, eNOS^{-/-} mice were used. Neither nNOS inhibitors nor nNOS knock-out mice were used due to reasons outlined in **Chapter 6**.

We observed no significant difference between the NMDA receptor-independent, L-VGCC-dependent LTP induced in slices from eNOS^{-/-} or age-, sex- and strain-matched wild-type mice (**Figure 5.7A**). However, in interleaved experiments, LTP in eNOS^{-/-} mice was significantly reduced by L-NNA (**Figure 5.7B**).

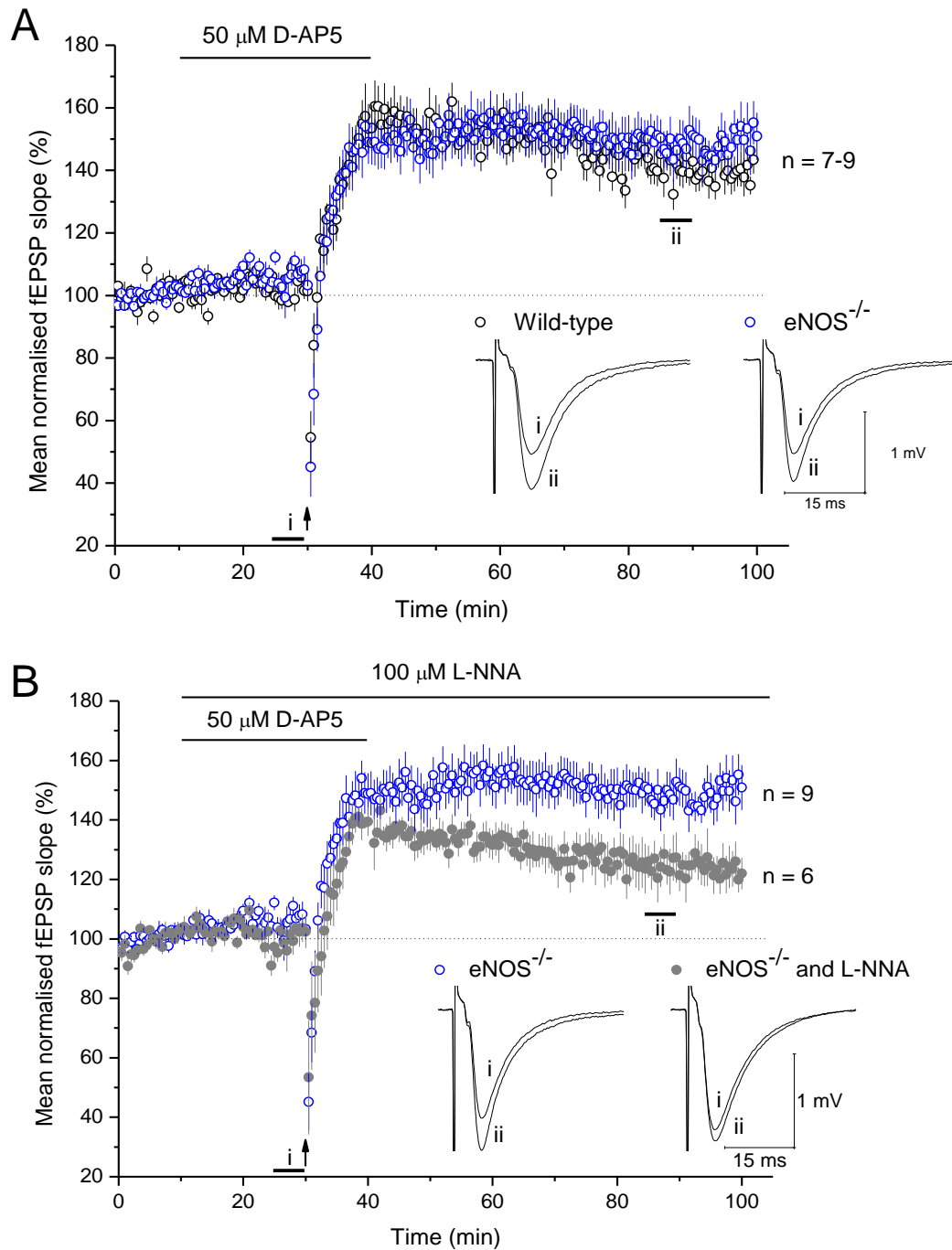


Figure 5.7 NMDA receptor-independent, L-VGCC-dependent LTP in eNOS^{-/-} mice. **A**) No significant difference was detected between the LTP induced in slices from eNOS^{-/-} and matched wild-type mice ($148 \pm 6\%$ vs. $141 \pm 5\%$ respectively; unpaired *t*-test, $p = 0.374$). **B**) The non-specific NOS inhibitor, L-NNA, significantly attenuated LTP in eNOS^{-/-} slices ($124 \pm 6\%$ vs. $148 \pm 6\%$; unpaired *t*-test, $p = 0.021$). All conditions were interleaved.

5.4.5 Relationship between NOS and L-VGCC's in LTP

L-VGCC-dependent LTP was reduced by a general NOS inhibitor and NO-targeted guanylyl cyclase antagonist (**Figure 5.5-7**), but expressed normally in eNOS^{-/-} slices. Since iNOS is not expressed in healthy hippocampus (Hopper and Garthwaite, 2006), these results are consistent with nNOS being the only NOS isoform required for L-VGCC-dependent LTP. The results shown in **Figure 5.4B-6** suggest that L-VGCCs, nNOS and NO-targeted guanylyl cyclase might act in series to affect L-VGCC-dependent LTP, because, the inhibition of LTP caused by the NOS antagonist, L-NNA, and the guanylyl cyclase antagonist, ODQ, was remarkably similar to that generated by nifedipine (compare τ in **Figure 5.4B-6**). This suggestion is supported by other lines of evidence (see **Discussion**). However, it was unclear whether L-VGCCs might activate nNOS-guanylyl cyclase, presumably via their Ca²⁺ conductance, or vice versa. Moreover, our results could not exclude the possibility that nNOS and L-VGCCs operate in parallel pathways, perhaps with a common target.

Previously, NOS activity has been measured in brain slices in response to depolarising agents, including K⁺ (Ferrendelli *et al.*, 1973). We took advantage of this to provide a simple test of whether, under conditions of crude synaptic stimulation, L-VGCC opening can cause nNOS activity in the hippocampus. Hippocampal slices were depolarised (presumably causing L-VGCC activation) by submersion in high K⁺-aCSF ([K⁺]_o ranged from 15-122.5 mM; note that standard aCSF contained 2.5mM K⁺) for 5 min and the effect of nifedipine or the L-VGCC agonist, FPL-64176 (reviewed in Rampe and Kane, 1994), on the resulting NOS-dependent cGMP accumulation was tested. Cyclic GMP was measured by radioimmunoassay since this represents the most sensitive assay of endogenous NOS activity currently widely available. Prior to stimulation with high K⁺ aCSF, slices were pre-treated with the PDE inhibitor, BAY 60-7550 (1 μ M, 30 min), to increase the sensitivity of the technique and allow direct measurement of cGMP production, D-AP5 (100 μ M, 35 min), to isolate NMDA receptor-independent cGMP accumulation, and TTX (1 μ M, 35 min), to negate the effects of network activity on the response.

As shown in **Figure 5.8A**, submersion of slices in high K^+ aCSF for 5 min induced cGMP accumulation in hippocampal slices in a manner that was dependent on the $[K^+]_o$ (black). This was blocked by pre-incubating slices with L-NNA (100 μ M, 35 min; red), ODQ (10 μ M, 35 min; blue) or in Ca^{2+} -free aCSF containing the Ca^{2+} chelator, EGTA (1 mM, 35 min; green). To place the amount of cGMP generated by K^+ into context, some slices were treated with a concentration of NMDA (100 μ M, 2 min) shown previously to evoke maximal NMDA-induced cGMP accumulation in 10-day-old rat hippocampal slices (Bartus, 2009). For these experiments, slices were maintained in standard aCSF (2.5 mM K^+) and were pre-treated with BAY 60-7550 (1 μ M, 30 min) and TTX (1 μ M, 35 min) but not D-AP5. The average response across all experiments was 19 ± 1 pmol/mg protein (grey bar; $n = 13$). Cyclic GMP accumulation was not significantly greater after treatment with 300 μ M NMDA for 2 min (24 ± 2 ; $p = 0.240$; $n = 2$), suggesting that 100 μ M NMDA was saturating.

To determine which isoform(s) of NOS was likely responsible for the cGMP response, eNOS^{-/-} mice were used. There was no significant difference between cGMP accumulation in wild-type and eNOS^{-/-} slices (**Figure 5.8B**), implying that the response was mediated by nNOS.

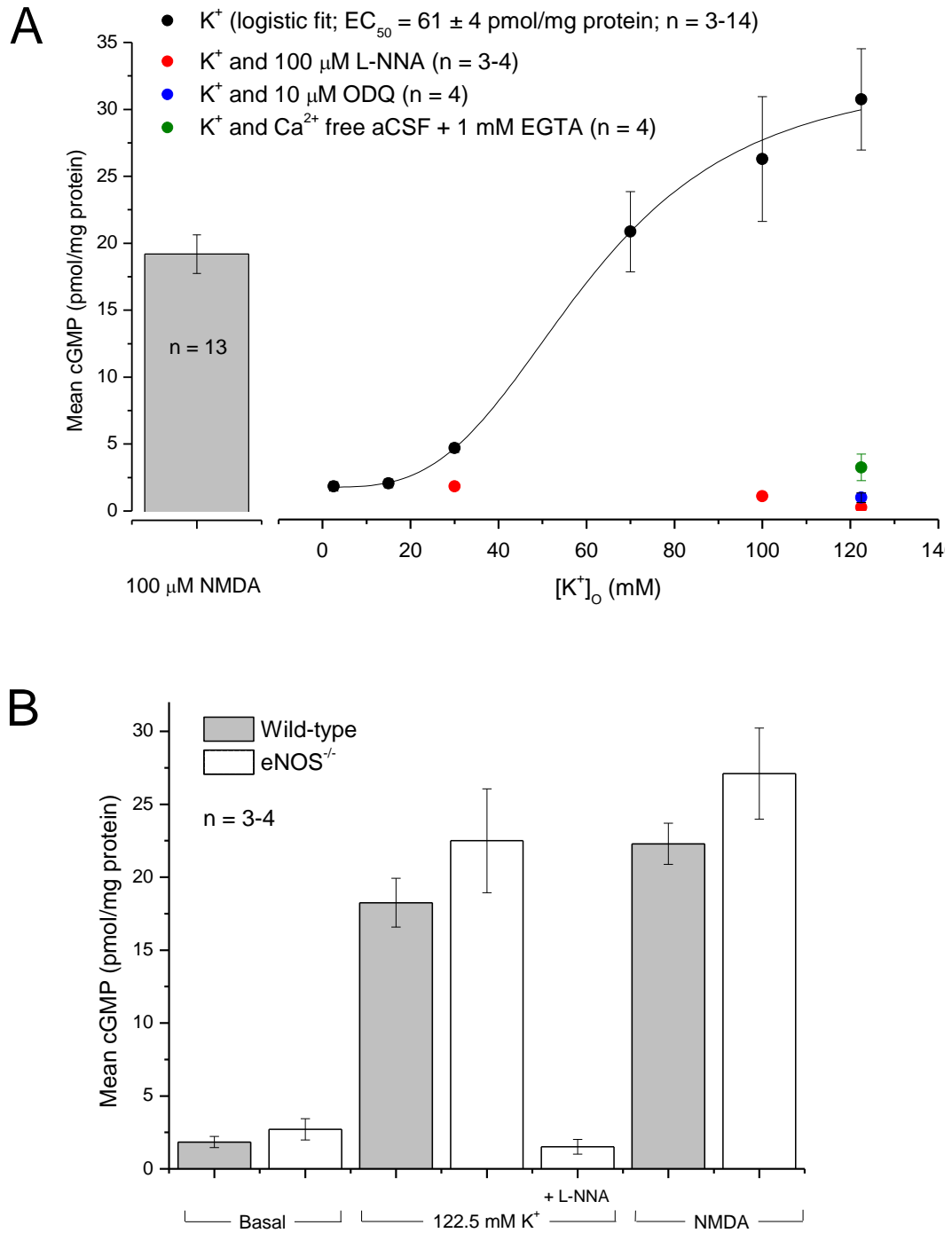


Figure 5.8 K^+ -induced cGMP accumulation in hippocampal slices. **A)** In slices incubated in standard aCSF (2.5 mM K) and pre-treated with BAY 60-7550, and TTX, NMDA (100 μM , 2 min) generated 19 ± 1 pmol cGMP/mg protein on average (grey bar). In slices pre-treated with BAY 60-7550, TTX and D-AP5, K^+ induced cGMP accumulation in a concentration-dependent manner (black) that was well described by a logistic equation ($R^2 = 0.997$; see **Chapter 2** for logistic equation). Slices treated with the highest concentration of K^+ (122.5 mM) produced significantly more cGMP than those treated with NMDA (ANOVA with Dunnett's test, $p < 0.01$). Where tested, K^+ -induced cGMP accumulation

was blocked in slices pre-incubated with L-NNA (100 μ M, 35 min; red), ODQ (10 μ M, 35 min; blue) or in Ca^{2+} free medium containing the Ca^{2+} chelator, EGTA (1mM; green). **B)** Following stimulation with 122.5 mM K^+ , cGMP accumulation was not significantly different between wild-type and $eNOS^{-/-}$ slices (wild-type: 18 ± 2 pmol/mg protein; $eNOS^{-/-}$: 22 ± 4 pmol/mg protein; unpaired *t*-test, $p = 0.322$). In all experiments, D-AP5 (100 μ M) and TTX (1 μ M) were pre-applied for 35 min and BAY 60-7550 (1 μ M) for 30 min.

Neither nifedipine (30 μ M, pre-incubated for 35 min) nor FPL 64176 (1 μ M, pre-incubated for 20 min) had any significant effect on the mean cGMP generated in hippocampal slices upon exposure to any $[K^+]_o$ used (**Figure 5.9**).

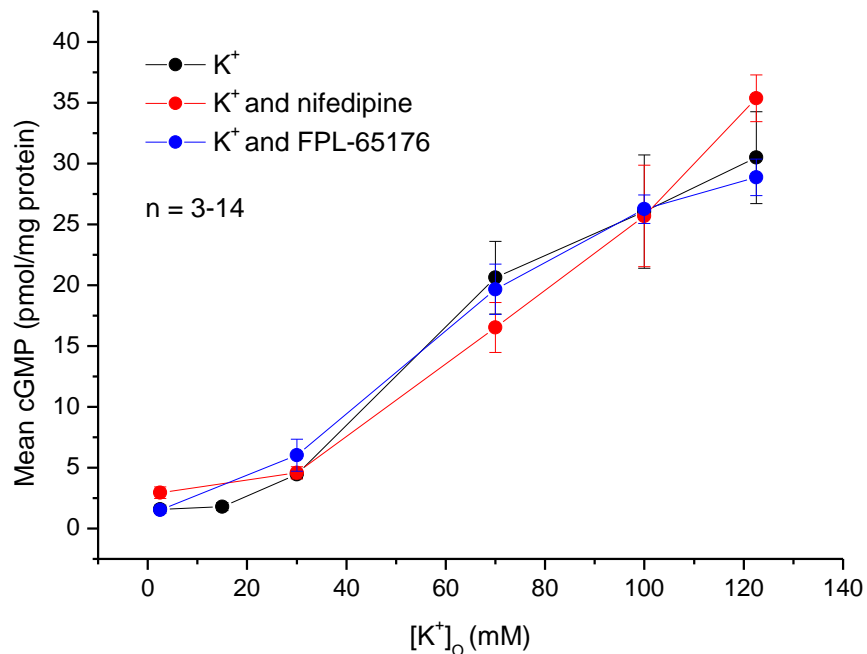


Figure 5.9 Effect of L-VGCC modulators on K^+ -induced cGMP accumulation. Slices were pre-incubated with nifedipine (red) or FPL-65176 (blue) and stimulated with various concentrations of K^+ for 2 min. There was no effect of nifedipine (30 μ M; 35 min pre-incubation; red) nor FPL-64176 (1 μ M; 35 min pre-incubation; blue) on cGMP accumulation in response to any $[K^+]_o$ tested (ANOVA with Dunnett's test, $p > 0.05$). All experiments were interleaved. In all experiments, D-AP5 (100 μ M) and TTX (1 μ M) were pre-applied for 35 min and BAY 60-7550 (1 μ M) for 30 min.

It could be argued that at the concentrations of K^+ used, membrane depolarisation was insufficient to activate L-VGCCs because they are high voltage activated. Estimates of the voltage at which L-VGCC receptors are half-maximally activated

($V_{0.5}$) vary in the literature and measurements are rarely made using native L-VGCCs. Instead L-VGCC subunits are usually expressed in dissociated cells. Many estimates for rodent neuronal $Ca_v1.2$ and 1.3 containing channels, which, as described above, are the predominant L-VGCCs in hippocampal pyramidal neurons, are between -15 to -20 mV (Catterall *et al.*, 2010a; Catterall *et al.*, 2010b). In a study by Helton *et al.* (2005), for example, the $V_{0.5}$ of Ca^{2+} currents recorded from tsA201 cells transiently co-expressing $Ca_v1.2$, $Ca_v\beta_3$, $Ca_v\alpha_2\delta_1$ subunit DNA was ~ 18 mV. In dissociated rat pyramidal neurons, the $V_{0.5}$ of native L-VGCCs has been reported to be ~ -14 mV (Mermelstein *et al.*, 2000). In this study, significant activation of L-VGCCs was also observed at more negative potentials (-30 mV).

To estimate the V_m of pyramidal neurons in hippocampal slices subject to varying $[K^+]_o$, and therefore, to identify whether L-VGCC's were likely to be active, the Goldman-Hodgkin-Katz equation was used (see **5.3.1** for details). As shown in **Figure 5.10**, exposure to 100 mM and 122.5 mM K^+ was predicted to depolarise the V_m of neurons to ~ -16 mV and -11 mV, respectively, and this was within the range of most estimates of the $V_{0.5}$ of rodent neuronal L-VGCCs (see **Discussion**).

It should be noted that the values for ion permeability and intracellular concentration used to calculate V_m were approximated and that our experiments do not control for L-VGCC inactivation during the K^+ stimulus. Nevertheless, the calculated V_m under basal conditions (standard aCSF in which $[K^+]_o = 2.5$ mM) was ~ -69 mV, the average resting V_m measured from pyramidal neurons in hippocampal slices under the same conditions as applied in this study (oxygenated aCSF, pH 7.4, 30 ± 1 °C) using intracellular sharp electrodes (see **Appendix 1** for details). The E_k was also calculated as a function of $[K^+]_o$ using the Nernst equation, since this relies on fewer approximated values than the calculated V_m . High concentrations of K^+ (100 - 122.5 mM) were predicted to cause ~ 100 mV shift in E_k , which would be very likely to activate L-VGCCs even if the true V_m varied from that predicted using the Goldman-Hodgkin-Katz equation.

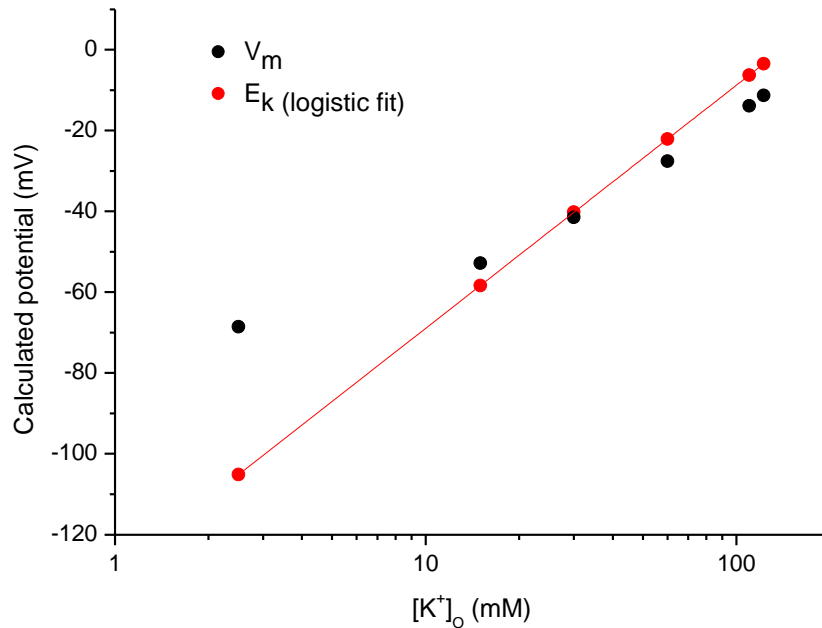


Figure 5.10 Estimating V_m and E_k as a function of $[K^+]_o$. As expected, E_k (red) was logistic (note log scale). As predicted by the Nernst equation, the slope of the line over a 10-fold change in $[K^+]_o = (RT/F) \cdot 2.3 = 60 \text{ mV}$, where 2.3 is the conversion factor of \ln to \log_{10} . As is standard, V_m deviated from E_k at low $[K^+]_o$. This reflects the influence of the other ions taken into consideration by the Goldman-Hodgkin-Katz equation, largely Na^+ , on V_m .

5.5 Discussion

In favour of the hypothesis that NO is required for NMDA receptor-independent, L-VGCC-dependent LTP at hippocampal CA1 synapses, the main finding of this study was that the non-selective NOS antagonist, L-NNA, caused a steady decline in the potentiation. This was remarkably similar to the effect of the L-VGCC antagonist, nifedipine (compare **Figure 5.4B-5**). The NO-targeted guanylyl cyclase antagonist, ODQ, also inhibited L-VGCC-dependent LTP, and in a similar manner (compare **Figure 5.4B** and **5.6**), suggesting that, in common with the vast majority of physiological NO signals (Garthwaite, 2008), the NO involved was transduced by cGMP.

Previously, NO has been shown to be required for other forms of NMDA receptor-independent LTP. For example, a slowly-rising form of NMDA-receptor independent LTP induced at synapses in slices of somatosensory cortex using long-lasting (10

min), 100-Hz burst stimulation has been reported to be blocked by the NOS antagonist, L-NAME, and in eNOS^{-/-} mice (Haul *et al.*, 1999). It has also been reported that LTP induced in the presence of D-AP5 at synapses between the dentate gyrus mossy fibres and the proximal-apical dendrites of CA3 pyramidal neurons using a 1-s, 100-Hz tetanus is reduced in eNOS^{-/-} mice (Doreulee *et al.*, 2001; although see Nicolarakis *et al.*, 1994). However, to our knowledge, this is the first report that endogenous NO is necessary for NMDA receptor-independent and L-VGCC-dependent LTP at CA1 synapses.

Following a 100-Hz, 1-s tetanus (HFS), LTP is, in our hands, NMDA receptor-dependent (**Chapter 3**). This LTP likely requires both nNOS and eNOS (Hopper and Garthwaite 2006). Endothelial NOS, which after phosphorylation can become tonically active (Fulton *et al.*, 2001), is thought to provide a continuous, low-level NO tone which may prime synapses for potentiation (Hopper and Garthwaite, 2006), perhaps by modulating basal levels of presynaptic transmitter release at CA1 synapses (Neitz *et al.*, 2011 and see **Chapter 4**). Neuronal NOS, on the other hand, is thought to produce a phasic, activity-dependent signal necessary for hippocampal LTP induction (Hopper and Garthwaite, 2006).

To characterise the NO signal necessary for the L-VGCC-dependent LTP, the NOS isoform(s) required was determined. Given previous evidence, it seemed reasonable that both sources of NO could be involved in L-VGCC-dependent LTP: NMDA receptor-independent nNOS activity has been previously reported (see below) and NMDA-receptor-independent forms of LTP at mossy fibre synapses (Doreulee *et al.*, 2001) and in the somatosensory cortex (Haul *et al.*, 1999) are reportedly reduced in eNOS^{-/-} mice. However, our experiments using eNOS^{-/-} mice favoured the conclusion that nNOS was the only source of the NO needed for L-VGCC-dependent LTP (**Figure 5.7**). Note that, unfortunately, selective nNOS inhibitors were unavailable for use (see **Chapter 6**) and mice lacking active splice variants in the hippocampus could not be obtained within the time constraints of this project. Taken together with previous findings (Hopper and Garthwaite, 2006), the lack of effect of eNOS knock-out on the L-VGCC-dependent LTP immediately suggested that the NO signal involved in the LTP was activity-dependent, rather than tonic, and synthesised in

neurons, rather than endothelial cells. The lack of effect also implies that eNOS and its effects on neurotransmission, for example, through the tonic modulation of neurotransmitter release onto CA1 cells (**Chapter 4** and Neitz *et al.*, 2011), are not necessary for all forms of CA1 LTP. Furthermore, the result provides important support for the role of nNOS in LTP, which has been disputed by findings that nNOS knock-out mice are capable of normal NOS-inhibitor sensitive LTP at CA1 synapses (O'Dell *et al.*, 1994; although it should be noted that the mice involved may have expressed active nNOS splice variants; Eliasson *et al.*, 1997), and that nNOS inhibitors shown previously to attenuate CA1 LTP (Hopper and Garthwaite, 2006), are not useably selective for nNOS over eNOS (see **Chapter 6**).

As discussed above (see **5.1 Introduction**), NO-, and L-VGCC-dependent forms of LTP at CA1 synapses have previously been shown to rely on similar mechanisms, and both NO and L-VGCCs have been found to modulate activity-dependent changes associated with gene expression, learning and memory in the hippocampus. It is also interesting to note that an interaction between NO and L-VGCC's during long-lasting synaptic activity, and perhaps learning and memory, may extend beyond CA1 synapses because L-VGCCs and NO have been found to be necessary for some forms of LTP in the lateral amygdala, as well as amygdala-dependent learning, such as auditory fear conditioning (Weisskopf *et al.*, 1999; Bauer *et al.*, 2002; Ota *et al.*, 2008). However, the critical role of NO in L-VGCC-dependent LTP was, to some extent, unexpected and this was for two main reasons.

Firstly, several groups have long-hypothesised that LTP induction protocols using high stimulus intensities favour the expression of NO-independent LTP (Haley *et al.*, 1993; Chetkovich *et al.*, 1993; O'Dell *et al.*, 1994; Wilson *et al.*, 1999), thus explaining why some forms of LTP are independent of NO (for example, Cummings *et al.*, 1994; Bannerman *et al.*, 1994b; Phillips *et al.*, 2008). This hypothesis has, arguably, received more attention than theories that other factors, such as the temperature at which the experiments were performed (Williams *et al.*, 1993), or the age and strain of the animals used (Holscher, 2002), determine whether NO is involved in LTP. However, we report clear evidence that NO-dependent LTP can be induced using an induction protocol delivered at relatively high stimulus intensities

(≥ 1 V higher than that typically used to evoke the baseline fEPSP (see **5.3 Methods** for details)). Our data suggest therefore suggest that some other variable(s) dictate the involvement of NO, or another factor capable of compensating for NO, in LTP and that the above hypothesis should be reconsidered. Furthermore, our results are accordant with more recent findings that postsynaptic somatic action potentials, the generation of which would be favoured by high vs. low intensity stimulation (and may also be necessary for L-VGCC activation), are necessary for NO-dependent LTP at CA1 synapses (Phillips *et al.*, 2008).

Secondly, physiological nNOS activation is thought to be achieved preferentially through NMDA receptors. It is well known that nNOS can bind the NMDA receptor subunit, NR2B, via PSD-95 (Christopherson *et al.*, 1999) and *in situ* hybridisation studies show that message for nNOS is co-localised with mRNA for PSD-95 throughout the brain (Brenman *et al.*, 1996). In the hippocampus, immunofluorescent staining has shown that nNOS, NR2B and PSD-95 co-localise in pyramidal cell dendritic spines (Burette *et al.*, 2002). NMDA has been shown to increase NO production in the hippocampus *in vivo* (Luo and Vincent, 1994) and *in vitro* (**Figure 5.8A**), and this has been shown to be nNOS- (Huang *et al.*, 1993) and PSD-95-dependent (Sattler *et al.*, 1999). A simple explanation for the requirement of L-VGCC-dependent LTP for nNOS, therefore, was incomplete antagonism of NMDA receptors during 200 Hz burst stimulation. Nevertheless, evidence presented by Grover and Teyler (1990, 1994) strongly suggests that glutamate released during this tetanus would be insufficient to overcome the concentrations of D-AP5 (50-100 μ M) used throughout this study. For example, they report that, in the presence of 50 μ M D/L-AP5 (equivalent to 25 μ M D-AP5), 95 % of NMDA receptors are blocked during 200 Hz burst stimulation, and that raising the concentration of D/L-AP5 to 200 μ M yields no further inhibition of NMDA receptors, nor any inhibition of L-VGCC-dependent LTP (Grover and Teyler, 1990). Therefore, the finding that NO was required for L-VGCC-dependent, NMDA receptor-independent LTP implies that, following 200 Hz burst stimulation, nNOS was activated by a source of Ca^{2+} influx other than NMDA receptors.

Several lines of evidence suggest that L-VGCCs might be responsible for nNOS activation during L-VGCC-dependent CA1 LTP. First, histological studies have shown that nNOS and L-VGCCs may co-localise in pyramidal cell soma, at the base of apical dendrites and in interneurons (Westenbroek *et al.*, 1990; Ahlijanian *et al.*, 1990; Hell *et al.*, 1993; Wendland *et al.*, 1994; Gonzalez-Hernandez *et al.*, 1996; Burette *et al.*, 2002). Interestingly, some histological and functional data also shows that Cav1.2 L-VGCCs are expressed in the postsynaptic densities of more distal pyramidal cell dendrites where they may lie in close proximity to NMDA receptors, and therefore, probably nNOS (Hell *et al.*, 1996). Second, as assessed using Fura-2 in hippocampal slices (Regehr and Tank, 1992; Christie *et al.*, 1995) and whole cell recordings of dissociated pyramidal neurons (Mermelstein *et al.*, 2000), L-VGCCs have been reported to cause significant (~ 30-50 % of the total) Ca²⁺ influx into pyramidal cell soma and dendrites during spikes and ramp depolarisations (to -30 mV) designed to approximate the effects of EPSPs. Third, as mentioned above, LTP induced in the presence of nifedipine, L-NNA and ODQ was characterised by a similar decay constant (**Figure 5.4B-6**). Fourth, L-VGCCs have previously been reported to activate nNOS in the nervous system. In the PNS, for example, in the enteric nervous system, Ca²⁺ influx via VGCCs, including L-VGCCs, is well-known to trigger NOS activation, leading to NANC transmission and smooth muscle relaxation (reviewed by Vincent, 2010). In primary cultures of mouse cortical neurons, in which non-neuronal cells constituted only ~ 5 % of the total, K⁺ (25-50 mM for 10-15 min) induced NOS-dependent, presumably nNOS-dependent, cGMP accumulation that was insensitive to TTX, MK-801 and CNQX but was attenuated by the L-VGCC antagonists, 4-(4-fluorophenyl)-2-methyl-6-(5-piperidinopentyloxy)pyrimidine hydrochloride (NS-7; Suma *et al.*, 1997; Tatsumi *et al.*, 1998) and nifedipine (Oka *et al.*, 1999). Furthermore, the L-VGCC agonist, BAY K-8644, concentration-dependently increased K⁺-induced cGMP accumulation and this was also attenuated by NS-7 and nifedipine (Oka *et al.*, 1999).

Nevertheless, it should be noted that the results presented in **Figure 5.4B-6** are equally consistent with two other possibilities, both consistent with another, unknown source of Ca²⁺ influx to neurons being responsible for stimulating nNOS. The first possibility is that NO could have activated L-VGCCs, as has been shown in

various biological systems, including the cardiac system (reviewed by Striessnig, 1999). In human atrial myocytes, for example, picomolar concentrations of the NO donor, 3-morpholinopyridone (SIN-1), and cGMP (500 nM) have been reported to increase L-VGCC-mediated currents, most likely via an effect on cGMP-inhibited PDE 3, leading to cAMP accumulation, PKA activation, L-VGCC phosphorylation and an increase in the open state probability of the channels (Kirstein *et al.*, 1995). The second possibility is that L-VGCCs and NO acted in parallel pathways, separated for example, by intracellular compartmentalisation, but with a common target necessary for LTP expression. In support of this, L-VGCC-dependent LTP is thought to require sources of Ca^{2+} influx to neurons other than L-VGCCs, such as metabotropic glutamate receptors (Little *et al.*, 1995). Furthermore, Kullmann *et al.* (1992) have shown that, although repeated depolarising pulses applied to CA1 neurons in hippocampal slices elicit a D-AP5-insensitive, nifedipine-sensitive increase in pyramidal cell EPSPs and EPSCs, this potentiation is transient (decaying back to baseline within ~ 30 min) and requires coincident synaptic activity for persistent expression. These findings suggest that another factor is required for L-VGCC-dependent LTP. This factor could be responsible for nNOS activation, and may also lend L-VGCC-dependent LTP its input-specificity, which, because L-VGCCs are most densely clustered in the pyramidal cell soma and at the base of apical dendrites, is difficult to explain.

Using a crude stimulus (2.5 – 122.5 mM K^+ , 5 min) to depolarise hippocampal slices and activate L-VGCCs, we found no evidence that L-VGCCs activate nNOS (**Figure 5.9**). The Goldman-Hodgkin-Katz equation predicts that the V_m of neurons exposed to the highest concentrations of K^+ used was close to or above the $V_{0.5}$ of the L-VGCC's present (**Figure 5.10**), suggesting that L-VGCCs were active under our conditions. Furthermore, cGMP generation was quantified using the cGMP radioimmunoassay, which provides the most sensitive measure of NOS activity currently widely available. Therefore at present, it is reasonable to assume that, in the hippocampus, L-VGCC-dependent, K^+ -induced nNOS activation is minimal or does not occur. Of course, this cannot rule out the possibility that during 200 Hz burst stimulation, L-VGCCs do activate nNOS. However, without any indication that L-

VGCCs can activate nNOS in the hippocampus, the relationship between L-VGCCs and nNOS in L-VGCC-dependent LTP remains an open question.

5.6 Conclusion

NO/cGMP appears to play a diverse role in hippocampal synaptic plasticity. In **Chapter 4** it was shown that, under our conditions, NMDA receptor-dependent LTP at CA1 synapses requires endogenous NO. In addition to this, the data presented in **Figures 5.4-6** suggest for the first time that NO/cGMP is also necessary for L-VGCC-dependent, NMDA receptor-independent CA1 LTP. Consistent with the results of experiments using eNOS^{-/-} mice (**Figure 5.7**) and the reported lack of iNOS in healthy hippocampus (Hopper and Garthwaite, 2006), nNOS may be the sole isoform of the NO required for L-VGCC-dependent LTP, implying that a NMDA receptor-independent mechanism, most likely involving an increase in intracellular Ca²⁺, is capable of activating nNOS during synaptic stimulation (**Figure 5.7**). This could hold considerable influence over NO physiology and pathology.

Taking advantage of previous findings that K⁺ induces NOS-dependent cGMP accumulation in hippocampal slices, and a highly sensitive assay for cGMP detection, experiments were performed to ascertain whether, under crude stimulation, L-VGCCs activate nNOS. Under these conditions, significant NMDA receptor-independent, NOS-dependent cGMP accumulation was recorded (**Figure 5.8**), consistent with the suggestion that nNOS can become activated by an unknown, NMDA receptor-independent mechanism(s). No evidence for L-VGCC-induced nNOS activity was found (**Figure 5.9**). This was not in favour of L-VGCC-induced nNOS activation during 200 Hz burst stimulation, although it must be emphasised that it is unclear how comparable the neuronal consequences of K⁺ and tetanic stimulation are. Experiments to identify the source(s) of Ca²⁺ influx responsible for K⁺-induced cGMP-accumulation have been performed (see **Appendix 1**), but were inconclusive. Interestingly, a cGMP sensor with picomolar sensitivity has been developed very recently (Batchelor *et al.*, 2010) and future application of this to hippocampal slices could allow L-VGCC-dependent NO synthesis to be re-investigated with improved sensitivity and following 200 Hz burst stimulation.

Finally, it is tempting to speculate that NO- and L-VGCC-dependent signalling pathways activated during LTP may converge on pathways linked to gene expression and/or BDNF release (see **5.2 Aim**). Concerning the former, NMDA receptor-independent NO synthesis during conditions also activating L-VGCCs could explain the discrepancy in the literature as to why NMDA receptors and NO are necessary for early-LTP induced by a 1-s, 100-Hz tetanus (HFS), but only the latter is required for late-LTP and some associated changes in gene expression induced by multiple HFS (see **5.1 Introduction**).

Chapter 6:

Evaluation of nNOS inhibitors using intact tissues

6.1 Introduction

This study resulted from attempts to identify the isoform of NOS involved in the NO-dependent plasticity's described in **Chapter 4-5** using nNOS inhibitors. The use of NOS inhibitors represents a major strategy for investigating NO physiology, as has been demonstrated throughout this thesis, and is also an attractive means of treating pathologies hypothesised to involve NO overproduction by NOS. These pathologies include disorders of the nervous system thought to involve nNOS, such as stroke and Parkinson's disease, and inflammatory diseases considered to involve iNOS, such as asthma and arthritis (reviewed in Gross and Wolin, 1995; Hobbs *et al.*, 1999; Vallance and Leiper, 2002).

The first series of NOS inhibitors to be developed were L-arginine derivatives such as L-NMMA, L-NNA (see **Table 6.1**) and its prodrug, L-NAME. These compete with L-arginine for binding to NOS and are non-selective for any NOS isozyme. They are actively transported into cells and typically have IC₅₀ values in the low micromolar range (Alderton *et al.*, 2001).

Early on, L-NNA and L-NMMA were reported to block eNOS-dependent, ACh-induced relaxation of rabbit aorta, which could be restored upon application of L-arginine or exogenous NO (Moore *et al.*, 1990). L-NMMA was also shown to dose-dependently increase blood pressure in two patients with septic shock who had failed to respond to conventional treatment. L-NAME was reported to have a similar effect in one of the patients (Petros *et al.*, 1991). Since then, the L-arginine-based inhibitors have been shown to inhibit various NO-dependent phenomena in different tissues and to benefit patients with other disorders involving NO overproduction, such as chronic tension-type headache (Ashina *et al.*, 1999b) and migraine (Lassen *et al.*, 1997), which may result from central sensitisation of noiceptive synapses by overactive nNOS (Ashina *et al.*, 1999a).

However, the interpretation of research using non-selective NOS inhibitors is limited because all three isoforms of NOS may be simultaneously active in one tissue. The therapeutic applications of non-selective NOS inhibitors are also hampered for the

same reason. For example, non-selective NOS inhibitors cannot be used to treat asthma, which may be augmented by excessive iNOS activity, because eNOS inhibition causes vasoconstriction in the airways (Hansel *et al.*, 2003). Likewise, nNOS and eNOS inhibition appear to have opposing consequences for tissue damage after ischemic insult (Huang *et al.*, 1994; Huang *et al.*, 1995; Huang *et al.*, 1996).

To avoid these problems, NOS inhibitors selective for one isozyme are necessary, but, unfortunately, their development has been demanding (Alderton *et al.*, 2001). The two most selective and potent nNOS inhibitors currently commercially available are L-VNIO (or Vinyl L-NIO; Babu and Griffith, 2008) and 1400-W (Garvey *et al.*, 1997; see **Table 6.1**). Both are competitive with L-arginine for binding to NOS. 1400-W is foremost known as a potent iNOS inhibitor, although it is also used as a nNOS inhibitor in healthy tissues, since in isolated enzyme assays it has been reported to exhibit significant selectivity for nNOS over eNOS (**Table 6.1**), and endogenous iNOS expression usually requires immune challenge (Kroncke *et al.*, 1998). Indeed, L-VNIO (0.1 μM) and 1400-W (1 μM) have been reported to block NMDA-induced cGMP accumulation in adult rat hippocampal slices, which is well-accepted to be nNOS-dependent (Huang *et al.*, 1993), and NO-dependent LTP at CA1-CA3 synapses in adult mouse hippocampal slices. The latter could be restored upon application of exogenous NO. At the same concentrations, neither compound affected cGMP accumulation in rat aortic rings upon stimulation with ACh (Hopper and Garthwaite, 2006), which is eNOS-dependent (Furchgott and Zawadzki, 1980; Huang *et al.*, 1995).

Since these findings were published, L-VNIO and 1400-W have been used at the above concentrations (0.1 μM and 1 μM , respectively) to test for the involvement of nNOS in the physiology of various tissues, including hippocampus, cortex and cerebellum (for example, Hall and Attwell, 2008; Taqatqeh *et al.*, 2009; Romberg *et al.*, 2009; Neitz *et al.*, 2011). However, recent findings indicate that their potency and selectivity may vary in different tissue preparations. First, it was reported that 10-fold higher concentrations of L-VNIO were required to block NMDA-induced cGMP accumulation in immature rat hippocampal slices and that this concentration also inhibited ACh-induced cGMP accumulation in aortic rings (Bartus, 2009).

Second, tests of the NOS isoform(s) involved in the modulation of basal neurotransmitter release (**Chapter 4**) and expression of NMDA receptor-independent LTP (**Chapter 5**) at CA1 synapses led us to the finding that 0.1 μM L-VNIO and 1 μM 1400-W have no effect on cGMP accumulation in slices of adult mouse hippocampus (see **Figure 6.1** and **6.3** below).

6.2 Aim

Given the diverse roles of nNOS in the mammalian CNS, the wealth of research being directed to understand these roles, and the potential therapeutic benefits of nNOS inhibition, alternative inhibitors to L-VNIO and 1400-W that are potent and selective for nNOS across different tissues are highly desirable.

Work in the laboratory of Professor R.B. Silverman (Northwestern University, Chicago, USA) has produced a series of pyrrolidine ($\text{C}_4\text{H}_9\text{N}$)-based compounds shown to potently inhibit nNOS in cell-free and cell-based assays with unrivalled selectivity over e- and iNOS (Ji *et al.*, 2009; Lawton *et al.*, 2009; Xue *et al.*, 2010a; Xue *et al.*, 2010b). One of the most recently developed compounds, described in Xue *et al.* (2010a) and called FX-5043 here, has a K_i (calculated using an IC_{50} measured in an isolated enzyme assay) of 80 nM, and is ~ 780 - and ~ 650 -fold selective over eNOS and iNOS, respectively (as calculated using K_i values; see **Table 6.1** for structure).

Concerns over the bioavailability of other pyrrolidine based nNOS inhibitors have been raised (Lawton *et al.*, 2009; Xue *et al.*, 2010a). However, unlike its parent compound (Compound 1 in **Table 6.1**), which, at physiological pH, is predicted to be mostly ($> 85\%$ as assessed using MarvinSketch 5.4.1.1, ChemAxon Kft., Budapest, Hungary) charged at both NH groups, FX-5043 is predicted to be mostly monocationic, because the CF_2 group, which is electron withdrawing, is expected to lower the pK_a of the adjacent NH (Xue *et al.*, 2010a). As a result, FX-5043 has been found to cross membranes ~ 2.5 -fold better than its parent compound (calculated by comparing ratios of IC_{50} values measured using cell-free and cell-based assays; Xue *et al.*, 2010a) and retain high potency for rat nNOS over-expressed in HEK T293

cells (~ IC₅₀ determined after 8 hr pre-incubation in the presence of a Ca²⁺ ionophore and 10 μM L-arginine = 19 μM; Xue *et al.*, 2010a; see Fang and Silverman, 2009 for further details of the cell-based assay). Therefore, we aimed to test the potential of the compound as a selective nNOS inhibitor using intact tissues. A second potential nNOS inhibitor, JK-5 (see **Table 6.1**), with a structure based upon FX-5043 was also tested.

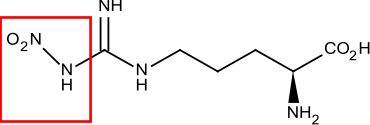
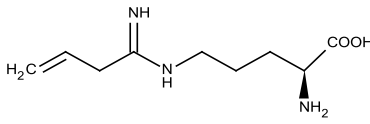
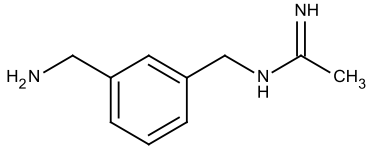
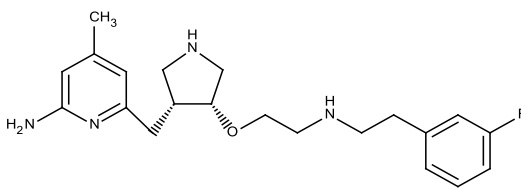
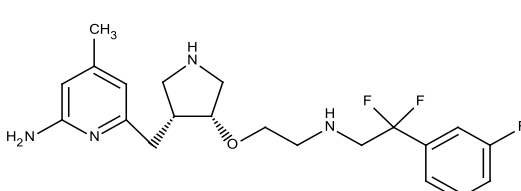
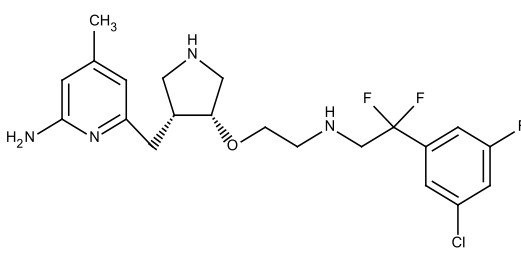
| Compound name and structure | ~ K_i (μM) | | | ~ Selectivity | | |
|---|---------------------------|-------|-------|---------------|-------|--------|
| | nNOS | eNOS | iNOS | e/n | i/n | e/i |
| L-NNAⁱ  | 0.015 | 0.039 | 4.4 | 2.6 | 293.3 | 0.009 |
| L-VNIOⁱⁱ  | 0.1 | 12 | 60 | 120 | 600 | 0.2 |
| 1400-Wⁱⁱⁱ  | 2 | 50 | 0.007 | 25 | 0.004 | > 7000 |
| Compound 1^{iv}  | 0.015 | 31 | 9.5 | > 2000 | 633.3 | 3.3 |
| FX-4053^{iv}  | 0.08 | 62 | 52 | 775 | 650 | 1.2 |
| JK-5^v  | - | - | - | - | - | - |

Table 6.1 Summary of NOS inhibitors discussed. Structures were taken from suppliers. For L-NNA, note that if the groups highlighted by the red box were replaced with NH_2 , the structure would show

L-arginine. Ki data were taken from: ⁱ Furfine et al. (1993) and Garvey et al. (1994); ⁱⁱ Babu and Griffith (1998); ⁱⁱⁱ Garvey et al. (1997); ^{iv} Xue et al. (2010a). ^v No published Ki is available. Selectivity was calculated as the ratio of Ki values.

6.3 Methods

6.3.1 Animals

Studies of the effect of L-VNIO and 1400-W on nNOS activity in hippocampus were performed using male 6-8 week-old C57/B16 mice from Charles River (Margate, UK). For all other experiments, male, 9-10 day-old Sprague Dawley rats (Charles River) were used.

6.3.2 Preparation of transverse hippocampal slices

Hippocampal slices, 400 µm-thick, were cut using the methods described in **Chapter 2.2.2.**

6.3.3 Preparation of cerebellar slices and aortic rings

Sprague Dawley rat pups were culled and decapitated. The cerebella were removed from the brains and 400 µm-thick sagittal slices were cut using a McIlwain tissue chopper (Campden Instruments, Loughborough, UK). In one experiment, aortic rings were prepared by Prof. John Garthwaite (UCL, London, UK). The aorta was exposed and the perivascular connective tissue was removed. The thoracic portion was dissected out into ice-cold Krebs solution containing (in mM) 120 NaCl, 2 KCl, 26 NaHCO₃, 1.19 MgSO₄, 1.18 KH₂PO₄, 11 D-glucose, 2 CaCl₂, equilibrated with 95 % O₂/ 5 % CO₂ (pH 7.4). Any remaining blood was washed away and 2-3 mm-wide rings were cut using a razor blade. Tissues were then recovered in oxygenated Krebs solution at 37°C for at least 1 hr.

6.3.4 Extracellular electrophysiological recordings at CA3-CA1 synapses

Extracellular electrophysiological recordings were made at CA3-CA1 synapses using the methods detailed in **Chapter 5.3.3**.

6.3.5 cGMP measurement

Hippocampal slices were randomly assigned to flasks of oxygenated aCSF (30°C) and cerebellar slices and aortic rings to flasks of oxygenated Krebs solution (37°C), all held in a shaking water-bath. Neuronal NOS dependent-cGMP production was stimulated in brain slices by exposure to NMDA (100 µM, 2 min). ACh (10 µM, 1 min exposure) was used to stimulate eNOS in aortic rings. In order that a significant accumulation of cGMP could be detected, hippocampal slices were pre-treated with the PDE 2 inhibitor, BAY 60-7550 (1 µM; 10 min pre-incubation) and aortic rings with the non-selective inhibitor, IBMX (1 mM; 20 min pre-incubation). PDE inhibition was not necessary to detect cGMP in cerebellar slices. Details of all other drugs applied are given in the text.

Immediately after stimulation (within 30 s), tissues were individually inactivated by submersion in 200 µl boiling buffer containing 50 mM tris-HCl and 4 mM EDTA (pH 7.4). Cyclic GMP was measured by radioimmunoassay and protein using the BCA method (see **Chapter 2.2.4-5** for methods). In every experiment, un-stimulated cGMP levels and the effect of the non-selective NOS inhibitor, L-NNA (100 µM, minimum 20 min pre-incubation) on the stimulated cGMP response were measured.

6.3.6 Liquid chromatography-mass spectrometry

Liquid chromatography-mass spectrometry was performed by Dr. Matthew Gooding (UCL, London, UK). Buffer for mass spectrometry contained formic acid, which added 1 proton to each sample compound.

6.3.7 Analysis and Statistics

Analysis of LTP

Values of LTP quoted in the text are means \pm SEM 55-60 min post HFS. Statistical significance was assessed using two-tailed unpaired t-tests.

Analysis of NOS activity assays

Values in the text are means \pm SEM. To assess statistical significance between data sets, two-tailed t-tests or one-factor ANOVA with Tukey-Kramer or Dunnett's multiple comparisons test were used.

6.4 Results

6.4.1 Effect of L-VNIO on NMDA-induced cGMP accumulation in adult mouse hippocampal slices

Hopper and Garthwaite (2006) determined that 0.1 μ M L-VNIO and 1 μ M 1400-W completely inhibit nNOS in adult rat hippocampal slices by measuring their effect on NMDA-induced cGMP accumulation. This is well-accepted to depend upon nNOS, since, in the hippocampus, Ca²⁺-dependent NO synthesis has been shown to be absent in nNOS-deficient mice (Huang *et al.*, 1993). They also showed that LTP at CA1 synapses in adult mouse hippocampal slices was blocked after 15 min incubation with 0.1 μ M L-VNIO.

In adult mouse hippocampal slices, it was therefore expected that L-VNIO would inhibit a form of CA1 LTP that was NO-dependent but eNOS-independent (see **Chapter 5** for details of the LTP). However, pre-incubation of slices for 15 min with 0.1 μ M of the compound had no effect on the potentiation (**Figure 6.1A**).

To control for the lack of effect of 0.1 μM L-VNIO on the LTP, its effect on NMDA-induced cGMP accumulation was tested. In slices pre-incubated with the PDE2 inhibitor, BAY-60 7550 (1 μM , 10 min), NMDA (100 μM , 2 min exposure) generated a significant accumulation of cGMP compared to the amount of cGMP measured in basal/un-stimulated slices. This response was abolished in slices pre-treated with 100 μM L-NNA for 25 min, but unaffected by L-VNIO (**Figure 6.1B**).

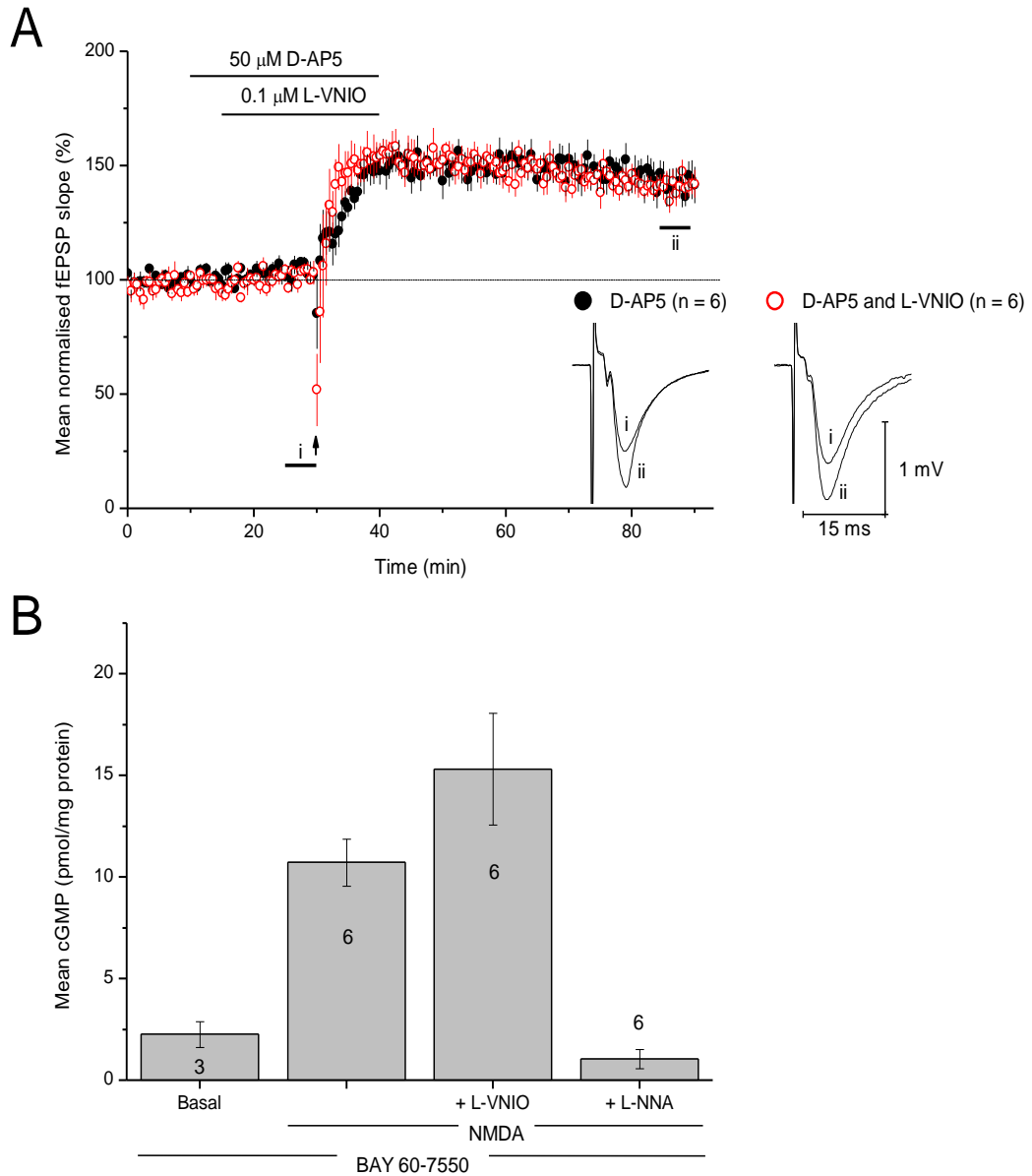


Figure 6.1 Effect of L-VNIO on NMDA-induced cGMP accumulation and nNOS-dependent LTP in adult mouse hippocampal slices. **A**) There was no significant effect of 0.1 μM L-VNIO on nNOS-dependent LTP at CA1 synapses (unpaired *t*-test, $p = 0.928$). High frequency burst stimulation was

applied at the arrow. The insets represent the mean fEPSP recorded at the time indicated by the numbered bars. The stimulus artefacts have been truncated. B) In slices pre-treated with 10 μ M BAY-60 7550, NMDA (100 μ M, 2 min exposure) induced a significant accumulation of cGMP from basal levels ($p < 0.05$). This was inhibited by pre-treatment with 100 μ M L-NNA ($p > 0.05$ compared to basal cGMP) but not with 0.1 μ M L-VNIO ($p > 0.05$ compared to NMDA-induced cGMP). Pre-incubation times for BAY-60 7550, L-NNA and L-VNIO were 10, 25 and 15 min, respectively.

Statistics are ANOVA with Tukey-Kramer. Numbers in bars are n values.

One simple explanation for the lack of effect of L-VNIO on NMDA-induced cGMP accumulation and nNOS-dependent LTP was that the compound was not authentic. Therefore a sample was processed for liquid chromatography-mass spectrometry. As shown in **Figure 6.2**, the compound appeared to be undegraded and free of major impurities.

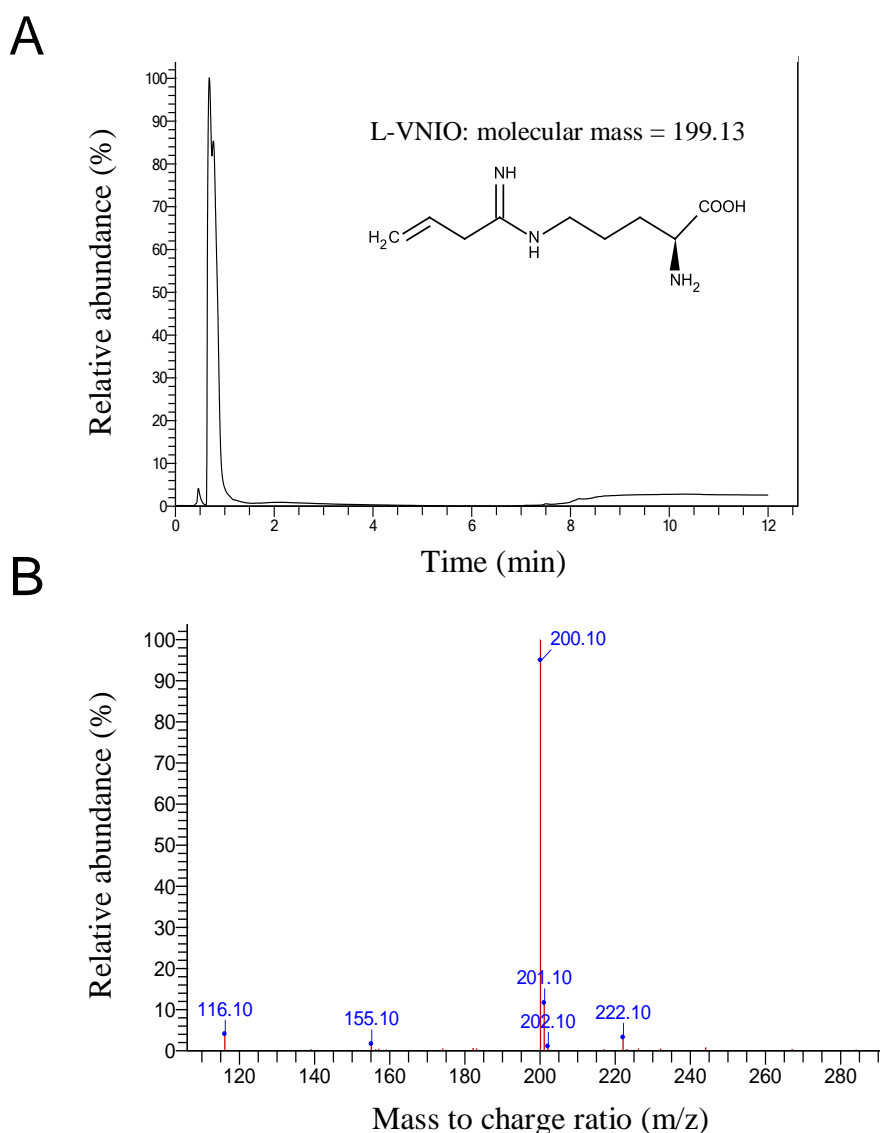


Figure 6.2 Chemical analysis of L-VNIO. **A)** Liquid-chromatography of L-VNIO yielded a single major peak in the chromatogram at ~ 45 s. Inset shows the structure and exact mass of L-VNIO. **B)** Analysis of this peak by mass spectrometry showed that the most abundant molecular ion present had a mass to charge ratio (blue) of 200.1, the predicted exact mass of L-VNIO (199.13) plus 1 proton.

6.4.2 Effect of 1400-W on NMDA-induced cGMP accumulation in adult mouse hippocampal slices

In light of the above results, the effect of 1400-W, the next most potent and selective nNOS inhibitor available, on NMDA-induced cGMP accumulation was tested. As shown in **Figure 6.3**, 1400-W applied at the same concentration and for the same duration as Hopper and Garthwaite (2006; 1 μ M, 15 min pre-incubation), failed to

inhibit cGMP accumulation in response to NMDA (100 μ M, 2 min exposure), although the response was blocked by 100 μ M L-NNA.

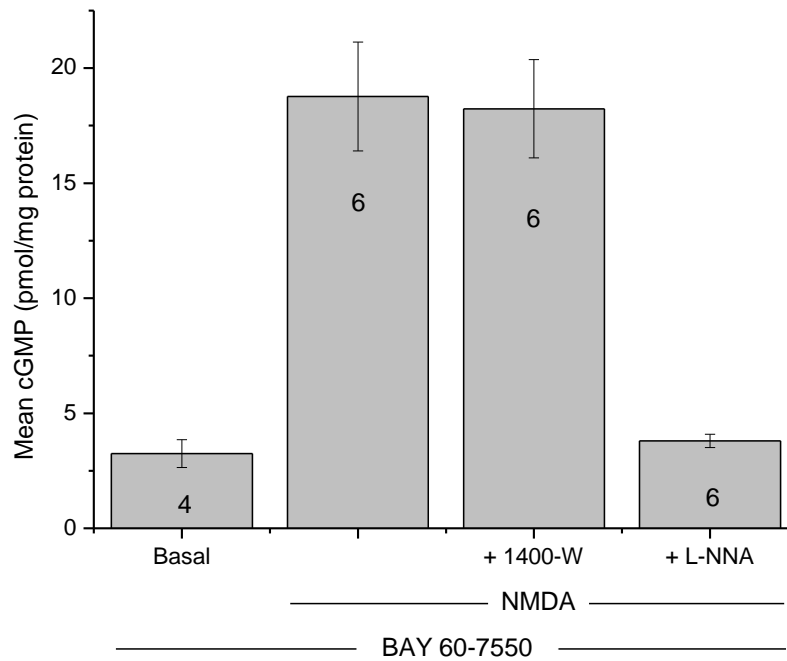


Figure 6.3 Effect of 1400-W on NMDA-induced cGMP accumulation in adult mouse hippocampal slices. In slices pre-treated with the PDE2 inhibitor, BAY 60-7550 (10 μ M) for 10 min, NMDA (100 μ M, 2 min exposure) generated a significant accumulation of cGMP ($p < 0.001$ compared to basal cGMP). This was not effected by 1400-W (1 μ M, 15 min pre-incubation; $p > 0.05$ compared to NMDA-induced cGMP), although it was abolished by L-NNA (100 μ M, 25 min; $p > 0.05$ compared to basal cGMP). Statistics are ANOVA with Tukey-Kramer. Numbers in bars are n values.

Using liquid chromatography-mass spectrometry, 1400-W was also found to be authentic, undegraded and free from major impurities (**Figure 6.4**).

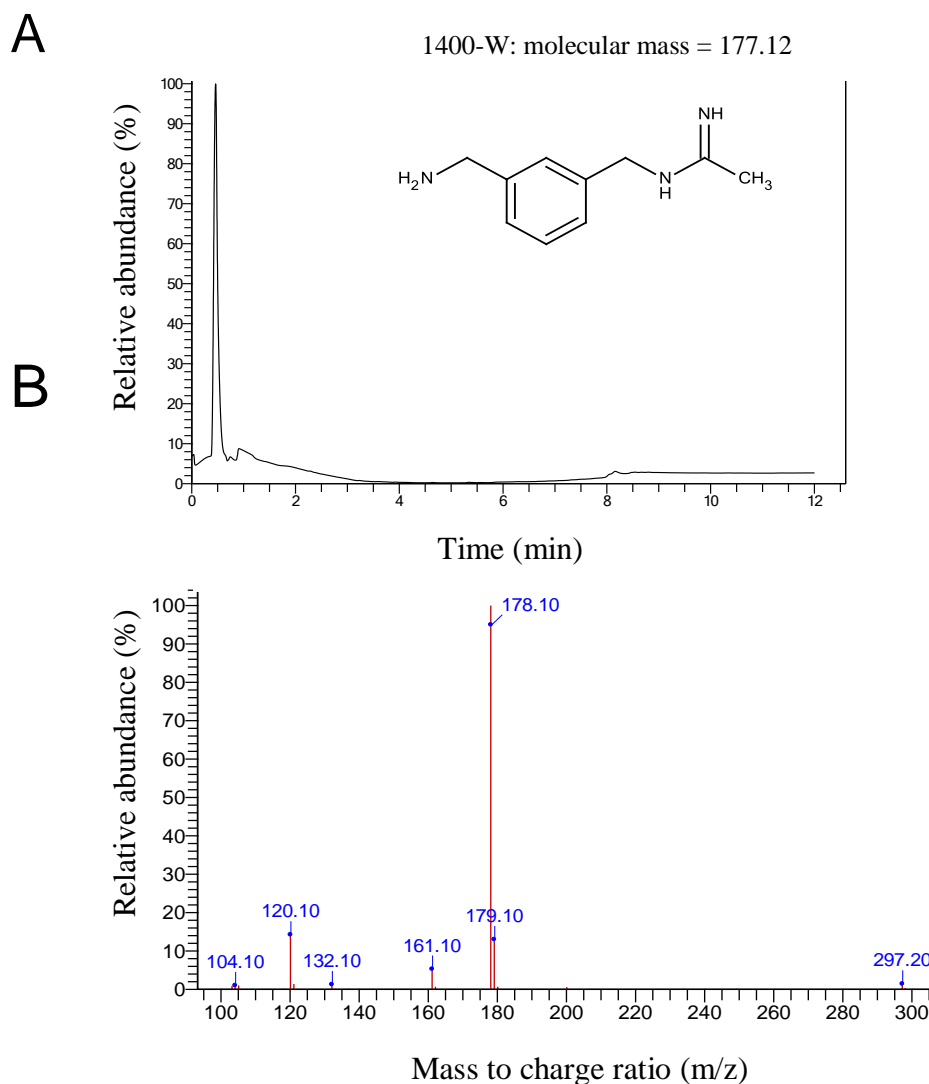


Figure 6.4 Chemical analysis of 1400-W. **A)** Chemical structure of 1400-W as specified by the manufacturer. **B)** A single peak in the chromatogram was recorded. **C)** Using mass spectrometry it was found that this peak was largely composed of a compound with a mass to charge ratio (blue) equal to the predicted exact mass of 1400-W, 177.12 (plus 1 proton donated by formic acid).

6.4.3 Effect of gem-difluorinated, pyrrolidine-based compounds on cGMP accumulation in immature rat tissues

The above results are contrary to previous reports that 0.1 μM L-VNIO and 1 μM 1400-W block NMDA-induced cGMP accumulation in adult rat hippocampal slices (Hopper and Garthwaite, 2006). As discussed above, L-VNIO (0.1 μM) has also been reported to be ineffective in blocking NMDA-induced cGMP accumulation in immature (10 day-old) rat hippocampal slices (Bartus, 2009). A 10-fold higher

concentration (1 μM) was effective but also inhibited eNOS-dependent, ACh-induced cGMP accumulation in immature rat aortic rings. Therefore, to address the lack of available potent and selective nNOS inhibitors which are effective across multiple tissues, two potentially highly potent and selective nNOS inhibitors (Xue *et al.*, 2010a; Xue *et al.*, 2010b) were obtained from Professor Richard B. Silverman (see FX-5043 and JK-5 in **Table 6.1**) and their efficacy in intact tissues was evaluated.

First, their effect on nNOS-dependent, NMDA-induced cGMP accumulation was determined. To improve the sensitivity of the assay and negate the requirement for PDE inhibition, rat immature cerebellar slices were used, since they have been shown in the laboratory to produce significantly more cGMP in response to NMDA than hippocampal slices.

In initial experiments, exposure to 100 μM NMDA for 2 min yielded 224 ± 21 pmol cGMP/mg protein ($n = 9$). This response was inhibited by L-NNA (100 μM , 25 min pre-incubation) and by FX-5043 or JK-5 (with 20 min pre-incubation) in a concentration-dependent manner (IC_{50} values were ~ 30 μM ; **Figure 6.5A**). Subsequently, it was found that inhibition by 30 μM FX-5043 increased exponentially with pre-incubation time (**Figure 6.5B**; note log scale), concordant with the idea that short pre-incubations are insufficient to allow for complete tissue penetration.

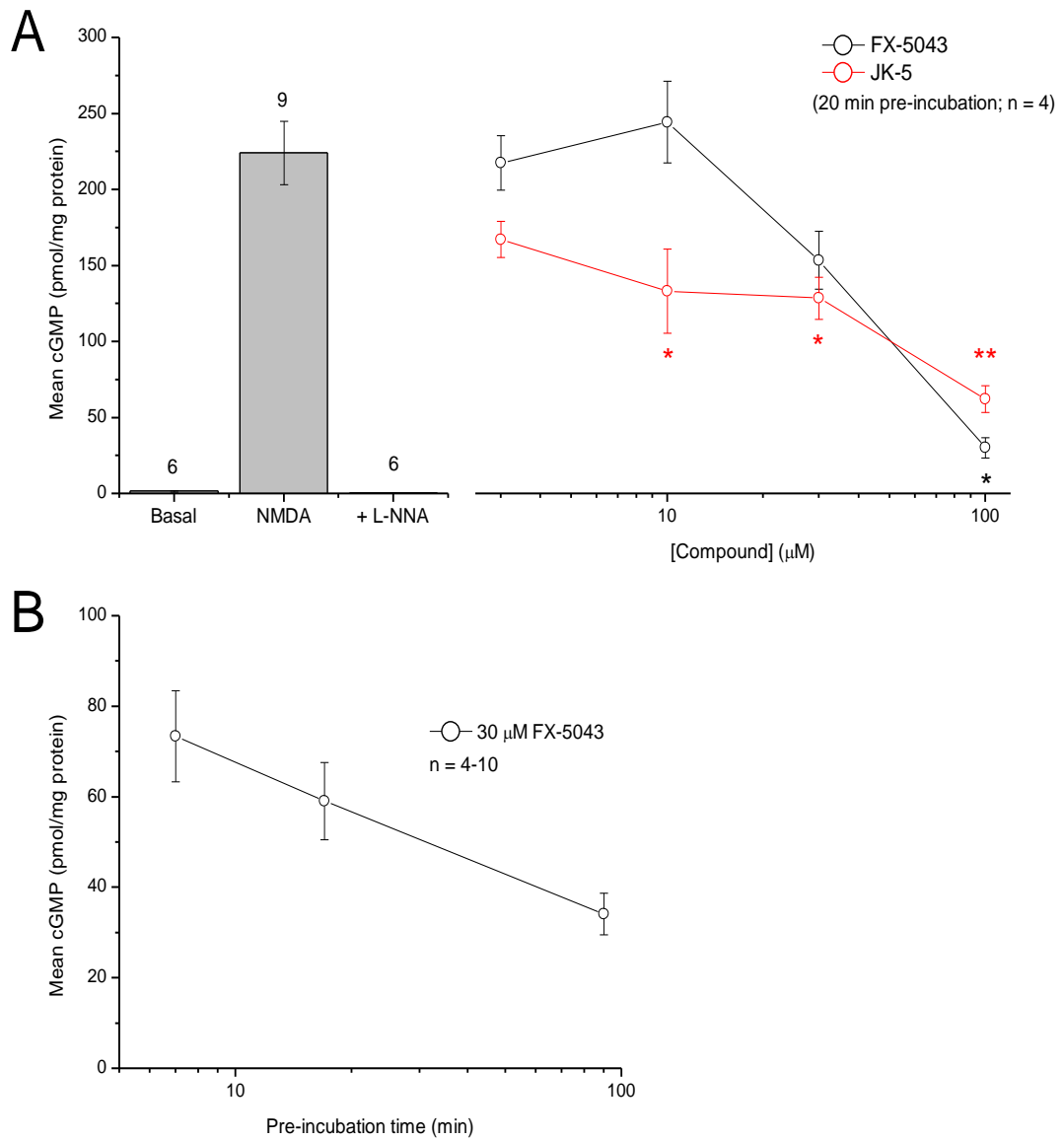


Figure 6.5 Characterisation of the putative nNOS inhibitors, FX-5043 and JK-5, using immature rat cerebellar slices. **A**) Exposure of slices to 100 μM NMDA for 2 min generated a significant increase in cGMP (ANOVA with Tukey-Kramer, $p < 0.001$ compared to basal cGMP) which was inhibited by L-NNA (100 μM pre-incubated for 25 min; $p > 0.05$ compared to basal cGMP) and by FX-5043 or JK-5 in a concentration-dependent manner (* $p < 0.05$, ** $p < 0.01$ compared to cGMP in slices treated with NMDA alone; ANOVA with Dunnett's test). **B**) Inhibition by 30 μM FX-5043 was improved with longer pre-incubation (note log scale). Numbers in bars are n values.

Following pre-incubation with 100 μ M FX-5043 or JK-5 for 90 min, NMDA-induced cGMP accumulation was blocked. Treatment with the vehicle (DMSO) alone had no effect (**Figure 6.6**).

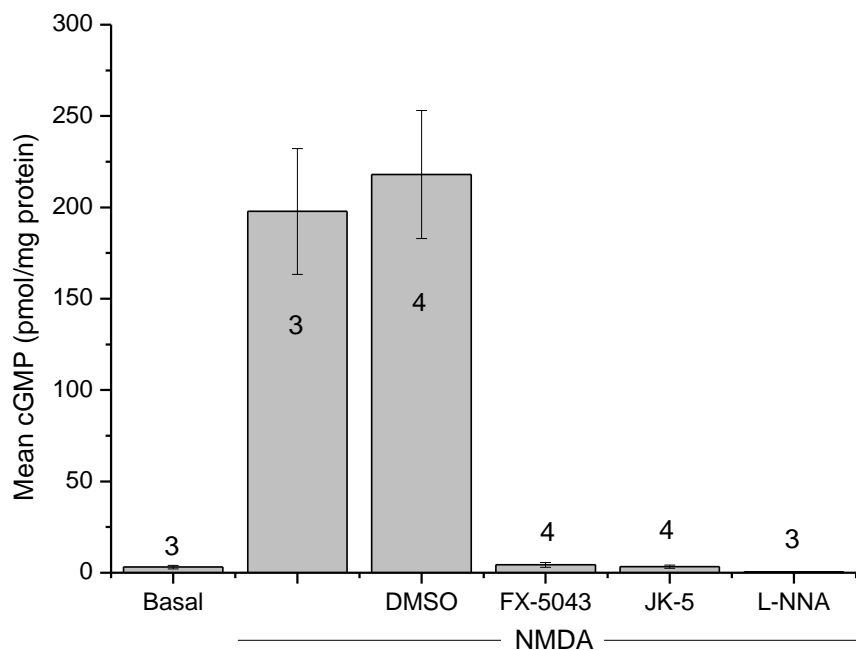


Figure 6.6 Effect of 100 μ M FX-5043 and JK-5, pre-incubated for 90 min, on NMDA-induced cGMP accumulation in rat cerebellar slices. NMDA-induced cGMP accumulation was reduced to basal levels by FX-5043, JK-5 and L-NNA (all 100 μ M, 90 min pre-incubation; ANOVA with Tukey-Kramer, $p > 0.05$ compared to basal). DMSO itself had no effect ($p > 0.05$ compared to cGMP in slices treated with NMDA alone). Numbers in bars are n values.

Finally the selectivity of the compounds was evaluated by measuring their effect on eNOS-dependent, ACh-induced cGMP accumulation in aortic rings. The same animals and conditions as in **Figure 6.6** were used. Rings were pre-treated with the non-selective PDE inhibitor, IBMX (1 mM), for 20 min. ACh (10 μ M for 1 min) generated a significant increase in cGMP from basal levels. This was reduced to basal levels by FX-5043 and JK-5. The vehicle, DMSO, had no effect (**Figure 6.7**).

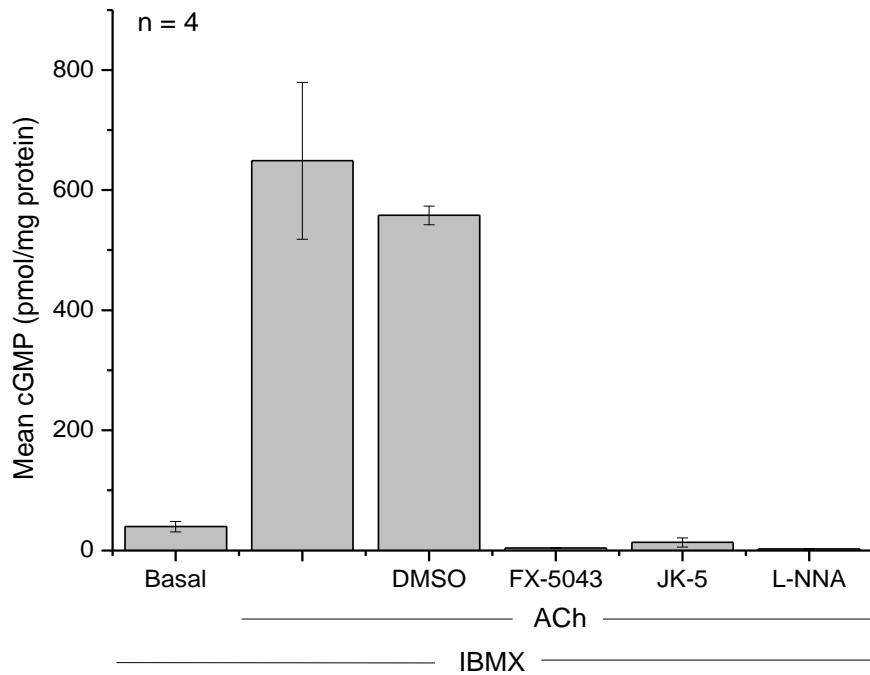


Figure 6.7 Effect of 100 μ M FX-5043 and JK-5, pre-incubated for 90 min, on ACh-induced cGMP accumulation in rat aortic rings. Aortic rings were pre-treated with 1 mM IBMX for 20 min. Animals and conditions were the same as **Figure 6.6**. ACh-induced significant cGMP accumulation from basal levels (ANOVA with Tukey-Kramer, $p < 0.001$). This was reduced to basal levels by FX-5043, JK-5 and L-NNA (all 100 μ M, 90 min pre-incubation; $p > 0.05$ compared to basal/un-stimulated levels). DMSO alone had no effect ($p > 0.05$ compared to cGMP in rings treated with ACh alone).

6.5 Discussion

Since the initial characterisation of the effect of L-VNIO and 1400-W on NMDA-induced cGMP accumulation and CA1 LTP in adult rat and mouse hippocampus, respectively (Hopper and Garthwaite, 2006), L-VNIO and 1400-W have been widely used at standard concentrations (0.1 μ M and 1 μ M, respectively) to affect selective nNOS inhibition in various tissues (for example, Hall and Attwell, 2008; Taqatqeh *et al.*, 2009; Romberg *et al.*, 2009; Neitz *et al.*, 2011). In one case, NO-dependent synaptic plasticity at CA1 synapses in adult mouse hippocampal slices that was insensitive to 0.1 μ M L-VNIO was assumed to be nNOS-independent (Neitz *et al.*, 2011). However, in accordance with previous findings in immature rat hippocampus (Bartus, 2009), one of the main conclusions of this study was that neither L-VNIO

(0.1 μM) nor 1400-W (1 μM) are at all effective in inhibiting NMDA-induced cGMP accumulation in adult mouse hippocampal slices (**Figure 6.1** and **6.3**).

There could be several reasons for the discrepancy between our findings and those of Hopper and Garthwaite (2006). Given that L-VNIO and 1400-W are competitive for binding to nNOS with L-arginine (Garvey *et al.*, 1997; Babu and Griffith, 1998), one explanation could be that the concentration of the amino acid varies between different tissues and tissue preparations. This is conceivable since L-arginine, which can be as concentrated as 80 μM in the cerebrospinal fluid of 8-week old rats (Takasugi *et al.*, 2003), is not normally included in solutions used to incubate tissues *in vitro*. Other reasons are likely to be related to the bioavailability of the compounds or their affinity for NOS in different tissues from different species. Factors underlying differences in bioavailability could include tissue and cell permeability, metabolism and transport of compounds. Differences in the compounds' affinity for NOS could arise, for example, through phosphorylation of the enzyme. The only clear methodological difference between the experiments performed by us and Hopper and Garthwaite (2006) to measure the effect of L-VNIO and 1400-W on NMDA-induced cGMP accumulation is the PDE 2 inhibitor used (BAY 60-7550 vs. EHNA). Experiments are planned to test whether these factors may account for the differences in potency of the inhibitors.

Regardless of the explanation, L-VNIO and 1400-W are clearly not ideal nNOS inhibitors and should not be used to determine the role of nNOS in biological phenomena without the appropriate tissue-specific controls for their potency. In light of the above results, published data on the effect of L-VNIO and 1400-W on biological phenomena should perhaps be re-interpreted and in future, the 'inhibitors' should be used cautiously, if at all.

The selectivity of other established nNOS inhibitors is also in doubt. For example, at the isolated enzyme level, the compound, N-propyl-L-arginine (NPA), reportedly displays high selectivity for nNOS over iNOS (3158-fold difference) and eNOS (149-fold difference) (Zhang *et al.*, 1997), but this has not been confirmed *in vivo* (Gowda *et al.*, 2004). 7-nitroindazole (7-NI) is also widely used as a selective nNOS

inhibitor *in vitro* and *in vivo*, although it has been reported to be completely non-selective at the isolated enzyme level (Alderton *et al.*, 2001). Its apparent selectivity in intact tissues could be explained if it accumulates preferentially in neurons rather than endothelial cells. Nevertheless, selective nNOS inhibition should ideally be achieved by the differential action of compounds on NOS isozymes, rather than through differences in compound bioavailability.

To address the lack of potent and selective nNOS inhibitors effective across multiple tissue preparations, we sought to evaluate two, new, gem-difluorinated, pyrrolidine-based compounds (FX-5043 and JK-5). As discussed above, FX-5043 has been shown to potently inhibit nNOS with unrivalled selectivity over both e- and iNOS in isolated enzyme and cell-based assays (Xue *et al.*, 2010a). However, under the conditions necessary to effect complete inhibition of nNOS-dependent, NMDA-induced cGMP accumulation in adult rat cerebellar slices (100 μ M, 90 min pre-incubation), we found that FX-5043 and JK-5 blocked eNOS-dependent, ACh-induced cGMP accumulation in adult rat aortic rings (**Figure 6.6** and **6.7**).

One possible explanation for the apparent lack of selectivity for nNOS over eNOS in intact tissues was that they also inhibit NO-targeted guanylyl cyclase. This could have explained why FX-5043 was observed to selectively inhibit nNOS over eNOS and iNOS using a cell-based assay, because this assay relied upon the measurement of the accumulation of nitrite, a metabolite of NO, in the medium (Fang and Silverman, 2009). However, tests of this possibility have since shown that the compounds have no significant effect on DEA/NONOate-induced cGMP production by purified bovine NO-targeted guanylyl cyclase (Prof. John Garthwaite, unpublished work).

Another reason for the apparent lack of selectivity of the compounds in intact tissues could be that they preferentially accumulate in endothelial cells over neurons to the extent that, at the concentration necessary to affect nNOS inhibition, the concentration in endothelial cells is so high that it inhibits eNOS. Given the reported K_i values of the compound (Xue *et al.*, 2010a), the difference in concentration between endothelial and neuronal cells would probably have to be ~ an order of

magnitude. Also, it cannot be ruled out that the compounds have some other, perhaps toxic, secondary effect on intact tissues, leading to a decrease in cGMP production.

Irrespective of the explanation, the main conclusion to be drawn from the data is that, while FX-5043 and JK-5 might be useful for selectively inhibiting nNOS at the level of the isolated enzyme or cell-based assay, their application to intact tissues is not appropriate. Since both compounds had a relatively high IC_{50} in cerebellar slices (~30 μ M following 20 min pre-incubation; **Figure 6.5A**), require long pre-incubation times to be effective, likely due to poor tissue penetration, and may have unknown secondary effects, they should also not be used as non-selective NOS inhibitors over L-arginine-based compounds such as L-NNA, which have IC_{50} values in the low micromolar range (see above for details), are actively transported into cells and have no known secondary effects in tissues (Alderton *et al.*, 2001).

Recently a symmetric, double headed aminopyridine has been developed that shows lower potency and selectivity for nNOS but increased cell permeability compared to the gem-difluorinated compounds used here (Xue *et al.*, 2011). This, as well as the above data, could be useful in directing the development of more compounds with high potency and selectivity for nNOS in its native state. Meanwhile, the results of studies using ‘selective’ nNOS inhibitors currently widely available should be interpreted with caution.

Chapter 7:

The location of NO-targeted guanylyl cyclase in adult mouse hippocampus

7.1 Introduction

As discussed previously (see **Chapter 1**), functional evidence has implicated NO/cGMP signalling to be active in multiple brain regions in several species in which it may contribute to the generation of diverse phenomena (Garthwaite, 2008). Accordingly, studies employing *in situ* hybridisation and immunohistochemistry have suggested the presence of NOS and NO-targeted guanylyl cyclase throughout the developing and mature rodent brain, albeit at varying levels in different regions (nNOS; Vincent and Kimura, 1992; Rodrigo *et al.*, 1994; eNOS ; Seidel *et al.*, 1997 ; Stanarius *et al.*, 1997; Topel *et al.*, 1998; Demas *et al.*, 1999; NO-targeted guanylyl cyclase; Matsuoka *et al.*, 1992; Gibb and Garthwaite, 2001; Ding *et al.*, 2004). Moreover, NADPH diaphorase histochemistry for NOS in rat brain has shown a remarkably coincident distribution with structures immunopositive for cGMP following *in vivo* perfusion of the NO donor, sodium nitroprusside (Southam and Garthwaite, 1993), consistent with functional evidence that guanylyl cyclase is the primary target of endogenous NO.

In the hippocampus, functional studies suggest that eNOS, nNOS and all three functionally relevant guanylyl cyclase subunits, $\alpha 1$, $\alpha 2$ and $\beta 1$, are present in area CA1 (**Chapters 3-6**; Hopper and Garthwaite, 2006; Taqatqeh *et al.*, 2009). This has largely been corroborated by histological data (see **Chapter 1**); however, the precise location of the guanylyl cyclase $\alpha 1$ subunit has recently come under question.

Studies employing NO-targeted guanylyl cyclase $\alpha 1$ - and $\alpha 2$ - lacking mice (NOGC $\alpha 1^{-/-}$ and NOGC $\alpha 2^{-/-}$, respectively) have shown that both the $\alpha 1\beta 1$ and $\alpha 2\beta 1$ isoforms are necessary for LTP in the visual cortex (Haghikia *et al.*, 2007) and hippocampus (Taqatqeh *et al.*, 2009). In the hippocampus, Taqatqeh *et al.* (2009) report that under basal conditions, and following LTP, PPF at CA1 synapses in NOGC $\alpha 1^{-/-}$ mice is increased compared to wild-type mice and recently, evidence in favour of $\alpha 1$ -dependent tonic modulation of transmitter release at CA1 synapses has been extended (Neitz *et al.* 2011 and **Chapter 4**). The results of these studies consistently imply that the $\alpha 1\beta 1$ isoform is located presynaptically and is responsible for transducing NO-dependent changes in transmitter release onto CA1 neurons.

Conversely, knocking-out the $\alpha 2$ subunit appears to have no effect on PPF or other measures of presynaptic transmitter release, such as miniature EPSC frequency (Taqatqeh *et al.*, 2009; Neitz *et al.*, 2011). One interpretation of this is that the $\alpha 2\beta 1$ isoform is postsynaptic.

Changes in PPF at CA1 synapses following plasticity are typically interpreted as a result of changes in presynaptic transmitter release occurring directly at Schaffer-collateral axon terminals. Much research has been directed to understanding these presynaptic forms of LTP and the involvement of NO in them (Arancio *et al.*, 1995; Arancio *et al.*, 1996; Arancio *et al.*, 2001). However, there is no unambiguous evidence that the $\alpha 1$ subunit is present at CA3-CA1 synapses. In a report by Gibb and Garthwaite (2001), low magnification images of hippocampus labelled for $\alpha 1$ mRNA showed message for the subunit to be located in the stratum radiatum, but it was unclear whether the subunit was in pyramidal neurons or interneurons. Rather, a key study using *in situ* hybridization and immunohistochemistry in conjunction with electron microscopy showed that $\alpha 2$ (which was co-localised with $\beta 1$) was expressed only in pyramidal cells and $\alpha 1$ (also co-localised with $\beta 1$) only in interneurons. These interneurons, the majority of which were parvalbumin- or cholecystokinin-positive and therefore probably basket cells, formed synapses on CA1 pyramidal cell soma, dendrites and axon initial segments. Neuronal NOS was found to be localised to the PSD of these synapses, suggesting that GABAergic inputs to CA1 pyramidal neurons may be retrogradely modulated by NO-targeted $\alpha 1\beta 1$ guanylyl cyclase activity (Szabadits *et al.*, 2007). This distribution of NOS and $\alpha 1\beta 1$ has since been confirmed in the developing hippocampus (Cserep *et al.*, 2011).

Taken together, the studies discussed above suggest that NO regulates transmitter release at the GABAergic, rather than glutamatergic, inputs to CA1 pyramidal neurons. Consistent with this, NO has been shown to modulate GABAergic transmission in several brain areas (for a review see Garthwaite, 2008). In the ventral tegmental area, for example, NO produced by dopaminergic neurons upon NMDA receptor activation has been found to retrogradely modulate GABA release from nearby inhibitory axon terminals, resulting in a heterosynaptic long-term potentiation of GABA_A-mediated synaptic transmission (Nugent *et al.*, 2007). In the

hippocampus, NO may act in conjunction with endocannabinoids as a retrograde messenger to depress GABAergic IPSCs (Makara *et al.*, 2007). Depression of GABAergic transmission in area CA1 by NO via the NO-targeted $\alpha 1\beta 1$ guanylyl cyclase isoform has also recently been reported to occur in slices from young (p5-p8) mice (Cserep *et al.*, 2011). However, the notion that apparent changes in transmitter release following LTP may be due to the effect of NO at GABAergic rather than glutamatergic synapses is at odds with findings that NO, produced postsynaptically may, through cGMP and PKG, induce a presynaptic LTP characterised by an increase in transmitter release between pairs of pyramidal neurons (identified by electrophysiological properties) in dissociated cell culture (Arancio *et al.*, 1995; Arancio *et al.*, 1996; Arancio *et al.*, 2001).

7.2 Aim

The pattern of $\alpha 1$ expression reported by Szabadits *et al.* (2007) was consistent following immunofluorescent, immunoperoxidase and *in situ* hybridization techniques in tissue fixed with 4 % PFA and accorded with immunostaining for $\alpha 1$ in sections of immature hippocampus, also fixed with 4 % PFA (Cserep *et al.*, 2011). However, it is known that the distribution of proteins as determined by histochemical methods can be significantly altered by the conditions under which the tissues are processed. Several groups have reported immunostaining for nNOS and the guanylyl cyclase $\beta 1$ subunit in pyramidal neurons in hippocampus fixed with 1 % PFA but not ≥ 4 % PFA (Wendland *et al.*, 1994; Gonzalez-Hernandez *et al.*, 1996; Burette *et al.*, 2002). It has been hypothesised that aldehyde cross-linking of proteins following strong fixation protocols may mask antibody epitopes and/or reduce the access of the antibody to its target protein. The latter circumstance may be particularly common when target proteins are located in PSD's or presynaptic varicosities. Therefore, we sought to re-investigate the distribution of $\alpha 1$ in the hippocampus, using weakly fixed tissue (1 % PFA). The aim was to either confirm the work of Szabadits *et al.* (2007), or to uncover new structures, perhaps pyramidal neurons, immunopositive for the NO-targeted guanylyl cyclase $\alpha 1$ subunit.

7.3 Methods

7.3.1 Animals

Unless otherwise stated, adult (8 week-old), male, C57/B16 mice were used. For some experiments, adult (2 8-9 week-old, 1 19 week-old), male, C57/B16/SV129 mice lacking the NO-receptor guanylyl cyclase $\alpha 1$ subunit (NOGC $\alpha 1^{-/-}$) were used. These were kindly provided by Dr Adrian Hobbs (UCL, London, UK). Male 8-9 week old wild-type siblings were used as controls. Rat brain lysate was prepared from an 8 day-old, male Sprague Dawley pup. All work was conducted in accordance with British Home Office regulations on laboratory animal use and welfare.

7.3.2 General Solutions

Phosphate buffer (PB; 0.2 M) was composed of 19 % 0.2 M NaH₂PO₄·2H₂O and 81 % 0.2 M Na₂HPO₄·2H₂O in double-distilled H₂O adjusted to pH 7.4.

Tris-buffered saline (TBS) comprised 48.4 mM trisma base and 150.2 mM NaCl in double-distilled H₂O equilibrated to pH 7.6 with concentrated HCl.

TBS-triton (TBS-T) additionally included 0.1 % triton X-100.

TBS-tween comprised TBS plus 0.05 % tween 20.

Tissue-lysis buffer consisted of 60 mM tris-HCl (pH 6.8), 1 % SDS, 1 % tween 20 and 1 x Halt protease inhibitor cocktail in double-distilled H₂O.

7.3.3 Immunohistochemistry

Preparation of transverse hippocampal sections

Mice were euthanized by cervical dislocation and decapitated. The hippocampi were either left in the brain during fixing and sectioning, or swiftly dissected out and sliced as described in **Chapter 2: General materials and methods**. In the former case, the brains were removed from the skulls and submerged in freshly prepared, ice-cold 1 % PFA prepared in 0.1 M PB and adjusted to pH 7.4. The anterior and posterior ends of the brains were cut (leaving the middle of the hippocampi intact) using a razor blade and the hemispheres were separated and fixed for 2 hr in 1 or 4 % PFA on a rocker at 4 °C. In the latter case, slices were left to recover in oxygenated aCSF for 1 hr before being fixed for 1 hr using 1 % PFA on a rocker at room temperature. Just prior to fixing of tissue from NOGC α 1^{-/-} and wild-type mice, the cerebellum was removed for Western blot analysis (see below for methods).

After fixing, tissues were washed with 0.1 M PB (4 times, 5 min) and cryoprotected with sucrose in 0.1 M PB (5 % sucrose for 4 h, then 20 % overnight, then 30 % for 4 hr and finally 50:50 30 % sucrose: OCT for 2 hr, all at 4 °C). They were then washed and embedded in OCT and swiftly frozen on dry ice made extra cold with isopentane. Tissue was stored at -80 °C prior to sectioning.

For sectioning, the embedded tissue was mounted on a cutting chuck using OCT. 10 μ m transverse hippocampal sections were made on 0.05 % chrome alum/ 0.5 % gelatine-coated slides using a cryostat (Model OTF, Bright Instruments Co Ltd., UK). During this process, some slides were stained with toluidine blue in order that the hippocampus proper could be visualised and the cutting plane adjusted as necessary. 1 % toluidine blue was prepared as a stock solution in 1 % borate. Before use, this was diluted 1/10 in tap H₂O and filtered. Slides were dried over a flame, washed with filtered toluidine blue for approximately 30 s, rinsed with tap H₂O, dried and mounted in di-N-butyle phthalate in xylene (DPX).

Slides were stored at -20 °C prior to immunohistochemistry.

Immunoperoxidase staining

The sections were rehydrated by washing with ice-cold TBS-T twice for 5 min and incubated for 15 min with a peroxidase suppressor obtained in a methanol solution, thereby reducing the probability of false positive staining due to endogenous peroxidase activity. After washing twice with cold TBS-T for 3 min, the tissue was incubated with 20 % filtered donkey serum (in TBS-T) for at least 1 hr and then with the primary antibody (see **Table 7.1**) in 1 % donkey serum in TBS-T overnight in a humid environment at 4 °C. Controls for the selectivity of secondary antibody binding were included in each experiment. These sections were from the same animal as experimental sections and were fixed and cut at the same time. They received 1 % donkey serum in the absence of primary antibody.

| Primary antibodies | | | |
|--|-------------|---------------------------|---|
| Antigen | Host | Concentration used | Catalogue number and/or supplier |
| Guanylyl cyclase α 1 subunit | Rabbit | 1:400 | G4280; Sigma |
| Guanylyl cyclase β 1 subunit | Rabbit | 1:250 | CAY-160897-1; Axxora (UK) Ltd. (Cayman Chemical) |
| | Rabbit | 1:600 | Prof. Soenke Behrends (see van Staveren <i>et al.</i> 2002) |
| nNOS | Rabbit | 1:700 | 61-7000; Invitrogen (Zymed) |
| Biotinylated secondary antibody | | | |
| Antigen | Host | Concentration used | Catalogue number and/or source |
| Rabbit | Donkey | 1:200 | AP182B; Chemicon |

Table 7.1 Antibodies used for immunoperoxidase staining, their concentration and supplier. Note that the α 1 primary antibody is the same as was used by Szabadits *et al.* (2007).

The next day, the sections were washed twice for 10 min with cold TBS-T and once with TBS, also 10 min. A donkey anti-rabbit biotinylated secondary antibody (see **Table 7.1**) was then applied at 1:200 TBS for 1h at room temperature in a humid

environment. Slides were then washed (3 times for 10 min in ice-cold TBS), incubated with Vectastain avidin biotin complex for 45 min at room temperature, stained for 4 min with 0.05% 3,3'-diaminobenzidine in TBS and then counterstained with Mayer's haemalum solution. Mayer's haemalum was applied for 2-10 s and the slides were then rinsed in tap H₂O for 25-30 s. After washing slides in double-distilled H₂O, they were left to dry overnight and then mounted in DPX. Slides were photographed using an upright microscope (Leitz, UK) fitted with a digital camera (Q-imaging, Canada).

Analysis

Experimental and control sections were photographed under the same conditions. Images were adjusted for brightness and contrast using Adobe Photoshop (Adobe, USA)/ Microsoft PowerPoint (Microsoft, USA).

All images are representative of at least two sections from at least two animals. Images of NOGC^{α1-/-} tissue are representative of sections from three animals. All NOGC^{α1-/-} mice were genotyped by Richard Burt (UCL). Additionally, we confirmed the phenotype of the NOGC^{α1-/-} mouse from which the sections imaged in this report were taken using Western blot analysis (see below).

7.3.4 Western Blotting

Tissue homogenisation and protein preparation

Animals were culled by cervical dislocation and decapitation. The head was immediately submerged in ice-cold PBS to cool the brain and remove excess blood. The brain was quickly removed to an ice-cold surface upon which the cerebellum was isolated and the hemispheres separated from each other. Each portion was transferred to a separate mortar containing 2 ml ice-cold tissue-lysis buffer. Tissue was smoothed using a glass pestle and the homogenate removed to tubes on ice. To further prevent protein degradation by proteases, the homogenates were heated for 10 min at 70 °C. They were then sheared using a 27 G needle to remove any outstanding

solid tissue and centrifuged for 10 min at 13,000 rpm (5 °C). The resulting supernatant, containing solubilised proteins, was removed and the pellet was discarded. Finally, the protein concentrations of the supernatants were measured using the BCA method, as described in **Chapter 2: General materials and methods**.

Sodium dodecyl sulphate polyacrylamide gel electrophoresis (SDS PAGE)

For SDS PAGE, 50 µg of sample protein was loaded per lane. Samples were brought to the same volume using tissue-lysis buffer (minus protease inhibitors). Then gel loading buffer, comprising 416 mM SDS, ~ 0.9 mM bromophenol blue, 778 mM dithiothreitol, 3 % 2 M tris (pH 6.8) and 47 % glycerol prepared in double-distilled H₂O, was added 1 in 3 to give a final volume of 13.3 µl.

SDS PAGE was run for 35 min at 200 V. A Mini-PROTEAN 3 Cell and 4-15 % Ready Gel (both Bio-Rad Laboratories, Hertfordshire, UK) were used. Running buffer contained (in mM): 25 tris; 192 glycine and 3.5 SDS. All 13.3 µl of sample were loaded per lane and one lane per gel contained 5 µl New England BioLabs ColourPlus prestained protein ladder.

Gel to membrane protein transfer

Following SDS PAGE, the gel was equilibrated for 30 min in transfer buffer additionally containing 0.2 % triton X-100. Transfer buffer comprised, in mM: 25 trisma base; 192 glycine; 3.5 SDS and 2.5 % methanol. Immediately before use, a polyvinylidene fluoride membrane was submerged in methanol for 30 s, rinsed with double-distilled H₂O and soaked in transfer buffer. A submerged transfer method was implemented at 0.38 A constant for 2 hr at 4 °C using the Amersham Bioscience (GE Healthcare Life Sciences, Buckinghamshire, UK) TE 22 Mighty Small Tank Transfer Unit.

Membrane probing

After transfer, the membrane was rinsed in double-distilled H₂O, then TBS and submerged in blocking buffer containing 3 % skimmed milk, 0.2 % tween 20, 0.5 % polyvinylpyrrolidone, and 1.5 % sodium azide in TBS. After 1 hr the membrane was washed for 5 min with TBS and the primary antibodies (see **Table 7.2**), diluted 1:500 in 50 % blocking buffer in TBS, were applied for 1 hr. The membrane was then washed 3 times for 5 min in TBS-tween, once for 5 min in TBS and submerged in an appropriate horseradish peroxidase-conjugated secondary antibody (**Table 7.2**) diluted in 50 % blocking buffer in TBS. After 1 hr, the membrane was washed 3 times in TBS-tween and once in TBS (all 5 min) and then blotted to remove excess solution. All treatments/washes were performed at room temperature on a shaking platform.

Antibody binding was visualised using the Thermo Scientific SuperSignal West Pico Chemiluminescent Substrate system. Luminol/enhancer solution and peroxide solution were mixed in equal measures and applied to the membrane for 5 min at room temperature on a shaker. The membrane was then blotted and covered in a plastic film. Luminescence was developed after exposure to High Performance Chemiluminescence Film for 5-20 min.

In order to control for protein loading, some membranes were stripped of guanylyl cyclase antibodies and probed for actin. Membranes were stored at room temperature. As necessary, they were re-hydrated in methanol, washed in double-distilled H₂O once for 2 min and then in TBS for 5 min. Thermo Scientific Restore Western Blot Stripping Buffer was applied for 10 min and membranes were rinsed for 5 min with TBS. The primary and secondary actin antibodies (see **Table 7.2**) were then applied following the method detailed above. Due to high background staining, the membranes were then washed copiously in TBS-tween (4 x 5 min; 5 x 15 min at room temperature). Antibody binding was exposed as above except that the membrane was exposed to the photographic film for 5-30 s.

| Primary antibodies | | | |
|---|-------------|---------------------------|---|
| Antigen | Host | Concentration used | Catalogue number and/or supplier |
| Guanylyl cyclase α 1 subunit | Rabbit | 1:500 | G4280; Sigma |
| Actin 1-19 | Goat | 1:500 | SC-1616; Santa Cruz Biotechnology |
| Horseradish peroxidase-conjugated secondary antibodies | | | |
| Antigen | Host | Concentration used | Catalogue number and/or source |
| Rabbit | Goat | 1:15000 | 31460; Perbio |
| Goat | Donkey | 1:20000 | SC-2020; Santa Cruz Biotechnology |

Table 7.2 Summary of antibodies used for Western blotting, their concentration and supplier.

Analysis

Films were scanned using a CanoScan LiDE (Canon UK Ltd., Surrey, UK). The presence/absence of bands was confirmed by calculating the average grey value across each row of pixels in each vertical lane, normalised to average grey values recorded outside a lane (background) using ImageJ (National Institutes of Health, USA). The area under each peak in grey values is indicative of total protein content.

Following grey value analysis, some blots were altered for brightness/contrast using Microsoft PowerPoint (Microsoft, USA). Blots within each figure were adjusted equally.

7.4 Results

7.4.1 Location of the NO-targeted guanylyl cyclase $\alpha 1$ subunit in adult mouse hippocampus

Evaluation using tissue fixed with 4 % PFA

Before testing the hypothesis that immunostaining of weakly fixed (1 % PFA) hippocampal sections would reveal the NO-targeted guanylyl cyclase $\alpha 1$ subunit to be present in pyramidal neurons, the distribution of the protein was evaluated by immunoperoxidase staining of sections fixed using 4 % PFA. After immunofluorescence and immunoperoxidase staining of hippocampus fixed with 4 % PFA using the same $\alpha 1$ primary antibody as employed in this study, Szabadits *et al.* (2007) found that only interneurons were immunopositive for $\alpha 1$. In accordance with this result, we found that cells outside the stratum pyramidale, presumably interneurons and/or glia, were most intensely stained (**Figure 7.1 C, E**). However, in the stratum pyramidale, cell soma and fibres resembling apical dendrites of pyramidal neurons were faintly immunopositive (**Figure 7.1 D, E, and F**). Although interneurons are found throughout this layer, the morphology and number of immunopositive cell soma favoured their classification as pyramidal neurons.

The neuropil in every strata was also densely stained compared to that in control sections not treated with the primary antibody (**Figure 7.1 A, B**), indicating that a wealth of $\alpha 1$ -containing fibres run through or terminate in the hippocampus. Particularly prominent were fibres running throughout the stratum polymorph of the dentate gyrus and the stratum lucidum (**Figure 7.1 A, F**). Given their position, it is likely that these were mossy fibres (labelled mf in **Figure 7.1 A, F**; Amaral and Witter, 1989) which, interestingly, have also been reported to be strongly immunoreactive for cGMP hydrolysing-PDE 2 (Stephenson *et al.*, 2009) and subject to NO-dependent LTP at synapses with CA3 neurons (Doreulee *et al.*, 2001; although see Nicolarakis *et al.*, 1994). As shown in **Figure 7.1 B and G** no non-selective secondary antibody binding was observed.

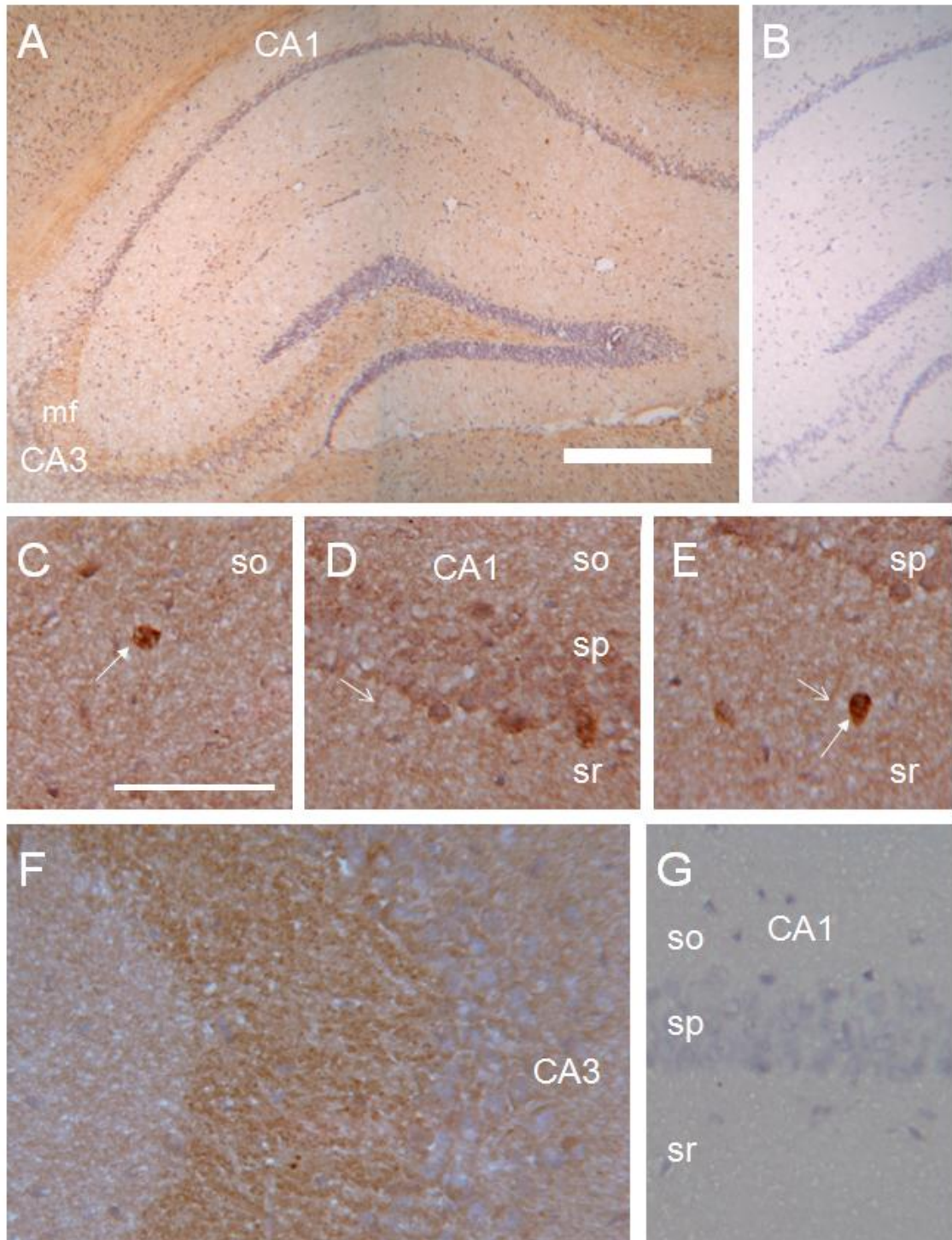


Figure 7.1 Immunoperoxidase staining for the NO-targeted guanylyl cyclase $\alpha 1$ subunit in transverse hippocampal sections fixed with 4 % PFA. **A)** The hippocampus major. Two juxtaposed images. **B)** Control for secondary antibody binding in A. mf = possible mossy fibres. **C-F)** Higher magnification images of a second section stained for $\alpha 1$ showing an area of the stratum oriens (so; C), stratum pyramidale (sp; D) and stratum radiatum (sr; E) of CA1, and an area of CA3/stratum lucidum (F). **G)** Control for secondary antibody binding in C-F. Unfilled arrows (D, E) indicate possible apical

dendrites of pyramidal neurons. Control sections were not treated with the primary antibody. Scale bar in A: 500 μ m, A-B; bar in C: 100 μ m, C-G. Filled arrows (C, E) indicate interneurons.

Evaluation using tissue fixed with 1 % PFA

In accordance with the distribution of staining observed in **Figure 7.1**, cells scattered outside the stratum pyramidale and fibres running throughout the dentate gyrus and stratum lucidum were strongly stained after identical treatment with tissue fixed with 1 % PFA (**Figure 7.2 A, C**). Unlike the staining observed in tissues fixed with 4 % PFA, however, and in favour with the hypothesis that pyramidal neurons express $\alpha 1$, cell soma and proximal apical dendrites in stratum pyramidale throughout Ammon's horn were very strongly immunopositive (**Figure 7.2 C**). Whether the rest of the dendritic arbour was also immunopositive, as is suggested by functional evidence implicating the $\alpha 1\beta 1$ guanylyl cyclase in synaptic plasticity (Taqatqeh *et al.*, 2009; Neitz *et al.*, 2011), was unclear because the dendrites of pyramidal neurons become rapidly thinner as they deviate from the apical fibre (Routh *et al.*, 2009), and using light microscopy, are usually indistinguishable from the rest of the neuropil.

Blood vessels throughout the hippocampus and subiculum were also immunopositive (**Figure 7.2 A, C**). This was not observed following staining of tissue fixed with 4 % PFA, but was consistent with functional evidence implicating NO-targeted guanylyl cyclase $\alpha 1\beta 1$ heterodimers in smooth muscle relaxation and vasodilation (Mergia *et al.*, 2006; Nimmegeers *et al.*, 2007). Moreover, some immunohistochemical data collected using a $\alpha 1\beta 1$ antibody also shows guanylyl cyclase to be present in endothelial, as well as smooth muscle cells surrounding blood vessels (Zhan *et al.*, 1999; Jarry *et al.*, 2003).

Some scattered cells, for example, in the stratum radiatum in **Figure 7.2 C** were immunonegative. Some non-selective staining was observed in the fimbrium and alveus surrounding the hippocampus and, to a lesser extent, in the lacunosum moleculare, (**Figure 7.2 B**).

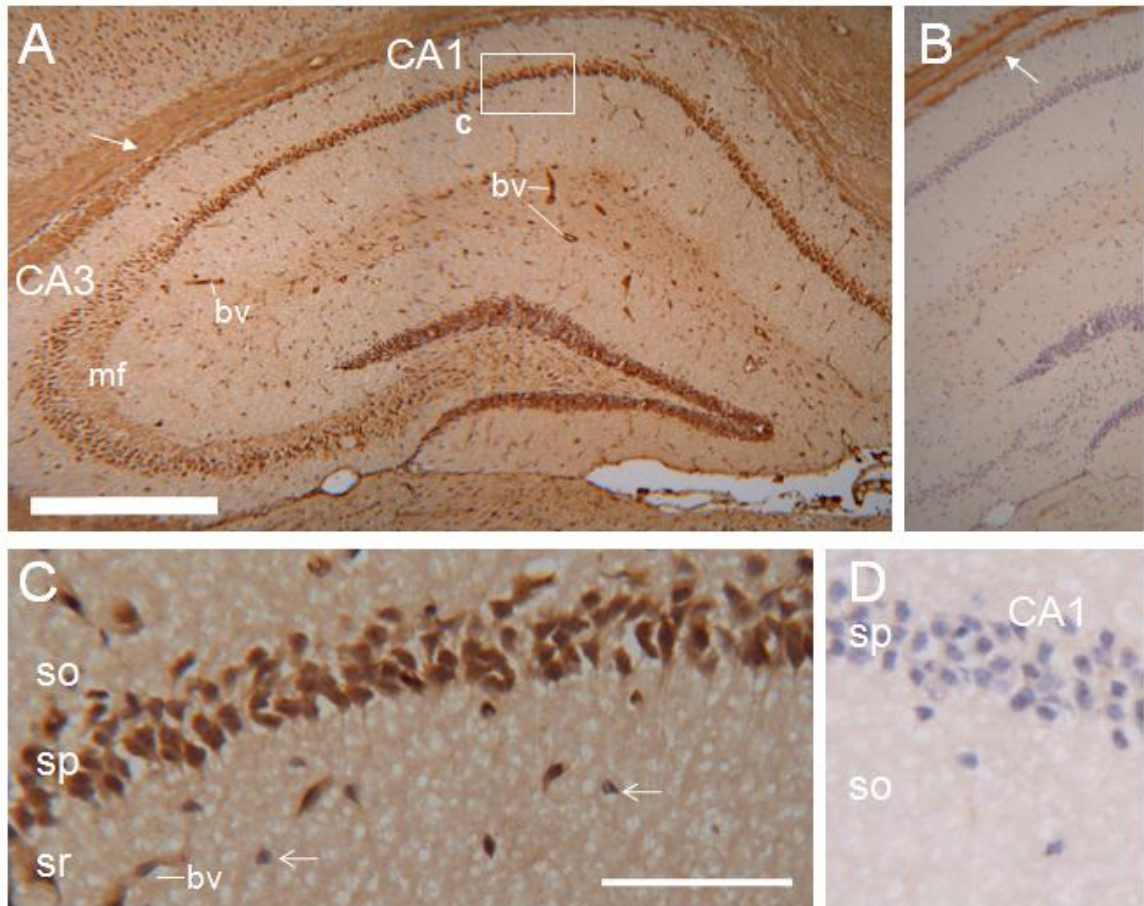


Figure 7.2 Immunoperoxidase staining for the NO-targeted guanylyl cyclase $\alpha 1$ subunit in transverse hippocampal sections fixed with 1 % PFA. **A)** The hippocampus major. Two juxtaposed images. *bv* = blood vessel; *mf* = possible mossy fibres. Inset box approximates location of image shown in **C**. **B)** Control for secondary antibody binding in **A**. Filled arrows (**A-B**) indicate non-selective staining. **C)** Higher magnification of area labelled **C** shown in **A**. Note the blood vessel (*bv*) in bottom left corner. Unfilled arrows indicate immunonegative cells in the stratum radiatum (*sr*). *so* = stratum oriens; *sp* = stratum pyramidale. **D)** Higher magnification of an area of CA1 in the section shown in **B**. Scale bar in **A** = 500, **A-B**; bar in **C** = 100 μm , **C-D**.

Although in the hippocampus and other brain areas, such as the molecular layer of the cerebellum, neuropil is not well preserved following 1 % PFA fixation, staining of a section of the same tissue as shown in **Figure 7.2** with toluidine blue indicated that the cells were healthy at the time of fixing and apical dendrites of pyramidal neurons were intact (**Figure 7.3**).

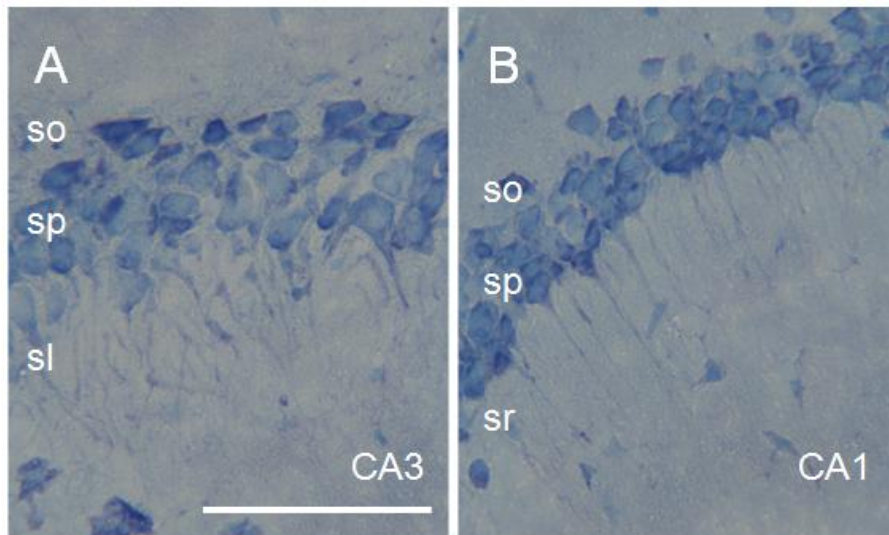


Figure 7.3 Toluidine blue staining of a section of the same tissue as shown in **Figure 7.2**. **A)** CA3. **B)** CA1. *sl* = stratum lucidum; *so* = stratum oriens; *sp* = stratum pyramidale; *sr* = stratum radiatum. Scale bar in A: 100 μ m, A-B.

7.4.2 Location of the NO-targeted guanylyl cyclase β 1 subunit and nNOS in adult mouse hippocampus

In favour of the hypothesis that pyramidal cells express α 1, **Figure 7.2** shows for the first time that, in tissues fixed with 1 % PFA, hippocampal pyramidal neurons can be immunostained for the NO-targeted guanylyl cyclase α 1 subunit using standard methods.

In immature granule cells of the developing cerebellum, mRNA for the NO-targeted α 2 subunit has been reported to be expressed without the β 1 subunit (Gibb and Garthwaite, 2001). Intense signals for β 1 subunit mRNA have also been detected in brain areas apparently with relatively little or no mRNA for either of the α subunits (Mergia *et al.*, 2003; Krumenacker *et al.*, 2006; Pifarre *et al.*, 2007). Since heterodimerisation of subunits is required for guanylyl cyclase catalytic activity, these data, if correct, suggest that individual NO-targeted guanylyl cyclase subunits may function in ways other than to transduce NO signals via cGMP.

Therefore, to determine the possible functional significance of our findings and their relevance to the role of $\alpha 1$ in NO/cGMP-mediated synaptic plasticity, we sought to investigate whether the structures found to express $\alpha 1$ in this study were immunopositive for $\beta 1$ under the same conditions. To assess the consistency of staining, two different primary antibodies raised against $\beta 1$ were used (see **Table 7.1** for details).

Figure 7.4 shows immunoperoxidase staining for $\beta 1$ in a section of tissue fixed with 4 % PFA using an antibody kindly provided by Prof. Soenke Behrends (antibody described in Behrends *et al.*, 2001; van Staveren *et al.*, 2004). All structures shown to be immunopositive for $\alpha 1$ in tissue fixed with 1 % PFA (**Figure 7.2**), including pyramidal neurons throughout Ammon's horn, cells scattered outside of the stratum pyramidale, potential mossy fibres and blood vessels, were immunopositive for $\beta 1$ (**Figure 7.4 A-E**). Staining of pyramidal cells in area CA1 (**Figure 7.4 A, C**) was in accordance with published results using this antibody (van Staveren *et al.*, 2004). No staining was observed in control sections treated only with the secondary antibody (**Figure 7.4 F**).

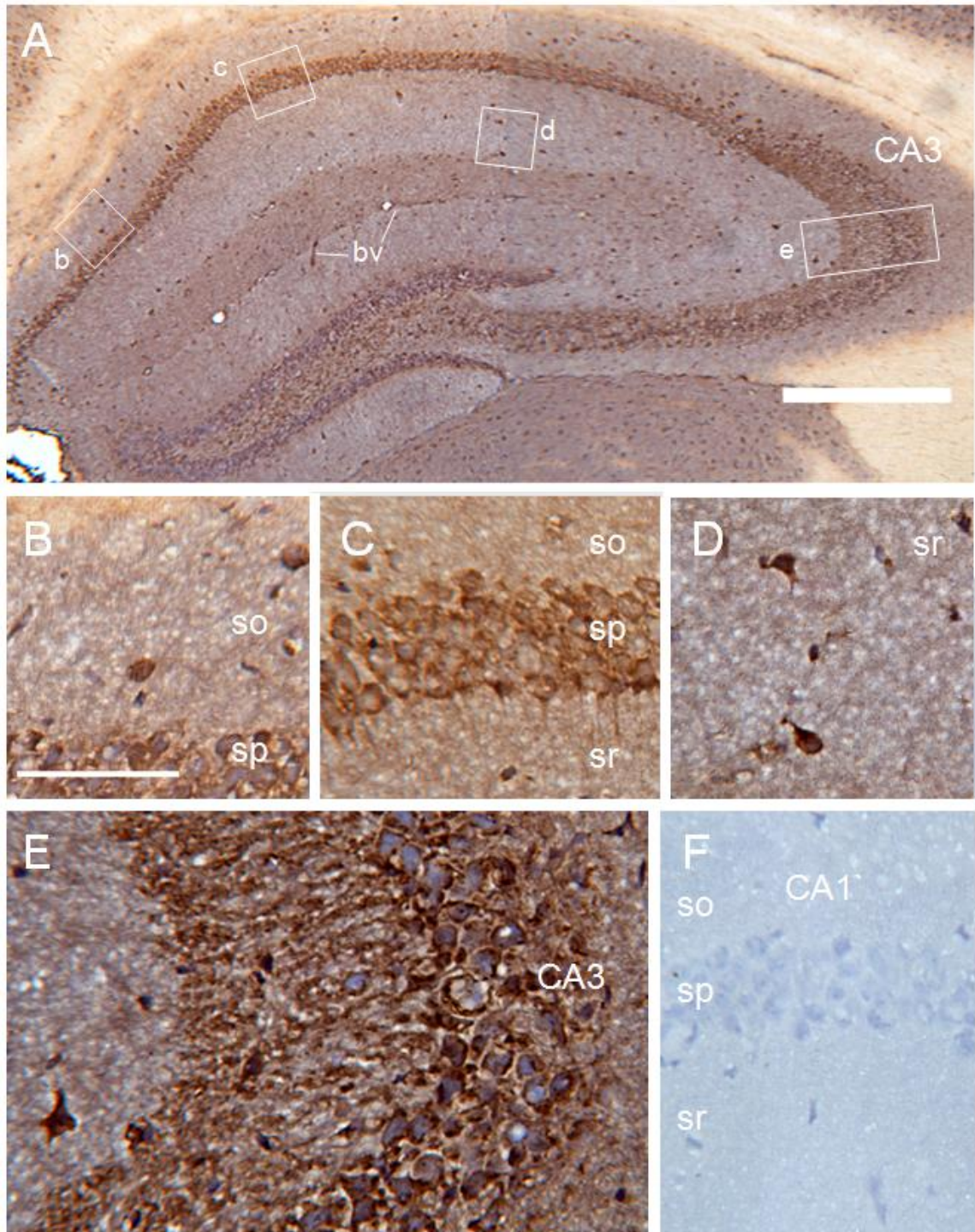


Figure 7.4 Immunoperoxidase staining for $\beta 1$ in transverse hippocampal sections fixed with 4 % PFA using a primary antibody kindly provided by Prof. Soenke Behrends. **A)** The hippocampus major. Two juxtaposed images. *bv* = blood vessel; boxes *b*, *c*, *d* and *e* show positions of higher magnification images below. **B-E)** Higher magnification images of the section presented in **A** showing the stratum oriens (*so*; **B**), stratum pyramidale (*sp*; **C**), stratum radiatum (*sr*; **D**) and area CA3/stratum lucidum (**E**). **F)** Control for the selectivity of secondary antibody in **A-E**. Scale bar in **A** = 500 μm . Scale in **B**: 100 μm , **B-F**.

The above results therefore suggested that all the structures that were found to be immunopositive for $\alpha 1$ in tissue fixed with 1 % PFA are capable of forming functional $\alpha 1\beta 1$ -containing guanylyl cyclase, and this was supported by immunoperoxidase staining of sections fixed with 1 % PFA using a $\beta 1$ antibody supplied by Cayman (see **Table 7.1** for antibody details). As shown in **Figure 7.5**, staining with this antibody was observed in the stratum pyramidale, blood vessels and a proportion of cells scattered throughout the hippocampus. As described by Burette *et al.* (2002), pyramidal cell staining was inhibited by strong (4 % PFA) tissue fixation.

Unlike the staining observed in **Figure 7.4**, fibres surrounding CA3 in the stratum lucidum were only very weakly immunopositive. This could have resulted from a difference in the overall efficacy of the two $\beta 1$ antibodies used, because, in the cerebellum, staining for $\beta 1$ using the Cayman antibody is weaker than staining observed using the antibody provided by Prof. Behrends (unpublished observations, Giti Garthwaite and Kathryn Harris, UCL, London, UK).

Some non-selective staining was observed in the alveus and fimbrium surrounding the hippocampus and, to a lesser extent, in the lacunosum moleculare (**Figure 7.5 B**).

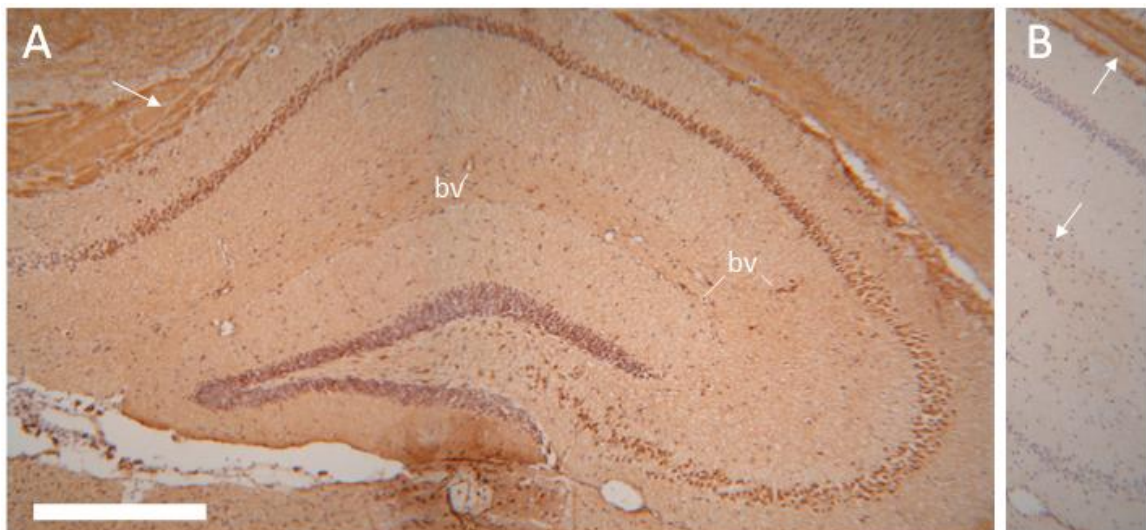


Figure 7.5 Immunoperoxidase staining for $\beta 1$ in transverse hippocampal sections fixed with 4 % PFA using a primary antibody obtained from Cayman. **A**) The hippocampus major. Two juxtaposed images. *bv* = blood vessel. **B**) Control for secondary antibody binding in B in which the primary

antibody was omitted. Filled arrows (A-B) indicate non-selective staining. Scale bar in A: 500 μ m, A-B.

Further to the functional significance of the above findings, and in accordance with previous results (Wendland *et al.*, 1994; Gonzalez-Hernandez *et al.*, 1996; Burette *et al.*, 2002), immunoperoxidase staining for nNOS suggested that it was present throughout the hippocampus and in a distribution complimentary to that of α 1 and β 1 (**Figure 7.6**). Immunopositive structures included cells and fibres in the stratum oriens, radiatum and pyramidale (**Figure 7.6 C-E**). As was previously found (Wendland *et al.*, 1994; Gonzalez-Hernandez *et al.*, 1996; Burette *et al.*, 2002), staining of pyramidal neurons was dependent on weak tissue fixation (1 vs. 4 % PFA). As expected, no staining of blood vessels was detected.

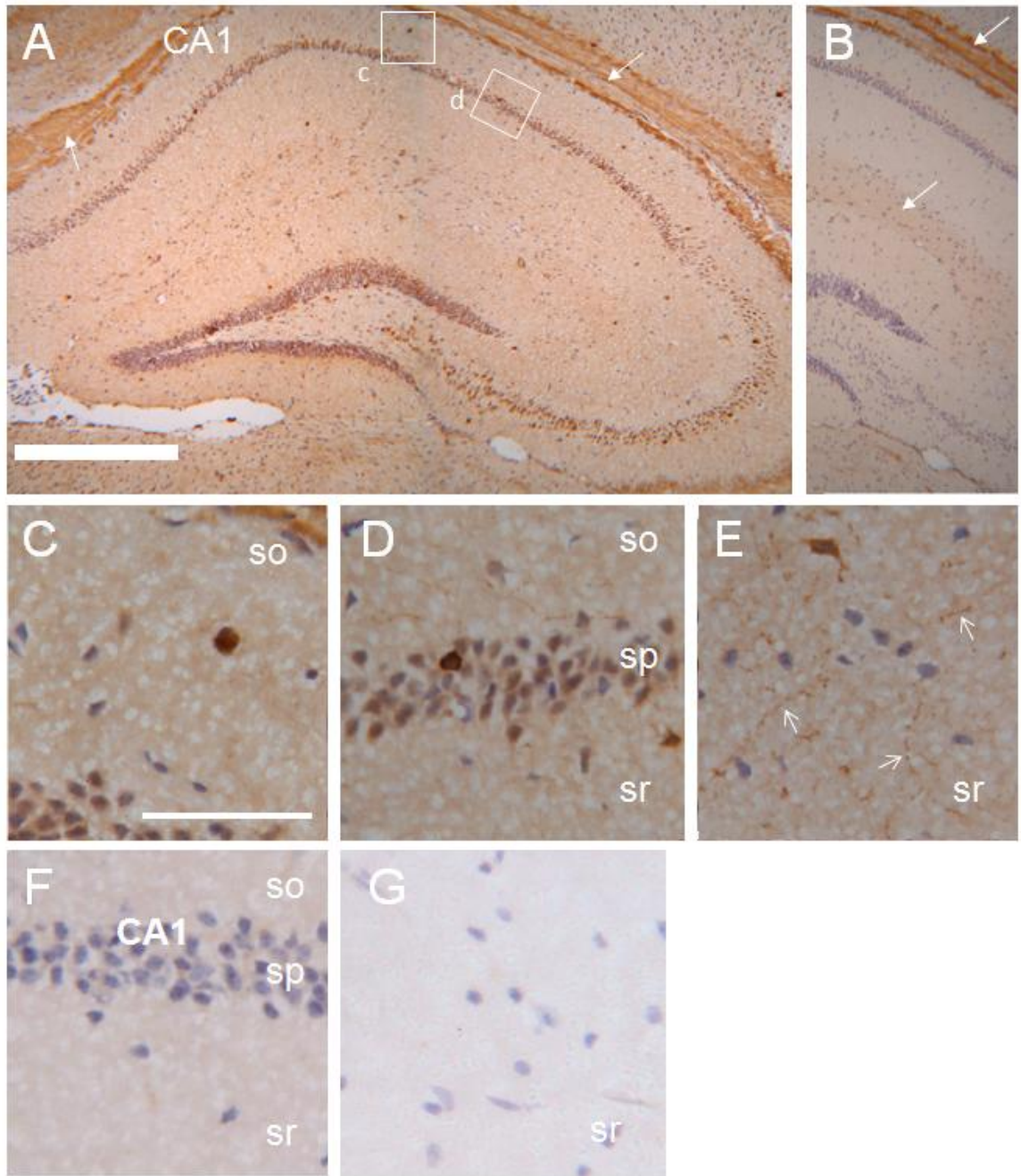


Figure 7.6 Immunoperoxidase staining for nNOS. Tissue was fixed with 1 % PFA. **A)** The hippocampus major. Two juxtaposed images. Boxes *c* and *d* show locations of higher magnification images below. **B)** Control for secondary antibody binding in **A**. Filled arrows (**A-B**) indicate non-selective staining. **C)** Stratum oriens. **D)** Stratum pyramidale. **E)** Stratum radiatum of a different section. Unfilled arrows indicate immunopositive fibres. **F)** Control for the selectivity of secondary antibody binding in **C-D**. **G)** Control for secondary antibody binding in **E**. Scale in bar in **A**: 500 μm , **A-B**. Scale in **C**: 100 μm , **C-G**.

7.4.3 Selectivity of the $\alpha 1$ primary antibody for $\alpha 1$ protein

As would typically be expected if the immunoperoxidase staining shown in **Figure 7.2** was representative of the true expression pattern of the protein *in vivo*, all the immunopositive structures also stained for $\beta 1$ and were in close proximity to those that stained for nNOS (**Figure 7.2-6**). However, the selectivity of the $\alpha 1$ antibody required testing because: 1) stringent-tests of its selectivity are absent in the literature, and tests should be performed under identical conditions to those in **Figure 7.2**; 2) other antibodies thought to selectively bind the $\alpha 1$ subunit have been found to bind the $\alpha 2$ subunit (Ding *et al.*, 2004), which would also be expected to be found in $\beta 1$ -containing structures close to nNOS; 3) the distribution of $\alpha 1$ staining observed in this study was strikingly different to that observed previously by Szabadits *et al.* (2007).

Therefore, Western blot analysis was performed. In order that weak, non-selective antibody binding might be detected, films were exposed until the strongest bands began to saturate. As shown in **Figure 7.7**, only one main antigen, which migrated at the molecular weight of rodent $\alpha 1$ (~ 80 kDa; Kamisaki *et al.*, 1986), was detected by the $\alpha 1$ antibody after incubation with blots of mouse and rat forebrain and cerebellum lysates.

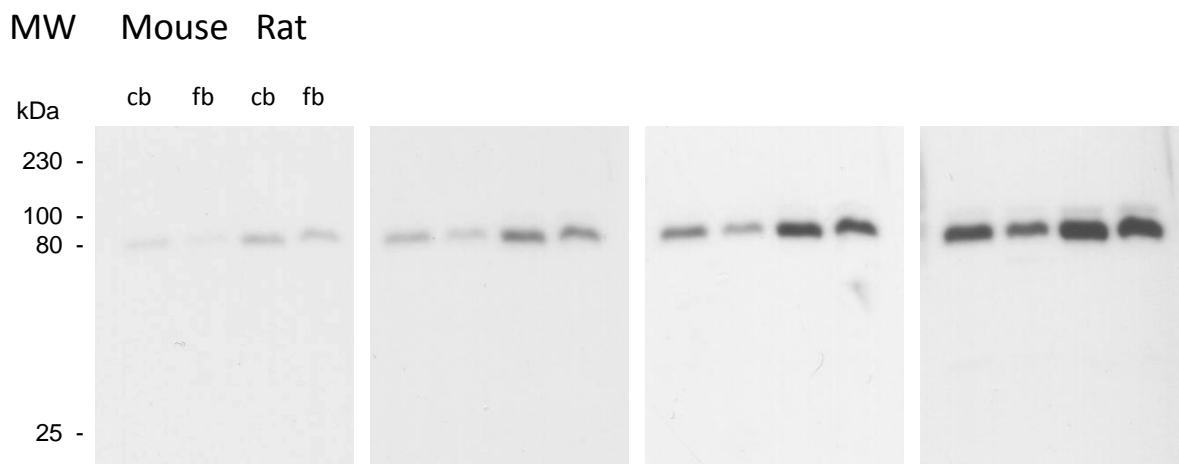


Figure 7.7 Western blots of rat and mouse cerebellum (cb) and forebrain (fb) lysates for $\alpha 1$. The first three films were exposed for 2, 5 and 10 min (left to right) to the membrane and show that the $\alpha 1$ antibody detected only one antigen which migrated at an apparent molecular weight (MW) of ~80

kDa. Very faint bands just heavier than 80 kDa are also detected in the last film which was exposed to the membrane for 20 min. MW as approximated from the ladder.

Following incubation of blots of NOGC $\alpha 1^{-/-}$ mouse cerebellum with the $\alpha 1$ antibody, no bands could be detected, although a band migrating at ~ 80 KDa could be detected in blots of cerebellum taken from a wild-type sibling. A very faint band, migrating at ~ 50 kDa, was detected following grey value analysis of lanes containing both wild-type and NOGC $\alpha 1^{-/-}$ lysate (**Figure 7.8 A**). Actin could also be detected in both lanes, and grey value analysis of the pixels contributing to each actin band indicated approximately equal protein loading in each lane (**Figure 7.8 B**).

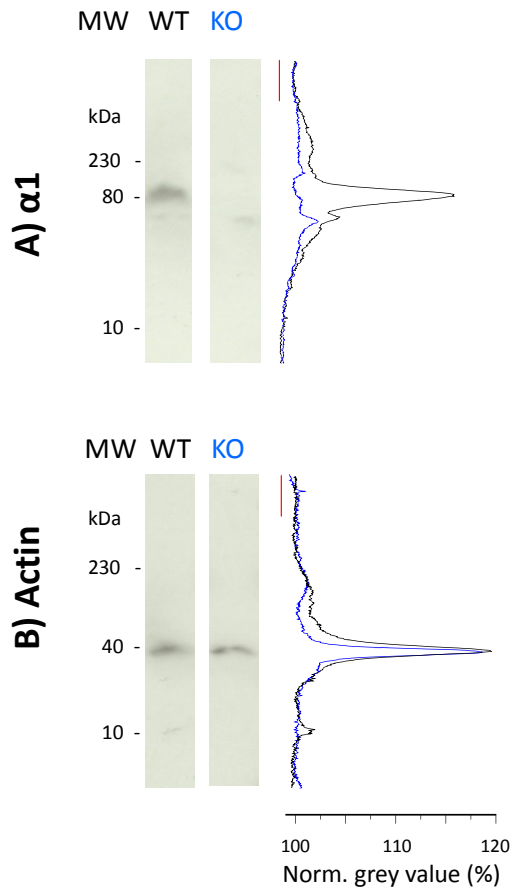


Figure 7.8 Western blot analysis of NOGC $\alpha 1^{-/-}$ cerebellum lysate. **A)** The $\alpha 1$ antibody detected one main antigen in lysate from a wild-type mouse (WT). This antigen displayed the same molecular weight (MW) as the $\alpha 1$ protein (~ 80 kDa) and was absent from lanes containing NOGC $\alpha 1^{-/-}$ lysate (KO). A very faint band was detected in both lanes at ~ 50 kDa following analysis of grey values. **B)** Stripping of the membrane and re-probing with an actin antibody revealed a band at the expected

molecular weight (~ 40 kDa) in both the WT and KO lanes. Analysis of grey values was indicative of approximately equal protein loading in each lane. Red bar in each panel indicates area of membrane to which grey values were normalised. Similar results were obtained following analysis of NOGC α 1^{-/-} forebrain lysate.

Under the conditions of Western blot, therefore, the α 1 antibody displayed high selectivity for the α 1 protein. However, immunoperoxidase staining of sections of NOGC α 1^{-/-} and wild-type hippocampus fixed with 4 % PFA was identical (**Figure 7.9**). All structures that had previously been identified as strongly immunopositive for α 1 in tissue from C57/Bl6 mice were intensely stained in sections from NOGC α 1^{-/-} mice, including cells outside the stratum pyramidale and fibres throughout the stratum polymorph, lucidum and the rest of the neuropil. Weak staining of pyramidal neurons was also observed. As before, blood vessels were immunonegative.

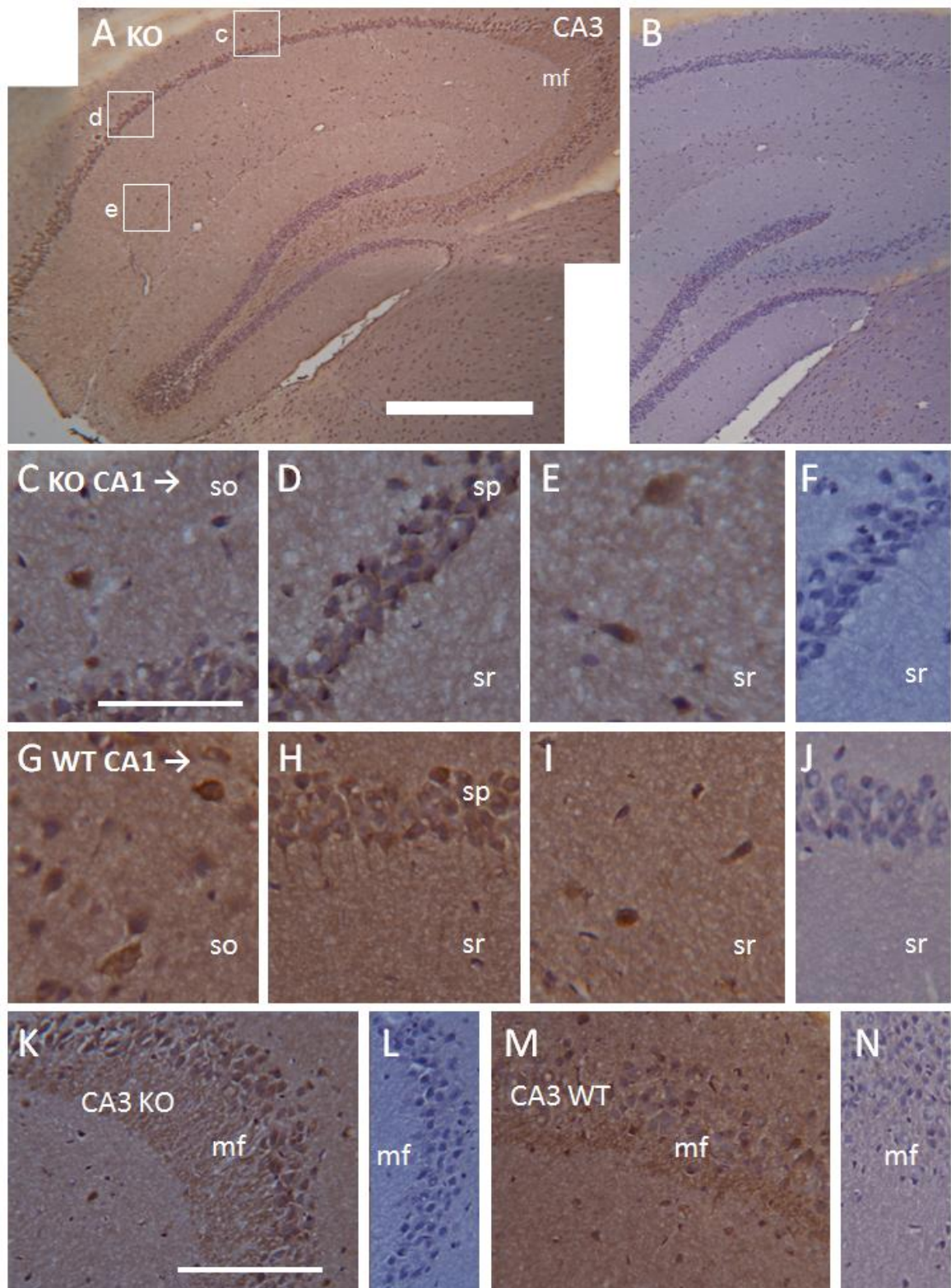


Figure 7.9 Immunoperoxidase staining of $NOGCa1^{-/-}$ (KO) and wild-type (WT) tissue for the NO-targeted guanylyl cyclase $\alpha 1$ subunit. Tissue fixed with 4 % PFA. **A-B**) Staining in the hippocampus proper and equivalent control for the selectivity of the secondary antibody. Two juxtaposed images. *mf* = possible mossy fibres; boxes *c-e* show approximate location of magnified images below. **C-F**)

Magnified images showing an area of the stratum oriens (so; C), stratum pyramidale (sp; D) and stratum radiatum (sr; E) of CA1 in A and stratum pyramidale of CA1 in B (F). G-I Images of CA1 in a section of wild-type tissue showing the stratum oriens (G), stratum pyramidale (H) and stratum radiatum (I). J) Equivalent control for the selectivity of secondary antibody in G-I. K-L) CA3 of a section of NOGCα1^{-/-} tissue and equivalent control for secondary antibody binding. M-N) CA3 of a section of wild-type tissue and equivalent control for secondary antibody binding. Scale bar in A: 500 μm, A-B. Scale in C: 100 μm, C-J. Scale in K: 100 μm, K-N. Note that the phenotype of mice used was confirmed by Western blot.

Immunostaining of NOGCα1^{-/-} and wild-type tissue fixed with 1% PFA was also identical (**Figure 7.10**). As found in C57/Bl6 tissue (**Figure 7.2**), pyramidal neurons and blood vessels were intensely stained.

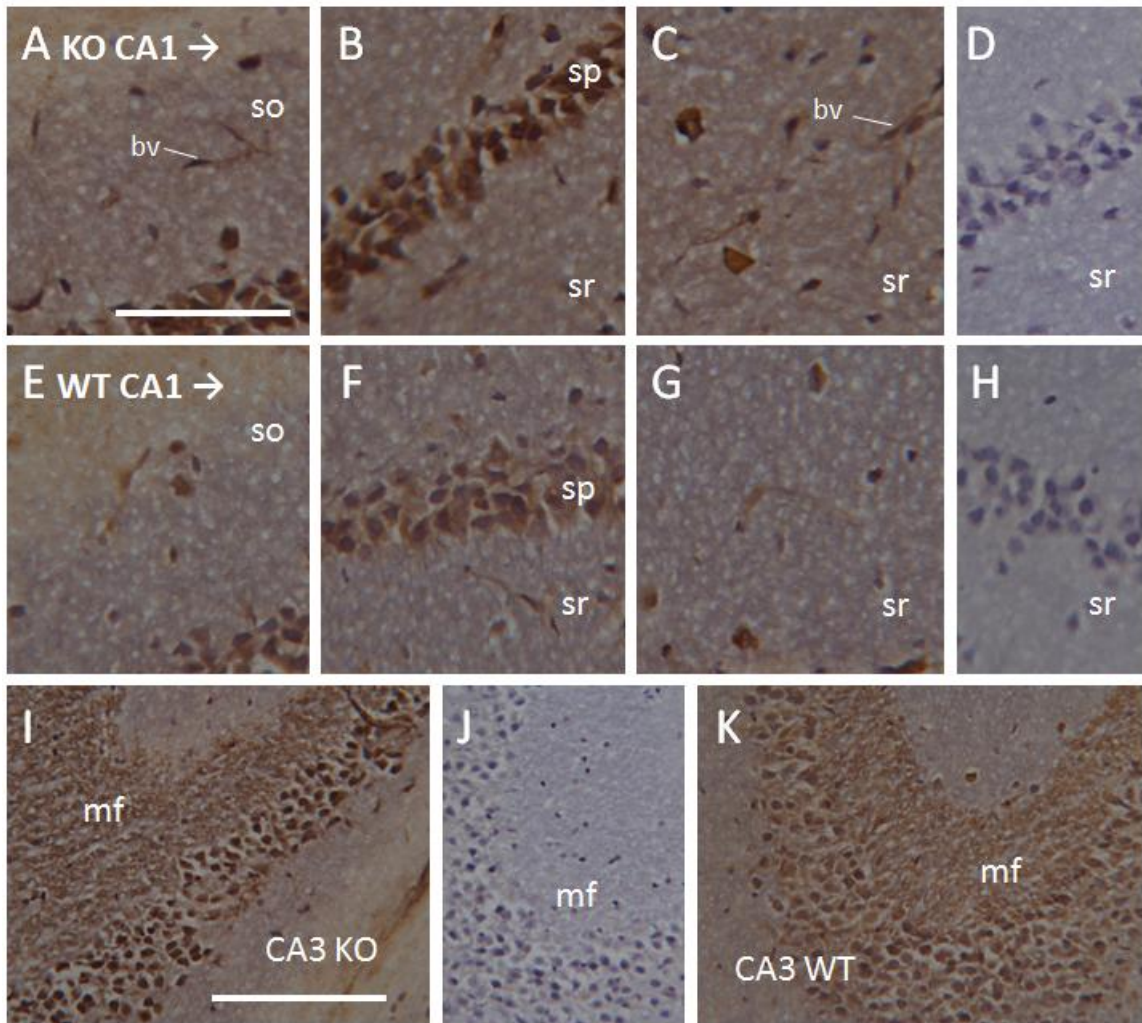


Figure 7.10 Immunoperoxidase staining of $NOGCa1^{-/-}$ (KO) and wild-type (WT) tissue for the NO-targeted guanylyl cyclase $\alpha 1$ subunit. Tissue fixed with 1 % PFA. **A-C**) Images showing an area of the stratum oriens (so; **A**), stratum pyramidale (sp; **B**) and stratum radiatum (sr; **C**) of CA1 in a section of $NOGCa1^{-/-}$ tissue. bv = blood vessel. **D**) Equivalent control for secondary antibody binding in **A-C**. **E-F**) Images of CA1 in a section of wild-type tissue showing the stratum oriens (**E**), stratum pyramidale (**F**) and stratum radiatum (**G**). **H**) Equivalent control for the selectivity of secondary antibody in **E-H**. **I-J**) CA3 of a section of $NOGCa1^{-/-}$ tissue and equivalent control for secondary antibody binding. **K**) CA3 of a section of wild-type tissue. Scale bar in for **A**: 100 μ m, **A-H**. Scale in **I**: 100 μ m, **I-K**. Note that the phenotype of mice used was confirmed by Western blot.

Clear staining for $\alpha 1$ in the cells and neuropil of the cortex was also observed in tissue from $NOGCa1^{-/-}$ mice, whether fixed with 4 % PFA (**Figure 7.11**) and 1 % PFA (not shown).

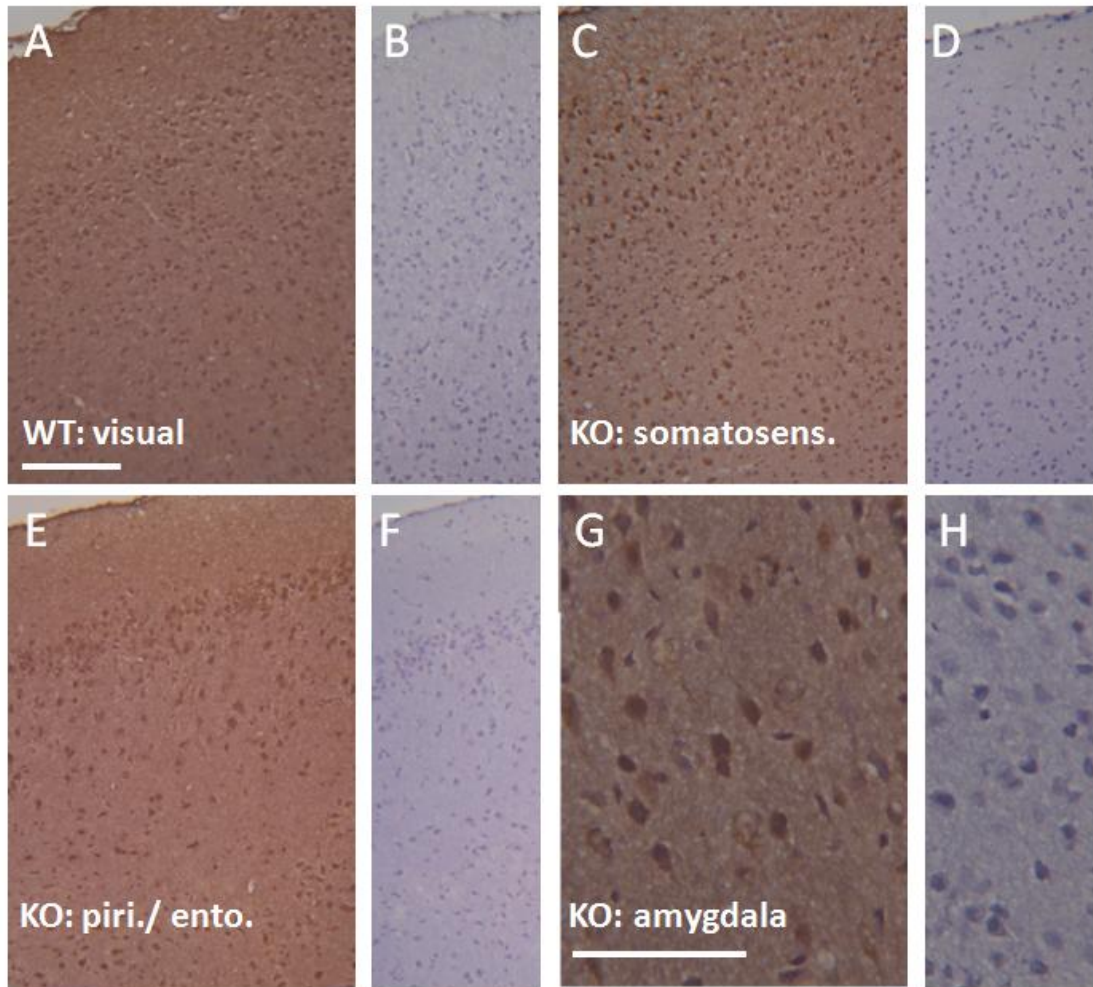


Figure 7.11 Immunoperoxidase staining for $\alpha 1$ in $NOGCaI^{-/-}$ (KO) and wild-type (WT) cortex (transverse sections) fixed with 4 % PFA. **A-B**) Primary visual cortex of wild-type mouse and corresponding control for secondary antibody binding. **C-D**) Primary somatosensory cortex of $NOGCaI^{-/-}$ mouse and equivalent control for secondary antibody binding. **E-F**) Piriform/ entorhinal cortex of $NOGCaI^{-/-}$ mouse and relevant control for secondary antibody. Layer 1 is at the top of each image. **G-H**) Cortical nucleus of the amygdala and equivalent control for secondary antibody. Scale bar in A: 200 μm , A to F. Scale in G: 100 μm , G-H. Note that the phenotype of the $NOGCaI^{-/-}$ mouse was confirmed by Western blot analysis.

7.4.4 Results summary

The above results are summarised in **Table 7.3**.

| Structure | Antibody | | | | | | |
|-------------------|------------|-----|-----|-----|------------|-----------|------|
| | $\alpha 1$ | | | | $\beta 1$ | $\beta 1$ | nNOS |
| | WT | | KO | | (Behrends) | (Cayman) | |
| | 4 % | 1 % | 4 % | 1 % | 4/1 % | 1 % | 1 % |
| Pyramidal neurons | + | +++ | + | +++ | +++ | ++ | ++ |
| Interneurons | +++ | +++ | +++ | +++ | +++ | +++ | +++ |
| Granule cells | + | + | + | + | + | + | + |
| Mossy fibres | ++ | ++ | ++ | ++ | ++ | + | - |
| Neuropil | + | + | + | + | + | + | + |
| Blood vessels | - | +++ | - | +++ | +++ | ++ | - |

Table 7.3 Summary of results. The relative intensity of staining in each of the structures listed (as judged by the experimenter) is indicated. Key: - = immunonegative/no staining; + = weak/inconsistent staining; ++ = moderate staining; +++ = strong/intense staining. WT = wild-type tissue; KO = *NOGCa1^{-/-}* tissue. Percentages indicate the concentration of PFA used to fix tissues.

7.5 Discussion

Given the role of NO/cGMP signalling in hippocampal physiology, and the possibility that NO may operate as a retrograde, anterograde and/or intracellular transmitter (Garthwaite, 2008), the precise location of NO sources and targets in the hippocampus is of great interest. As discussed above (see **7.1 Introduction**), the location of the NO-targeted guanylyl cyclase $\alpha 1$ subunit is contentious. Using immunohistochemical techniques, the subunit has been found in interneurons in the adult (Szabadits *et al.* 2007) and developing (Cserep *et al.*, 2011) hippocampus, suggesting that, if functional studies are correct (Taqatqeh *et al.*, 2009; Neitz *et al.*, 2011), presynaptic effects of NO may be restricted to synapses involving these cells.

Szabadits *et al.* (2007) and Cserep *et al.* (2011) used tissues fixed with 4 % PFA to perform their immunohistochemical studies but it has been reported that this concentration of PFA inhibits immunostaining of hippocampal pyramidal neurons for synaptic proteins including nNOS and the $\beta 1$ NO-targeted guanylyl cyclase subunit (Wendland *et al.*, 1994; Gonzalez-Hernandez *et al.*, 1996; Burette *et al.*, 2002). Possible explanations for this inhibition are that high concentrations of PFA (4% vs. 1 %) mask antibody epitopes and/or restrict the access of antibodies to their target proteins by excessively cross-linking proteins. In PSD's and presynaptic varicosities, where protein density is high and nNOS, $\beta 1$ and $\alpha 1$ are expected to reside, the latter circumstance may be particularly likely. Therefore we reinvestigated the distribution of $\alpha 1$ in the hippocampus by immunoperoxidase staining of weakly fixed (1 % PFA) tissue to see whether evidence for the $\alpha 1$ subunit in pyramidal neurons had been overlooked.

In accordance with Szabadits *et al.* (2007) and Cserep *et al.* (2011), we found that cells scattered outside of the stratum pyramidale, presumably interneurons and/or glia, were most intensely immunopositive for $\alpha 1$ after staining of tissues fixed with 4 % PFA. The same antibody as employed by Szabadits *et al.* (2007) and Cserep *et al.* (2011) was used. However, pyramidal cell soma and apical dendrites throughout Ammon's horn were also weakly immunopositive (**Figure 7.1**) and, in accordance with the notion that pyramidal neurons must be weakly fixed to be immunostained for some synaptic proteins, staining of these cells was intensified after identical treatment of tissues fixed with 1 % PFA.

Considering that pyramidal neurons were also found to be immunopositive for the $\beta 1$ NO-targeted guanylyl cyclase subunit and nNOS (**Figure 7.4-6**), and in light of the studies by Taqatqeh *et al.* (2009) and Cserep *et al.* (2011), the distribution of $\alpha 1$ staining that we observed in tissues fixed with 1 % PFA suggested that $\alpha 1\beta 1$ -dependent NO-induced modulation of transmitter release might occur at CA1-CA3 synapses. NO-regulated neurotransmitter release at CA1-CA3 synapses is consistent with the effect of NO at synapses between pairs of dissociated pyramidal neurons during LTP (Arancio *et al.*, 1995; Arancio *et al.*, 1996; Arancio *et al.*, 2001).

The distributions of staining for $\alpha 1$, $\beta 1$ and nNOS observed in tissues fixed with 1 % PFA (see **Figure 7.2-7.6**) were remarkably similar. This was in favour of the $\alpha 1$ antibody selectively binding protein for the $\alpha 1$ subunit, and therefore, with the distribution of $\alpha 1$ protein observed in tissues fixed with 1 % PFA being physiologically relevant. Indeed, these possibilities were supported by several other observations.

First, blood vessels were found to be intensely immunopositive for $\alpha 1$ following staining of tissue fixed with 1 % but not 4 % PFA (**Figure 7.1-2**). This was consistent with immunohistochemical and functional evidence suggesting the presence of $\alpha 1\beta 1$ in the smooth muscle of blood vessels, such as arteries (Mergia *et al.*, 2006; Nimmegeers *et al.*, 2007). Notably, smaller blood vessels, such as those that were found to be immunopositive in this study, also contain smooth muscle (for example, venules measure on average $\sim 20 \mu\text{M}$; Germann and Stanfield, 2002). Moreover, endothelial cells in kidney and lung have also been reported to express $\alpha 1\beta 1$ (Zhan *et al.*, 1999; Jarry *et al.*, 2003). Second, and in apparent discord with the notion that all structures in the hippocampus were non-selectively stained, some cells scattered outside the stratum pyramidale, for example, in the stratum granulare, were immunonegative for $\alpha 1$ in tissues fixed with 1 % PFA (**Figure 7.2**). Third, and most importantly, Western blot analysis showed that, in tissue lysates prepared from C57/Bl6 mice, the $\alpha 1$ antibody detected only one main antigen which had the same molecular weight as the $\alpha 1$ subunit ($\sim 80 \text{ kDa}$; Kamisaki *et al.*, 1986) and was absent from lysates prepared from NOGC $\alpha 1^{-/-}$ tissue (**Figure 7.7-7.8**).

However, immunoperoxidase staining of sections from mice lacking the $\alpha 1$ subunit, as confirmed by Western blotting, revealed that, at least under our conditions, the $\alpha 1$ antibody was not selective for the $\alpha 1$ protein. As shown in **Figure's 7.9-10**, all the structures found to be immunopositive after staining of tissues prepared from C57/Bl6 or NOGC $\alpha 1^{-/-}$ wild-type mice were also immunopositive in sections prepared from NOGC $\alpha 1^{-/-}$, regardless of fixing with 1 or 4 % PFA. Similarly, immunostaining was prevalent throughout sections of cortex prepared from NOGC $\alpha 1^{-/-}$ mice (**Figure 7.11**).

Since the protein sequence for the $\alpha 1$ antibody epitope is not present anywhere else in the mouse proteome (as assessed using the Basic Local Alignment Search Tool (BLAST); www.ncbi.nlm.nih.gov/genome/seq/BlastGen/BlastGen.cgi?taxid=100901; accessed 20/01/2011) it is hard to make a firm hypothesis as to what the $\alpha 1$ antibody was binding to. The distribution of staining for $\alpha 1$ was remarkably coincident with the distribution of staining for $\beta 1$ (**Figure 7.2** and **7.3**), so it could be hypothesised that the $\alpha 1$ antibody binds the $\beta 1$ subunit. Alternatively, it could be speculated that the $\alpha 1$ antibody recognises the $\alpha 2$ subunit, which weighs ~ 82 kDa ($\beta 1$ weighs ~ 70 kDa; Kamisaki *et al.*, 1986; Harteneck *et al.*, 1991), because following Western blotting of lysates of rat forebrain and cerebellum for $\alpha 1$, faint bands surrounding the major signal at ~ 80 kDa could be detected after a long (20 min) exposure of the blotting membrane to film (**Figure 7.6**). This would also explain why the $\beta 1$ antibodies yielded similar distributions of immunoperoxidase staining to the $\alpha 1$ antibody. Notably, another antibody thought to selectively bind the $\alpha 1$ subunit has been found to bind protein for the $\alpha 2$ subunit (Ding *et al.*, 2004). One way to test the possibility that the $\alpha 1$ antibody bound protein for the $\alpha 2$ or $\beta 1$ protein would be to stain tissues prepared from animals deficient in these subunits. However, it should be noted that the $\alpha 1$ subunit may have bound a protein unrelated to guanylyl cyclase. Consistent with this, grey analysis of images of Western blots probed with the $\alpha 1$ antibody revealed a very faint signal in both NOGC $\alpha 1^{-/-}$ and wild-type lysates that was unlikely to be a guanylyl cyclase subunit (~ 50 kDa; **Figure 7.7**).

The conditions used for immunohistochemistry vary widely between groups of experimenters and therefore, it cannot be said that other observations made using the $\alpha 1$ antibody (for example, Szabadits *et al.*, 2007; Fukutani *et al.*, 2009; Wilson and Garthwaite, 2010; Cserep *et al.*, 2011), are artefactual. Indeed, the lack of any major signal following Western blotting of NOGC $\alpha 1^{-/-}$ tissue with the $\alpha 1$ antibody shows that the antibody does selectively bind the $\alpha 1$ subunit under some conditions. Furthermore, in the study by Szabadits *et al.* (2007), the reported distributions of $\alpha 1$ and $\alpha 2$ subunit mRNA, as assessed using *in situ* hybridisation, were distinct from each other, and the distribution of $\alpha 1$ mRNA was complementary with the distribution of the $\alpha 1$ protein, as judged by immunofluorescence and

immunoperoxidase, consistent with the distribution of immunostaining for $\alpha 1$ reflecting the true expression pattern of this subunit.

Unfortunately, indicators of selective binding like those included in the study by Szabadits *et al.* (2007) are absent in other studies using the $\alpha 1$ antibody and stringent, relevant-tests of the antibody's selectivity are, inexplicably, missing in the literature. Therefore, the present work clearly complicates the interpretation of the results of published studies employing the antibody. (It should be noted that adequate controls for the selectivity of both of the $\beta 1$ antibodies used here are also lacking and, until they are provided, the precise location of $\beta 1$ in the hippocampus will also remain uncertain). To clarify the location of the $\alpha 1$ subunit in hippocampus, future work must determine the conditions, if any, under which the $\alpha 1$ antibody is selective for its target. Interestingly, precedent for selective antibody binding under the conditions of Western blotting but not conventional immunoperoxidase staining exists in the literature (Watanabe *et al.*, 1998). Watanabe *et al.* (1998) found that the selective binding (as assessed using knock-out tissue) of primary antibodies for the NMDA receptor subunits NR1 and NR2A and B in 4% PFA-fixed sections of mouse brain, including the hippocampus, was dependent on the pre-treatment of sections with pepsin, which facilitated the access of very low, previously sub-threshold concentrations of the antibodies to their targets. The resulting pattern of staining was drastically different to that observed in pepsin-untreated sections using higher antibody concentrations that were non-specific. In fact, they accorded better with expectations of the distribution of a synaptic protein (since, for example, dendritic staining in the hippocampus became stronger than staining of cell soma) and with the distribution of the NMDA receptor subunits' mRNA, as assessed by *in situ* hybridisation. Similar results have been reported following the combined use of pepsin and very low concentrations of antibodies to stain for other synaptic proteins, such as PSD-95 (Fukaya and Watanabe, 2000), and it is noteworthy that the distribution of the non-specific staining for NMDA receptor subunits observed in pepsin un-treated sections by Watanabe *et al.* (1998) was remarkably similar to the distribution of staining that we observed following immunoperoxidase staining for the NO-targeted guanylyl cyclase $\alpha 1$ subunit in 1 % PFA-fixed tissue. Therefore

pepsin treatment could represent a strategy for obtaining selective binding of the NO-targeted guanylyl cyclase $\alpha 1$ antibody.

If no conditions for selective antibody binding are found, the development of an alternative antibody with higher selectivity for the $\alpha 1$ protein will be desirable. Considering that functional evidence implies that presynaptic effects of NO are $\alpha 1$ -dependent (Taqatqeh *et al.*, 2009; Neitz *et al.*, 2011), the true location of $\alpha 1$, whether in interneurons and/or pyramidal neurons will be very interesting and could be of critical importance to researchers seeking to understand NO/cGMP-dependent plasticity.

Chapter 8:

Summary

8.1 NO and NMDA receptor-dependent LTP

It is well accepted that various forms of synaptic plasticity require NO. Brain areas in which NO-dependent forms of LTP have been studied include the hippocampus (for example, Son *et al.*, 1996; Doreulee *et al.*, 2001; Hopper and Garthwaite, 2006), the neocortex (for example, Haul *et al.*, 1999; Hardingham and Fox, 2006; Haghikia *et al.*, 2007) and amygdala (Watanabe *et al.*, 1995). At CA1 synapses, where LTP is archetypal, both endothelium-derived and neuronal NO signals are thought to be required for stable NMDA receptor- and NO-dependent LTP (Son *et al.*, 1996; Hopper and Garthwaite, 2006).

8.1.1 Role of nNOS

Given the physical link between nNOS and NMDA receptors in neurons, and that NO is a putative retrograde transmitter at synapses, thoughts on the role of NO in LTP usually centre around its generation upon NMDA receptor channel opening and action on presynaptic targets (Feil and Kleppisch, 2008; Garthwaite, 2008). Compelling evidence for retrograde NO transmission has been provided by studies of LTP at synapses between dissociated hippocampal neurons. However, there are few examples of presynaptic effects of NO (consistent with retrograde transmission) during LTP at synapses in intact, wild-type tissues (see **Table 3.1**).

Given the above, the study presented in **Chapter 3** was designed to test the prediction that exogenous NO, when paired with HFS, would restore the NO-dependent component of NMDA receptor-dependent LTP at CA1 synapses when NMDA receptors were blocked. In this way we aimed to isolate the NO-dependent component and test its locus (pre- or postsynaptic). Consistent with the prediction, we report for the first time that the NO donor, PAPA/NONOate, generated a persistent enhancement of CA1 fEPSPs when paired with HFS in the presence of the NMDA antagonist, D-AP5. In accordance with the typical effect of NOS inhibition on NMDA receptor-dependent LTP (see **Figure 3.4**), this NO-induced potentiation was of slow onset but reached a magnitude similar to HFS-induced LTP. Further characterisation of this NO-induced potentiation was consistent with it being

representative of a NO-dependent component of LTP (although see **Chapter 3** for a broader discussion), suggesting that the potentiation may be useful tool for the study of long-lasting NO-dependent potentiation in isolation of other mechanisms underlying LTP.

The hypothesis that NO acts as a retrograde messenger during LTP at synapses in intact tissues, in conjunction with studies of LTP at synapses between dissociated cells, predicted that the NO-induced potentiation would be presynaptic. However, we found no evidence for this. While our data cannot rule out a presynaptic effect of NO during HFS-induced and other types of LTP, including those that may occur naturally *in vivo*, they are not consistent with this possibility. Furthermore, much of the evidence in favour of a presynaptic effect of NO during LTP in intact tissues is also consistent with NO acting postsynaptically. Additionally, the data imply that conclusions drawn from studying synapses between dissociated neurons may not be applicable to synapses in intact tissues (perhaps due to a lack of eNOS in the former preparation; see below).

In the future, fluorescent indicators of presynaptic efficacy (reviewed by Blundon and Zakharenko, 2008) could be used to further test the possible presynaptic effect of NO during LTP at synapses in intact tissues. At present, we conclude that an action on both sides of the synapse is most parsimonious with the current data on the role of NO/cGMP in LTP (see Garthwaite, 2008; Feil and Kleppisch, 2008 for a review). Such a role for NO in LTP may enable it to coordinate synaptic plasticity across the synapse; a potentially important action of which few other molecules would be capable.

8.1.2 Role of eNOS

The NO-induced potentiation detailed in **Chapter 3** was facilitated by endogenous NO. Based on the current literature (Hopper and Garthwaite, 2006), the endogenous NO required was probably endothelium-derived. Endothelial NOS has been reported to generate a low-level, activity-independent NO tone in optic nerve and hippocampus. In optic nerve, this NO signal causes the tonic depolarisation of axons

via a pathway involving HCN channels (Garthwaite *et al.*, 2006). In hippocampus, the NO tone has been postulated to prime synapses for LTP (Hopper and Garthwaite, 2006), but, prior to the present study, it had no defined role.

The data presented in **Chapter 4** imply that eNOS activity elicits the tonic facilitation of neurotransmitter release at CA1 synapses under conditions of basal stimulation (i.e. stimulation causing no observable change in synaptic efficacy). Although our data are limited, our conclusion is consistent with a recent study by Neitz *et al.* (2011), and proposes a novel role for the endothelium-derived, activity-independent NO tone in the hippocampus. The consequences of such a role for eNOS may be of critical importance to NO-dependent plasticity, since factors that influence neurotransmitter release during LTP induction likely influence LTP expression. Indeed, it is noteworthy that the effect of (e)NOS inhibition on PPF under basal conditions was observed when the ISI was 10 ms- the same ISI as occurs during HFS. We hypothesise that the facilitation of neurotransmitter release at CA1 synapses by eNOS may regulate the stimulus threshold for the induction of stable LTP, thus explaining why some forms of LTP require endothelium-derived NO (for example, Haul *et al.*, 1999; Son *et al.*, 1996; Hopper and Garthwaite, 2006). Since eNOS activity is subject to dynamic regulation (**Chapter 1**), it is, given the above hypothesis, also tempting to speculate that endothelium-derived NO may contribute to metaplasticity. On this point it is interesting to note that exercise, which causes an increase in eNOS activity in the cardiovascular system and brain, probably via the shear stress of endothelial cells (reviewed by Walther *et al.*, 2004; Faraci, 2006), has been proposed by those studying adult neurogenesis in the dentate gyrus, LTP and learning in spatial tasks to prime the hippocampus for plasticity as animals move through environments and increase their capacity for experience (Kempermann, 2002; Kempermann *et al.*, 2010).

Recently, it has been reported that the regulation of neurotransmitter release under basal conditions by NO (eNOS) requires the $\alpha 1\beta 1$ isoform of NO-targeted guanylyl cyclase (Taqatqeh *et al.*, 2009; Neitz *et al.*, 2011). Message and protein for the $\alpha 1$ NO-targeted guanylyl cyclase has been detected in hippocampal interneurons but not pyramidal cells (Szabadits *et al.*, 2007; Cserep *et al.*, 2011).

Using conditions that have been reported to enhance the staining of other presumed synaptic proteins in fibres and principal cells (Burette *et al.*, 2002; Wendland *et al.*, 1994; Gonzalez-Hernandez *et al.*, 1996), we made attempts to determine whether the NO-targeted guanylyl cyclase $\alpha 1$ subunit was also present in hippocampal pyramidal neurons, as effects of NO on neurotransmitter release at synapses between pairs of dissociated pyramidal neurons would suggest (see **Table 3.1**). Under these conditions, immunoperoxidase staining for the $\alpha 1$ subunit was detected in pyramidal neurons (**Chapter 7**). However, the staining was found to be entirely non-specific based on the use of $\alpha 1$ -null mice. Importantly, interneuron staining, regardless of the conditions used, was also non-specific. Although the $\alpha 1$ antibody that we used is the most commonly employed for immunohistochemistry, no other stringent tests of its specificity have been reported. The specificity of antibodies used for the detection of the $\beta 1$ subunit is also unclear and tests of this are hampered by a lack of viable $\beta 1$ -deficient mice. Given the wealth of physiological processes and pathologies thought to involve NO/cGMP, and the intriguing possibility that pre- and postsynaptic effects of NO might be differentially transduced by the $\alpha 1$ - and $\alpha 2$ -containing NO-targeted guanylyl cyclase isoforms, further, controlled tests of the location of NO-targeted guanylyl cyclase are required (see **Chapter 7** for a strategy).

8.2 NO and NMDA receptor-independent LTP

The data presented in **Chapter 5** show for the first time that a form of NMDA receptor-independent, L-VGCC-dependent LTP at CA1 synapses requires NO, in this case, apparently generated solely by nNOS. This finding challenges the view that neuronal NO is preferentially synthesised by NMDA receptor channel opening. L-VGCC-dependent forms of synaptic plasticity have been correlated with learning and memory (Borroni *et al.*, 2000; Kleppisch *et al.*, 2004; Woodside *et al.*, 2004; Moosmang *et al.*, 2005a), and may be particularly important for changes in gene expression during synaptic plasticity (Murphy *et al.*, 1991; Bading *et al.*, 1993; Impey *et al.*, 1996). Therefore, our data indicate that a potentially important role for NO in the regulation of synaptic efficacy may have been previously overlooked.

Neuronal NOS activation during NMDA receptor-independent, L-VGCC-dependent LTP likely results from a rise in intradendritic Ca^{2+} . Although we were unable to identify a potential source of Ca^{2+} responsible for nNOS activation during L-VGCC-dependent LTP (**Chapter 5** and **Appendix 2**), the use of a new biosensor with unrivalled sensitivity to NO (described in Batchelor *et al.*, 2010; Wood *et al.*, 2011) may, in the future, enable the elucidation of the signalling pathway(s) responsible.

The role of nNOS in L-VGCC-dependent LTP was deduced from studies using a non-selective NOS inhibitor (L-NNA) in conjunction with eNOS-deficient mice. Ideally, the role of nNOS would also have been tested using a selective inhibitor. Unfortunately, the study described in **Chapter 5** led to the discovery that the most potent nNOS inhibitors (L-VNIO and 1400-W) currently available, were, at the standard concentrations for use (0.1 μM and 1 μM , respectively), ineffective in blocking NMDA-induced, NOS-dependent cGMP synthesis in adult mouse hippocampal slices (see **Chapter 6**). Prior to our discovery, similar findings were made using slices of immature mouse hippocampus (Bartus, 2009). Our data were particularly surprising since the original characterisation of L-VNIO (0.1 μM) and 1400-W (1 μM) as selective nNOS inhibitors in intact tissues was done using adult hippocampus (Hopper and Garthwaite, 2006). Taken together, the data presented in **Chapter 6** and by Bartus (2009) suggest that the compounds, which, have been widely used at the above concentrations, are inadequately selective for nNOS over eNOS to be of use diagnostically. Experiments to address the difference between the results of the present study and those of Hopper and Garthwaite (2006) are in progress. Since a wealth of studies using these compounds lack appropriate controls for selective nNOS inhibition (for example, Neitz *et al.*, 2011), the related data should be re-interpreted.

To address the lack of useable nNOS inhibitors, we tested another compound (FX-5043), shown previously to inhibit nNOS with unrivalled potency and selectivity in cell-free and cell-based assays (Xue *et al.*, 2010a). In testament to the challenges that face that the development of selective NOS inhibitors (reviewed by Alderton *et al.*, 2001), neither FX-5043, nor a similar compound, JK-5, were found to be appropriate for use in intact tissues (**Chapter 5**). Therefore more work is needed to develop

selective nNOS inhibitors for research, and potentially clinical (see Gross and Wolin, 1995; Hobbs *et al.*, 1999; Vallance and Leiper, 2002), use.

8.3 Some general outstanding issues

The data presented here add support to some key hypotheses of the role of NO in LTP, and show novel roles for NO in synaptic plasticity. Additionally, a scheme for NMDA receptor and NO-dependent, HFS-induced LTP laid out in **Figure 3.21** may be a useful foundation for further tests of the role of NO in LTP.

Overall, the results are consistent with the view that physiological NO signals are transduced by NO-targeted guanylyl cyclase and cGMP accumulation, but the mechanisms downstream of NO/cGMP in synaptic plasticity largely remain to be elucidated (see **Chapter 1** for review). The definition of mechanisms downstream of NO/cGMP during LTP may help to explain how two NO/cGMP signals (endothelium-derived and neuronal) act upon one synapse simultaneously. Based on recent work by others (Taqatqeh *et al.*, 2009; Neitz *et al.*, 2011), it is tempting to speculate that NO signals produced by eNOS and nNOS may differentially target the $\alpha 1\beta 1$ and $\alpha 2\beta 1$ cyclases, and that these may be confined to different sides of the synapse. If eNOS and nNOS act on the same sides of the synapse, but have distinct roles, the compartmentalisation of NO/cGMP signals by PDEs may be important, as may be the involvement of downstream effectors with different sensitiveness to cGMP, such as PKGI and PKGII (see **Chapter 1**).

There are, of course, many alternatives to the ‘one synapse’ hypothesis for NO action in LTP. Immunohistochemical evidence, for example, suggests that astrocytes respond to NO in multiple brain areas (de Vente *et al.*, 1998). Interestingly astrocytes have low PDE activity, and are therefore highly sensitive to NO (Garthwaite, 2005). Although little is known about the physiological significance of possible signals conveyed to astrocytes by NO, astrocytes are well-placed to regulate synaptic plasticity. Actions that may influence LTP include: the regulation of synaptogenesis; neurotransmitter uptake; and the release of gliotransmitters (reviewed by Barker and Ullian, 2010). Many of these actions could conceivably be influenced by changes in

astrocyte morphology and, considering the potential role of NO in structural synaptic plasticity (Nikonenko *et al.*, 2003; Nikonenko *et al.*, 2008), it is interesting that the NO pathway has been found to regulate the morphology of rat cerebellar astroglia in culture (Boran and Garcia, 2007), in this case via cGMP/PKG, and astrocyte-like cells in hypothalamus (De Seranno *et al.*, 2004).

Additionally, an emerging focus of research with relevance to the involvement of NO in synaptic plasticity is on the role of NO in GABAergic transmission at interneuron synapses. It has long been recognised that NO regulates the release of GABA at synapses in various brain regions (reviewed by Prast and Philippu, 2001). In the ventral tegmental area (Nugent *et al.*, 2007) and the hippocampus (Makara *et al.*, 2007; Cserep *et al.*, 2011), evidence consistent with the activity-dependent synthesis of NO in pyramidal neurons and subsequent down-regulation of GABAergic transmission via retrograde transmission has been reported (see **Chapter 7, 7.1** for discussion). In the hippocampus, it is tempting to speculate that such an NO-mediated depolarisation-induced suppression of inhibition would influence the LTP induction threshold at pyramidal cell synapses. The effects of NO on GABAergic transmission in the developing hippocampus appeared to be regulated by the $\alpha 1\beta 1$ -containing guanylyl cyclase (Cserep *et al.*, 2011), which has recently been identified as presynaptic and tonically active on the basis of functional evidence (Taqatqeh *et al.*, 2009; Neitz *et al.*, 2011; **Chapter 4**).

Excitingly, the future use of a new biosensor able to detect picomolar concentrations of NO/cGMP in real-time (Batchelor *et al.*, 2010; Wood *et al.*, 2011) may enable a multitude of questions regarding the physiology of NO and its role in synaptic plasticity to be answered. If the biosensor can be transfected into hippocampal cells, it may permit direct tests of questions as fundamental as whether or not neuronal NO signals generated during LTP are synapse specific (see above) and/or subject to potentiation themselves.

Appendix 1:

Intracellular recording of synaptic activity in area CA1 using sharp electrodes

We investigated the effects of HFS-induced LTP and the NO-induced potentiation described in **Chapter 3** on PPF in individual pyramidal neurons in area CA1 in hippocampal slices using standard methods for intracellular electrophysiological recording with sharp electrodes. Sharp electrode recording offered three major advantages over patch-clamp recording. First, sharp electrode recordings can be maintained for longer than patch-clamp recordings because sharp electrodes confer experiments with greater physical and biochemical stability. Second, and in accordance with the first advantage, sharp electrode recording has less effect on the postsynaptic cell cytoplasm. Third, sharp electrodes can be advanced into the slice to the depth where field recordings are typically made and away from tissue damage caused by slicing. This point was especially important since the concentration of bath-applied exogenous NO that penetrates a brain slice is known to decline steeply as a function of depth into the slice (Hall and Garthwaite, 2006).

Intracellular sharp electrodes, ~ 70-120 M Ω when filled with 2-3 M KMeSO₄, were placed within the stratum pyramidale in area CA1, adjacent to an extracellular recording electrode in the stratum radiatum (**Figure 9.1**; see **Chapter 2** for details of field electrode recording). Pyramidal neurons were identified by their electrophysiological properties, including their resting V_m (~ -69 mV), action potential threshold (~ 50 mV), slow after-hyperpolarisation (AHP) and spike frequency adaptation (**Figure 9.1B-C**; see Spruston and McBain, 2007 for comparison). Presumed pyramidal cell EPSPs were largely inhibited by CNQX (10 μ M). A slower, CNQX-resistant, D-AP5 (50 μ M)-sensitive EPSP could be observed on raising the stimulation amplitude. These findings were consistent with the synaptic activation of AMPA/kainate and NMDA receptors (**Figure 9.1C**).

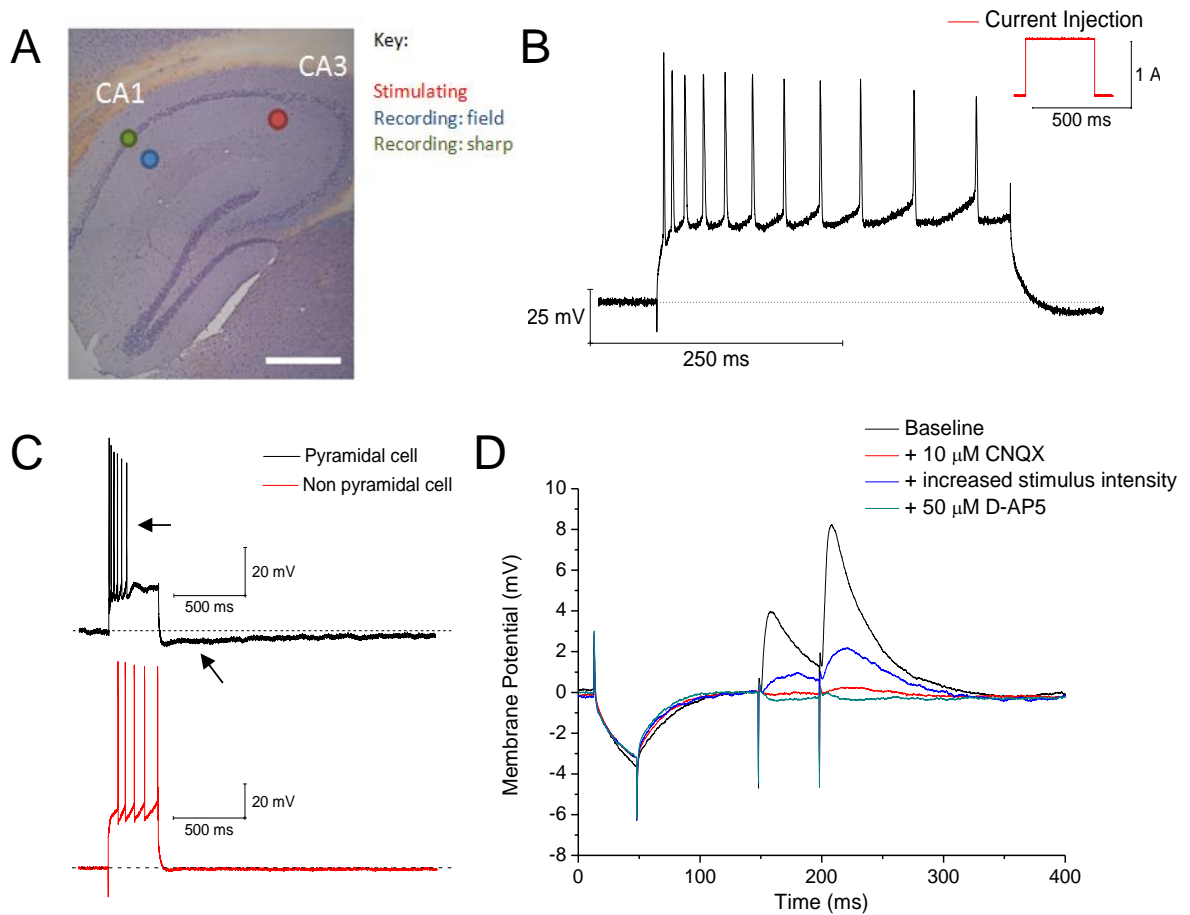


Figure 9.1 Intracellular recording of pyramidal cell activity in hippocampal slices using sharp electrodes. **A)** The target sites of the stimulating and recording electrodes are indicated using a Mayer's Hemalum-stained transverse section of the hippocampus. Scale = 500 μm . **B)** Typical response of a pyramidal neuron recorded using a sharp electrode in response to the current injection shown in the inset. **C)** Typical responses of cells presumed to be pyramidal and non-pyramidal neurons in response to identical current injection. Note the AHP and accommodation (indicated by the arrows) shown by the pyramidal but not the non-pyramidal cell. **D)** EPSPs were recorded from a typical pyramidal cell following a pair of stimuli delivered 50 ms apart. Note the PPF of the second EPSP. The AMPA/kainate receptor antagonist, CNQX (10 μM), and the NMDA receptor antagonist, D-AP5 (25 μM), were applied in the order shown in the legend (top to bottom). The EPSPs were found to be composed of a large CNQX (10 μM)-sensitive, AMPA receptor-dependent potential, a slow D-AP5 (50 μM)-sensitive, NMDA receptor-dependent potential and a small IPSP (shown in green). Traces are means of consecutive EPSPs recorded from one typical slice.

Paired-pulse stimulation resulted in PPF of EPSPs (**Figure 9.1**) which lasted at least 400 ms (**Figure 9.2**). As is standard, the PPR (response 2/response 1) decreased as

the ISI was increased. Remarkably, PPF of EPSPs was similar to PPF of adjacent fEPSPs (**Figure 9.2**), suggesting that extracellular measurements of PPF across multiple dendrites were representative of PPF occurring in single cells.

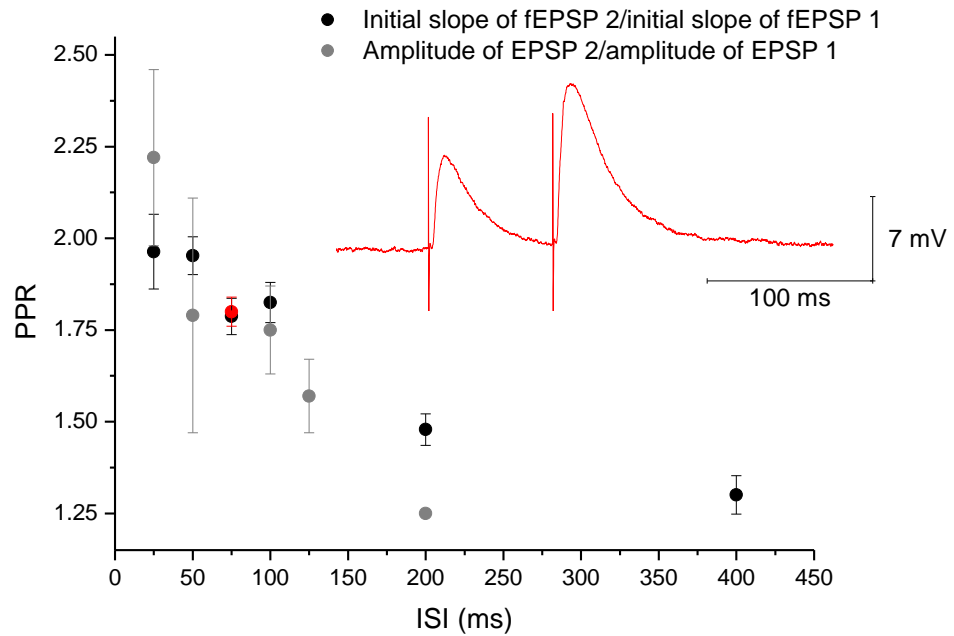


Figure 9.2 PPF of pyramidal cell EPSPs and fEPSPs in hippocampal slices. Pairs of stimuli were delivered at the ISI indicated and the PPRs of the resulting responses were measured as the slope of fEPSP 2/fEPSP 1 (black) or the peak amplitude of EPSP 2/EPSP 1 from baseline (grey). $n = 2-15$ slices. Inset EPSPs (ISI = 75 ms) are a mean of 10-15 consecutive traces and were recorded at the ISI indicated by the filled red data point.

In a proportion of intracellular recordings, HFS of Schaffer collaterals/commissural fibres yielded LTP of fEPSPs and EPSPs in area CA1 (**Figure 9.3**).

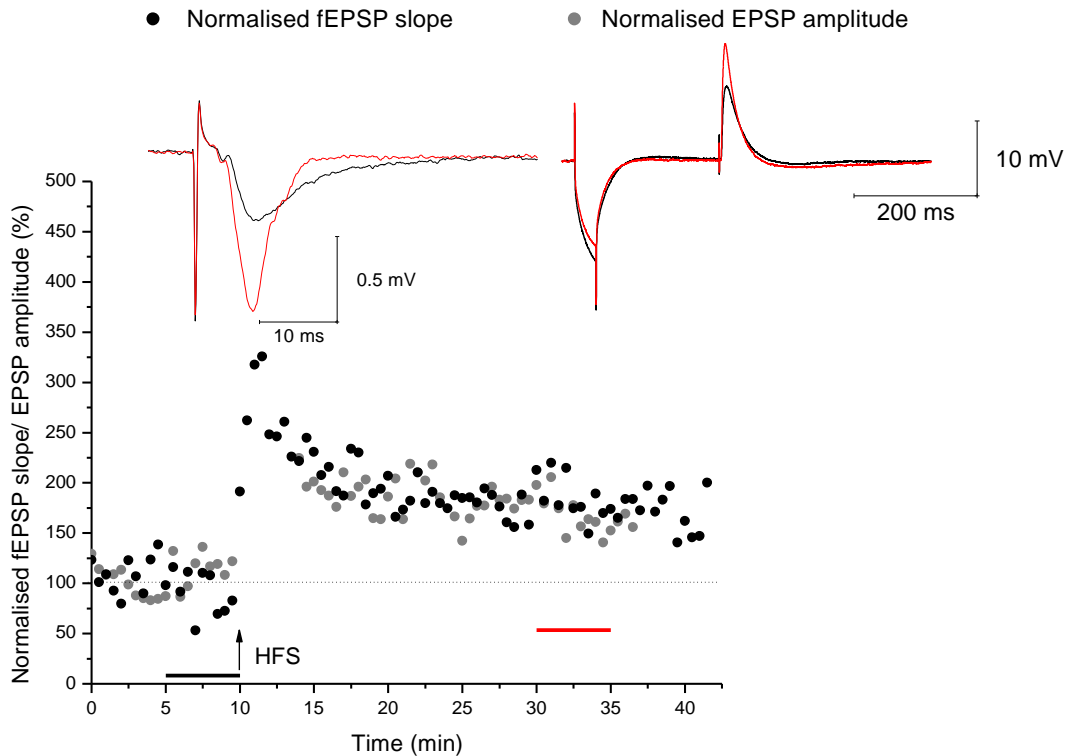


Figure 9.3 LTP of adjacent fEPSPs and pyramidal neuron EPSPs. A typical example of CA1 LTP induced by HFS (1-s, 100-Hz tetanus) of Schaffer collaterals/commissural fibres and recorded using an extracellular field electrode in the stratum radiatum (black) and an adjacent sharp electrode within a presumed pyramidal neuron in the stratum pyramidale (grey). The data recorded intracellularly has been truncated since the cell fired during PTP. Sample traces are the mean response recorded at the times indicated by the colour-coded bars.

However, ~ 50 % of recordings could not be maintained for the duration required, and ~ 50 % of neurons from which stable recordings were made were unable to support LTP (induction and expression). The lack of stable LTP could have resulted from a combination of factors, including poor slice or neuron health, instability of the intracellular electrode or the possibility that not all neurons adjacent to the field electrode contributed to LTP of the fEPSP. In support of the latter possibility, studies of LTP and LTD at CA1 synapses in transverse hippocampal slices and organotypic hippocampal slice cultures suggest that a small proportion of CA1 synapses do not exhibit synaptic plasticity (Petersen *et al.*, 1998; Debanne *et al.*, 1999). We favour this possibility as an explanation for the lack of LTP because, in all cases, the fEPSP appeared to be healthy and could be potentiated, baseline EPSPs were maintained despite the lack of LTP, and PTP was not observed in cells that failed to potentiate.

Given the above, extracellular recording was taken as the sole approach to the investigation of the effect of LTP and the NO-induced potentiation on PPF. To determine whether statistically significant changes in PPF of fEPSP could be detected, experiments using two compounds, 2-Cl-adenosine and forskolin, shown previously to affect opposite changes in PPF were performed (see **Chapter 3**).

Appendix 2:

Mechanism of K⁺-induced, NOS-dependent cGMP accumulation in hippocampus

Neuronal NOS is thought to be preferentially activated by NMDA receptor channel opening. However, nNOS activity appears to be critical for the expression of NMDA receptor-independent, L-VGCC-dependent LTP at CA1 synapses in the hippocampus. As shown in **Chapter 5**, exposure of hippocampal slices to high concentrations of extracellular K⁺ ([K⁺]_o) elicited D-AP5-insensitive, nNOS-dependent cGMP accumulation in a concentration-dependent manner (**Figure 5.8**). Following stimulation with the highest [K⁺]_o tested (122.5 mM), cGMP accumulation was significantly greater than that induced by a maximal concentration of NMDA, implying that if the mechanism(s) underlying the K⁺-induced cGMP response were active following more physiological stimuli, they could hold considerable influence over NO physiology and/or pathology in the hippocampus, including during synaptic plasticity and conditions of excitotoxicity. Therefore a preliminary set of experiments aimed at identifying the mechanism(s) underlying the K⁺-induced cGMP accumulation in hippocampal slices were performed.

Hippocampal slices were stimulated with 122.5 mM K⁺ for 5 min. In all experiments, slices were pre-incubated with D-AP5 (100 μM, 35 min), to block NMDA receptor-dependent cGMP accumulation, TTX (1 μM, 35 min), to block network activity, and BAY 60-7550 (1 μM, 30 min), to inhibit the major PDE present in the hippocampus (PDE 2; van Staveren *et al.*, 2001; Suvarna and O'Donnell, 2002; van Staveren *et al.*, 2003), thus increasing the sensitivity of the measurement of cGMP production (see **Chapter 5** for full methods). In interleaved experiments slices were pre-incubated for 35 min with one of the inhibitors listed in **Table 10.1**, or with thapsigargin (10 μM, 100 min). Statistical significance was tested using one-factor ANOVA with Dunnett's test.

| Inhibitor | Conc. (μM) | Primary target | Reason for use |
|----------------------------------|------------|------------------------|--|
| NBQX disodium | 10 | AMPA/kainate receptors | AMPA reportedly induces NOS-dependent cGMP production in rat cerebellar slices (Southam <i>et al.</i> , 1991; Okada, 1992) and conversion of radiolabelled L-arginine to citrulline in adult rat hippocampus <i>in vivo</i> (Bhardwaj <i>et al.</i> , 1997b). |
| LY 341495 | 100 | All mGluRs | mGluR agonism shown to induce NOS-dependent cGMP generation in rat cerebellar slices (Okada, 1992), and conversion of radiolabelled L-arginine to citrulline in adult rat hippocampus <i>in vivo</i> (Bhardwaj <i>et al.</i> , 1997a), likely via Ca ²⁺ release from InsP ₃ -sensitive intracellular stores. |
| S-MCPG | 500 | Group I/II mGluRs | Shown to block NMDA receptor-independent, L-VGCC-dependent LTP at CA1 synapses in adult hippocampal slices (Little <i>et al.</i> , 1995). Also see reason for using LY 341495. |
| (+)- MK-801 | 10 | NMDA receptors | NMDA causes NO synthesis in the hippocampus <i>in vitro</i> (Chapter 5) and <i>in vivo</i> (Luo and Vincent, 1994). |
| Cadmium sulphate | 200 | All VGCCs | See reasons for using ω-agatoxin IVA, ω-conotoxin GVIA and nickel (II) chloride. |
| ω-conotoxin GVIA | 1 | N-VGCCs | N-VGCCs necessary for some forms of NO-dependent, NANC transmission and smooth muscle contraction in the PNS (reviewed in Vincent, 2010). |
| Nickel (II) chloride | 50 | R/T-VGCCs | Reported to inhibit un-stimulated, basal NOS-dependent cGMP accumulation in immature rat hippocampal (Bartus, 2009). |
| ω-agatoxin IVA | 1 | P/Q-VGCCs | Shown to attenuate K ⁺ -induced, NOS-dependent cGMP generation in isolated mouse cortical neurons (Tatsumi <i>et al.</i> , 1998) and conversion of L-arginine to L-citrulline in rat cerebrocortical slices (Alagarsamy <i>et al.</i> , 1994). |
| Gadolinium (III) chloride | 30 | Some TRP channels | Reportedly inhibits un-stimulated, basal NOS-dependent cGMP accumulation in immature rat hippocampal slices (Bartus, 2009). |

Table 10.1 Inhibitors used to identify the molecular mechanism of K⁺-induced, nNOS-dependent cGMP accumulation in hippocampal slices. The names, concentrations used, primary targets and reasons for use of each antagonist are given. All compounds were pre-applied for 35 min. Abbreviations: mGluR = metabotropic glutamate receptor; IP₃ = inositol trisphosphate; NANC = non-adrenergic, non-cholinergic; TRP = transient receptor potential. Note that many of the compounds used affect secondary targets

As shown above (**Figure 5.8**) and again in **Figure 10.1** for ease of comparison, application of 122.5 mM K⁺ for 5 min caused a significant increase in cGMP accumulation relative to that recorded in un-stimulated slices. This rise in cGMP was blocked by the NOS antagonist, L-NNA, the NO-targeted guanylyl cyclase antagonist, ODQ, and was unaltered in slices from mice lacking eNOS, suggesting the response was mediated by the nNOS/NO/cGMP pathway. The response was also significantly attenuated in slices incubated in Ca²⁺-free aCSF containing the membrane impermeable Ca²⁺ chelator, EGTA, consistent with NOS being Ca²⁺/CaM-dependent (Alderton *et al.*, 2001) and implying that Ca²⁺ influx across the neuronal membrane was required for the cGMP response, either to directly activate nNOS or to maintain intracellular Ca²⁺ stores necessary for indirect nNOS activation.

Since high [K⁺]_o would depolarise neurons, the above results were consistent with nNOS activation by the voltage-gated entry of Ca²⁺ into cells, and therefore, the effect of VGCC inhibition (various inhibitors, 35 min) on the K⁺-induced cGMP accumulation was tested. It was found that the general Ca²⁺ channel antagonist, cadmium sulphate (200 µM; Cd²⁺) significantly reduced the cGMP response to K⁺, but neither the R/T VGCC inhibitor, Ni²⁺ (50 µM), nor the highly selective toxins, ω-conotoxin GVIA (1 µM) and ω-agatoxin IVA (1 µM), which block N and P/Q VGCCs respectively, had any significant effect on the K⁺-induced cGMP rise (**Figure 10.1**; note that the effect of L-VGCC inhibition on the cGMP response was tested in **Chapter 5** using nifedipine).

To try to determine what other mechanism(s) could render the response to high [K⁺]_o dependent on extracellular Ca²⁺, we tested whether the cGMP response required glutamate receptor activity because glutamate release would be expected to be Ca²⁺-dependent. To test the possibility that K⁺-induced glutamate release had overcome the competitive blockade of NMDA receptors by the D-AP5 present in our experiments, leading to NMDA receptor-dependent nNOS activation, slices were pre-incubated with the non-competitive, use-dependent NMDA receptor-antagonist, (+)-MK-801 (10 µM, 35 min), in conjunction with D-AP5 (100 µM, 35 min). This had no significant effect on the mean cGMP response (**Figure 10.1**). Neither did pre-incubation of slices with the AMPA/kainate inhibitor, NBQX (10 µM), or the

metabotropic glutamate receptor inhibitors, LY 341495 (100 μM) or S-MCPG (**Figure 10.1**).

To test the potential involvement of Ca²⁺ released from intracellular stores, slices were pre-incubated with 10 μM thapsigargin for 70 min prior to the addition of the PDE inhibitor, BAY 60-7550 (100 min prior to stimulation with K⁺). This was expected to inhibit the sarco/endoplasmic reticulum Ca²⁺ ATPase (SERCA), therefore causing intracellular Ca²⁺ stores to empty prior to K⁺ stimulation (Treiman *et al.*, 1998). We found no effect of thapsigargin was found on the K⁺-induced cGMP rise (**Figure 10.1**).

Finally, to test the potential involvement of transient receptor potential (TRP) channels in the K⁺-induced cGMP accumulation, Gd³⁺ (30 μM) was used. Pyramidal cell Ca²⁺ influx has previously been reported via TRP channels, which are a large family of mixed-cation channels that are active at basal conditions and in response to factors such as temperature and BDNF (reviewed by Moran *et al.*, 2004). Gd³⁺ is one of the most commonly used TRP channel inhibitors. However, it also attenuates the activity of non-TRP channels, such as VGCCs (reviewed by Caldwell *et al.*, 1998). It was found that Gd³⁺ significantly inhibited cGMP accumulation (**Figure 10.1**), but to a lesser extent than Cd²⁺.

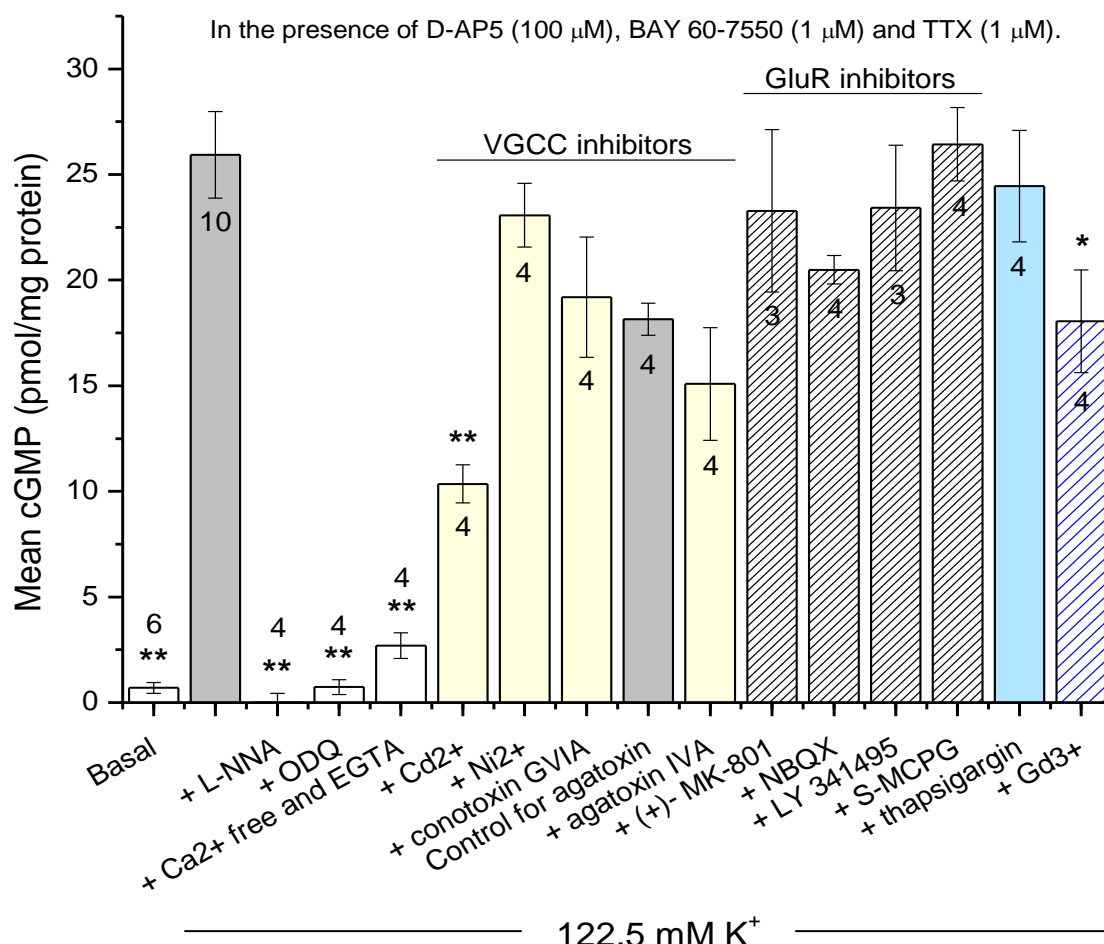


Figure 10.1 Pharmacological profile of high $[K^+]_o$ -evoked cGMP accumulation in hippocampal slices. Data showing cGMP accumulation in un-stimulated slices (basal), and in slices stimulated with 122.5 mM K^+ (5 min) but pre-incubated with the NO-targeted guanylyl cyclase antagonist, ODQ (10 μ M, 35 min), the NOS antagonist, L-NNA (100 μ M, 35 min), or in Ca^{2+} -free media containing 1 mM of the extracellular Ca^{2+} chelator, EGTA, (35 min) has been shown previously in **Chapter 5** but is shown here for ease of comparison. Compared to the mean cGMP response in K^+ -treated slices, the non-selective Ca^{2+} channel antagonist, Cd^{2+} (200 μ M), significantly attenuated the mean cGMP response to 122.5 mM extracellular K^+ ($p < 0.01$ compared to untreated controls; first yellow vs. first grey bar). None of the class-selective VGCC inhibitors (Ni^{2+} , 50 μ M; ω -conotoxin GVIA, 1 μ M; ω -agatoxin IVA, 1 μ M) had any effect on the cGMP response (yellow vs. grey bars). Neither the NMDA receptor inhibitor, (+)-MK-801 (10 μ M), the AMPA/kainate inhibitor, NBQX (10 μ M), nor the metabotropic glutamate receptor antagonists, LY 341495 (100 μ M) or S-MCPG (500 μ M), had any effect on the cGMP response ($p > 0.05$; hatched bars vs. grey bar). The SERCA inhibitor, thapsigargin, was also without effect ($p > 0.05$; blue vs. grey bar). The TRP channel blocker, Gd^{3+} (30 μ M), significantly reduced the K^+ -induced cGMP response ($p < 0.05$ compared to untreated controls; blue hatched vs. grey bar). All experiments were interleaved. All inhibitors were pre-applied for 35 min, except thapsigargin, which was pre-applied for 100 min. Statistics are ANOVA with Dunnett's test where ** = $p < 0.01$, * = $p < 0.05$ compared to slices treated with K^+ alone (first grey bar). Numbers in bars are n values.

In summary, the results presented here and in **Chapter 5** show that significant NMDA receptor-independent, nNOS-dependent cGMP accumulation is possible in the hippocampus and requires a rise in intracellular Ca²⁺. This finding is accordant with a role for NO in NMDA receptor-independent CA1 LTP. Of the inhibitors used to identify the source of the rise in intracellular Ca²⁺ responsible for the K⁺-induced cGMP accumulation, Cd²⁺ most potently inhibited the NMDA receptor-independent, K⁺-induced cGMP response. However, a residual Cd²⁺-insensitive cGMP accumulation was observed. This might represent incomplete Ca²⁺ channel inhibition during depolarisation (Thevenod and Jones, 1992), an inadequate Cd²⁺ concentration for complete Ca²⁺ channel block, or a Cd²⁺-induced increase in intracellular Ca²⁺ caused, for example, by SERCA inhibition and the release of Ca²⁺ from intracellular stores (Visser *et al.*, 1993). Previous work in the laboratory has shown that 200 µM Cd²⁺ does not inhibit exogenous NO-induced cGMP production in immature hippocampal slices (Bartus, 2009), ruling out the possibility that the inhibitory effect we observed was due to a direct effect of Cd²⁺ on the NO/cGMP pathway, and against a toxic influence of Cd²⁺ (Li *et al.*, 2000).

No selective VGCC inhibitor could account for the effect of Cd²⁺ on the cGMP response, suggesting that the compound was acting on a Ca²⁺ channel whose involvement was not-tested, or a combination of Ca²⁺ channels activated by the relatively crude stimulus. Perhaps because Ca²⁺ is such a ubiquitous signalling molecule, it is not completely surprising that significant NO-induced cGMP accumulation can occur in neurons independent of NMDA receptor activation and that a single source of Ca²⁺ necessary for the K⁺-induced, nNOS-cGMP accumulation could not be isolated in these experiments. Taking into account the non-physiological nature of the stimulation, the lack of selective pharmacological tools and the potential complexity of investigating a combinatorial effect of Ca²⁺ on NOS, we did not make any further attempts to isolate the source of Ca²⁺ responsible for the K⁺-induced cGMP response.

References

- Abeliovich A, Schmitz Y, Farinas I, Choi-Lundberg D, Ho WH, Castillo PE, Shinsky N, Verdugo JM, Armanini M, Ryan A, Hynes M, Phillips H, Sulzer D, Rosenthal A (2000) Mice lacking alpha-synuclein display functional deficits in the nigrostriatal dopamine system. *Neuron* **25**: 239-252.
- Abraham WC (2008) Metaplasticity: tuning synapses and networks for plasticity. *Nat. Rev. Neurosci.* **9**: 387.
- Abraham WC, Logan B, Greenwood JM, Dragunow M (2002) Induction and experience-dependent consolidation of stable long-term potentiation lasting months in the hippocampus. *J. Neurosci* **22**: 9626-9634.
- Ahlijanian MK, Westenbroek RE, Catterall WA (1990) Subunit structure and localization of dihydropyridine-sensitive calcium channels in mammalian brain, spinal cord, and retina. *Neuron* **4**: 819-832.
- Alagarsamy S, Lonart G, Johnson KM (1994) The role of P-type calcium channels in the depolarization-induced activation of nitric oxide synthase in frontal cortex. *J. Neurochem.* **62**: 400-403.
- Alderton WK, Cooper CE, Knowles RG (2001) Nitric oxide synthases: structure, function and inhibition. *Biochem. J.* **357**: 593-615.
- Amaral D, Lavenex P (2007) Hippocampal neuroanatomy. In: The hippocampus book (Andersen P, Morris R, Amaral D, Bliss T.V.P., O'Keefe J, eds), pp 37-114. Oxford: Oxford University Press.
- Amaral DG, Witter MP (1989) The three-dimensional organization of the hippocampal formation: A review of anatomical data. *Neuroscience* **31**: 571-591.
- Andersen P, Morris R, Amaral D, Bliss T.V.P., O'Keefe J (2007) Historical perspective: proposed functions, biological characteristics, and neurobiological models of the hippocampus. In: The hippocampus book (Andersen P, Morris R, Amaral D, Bliss TVP, O'Keefe J, eds), pp 9-36. Oxford: Oxford University Press.
- Andersen P, Sundberg SH, Sveen O, Wigstrom H (1977) Specific long-lasting potentiation of synaptic transmission in hippocampal slices. *Nature* **266**: 736-737.
- Anekonda TS, Quinn JF, Harris C, Frahler K, Wadsworth TL, Woltjer RL (2011) L-type voltage-gated calcium channel blockade with isradipine as a therapeutic strategy for Alzheimer's disease. *Neurobiol. Dis.* **41**: 62-70.
- Aniksztejn L, Ben-Ari Y (1991) Novel form of long-term potentiation produced by a K⁺ channel blocker in the hippocampus. *Nature* **349**: 67-69.
- Antonova I, Arancio O, Trillat AC, Wang HG, Zablow L, Udo H, Kandel ER, Hawkins RD (2001) Rapid increase in clusters of presynaptic proteins at onset of long-lasting potentiation. *Science* **294**: 1547-1550.
- Arancio O, Kandel ER, Hawkins RD (1995) Activity-dependent long-term enhancement of transmitter release by presynaptic 3',5'-cyclic GMP in cultured hippocampal neurons. *Nature* **376**: 74-80.
- Arancio O, Antonova I, Gambaryan S, Lohmann SM, Wood JS, Lawrence DS, Hawkins RD (2001) Presynaptic role of cGMP-dependent protein kinase during long-lasting potentiation. *J. Neurosci.* **21**: 143-149.

- Arancio O, Kiebler M, Lee CJ, Lev-Ram V, Tsien RY, Kandel ER, Hawkins RD (1996) Nitric oxide acts directly in the presynaptic neuron to produce long-term potentiation in cultured hippocampal neurons. *Cell* **87**: 1025-1035.
- Arnold WP, Mittal CK, Katsuki S, Murad F (1977) Nitric oxide activates guanylate cyclase and increases guanosine 3':5'-cyclic monophosphate levels in various tissue preparations. *Proc. Natl. Acad. Sci. U. S. A* **74**: 3203-3207.
- Ashina M, Bendtsen L, Jensen R, Lassen LH, Sakai F, Olesen J (1999a) Possible mechanisms of action of nitric oxide synthase inhibitors in chronic tension-type headache. *Brain* **122** (Pt 9): 1629-1635.
- Ashina M, Lassen LH, Bendtsen L, Jensen R, Olesen J (1999b) Effect of inhibition of nitric oxide synthase on chronic tension-type headache: a randomised crossover trial. *Lancet* **353**: 287-289.
- Babu BR, Griffith OW (1998) N5-(1-Imino-3-butenyl)-L-ornithine. A neuronal isoform selective mechanism-based inactivator of nitric oxide synthase. *J. Biol. Chem.* **273**: 8882-8889.
- Bading H, Ginty DD, Greenberg ME (1993) Regulation of gene expression in hippocampal neurons by distinct calcium signaling pathways. *Science* **260**: 181-186.
- Bannerman DM, Chapman PF, Kelly PA, Butcher SP, Morris RG (1994a) Inhibition of nitric oxide synthase does not impair spatial learning. *J. Neurosci* **14**: 7404-7414.
- Bannerman DM, Chapman PF, Kelly PA, Butcher SP, Morris RG (1994b) Inhibition of nitric oxide synthase does not prevent the induction of long-term potentiation *in vivo*. *J. Neurosci* **14**: 7415-7425.
- Bannerman DM, Good MA, Butcher SP, Ramsay M, Morris RG (1995) Distinct components of spatial learning revealed by prior training and NMDA receptor blockade. *Nature* **378**: 182-186.
- Barker AJ, Ullian EM (2010) Astrocytes and synaptic plasticity. *Neuroscientist* **16**: 40-50.
- Bartus K (2009) Nitric oxide-mediated cGMP signal transduction in the central nervous system. PhD Thesis, University College London, London, UK.
- Batchelor AM, Bartus K, Reynell C, Constantinou S, Halvey EJ, Held KF, Dostmann WR, Vernon J, Garthwaite J (2010) Exquisite sensitivity to subsecond, picomolar nitric oxide transients conferred on cells by guanylyl cyclase-coupled receptors. *Proc. Natl. Acad. Sci. U. S. A* **107**: 22060-22065.
- Bauer EP, Schafe GE, LeDoux JE (2002) NMDA receptors and L-type voltage-gated calcium channels contribute to long-term potentiation and different components of fear memory formation in the lateral amygdala. *J. Neurosci.* **22**: 5239-5249.
- Bayazitov IT, Richardson RJ, Fricke RG, Zakharenko SS (2007) Slow presynaptic and fast postsynaptic components of compound long-term potentiation. *J. Neurosci.* **27**: 11510-11521.
- Baylor D (1996) How photons start vision. *Proc. Natl. Acad. Sci. U. S. A* **93**: 560-565.
- Behrends S, Kempfert J, Mietens A, Koglin M, Scholz H, Middendorff R (2001) Developmental changes of nitric oxide-sensitive guanylyl cyclase expression in pulmonary arteries. *Biochem. Biophys. Res. Commun.* **283**: 883-887.
- Bekkers JM, Stevens CF (1990) Presynaptic mechanism for long-term potentiation in the hippocampus. *Nature* **346**: 724-729.
- Bellamy TC, Garthwaite J (2002) The receptor-like properties of nitric oxide-activated soluble guanylyl cyclase in intact cells. *Mol. Cell Biochem.* **230**: 165-176.

- Bellamy TC, Griffiths C, Garthwaite J (2002) Differential sensitivity of guanylyl cyclase and mitochondrial respiration to nitric oxide measured using clamped concentrations. *J. Biol. Chem.* **277**: 31801-31807.
- Bender AT, Beavo JA (2006) Cyclic nucleotide phosphodiesterases: molecular regulation to clinical use. *Pharmacol. Rev.* **58**: 488-520.
- Bender VA, Pugh JR, Jahr CE (2009) Presynaptically expressed long-term potentiation increases multivesicular release at parallel fiber synapses. *J. Neurosci.* **29**: 10974-10978.
- Bhardwaj A, Northington FJ, Martin LJ, Hanley DF, Traystman RJ, Koehler RC (1997a) Characterization of metabotropic glutamate receptor-mediated nitric oxide production *in vivo*. *J. Cereb. Blood Flow Metab.* **17**: 153-160.
- Bhardwaj A, Northington FJ, Ichord RN, Hanley DF, Traystman RJ, Koehler RC (1997b) Characterization of ionotropic glutamate receptor mediated nitric oxide production *in vivo* in rats. *Stroke* **28**: 850-857.
- Biel M, Wahl-Schott C, Michalakis S, Zong X (2009) Hyperpolarization-activated cation channels: from genes to function. *Physiol Rev.* **89**: 847-885.
- Bird CM, Burgess N (2008) The hippocampus and memory: insights from spatial processing. *Nat. Rev. Neurosci.* **9**: 182-194.
- Blackshaw S, Eliasson MJL, Sawa A, Watkins CC, Krug D, Gupta A, Arai T, Ferrante RJ, Snyder SH (2003) Species, strain and developmental variations in hippocampal neuronal and endothelial nitric oxide synthase clarify discrepancies in nitric oxide-dependent synaptic plasticity. *Neuroscience* **119**: 979-990.
- Bliss TVP, Collingridge GL, Morris RG (2007) Synaptic plasticity in the hippocampus. In: *The hippocampus book*. (Andersen P, Morris RG, Amaral D, Bliss T.V.P., O'Keefe J, eds), pp 343-474. New York: Oxford University Press, Inc.
- Bliss TVP, Gardner-Medwin AR (1973) Long-lasting potentiation of synaptic transmission in the dentate area of the unanaesthetized rabbit following stimulation of the perforant path. *J. Physiol.* **232**: 357-374.
- Bliss TVP, Lomo T (1973) Long-lasting potentiation of synaptic transmission in the dentate area of the anaesthetized rabbit following stimulation of the perforant path. *J. Physiol. (Lond.)* **232**: 331-356.
- Bliss TVP, Richter-Levin G (1993) Spatial learning and the saturation of long-term potentiation. *Hippocampus* **3**: 123-125.
- Blokland A, de VJ, Prickaerts J, Honig W, Markerink-Van IM, Steinbusch H (1999) Local inhibition of hippocampal nitric oxide synthase does not impair place learning in the Morris water escape task in rats. *Eur. J. Neurosci* **11**: 223-232.
- Blundon JA, Zakharenko SS (2008) Dissecting the components of long-term potentiation. *Neuroscientist.* **14**: 598-608.
- Boehning D, Snyder SH (2003) Novel neural modulators. *Annu. Rev. Neurosci.* **26**: 105-131.
- Boess FG, Hendrix M, van der Staay FJ, Erb C, Schreiber R, van SW, de VJ, Prickaerts J, Blokland A, Koenig G (2004) Inhibition of phosphodiesterase 2 increases neuronal cGMP, synaptic plasticity and memory performance. *Neuropharmacology* **47**: 1081-1092.
- Bohme GA, Bon C, Lemaire M, Reibaud M, Piot O, Stutzmann JM, Doble A, Blanchard JC (1993) Altered synaptic plasticity and memory formation in nitric oxide synthase inhibitor-treated rats. *Proc. Natl. Acad. Sci. U. S. A* **90**: 9191-9194.

- Bohme GA, Bon C, Stutzmann JM, Doble A, Blanchard JC (1991) Possible involvement of nitric oxide in long-term potentiation. *Eur. J. Pharmacol.* **199**: 379-381.
- Bon CL, Garthwaite J (2001) Exogenous nitric oxide causes potentiation of hippocampal synaptic transmission during low-frequency stimulation via the endogenous nitric oxide-cGMP pathway. *Eur. J. Neurosci.* **14**: 585-594.
- Bon CL, Garthwaite J (2003) On the role of nitric oxide in hippocampal long-term potentiation. *J. Neurosci.* **23**: 1941-1948.
- Bonigk W, Altenhofen W, Muller F, Dose A, Illing M, Molday RS, Kaupp UB (1993) Rod and cone photoreceptor cells express distinct genes for cGMP-gated channels. *Neuron* **10**: 865-877.
- Boran MS, Garcia A (2007) The cyclic GMP-protein kinase G pathway regulates cytoskeleton dynamics and motility in astrocytes. *J. Neurochem.* **102**: 216-230.
- Borroni AM, Fichtenholtz II, Woodside BL, Teyler TJ (2000) Role of voltage-dependent calcium channel long-term potentiation (LTP) and NMDA LTP in spatial memory. *J. Neurosci.* **20**: 9272-9276.
- Boulton CL, Southam E, Garthwaite J (1995) Nitric oxide-dependent long-term potentiation is blocked by a specific inhibitor of soluble guanylyl cyclase. *Neuroscience* **69**: 699-703.
- Bredt DS, Glatt CE, Hwang PM, Fotuhi M, Dawson TM, Snyder SH (1991a) Nitric oxide synthase protein and mRNA are discretely localized in neuronal populations of the mammalian CNS together with NADPH diaphorase. *Neuron* **7**: 615-624.
- Bredt DS, Hwang PM, Glatt CE, Lowenstein C, Reed RR, Snyder SH (1991b) Cloned and expressed nitric oxide synthase structurally resembles cytochrome P-450 reductase. *Nature* **351**: 714-718.
- Bredt DS, Hwang PM, Snyder SH (1990) Localization of nitric oxide synthase indicating a neural role for nitric oxide. *Nature* **347**: 768-770.
- Bredt DS, Snyder SH (1990) Isolation of nitric oxide synthetase, a calmodulin-requiring enzyme. *Proc. Natl. Acad. Sci. U. S. A* **87**: 682-685.
- Brenman JE, Chao DS, Gee SH, McGee AW, Craven SE, Santillano DR, Wu Z, Huang F, Xia H, Peters MF, Froehner SC, Bredt DS (1996) Interaction of nitric oxide synthase with the postsynaptic density protein PSD-95 and alpha1-syntrophin mediated by PDZ domains. *Cell* **84**: 757-767.
- Brun VH, Ytterbo K, Morris RG, Moser MB, Moser EI (2001) Retrograde amnesia for spatial memory induced by NMDA receptor-mediated long-term potentiation. *J. Neurosci.* **21**: 356-362.
- Brune B, Ullrich V (1987) Inhibition of platelet aggregation by carbon monoxide is mediated by activation of guanylate cyclase. *Mol. Pharmacol.* **32**: 497-504.
- Bucci M, Gratton JP, Rudic RD, Acevedo L, Roviezzo F, Cirino G, Sessa WC (2000) *In vivo* delivery of the caveolin-1 scaffolding domain inhibits nitric oxide synthesis and reduces inflammation. *Nat. Med.* **6**: 1362-1367.
- Buechler WA, Nakane M, Murad F (1991) Expression of soluble guanylate cyclase activity requires both enzyme subunits. *Biochem. Biophys. Res. Commun.* **174**: 351-357.
- Burette A, Zabel U, Weinberg RJ, Schmidt HH, Valtchanoff JG (2002) Synaptic localization of nitric oxide synthase and soluble guanylyl cyclase in the hippocampus. *J. Neurosci.* **22**: 8961-8970.
- Caldwell RA, Clemo HF, Baumgarten CM (1998) Using gadolinium to identify stretch-activated channels: technical considerations. *Am. J. Physiol.* **275**: C619-C621.

- Casamassima F, Hay AC, Benedetti A, Lattanzi L, Cassano GB, Perlis RH (2010) L-type calcium channels and psychiatric disorders: A brief review. *Am. J. Med. Genet. B Neuropsychiatr. Genet.* **153B**: 1373-1390.
- Catterall WA (2000) Structure and regulation of voltage-gated Ca^{2+} channels. *Annu. Rev. Cell Dev. Biol.* **16**: 521-555.
- Catterall WA, Perez-Reyes E, Snutch TP, Striessnig J (2009) Voltage-gated calcium channels, introductory chapter. IUPHAR database.
- Catterall WA, Perez-Reyes E, Snutch TP, Striessnig J (2005) International Union of Pharmacology. XLVIII. Nomenclature and structure-function relationships of voltage-gated calcium channels. *Pharmacol. Rev.* **57**: 411-425.
- Catterall WA, Perez-Reyes E, Snutch TP, Striessnig J (2010a) Voltage-Gated Calcium Channels: $\text{Ca}_v1.3$. IUPHAR database.
- Catterall WA, Perez-Reyes E, Snutch TP, Striessnig J (2010b) Voltage-Gated Calcium Channels: $\text{Ca}_v1.2$. IUPHAR database.
- Catterall WA, Striessnig J (1992) Receptor sites for Ca^{2+} channel antagonists. *Trends Pharmacol. Sci.* **13**: 256-262.
- Cavus I, Teyler T (1996) Two forms of long-term potentiation in area CA1 activate different signal transduction cascades. *J. Neurophysiol.* **76**: 3038-3047.
- Chan Y, Fish JE, D'Abreo C, Lin S, Robb GB, Teichert AM, Karantzoulis-Fegaras F, Keightley A, Steer BM, Marsden PA (2004) The cell-specific expression of endothelial nitric-oxide synthase: a role for DNA methylation. *J. Biol. Chem.* **279**: 35087-35100.
- Chapman PF, Atkins CM, Allen MT, Haley JE, Steinmetz JE (1992) Inhibition of nitric oxide synthesis impairs two different forms of learning. *NeuroReport* **3**: 567-570.
- Chen C, Regehr WG (1997) The mechanism of cAMP-mediated enhancement at a cerebellar synapse. *J. Neurosci.* **17**: 8687-8694.
- Chen HX, Roper SN (2003) PKA and PKC enhance excitatory synaptic transmission in human dentate gyrus. *J. Neurophysiol.* **89**: 2482-2488.
- Chetkovich DM, Klann E, Sweatt JD (1993) Nitric oxide synthase-independent long-term potentiation in area CA1 of hippocampus. *NeuroReport* **4**: 919-922.
- Chiang LW, Schweizer FE, Tsien RW, Schulman H (1994) Nitric oxide synthase expression in single hippocampal neurons. *Brain Res. Mol Brain Res.* **27**: 183-188.
- Chien WL, Liang KC, Teng CM, Kuo SC, Lee FY, Fu WM (2003) Enhancement of long-term potentiation by a potent nitric oxide-guanylyl cyclase activator, 3-(5-hydroxymethyl-2-furyl)-1-benzyl-indazole. *Mol. Pharmacol.* **63**: 1322-1328.
- Chien WL, Liang KC, Teng CM, Kuo SC, Lee FY, Fu WM (2005) Enhancement of learning behaviour by a potent nitric oxide-guanylate cyclase activator YC-1. *Eur. J. Neurosci.* **21**: 1679-1688.
- Christie BR, Eliot LS, Ito K, Miyakawa H, Johnston D (1995) Different Ca^{2+} channels in soma and dendrites of hippocampal pyramidal neurons mediate spike-induced Ca^{2+} influx. *J. Neurophysiol.* **73**: 2553-2557.

- Christopherson KS, Hillier BJ, Lim WA, Brecht DS (1999) PSD-95 assembles a ternary complex with the N-methyl-D-aspartic acid receptor and a bivalent neuronal NO synthase PDZ domain. *J. Biol. Chem.* **274**: 27467-27473.
- Clark NC, Nagano N, Kuenzi FM, Jarolimiek W, Huber I, Walter D, Wietzorrek G, Boyce S, Kullmann DM, Striessnig J, Seabrook GR (2003) Neurological phenotype and synaptic function in mice lacking the Ca_v1.3 α subunit of neuronal L-type voltage-dependent Ca²⁺ channels. *Neuroscience* **120**: 435-442.
- Clutton-Brock J (1967) Two cases of poisoning by contamination of nitrous oxide with higher oxides of nitrogen during anaesthesia. *Br. J. Anaesth.* **39**: 388-392.
- Collingridge GL, Kehl SJ, McLennan H (1983a) Excitatory amino acids in synaptic transmission in the Schaffer collateral-commissural pathway of the rat hippocampus. *J. Physiol.* **334**: 33-46.
- Collingridge GL, Kehl SJ, McLennan H (1983b) The antagonism of amino acid-induced excitations of rat hippocampal CA1 neurones *in vitro*. *J. Physiol.* **334**: 19-31.
- Contestabile A (2000) Roles of NMDA receptor activity and nitric oxide production in brain development. *Brain Res. Rev.* **32**: 476-509.
- Cooke SF, Bliss TVP (2006) Plasticity in the human central nervous system. *Brain* **129**: 1659-1673.
- Cooke SF, Wu J, Plattner F, Errington M, Rowan M, Peters M, Hirano A, Bradshaw KD, Anwyl R, Bliss TVP, Giese KP (2006) Autophosphorylation of α CaMKII is not a general requirement for NMDA receptor-dependent LTP in the adult mouse. *J. Physiol.* **574**: 805-818.
- Corbin JD, Turko IV, Beasley A, Francis SH (2000) Phosphorylation of phosphodiesterase-5 by cyclic nucleotide-dependent protein kinase alters its catalytic and allosteric cGMP-binding activities. *Eur. J. Biochem.* **267**: 2760-2767.
- Corkin S (2002) What's new with the amnesic patient H.M.? *Nat. Rev. Neuro.* **3**: 153-160.
- Craven KB, Zagotta WN (2006) CNG and HCN channels: two peas, one pod. *Annu. Rev. Physiol* **68**: 375-401.
- Craven PA, DeRubertis FR (1978) Restoration of the responsiveness of purified guanylate cyclase to nitrosoguanidine, nitric oxide, and related activators by heme and heme proteins. Evidence for involvement of the paramagnetic nitrosyl-heme complex in enzyme activation. *J. Biol. Chem.* **253**: 8433-8443.
- Creager R, Dunwiddie T, Lynch G (1980) Paired-pulse and frequency facilitation in the CA1 region of the *in vitro* rat hippocampus. *J. Physiol.* **299**: 409-424.
- Cserep C, Szonyi A, Veres JM, Nemeth B, Szabadits E, de VJ, Hajos N, Freund TF, Nyiri G (2011) Nitric oxide signaling modulates synaptic transmission during early postnatal development. *Cereb. Cortex.* **9**: 2065-2074.
- Cukkemane A, Seifert R, Kaupp UB (2011) Cooperative and uncooperative cyclic-nucleotide-gated ion channels. *Trends Biochem. Sci.* **36**: 55-64.
- Cummings JA, Nicola SM, Malenka RC (1994) Induction in the rat hippocampus of long-term potentiation (LTP) and long-term depression (LTD) in the presence of a nitric oxide synthase inhibitor. *Neurosci. Lett.* **176**: 110-114.
- Daff S (2010) NO synthase: structures and mechanisms. *Nitric Oxide* **23**: 1-11.

- Daff S, Sagami I, Shimizu T (1999) The 42-amino acid insert in the FMN domain of neuronal nitric-oxide synthase exerts control over Ca²⁺/calmodulin-dependent electron transfer. *J. Biol. Chem.* **274**: 30589-30595.
- Davies SN, Collingridge GL (1989) Role of excitatory amino acid receptors in synaptic transmission in area CA1 of rat hippocampus. *Proc. R. Soc. Lond B Biol. Sci.* **236**: 373-384.
- Davy H (1800) Researches clinical and philosophical, chiefly concerning nitrous oxide or dephlogisticated nitrous air. Volume published for J Johnson, London by Biggs and Cottle, Bristol.
- Dawson TM, Snyder SH (1994) Gases as biological messengers: nitric oxide and carbon monoxide in the brain. *J. Neurosci.* **14**: 5147-5159.
- De Seranno S, Estrella C, Loyens A, Cornea A, Ojeda SR, Beauvillain JC, Prevot V (2004) Vascular endothelial cells promote acute plasticity in ependymogial cells of the neuroendocrine brain. *J. Neurosci.* **24**: 10353-10363.
- de Vente J, Asan E, Gambaryan S, Markerink-Van IM, Axer H, Gallatz K, Lohmann SM, Palkovits M (2001) Localization of cGMP-dependent protein kinase type II in rat brain. *Neuroscience* **108**: 27-49.
- de Vente J, Hopkins DA, Markerink-Van IM, Emson PC, Schmidt HH, Steinbusch HW (1998) Distribution of nitric oxide synthase and nitric oxide-receptive, cyclic GMP-producing structures in the rat brain. *Neuroscience* **87**: 207-241.
- Debanne D, Gahwiler BH, Thompson SM (1999) Heterogeneity of synaptic plasticity at unitary CA3-CA1 and CA3-CA3 connections in rat hippocampal slice cultures. *J. Neurosci.* **19**: 10664-10671.
- Dedio J, Konig P, Wohlfart P, Schroeder C, Kummer W, Muller-Esterl W (2001) NOSIP, a novel modulator of endothelial nitric oxide synthase activity. *FASEB J.* **15**: 79-89.
- Degerman E, Belfrage P, Manganiello VC (1997) Structure, localization, and regulation of cGMP-inhibited phosphodiesterase (PDE3). *J. Biol. Chem.* **272**: 6823-6826.
- Deguchi T, Yoshioka M (1982) L-Arginine identified as an endogenous activator for soluble guanylate cyclase from neuroblastoma cells. *J. Biol. Chem.* **257**: 10147-10151.
- Demas GE, Kriegsfeld LJ, Blackshaw S, Huang P, Gammie SC, Nelson RJ, Snyder SH (1999) Elimination of aggressive behavior in male mice lacking endothelial nitric oxide synthase. *J. Neurosci.* **19**: RC30.
- Detre JA, Nairn AC, Aswad DW, Greengard P (1984) Localization in mammalian brain of G-substrate, a specific substrate for guanosine 3',5'-cyclic monophosphate-dependent protein kinase. *J. Neurosci.* **4**: 2843-2849.
- Dhallan RS, Yau KW, Schrader KA, Reed RR (1990) Primary structure and functional expression of a cyclic nucleotide-activated channel from olfactory neurons. *Nature* **347**: 184-187.
- Dinerman JL, Dawson TM, Schell MJ, Snowman A, Snyder SH (1994) Endothelial nitric oxide synthase localized to hippocampal pyramidal cells: implications for synaptic plasticity. *Proc. Natl. Acad. Sci. U. S. A* **91**: 4214-4218.
- Ding JD, Burette A, Nedvetsky PI, Schmidt HH, Weinberg RJ (2004) Distribution of soluble guanylyl cyclase in the rat brain. *J. Comp. Neurol.* **472**: 437-448.
- Dityatev AE, Bolshakov VY (2005) Amygdala, long-term potentiation, and fear conditioning. *Neuroscientist* **11**: 75-88.
- Dolphin AC, Errington ML, Bliss TV (1982) Long-term potentiation of the perforant path *in vivo* is associated with increased glutamate release. *Nature* **297**: 496-498.

- Doreulee N, Brown RE, Yanovsky Y, Godecke A, Schrader J, Haas HL (2001) Defective hippocampal mossy fiber long-term potentiation in endothelial nitric oxide synthase knockout mice. *Synapse* **41**: 191-194.
- Doreulee N, Sergeeva OA, Yanovsky Y, Chepkova AN, Selbach O, Godecke A, Schrader J, Haas HL (2003) Cortico-striatal synaptic plasticity in endothelial nitric oxide synthase deficient mice. *Brain Res.* **964**: 159-163.
- Doyle CA, Slater P (1997) Localization of neuronal and endothelial nitric oxide synthase isoforms in human hippocampus. *Neuroscience* **76**: 387-395.
- Drab M, Verkade P, Elger M, Kasper M, Lohn M, Lauterbach B, Menne J, Lindschau C, Mende F, Luft FC, Schedl A, Haller H, Kurzchalia TV (2001) Loss of caveolae, vascular dysfunction, and pulmonary defects in caveolin-1 gene-disrupted mice. *Science* **293**: 2449-2452.
- Dreyer J, Schleicher M, Tappe A, Schilling K, Kuner T, Kusumawidijaja G, Muller-Esterl W, Oess S, Kuner R (2004) Nitric oxide synthase (NOS)-interacting protein interacts with neuronal NOS and regulates its distribution and activity. *J. Neurosci.* **24**: 10454-10465.
- Dudzinski DM, Igarashi J, Greif D, Michel T (2006) The regulation and pharmacology of endothelial nitric oxide synthase. *Annu. Rev. Pharmacol. Toxicol.* **46**: 235-276.
- Dumas TC, Foster TC (1998) Late developmental changes in the ability of adenosine A1 receptors to regulate synaptic transmission in the hippocampus. *Brain Res. Dev. Brain Res.* **105**: 137-139.
- Dun NJ, Dun SL, Wong RK, Forstermann U (1994) Colocalization of nitric oxide synthase and somatostatin immunoreactivity in rat dentate hilar neurons. *Proc. Natl. Acad. Sci. U. S. A* **91**: 2955-2959.
- Dunwiddie TV, Haas HL (1985) Adenosine increases synaptic facilitation in the *in vitro* rat hippocampus: evidence for a presynaptic site of action. *J. Physiol.* **369**: 365-377.
- East SJ, Garthwaite J (1991) NMDA receptor activation in rat hippocampus induces cyclic GMP formation through the L-arginine-nitric oxide pathway. *Neurosci. Lett.* **123**: 17-19.
- el-Husseini AE, Bladen C, Vincent SR (1995) Molecular characterization of a type II cyclic GMP-dependent protein kinase expressed in the rat brain. *J. Neurochem.* **64**: 2814-2817.
- Eliasson MJ, Blackshaw S, Schell MJ, Snyder SH (1997) Neuronal nitric oxide synthase alternatively spliced forms: prominent functional localizations in the brain. *Proc. Natl. Acad. Sci. U. S. A* **94**: 3396-3401.
- Enoki R, Hu YL, Hamilton D, Fine A (2009) Expression of long-term plasticity at individual synapses in hippocampus is graded, bidirectional, and mainly presynaptic: optical quantal analysis. *Neuron* **62**: 242-253.
- Erusalimsky JD, Moncada S (2007) Nitric oxide and mitochondrial signaling: from physiology to pathophysiology. *Arterioscler. Thromb. Vasc. Biol.* **27**: 2524-2531.
- Fang J, Silverman RB (2009) A cellular model for screening neuronal nitric oxide synthase inhibitors. *Anal. Biochem.* **390**: 74-78.
- Faraci FM (2006) Protecting the brain with eNOS: run for your life. *Circ. Res.* **99**: 1029-1030.
- Feelisch M (1998) The use of nitric oxide donors in pharmacological studies. *Naunyn Schmiedeberg's Arch. Pharmacol.* **358**: 113-122.
- Feil R, Hofmann F, Kleppisch T (2005a) Function of cGMP-dependent protein kinases in the nervous system. *Rev. Neurosci.* **16**: 23-41.

- Feil R, Kleppisch T (2008) NO/cGMP-dependent modulation of synaptic transmission. *Handb. Exp. Pharmacol.* **184**: 529-560.
- Feil S, Zimmermann P, Knorn A, Brummer S, Schlossmann J, Hofmann F, Feil R (2005b) Distribution of cGMP-dependent protein kinase type I and its isoforms in the mouse brain and retina. *Neuroscience* **135**: 863-868.
- Feldman D (2009) Synaptic mechanisms for plasticity in neocortex. *Annu. Rev. Neurosci.* **32**: 33-55.
- Feron O, Saldana F, Michel JB, Michel T (1998) The endothelial nitric-oxide synthase-caveolin regulatory cycle. *J. Biol. Chem.* **273**: 3125-3128.
- Ferrendelli JA, Chang MM, Kinscherf DA (1974) Elevation of cyclic GMP levels in central nervous system by excitatory and inhibitory amino acids. *J. Neurochem.* **22**: 535-540.
- Ferrendelli JA, Kinscherf DA, Chang MM (1973) Regulation of levels of guanosine cyclic 3',5'-monophosphate in the central nervous system: effects of depolarizing agents. *Mol. Pharmacol.* **9**: 445-454.
- Ferrendelli JA, Rubin EH, Kinscherf DA (1976) Influence of divalent cations on regulation of cyclic GMP and cyclic AMP levels in brain tissue. *J. Neurochem.* **26**: 741-748.
- Ferrero R, Rodriguez-Pascual F, Miras-Portugal MT, Torres M (2000) Nitric oxide-sensitive guanylyl cyclase activity inhibition through cyclic GMP-dependent dephosphorylation. *J. Neurochem.* **75**: 2029-2039.
- Fesenko EE, Kolesnikov SS, Lyubarsky AL (1985) Induction by cyclic GMP of cationic conductance in plasma membrane of retinal rod outer segment. *Nature* **313**: 310-313.
- Fischmeister R, Castro L, Abi-Gerges A, Rochais F, Vandecasteele G (2005) Species- and tissue-dependent effects of NO and cyclic GMP on cardiac ion channels. *Comp. Biochem. Physiol A Mol. Integr. Physiol.* **142**: 136-143.
- Foerster J, Harteneck C, Malkewitz J, Schultz G, Koesling D (1996) A functional heme-binding site of soluble guanylyl cyclase requires intact N-termini of alpha 1 and beta 1 subunits. *Eur. J. Biochem.* **240**: 380-386.
- Fontinha BM, Delgado-Garcia JM, Madronal N, Ribeiro JA, Sebastiao AM, Gruart A (2009) Adenosine A(2A) receptor modulation of hippocampal CA3-CA1 synapse plasticity during associative learning in behaving mice. *Neuropsychopharmacology* **34**: 1865-1874.
- Francis SH, Busch JL, Corbin JD, Sibley D (2010) cGMP-dependent protein kinases and cGMP phosphodiesterases in nitric oxide and cGMP action. *Pharmacol. Rev.* **62**: 525-563.
- Freund TF, Buzsaki G (1996) Interneurons of the hippocampus. *Hippocampus* **6**: 347-470.
- Friebe A, Mergia E, Dangel O, Lange A, Koesling D (2007) Fatal gastrointestinal obstruction and hypertension in mice lacking nitric oxide-sensitive guanylyl cyclase. *Proc. Natl. Acad. Sci. U. S. A* **104**: 7699-7704.
- Fuenzalida M, Fernandez de SD, Couve A, Buno W (2010) Role of AMPA and NMDA receptors and back-propagating action potentials in spike timing-dependent plasticity. *J. Neurophysiol.* **103**: 47-54.
- Fukaya M, Watanabe M (2000) Improved immunohistochemical detection of postsynaptically located PSD-95/SAP90 protein family by protease section pretreatment: a study in the adult mouse brain. *J. Comp. Neurol.* **426**: 572-586.
- Fukutani T, Iino S, Nojyo Y (2009) The expression of soluble guanylate cyclase in the vasculature of rat skeletal muscle. *Arch. Histol. Cytol.* **72**: 117-126.

- Fulton D, Gratton JP, Sessa WC (2001) Post-translational control of endothelial nitric oxide synthase: why isn't calcium/calmodulin enough? *J. Pharmacol. Exp. Ther.* **299**: 818-824.
- Furchgott RF, Martin W (1985) Interactions of endothelial cells and smooth muscle cells of arteries. *Chest* **88**: 210S-213S.
- Furchgott RF, Zawadzki JV (1980) The obligatory role of endothelial cells in the relaxation of arterial smooth muscle by acetylcholine. *Nature* **288**: 373-376.
- Furfine ES, Harmon MF, Paith JE, Garvey EP (1993) Selective inhibition of constitutive nitric oxide synthase by L-NG-nitroarginine. *Biochemistry* **32**: 8512-8517.
- Galle J, Zabel U, Hubner U, Hatzelmann A, Wagner B, Wanner C, Schmidt HH (1999) Effects of the soluble guanylyl cyclase activator, YC-1, on vascular tone, cyclic GMP levels and phosphodiesterase activity. *Br. J. Pharmacol.* **127**: 195-203.
- Gamm DM, Francis SH, Angelotti TP, Corbin JD, Uhler MD (1995) The type II isoform of cGMP-dependent protein kinase is dimeric and possesses regulatory and catalytic properties distinct from the type I isoforms. *J. Biol. Chem.* **270**: 27380-27388.
- Garcia-Cardena G, Fan R, Shah V, Sorrentino R, Cirino G, Papapetropoulos A, Sessa WC (1998) Dynamic activation of endothelial nitric oxide synthase by Hsp90. *Nature* **392**: 821-824.
- Garcia-Cardena G, Martasek P, Masters BS, Skidd PM, Couet J, Li S, Lisanti MP, Sessa WC (1997) Dissecting the interaction between nitric oxide synthase (NOS) and caveolin. Functional significance of the nos caveolin binding domain *in vivo*. *J. Biol. Chem.* **272**: 25437-25440.
- Garcia-Cardena G, Oh P, Liu J, Schnitzer JE, Sessa WC (1996) Targeting of nitric oxide synthase to endothelial cell caveolae via palmitoylation: implications for nitric oxide signaling. *Proc. Natl. Acad. Sci. U. S. A* **93**: 6448-6453.
- Garthwaite G, Bartus K, Malcolm D, Goodwin D, Kollb-Sielecka M, Dooleniya C, Garthwaite J (2006) Signaling from blood vessels to CNS axons through nitric oxide. *J. Neurosci.* **26**: 7730-7740.
- Garthwaite J (1985) Cellular uptake disguises action of L-glutamate on N-methyl-D-aspartate receptors. With an appendix: diffusion of transported amino acids into brain slices. *Br. J. Pharmacol.* **85**: 297-307.
- Garthwaite J (2005) Dynamics of cellular NO-cGMP signaling. *Front Biosci.* **10**: 1868-1880.
- Garthwaite J (2007) Neuronal nitric oxide synthase and the serotonin transporter get harmonious. *Proc. Natl. Acad. Sci. U. S. A* **104**: 7739-7740.
- Garthwaite J (2008) Concepts of neural nitric oxide-mediated transmission. *Eur. J. Neurosci.* **11**: 2783-2802.
- Garthwaite J, Charles SL, Chess Williams R (1988) Endothelium-derived relaxing factor release on activation of NMDA receptors suggests role as intercellular messenger in the brain. *Nature* **336**: 385-388.
- Garthwaite J, Garthwaite G (1987) Cellular origins of cyclic GMP responses to excitatory amino acid receptor agonists in rat cerebellum *in vitro*. *J. Neurochem.* **48**: 29-39.
- Garthwaite J, Garthwaite G, Palmer RM, Moncada S (1989) NMDA receptor activation induces nitric oxide synthesis from arginine in rat brain slices. *Eur. J. Pharmacol.* **172**: 413-416.
- Garthwaite J, Southam E, Boulton CL, Nielsen EB, Schmidt K, Mayer B (1995) Potent and selective inhibition of nitric oxide-sensitive guanylyl cyclase by 1H-[1,2,4]oxadiazolo[4,3-a]quinoxalin-1-one. *Mol. Pharmacol.* **48**: 184-188.

- Garvey EP, Oplinger JA, Furfine ES, Kiff RJ, Laszlo F, Whittle BJ, Knowles RG (1997) 1400W is a slow, tight binding, and highly selective inhibitor of inducible nitric-oxide synthase *in vitro* and *in vivo*. *J. Biol. Chem.* **272**: 4959-4963.
- Garvey EP, Tuttle JV, Covington K, Merrill BM, Wood ER, Baylis SA, Charles IG (1994) Purification and characterization of the constitutive nitric oxide synthase from human placenta. *Arch. Biochem. Biophys.* **311**: 235-241.
- Germann WJ, Stanfield CL (2002) Principles of human physiology. Pearson Education Inc., San Francisco, CA.
- Gerzer R, Bohme E, Hofmann F, Schultz G (1981) Soluble guanylate cyclase purified from bovine lung contains heme and copper. *FEBS Lett.* **132**: 71-74.
- Gibb BJ, Garthwaite J (2001) Subunits of the nitric oxide receptor, soluble guanylyl cyclase, expressed in rat brain. *Eur. J. Neurosci* **13**: 539-544.
- Gibb BJ, Wykes V, Garthwaite J (2003) Properties of NO-activated guanylyl cyclases expressed in cells. *Br. J. Pharmacol.* **139**: 1032-1040.
- Giese KP, Fedorov NB, Filipkowski RK, Silva AJ (1998) Autophosphorylation at Thr286 of the α Calcium-Calmodulin Kinase II in LTP and Learning. *Science* **279**: 870-873.
- Golderer G, Werner ER, Leitner S, Grobner P, Werner-Felmayer G (2001) Nitric oxide synthase is induced in sporulation of *Physarum polycephalum*. *Genes Dev.* **15**: 1299-1309.
- Gonzalez-Hernandez T, Perez de la Cruz MA, Mantolan-Sarmiento B (1996) Histochemical and immunohistochemical detection of neurons that produce nitric oxide: effect of different fixative parameters and immunoreactivity against non-neuronal NOS antisera. *J. Histochem. Cytochem.* **44**: 1399-1413.
- Goosens KA, Maren S (2001) Contextual and auditory fear conditioning are mediated by the lateral, basal, and central amygdaloid nuclei in rats. *Learn. Mem.* **8**: 148-155.
- Gowda C, Toomayan GA, Qi WN, Chen LE, Cai Y, Allen DM, Seaber AV, Urbaniak JR (2004) The effects of N Ω -propyl-L-arginine on reperfusion injury of skeletal muscle. *Nitric Oxide* **11**: 17-24.
- Gratton JP, Fontana J, O'Connor DS, Garcia-Cardena G, McCabe TJ, Sessa WC (2000) Reconstitution of an endothelial nitric-oxide synthase (eNOS), hsp90, and caveolin-1 complex *in vitro*. Evidence that hsp90 facilitates calmodulin stimulated displacement of eNOS from caveolin-1. *J. Biol. Chem.* **275**: 22268-22272.
- Green LC, Ruiz de LK, Wagner DA, Rand W, Istfan N, Young VR, Tannenbaum SR (1981a) Nitrate biosynthesis in man. *Proc. Natl. Acad. Sci. U. S. A* **78**: 7764-7768.
- Green LC, Tannenbaum SR, Goldman P (1981b) Nitrate synthesis in the germfree and conventional rat. *Science* **212**: 56-58.
- Gross SS, Wolin MS (1995) Nitric oxide: pathophysiological mechanisms. *Annu. Rev. Physiol.* **57**: 737-769.
- Grover LM (1998) Evidence for postsynaptic induction and expression of NMDA receptor independent LTP. *J. Neurophysiol.* **79**: 1167-1182.
- Grover LM, Teyler TJ (1990) Two components of long-term potentiation induced by different patterns of afferent activation. *Nature* **347**: 477-479.

- Grover LM, Teyler TJ (1992) N-methyl-d-aspartate receptor-independent long-term potentiation in area CA1 of rat hippocampus: Input-specific induction and preclusion in a non-tetanized pathway. *Neuroscience* **49**: 7-11.
- Grover LM, Teyler TJ (1994) Activation of NMDA receptors in hippocampal area CA1 by low and high frequency orthodromic stimulation and their contribution to induction of long-term potentiation. *Synapse* **16**: 66-75.
- Gruart A, Munoz MD, Delgado-Garcia JM (2006) Involvement of the CA3-CA1 synapse in the acquisition of associative learning in behaving mice. *J. Neurosci.* **26**: 1077-1087.
- Gruart A, Sciarretta C, Valenzuela-Harrington M, Delgado-Garcia JM, Minichiello L (2007) Mutation at the TrkB PLC γ -docking site affects hippocampal LTP and associative learning in conscious mice. *Learn. Mem.* **14**: 54-62.
- Gruetter CA, Barry BK, McNamara DB, Kadowitz PJ, Ignarro LJ (1980a) Coronary arterial relaxation and guanylate cyclase activation by cigarette smoke, N'-nitrosornicotine and nitric oxide. *J. Pharmacol. Exp. Ther.* **214**: 9-15.
- Gruetter DY, Gruetter CA, Barry BK, Baricos WH, Hyman AL, Kadowitz PJ, Ignarro LJ (1980b) Activation of coronary arterial guanylate cyclase by nitric oxide, nitroprusside, and nitrosoguanidine--inhibition by calcium, lanthanum, and other cations, enhancement by thiols. *Biochem. Pharmacol.* **29**: 2943-2950.
- Gupta G, Azam M, Yang L, Danziger RS (1997) The beta2 subunit inhibits stimulation of the alpha1/beta1 form of soluble guanylyl cyclase by nitric oxide. Potential relevance to regulation of blood pressure. *J. Clin. Invest* **100**: 1488-1492.
- Hada J, Kaku T, Jiang MH, Morimoto K, Hayashi Y (2003) Inhibition of high K⁺-evoked gamma-aminobutyric acid release by sodium nitroprusside in rat hippocampus. *Eur. J. Pharmacol.* **467**: 119-123.
- Haghikia A, Mergia E, Friebe A, Eysel UT, Koesling D, Mittmann T (2007) Long-term potentiation in the visual cortex requires both nitric oxide receptor guanylyl cyclases. *J. Neurosci.* **27**: 818-823.
- Haley JE, Malen PL, Chapman PF (1993) Nitric oxide synthase inhibitors block long-term potentiation induced by weak but not strong tetanic stimulation at physiological brain temperatures in rat hippocampal slices. *Neurosci. Lett.* **160**: 85-88.
- Hall CN, Attwell D (2008) Assessing the physiological concentration and targets of nitric oxide in brain tissue. *J. Physiol.* **586**: 3597-3615.
- Hall CN, Garthwaite J (2006) Inactivation of nitric oxide by rat cerebellar slices. *J. Physiol.* **577**: 549-567.
- Hall CN, Garthwaite J (2009) What is the real physiological NO concentration *in vivo*? *Nitric Oxide* **21**: 92-103.
- Hansel TT, Kharitonov SA, Donnelly LE, Erin EM, Currie MG, Moore WM, Manning PT, Recker DP, Barnes PJ (2003) A selective inhibitor of inducible nitric oxide synthase inhibits exhaled breath nitric oxide in healthy volunteers and asthmatics. *FASEB J.* **17**: 1298-1300.
- Hardingham N, Fox K (2006) The role of nitric oxide and GluR1 in presynaptic and postsynaptic components of neocortical potentiation. *J. Neurosci.* **26**: 7395-7404.
- Harteneck C, Wedel B, Koesling D, Malkewitz J, Bohme E, Schultz G (1991) Molecular cloning and expression of a new alpha-subunit of soluble guanylyl cyclase. Interchangeability of the alpha-subunits of the enzyme. *FEBS Lett.* **292**: 217-222.

- Haul S, Godecke A, Schrader J, Haas HL, Luhmann HJ (1999) Impairment of neocortical long-term potentiation in mice deficient of endothelial nitric oxide synthase. *J. Neurophysiol.* **81**: 494-497.
- Hawkins RD, Zhuo M, Arancio O (1994) Nitric oxide and carbon monoxide as possible retrograde messengers in hippocampal long-term potentiation. *J. Neurobiol.* **25**: 652-665.
- Hayes J, Li S, Anwyl R, Rowan MJ (2008) A role for protein kinase A and protein kinase M zeta in muscarinic acetylcholine receptor-initiated persistent synaptic enhancement in rat hippocampus *in vivo*. *Neuroscience* **151**: 604-612.
- Hebb DO (1949) The organisation of behaviour. New York: Wiley.
- Hegesh E, Shiloah J (1982) Blood nitrates and infantile methemoglobinemia. *Clin. Chim. Acta* **125**: 107-115.
- Hell JW, Westenbroek RE, Breeze LJ, Wang KK, Chavkin C, Catterall WA (1996) N-methyl-D-aspartate receptor-induced proteolytic conversion of postsynaptic class C L-type calcium channels in hippocampal neurons. *Proc. Natl. Acad. Sci. U. S. A* **93**: 3362-3367.
- Hell JW, Westenbroek RE, Warner C, Ahljianian MK, Prystay W, Gilbert MM, Snutch TP, Catterall WA (1993) Identification and differential subcellular localization of the neuronal class C and class D L-type calcium channel alpha 1 subunits. *J. Cell Biol.* **123**: 949-962.
- Helton TD, Xu W, Lipscombe D (2005) Neuronal L-type calcium channels open quickly and are inhibited slowly. *J. Neurosci.* **25**: 10247-10251.
- Hibbs JB, Jr., Taintor RR, Vavrin Z, Rachlin EM (1988) Nitric oxide: a cytotoxic activated macrophage effector molecule. *Biochem. Biophys. Res. Commun.* **157**: 87-94.
- Hibbs JB, Jr., Vavrin Z, Taintor RR (1987) L-arginine is required for expression of the activated macrophage effector mechanism causing selective metabolic inhibition in target cells. *J. Immunol.* **138**: 550-565.
- Hobbs AJ, Higgs A, Moncada S (1999) Inhibition of nitric oxide synthase as a potential therapeutic target. *Annu. Rev. Pharmacol. Toxicol.* **39**: 191-220.
- Hockerman GH, Peterson BZ, Johnson BD, Catterall WA (1997) Molecular determinants of drug binding and action on L-type calcium channels. *Annu. Rev. Pharmacol. Toxicol.* **37**: 361-396.
- Holscher C (2002) Different strains of rats show different sensitivity to block of long-term potentiation by nitric oxide synthase inhibitors. *Eur. J. Pharmacol* **457**: 99-106.
- Hopper R, Lancaster B, Garthwaite J (2004) On the regulation of NMDA receptors by nitric oxide. *Eur. J. Neurosci.* **19**: 1675-1682.
- Hopper RA, Garthwaite J (2006) Tonic and phasic nitric oxide signals in hippocampal long-term potentiation. *J. Neurosci.* **26**: 11513-11521.
- Huang PL, Dawson TM, Brecht DS, Snyder SH, Fishman MC (1993) Targeted disruption of the neuronal nitric oxide synthase gene. *Cell* **75**: 1273-1286.
- Huang PL, Huang Z, Mashimo H, Bloch KD, Moskowitz MA, Bevan JA, Fishman MC (1995) Hypertension in mice lacking the gene for endothelial nitric oxide synthase. *Nature* **377**: 239-242.
- Huang YY, Malenka RC (1993) Examination of TEA-induced synaptic enhancement in area CA1 of the hippocampus: the role of voltage-dependent Ca²⁺ channels in the induction of LTP. *J. Neurosci.* **13**: 568-576.

Huang Z, Huang PL, Ma J, Meng W, Ayata C, Fishman MC, Moskowitz MA (1996) Enlarged infarcts in endothelial nitric oxide synthase knockout mice are attenuated by nitro-L-arginine. *J. Cereb. Blood Flow Metab.* **16**: 981-987.

Huang Z, Huang PL, Panahian N, Dalkara T, Fishman MC, Moskowitz MA (1994) Effects of cerebral ischemia in mice deficient in neuronal nitric oxide synthase. *Science* **265**:1883-1885.

Ignarro LJ, Buga GM, Wood KS, Byrns RE, Chaudhuri G (1987) Endothelium-derived relaxing factor produced and released from artery and vein is nitric oxide. *Proc. Natl. Acad. Sci. U. S. A* **84**: 9265-9269.

Ignarro LJ, Lipton H, Edwards JC, Baricos WH, Hyman AL, Kadowitz PJ, Gruetter CA (1981) Mechanism of vascular smooth muscle relaxation by organic nitrates, nitrites, nitroprusside and nitric oxide: evidence for the involvement of S-nitrosothiols as active intermediates. *J. Pharmacol. Exp. Ther.* **218**: 739-749.

Impey S, Mark M, Villacres EC, Poser S, Chavkin C, Storm DR (1996) Induction of CRE-mediated gene expression by stimuli that generate long-lasting LTP in area CA1 of the hippocampus. *Neuron* **16**: 973-982.

Irvine EE, Vernon J, Giese KP (2005) AlphaCaMKII autophosphorylation contributes to rapid learning but is not necessary for memory. *Nat. Neurosci.* **8**: 411-412.

Ito M (2001) Cerebellar long-term depression: characterization, signal transduction, and functional roles. *Physiol. Rev.* **81**: 1143-1195.

Iyengar R, Stuehr DJ, Marletta MA (1987) Macrophage synthesis of nitrite, nitrate, and N-nitrosamines: precursors and role of the respiratory burst. *Proc. Natl. Acad. Sci. U. S. A* **84**: 6369-6373.

Jacoby S, Sims RE, Hartell NA (2001) Nitric oxide is required for the induction and heterosynaptic spread of long-term potentiation in rat cerebellar slices. *J. Physiol.* **535**: 825-839.

Jaffrey SR, Benfenati F, Snowman AM, Czernik AJ, Snyder SH (2002) Neuronal nitric-oxide synthase localization mediated by a ternary complex with synapsin and CAPON. *Proc. Natl. Acad. Sci. U. S. A* **99**: 3199-3204.

Jaffrey SR, Snowman AM, Eliasson MJ, Cohen NA, Snyder SH (1998) CAPON: a protein associated with neuronal nitric oxide synthase that regulates its interactions with PSD95. *Neuron* **20**: 115-124.

Jarrard LE (1993) On the role of the hippocampus in learning and memory in the rat. *Behav. Neural Biol.* **60**: 9-26.

Jarry A, Renaudin K, Denis MG, Robard M, Buffin-Meyer B, Karam G, Buzelin F, Paris H, Labois CL, Vallette G (2003) Expression of NOS1 and soluble guanylyl cyclase by human kidney epithelial cells: morphological evidence for an autocrine/paracrine action of nitric oxide. *Kidney Int.* **64**: 170-180.

Ji H, Li H, Martasek P, Roman LJ, Poulos TL, Silverman RB (2009) Discovery of highly potent and selective inhibitors of neuronal nitric oxide synthase by fragment hopping. *J. Med. Chem.* **52**: 779-797.

Ji RR, Kohno T, Moore KA, Woolf CJ (2003) Central sensitization and LTP: do pain and memory share similar mechanisms? *Trends Neurosci.* **26**: 696-705.

Kahle JS, Cotman CW (1993) Adenosine, L-AP4, and baclofen modulation of paired-pulse potentiation in the dentate gyrus: interstimulus interval-dependent pharmacology. *Exp. Brain Res.* **94**: 97-104.

- Kamisaki Y, Saheki S, Nakane M, Palmieri JA, Kuno T, Chang BY, Waldman SA, Murad F (1986) Soluble guanylate cyclase from rat lung exists as a heterodimer. *J. Biol. Chem.* **261**: 7236-7241.
- Kandel ER, O'Dell TJ (1992) Are adult learning mechanisms also used for development? *Science* **258**: 243-245.
- Kantor DB, Lanzrein M, Stary SJ, Sandoval GM, Smith WB, Sullivan BM, Davidson N, Schuman EM (1996) A role for endothelial NO synthase in LTP revealed by adenovirus-mediated inhibition and rescue. *Science* **274**: 1744-1748.
- Kato K, Clifford DB, Zorumski CF (1993) Long-term potentiation during whole-cell recording in rat hippocampal slices. *Neuroscience* **53**: 39-47.
- Katsuki S, Arnold W, Mittal C, Murad F (1977a) Stimulation of guanylate cyclase by sodium nitroprusside, nitroglycerin and nitric oxide in various tissue preparations and comparison to the effects of sodium azide and hydroxylamine. *J. Cyclic. Nucleotide. Res.* **3**: 23-35.
- Katsuki S, Arnold WP, Murad F (1977b) Effects of sodium nitroprusside, nitroglycerin, and sodium azide on levels of cyclic nucleotides and mechanical activity of various tissues. *J. Cyclic. Nucleotide. Res.* **3**: 239-247.
- Katzoff A, Ben-Gedalya T, Susswein AJ (2002) Nitric oxide is necessary for multiple memory processes after learning that a food is inedible in aplysia. *J. Neurosci.* **22**: 9581-9594.
- Kaupp UB, Seifert R (2002) Cyclic nucleotide-gated ion channels. *Physiol. Rev.* **82**: 769-824.
- Kazerounian S, Pitari GM, Ruiz-Stewart I, Schulz S, Waldman SA (2002) Nitric oxide activation of soluble guanylyl cyclase reveals high and low affinity sites that mediate allosteric inhibition by calcium. *Biochemistry* **41**: 3396-3404.
- Keefer LK, Nims RW, Davies KM, Wink DA (1996) "NONOates" (1-substituted diazen-1-ium-1,2-diolates) as nitric oxide donors: convenient nitric oxide dosage forms. *Methods Enzymol.* **268**: 281-293.
- Keilhoff G, Seidel B, Noack H, Tischmeyer W, Stanek D, Wolf G (1996) Patterns of nitric oxide synthase at the messenger RNA and protein levels during early rat brain development. *Neuroscience* **75**: 1193-1201.
- Kempermann G (2002) Why new neurons? Possible functions for adult hippocampal neurogenesis. *J. Neurosci.* **22**: 635-638.
- Kempermann G, Fabel K, Ehninger D, Babu H, Leal-Galicia P, Garthe A, Wolf SA (2010) Why and how physical activity promotes experience-induced brain plasticity. *Front Neurosci.* **4**: 189.
- Kerchner GA, Nicoll RA (2008) Silent synapses and the emergence of a postsynaptic mechanism for LTP. *Nat. Rev. Neurosci.* **9**: 813-825.
- Kessels HW, Malinow R (2009) Synaptic AMPA receptor plasticity and behavior. *Neuron* **61**: 340-350.
- Kim HY, Kim SJ, Kim J, Oh SB, Cho H, Jung SJ (2005) Effect of nitric oxide on hyperpolarization-activated current in substantia gelatinosa neurons of rats. *Biochem. Biophys. Res. Commun.* **338**: 1648-1653.
- Kirstein M, Rivet-Bastide M, Hatem S, Benardeau A, Mercadier JJ, Fischmeister R (1995) Nitric oxide regulates the calcium current in isolated human atrial myocytes. *J. Clin. Invest.* **95**: 794-802.

- Kishi Y, Watanabe T, Makita T, Sakita S, Watanabe R, Ashikaga T, Numano F (1995) Effect of nifedipine on cyclic GMP turnover in cultured coronary smooth muscle cells. *J. Cardiovasc. Pharmacol.* **26**: 590-595.
- Kleppisch T, Moosmang S, Adelsberger H, Lacinova L, Langwieser N, Muller J, Kurzeder S, Marais E, Schulla V, Goebbels S, Nave KA, Klugbauer N, Hofmann F (2004) Pivotal function of Ca_v1.2 L-type calcium channels in hippocampal long-term potentiation and learning. *Naunyn Schmiedeberg's Arch. Pharmacol* **369**: R83.
- Ko FN, Wu CC, Kuo SC, Lee FY, Teng CM (1994) YC-1, a novel activator of platelet guanylate cyclase. *Blood* **84**: 4226-4233.
- Koesling D, Harteneck C, Humbert P, Bosserhoff A, Frank R, Schultz G, Bohme E (1990) The primary structure of the larger subunit of soluble guanylyl cyclase from bovine lung. Homology between the two subunits of the enzyme. *FEBS Lett.* **266**: 128-132.
- Koesling D, Herz J, Gausepohl H, Niroomand F, Hinsch KD, Mulsch A, Bohme E, Schultz G, Frank R (1988) The primary structure of the 70 kDa subunit of bovine soluble guanylate cyclase. *FEBS Lett.* **239**: 29-34.
- Koesling D, Russwurm M, Mergia E, Mullershausen F, Friebe A (2004) Nitric oxide-sensitive guanylyl cyclase: structure and regulation. *Neurochem. Int.* **45**: 813-819.
- Koglin M, Behrends S (2003) A functional domain of the alpha1 subunit of soluble guanylyl cyclase is necessary for activation of the enzyme by nitric oxide and YC-1 but is not involved in heme binding. *J. Biol. Chem.* **278**: 12590-12597.
- Korn H, Faber DS (1991) Quantal analysis and synaptic efficacy in the CNS. *Trends Neurosci.* **14**: 439-445.
- Kroncke KD, Fehsel K, Kolb-Bachofen V (1998) Inducible nitric oxide synthase in human diseases. *Clin. Exp. Immunol.* **113**: 147-156.
- Krumenacker JS, Katsuki S, Kots A, Murad F (2006) Differential expression of genes involved in cGMP-dependent nitric oxide signaling in murine embryonic stem (ES) cells and ES cell-derived cardiomyocytes. *Nitric Oxide* **14**: 1-11.
- Kullmann DM, Perkel DJ, Manabe T, Nicoll RA (1992) Ca²⁺ entry via postsynaptic voltage-sensitive Ca²⁺ channels can transiently potentiate excitatory synaptic transmission in the hippocampus. *Neuron* **9**: 1175-1183.
- Lacinova L, Moosmang S, Langwieser N, Hofmann F, Kleppisch T (2008) Ca_v1.2 calcium channels modulate the spiking pattern of hippocampal pyramidal cells. *Life Sci.* **82**: 41-49.
- Lacza Z, Pankotai E, Csordas A, Gero D, Kiss L, Horvath EM, Kollai M, Busija DW, Szabo C (2006) Mitochondrial NO and reactive nitrogen species production: does mtNOS exist? *Nitric Oxide* **14**: 162-168.
- Lassen LH, Ashina M, Christiansen I, Ulrich V, Olesen J (1997) Nitric oxide synthase inhibition in migraine. *Lancet* **349**: 401-402.
- Lawton GR, Ralay RH, Chico LK, Ji H, Xue F, Martasek P, Roman LJ, Watterson DM, Silverman RB (2009) Analogues of 2-aminopyridine-based selective inhibitors of neuronal nitric oxide synthase with increased bioavailability. *Bioorg. Med. Chem.* **17**: 2371-2380.
- Leinders-Zufall T, Zufall F (1995) Block of cyclic nucleotide-gated channels in salamander olfactory receptor neurons by the guanylyl cyclase inhibitor LY83583. *J. Neurophysiol.* **74**: 2759-2762.

- Lessmann V, Stroh-Kaffei S, Steinbrecher V, Edelmann E, Brigadski T, Kilb W, Luhmann HJ (2011) The expression mechanism of the residual LTP in the CA1 region of BDNF k.o. mice is insensitive to NO synthase inhibition. *Brain Res.* **1391**: 14-23.
- Li M, Kondo T, Zhao QL, Li FJ, Tanabe K, Arai Y, Zhou ZC, Kasuya M (2000) Apoptosis induced by cadmium in human lymphoma U937 cells through Ca²⁺-calpain and caspase-mitochondria-dependent pathways. *J. Biol. Chem.* **275**: 39702-39709.
- Li S, Cullen WK, Anwyl R, Rowan MJ (2007) Muscarinic acetylcholine receptor-dependent induction of persistent synaptic enhancement in rat hippocampus *in vivo*. *Neuroscience* **144**: 754-761.
- Lin H, Totterdell S (1998) Light and electron microscopic study of neuronal nitric oxide synthase-immunoreactive neurons in the rat subiculum. *J. Comp. Neurol.* **395**: 195-208.
- Lipton SA, Choi YB, Takahashi H, Zhang D, Li W, Godzik A, Bankston LA (2002) Cysteine regulation of protein function--as exemplified by NMDA-receptor modulation. *Trends Neurosci.* **25**: 474-480.
- Lisman J, Schulman H, Cline H (2002) The molecular basis of CaMKII function in synaptic and behavioural memory. *Nat. Rev. Neurosci.* **3**: 175-190.
- Little Z, Grover LM, Teyler TJ (1995) Metabotropic glutamate receptor antagonist, (R,S)-alpha-methyl-4-carboxyphenylglycine, blocks two distinct forms of long-term potentiation in area CA1 of rat hippocampus. *Neurosci. Lett.* **201**: 73-76.
- Liu S, Fa M, Ninan I, Trinchese F, Dauer W, Arancio O (2007) Alpha-synuclein involvement in hippocampal synaptic plasticity: role of NO, cGMP, cGK and CaMKII. *Eur. J. Neurosci.* **25**: 3583-3596.
- Liu S, Ninan I, Antonova I, Battaglia F, Trinchese F, Narasanna A, Kolodilov N, Dauer W, Hawkins RD, Arancio O (2004) alpha-Synuclein produces a long-lasting increase in neurotransmitter release. *EMBO J.* **23**: 4506-4516.
- Logue SF, Paylor R, Wehner JM (1997) Hippocampal lesions cause learning deficits in inbred mice in the Morris water maze and conditioned-fear task. *Behav. Neurosci.* **111**: 104-113.
- Lonart G, Wang J, Johnson KM (1992) Nitric oxide induces neurotransmitter release from hippocampal slices. *Eur. J. Pharmacol.* **220**: 271-272.
- Lovick TA, Brown LA, Key BJ (1999) Neurovascular relationships in hippocampal slices: physiological and anatomical studies of mechanisms underlying flow-metabolism coupling in intraparenchymal microvessels. *Neuroscience* **92**: 47-60.
- Lu KT, Gean PW (1999) Masking of forskolin-induced long-term potentiation by adenosine accumulation in area CA1 of the rat hippocampus. *Neuroscience* **88**: 69-78.
- Lu YF, Kandel ER, Hawkins RD (1999) Nitric oxide signaling contributes to late-phase LTP and CREB phosphorylation in the hippocampus. *J. Neurosci.* **19**: 10250-10261.
- Lucas KA, Pitari GM, Kazerounian S, Ruiz-Stewart I, Park J, Schulz S, Chepenik KP, Waldman SA (2000) Guanylyl cyclases and signaling by cyclic GMP. *Pharmacol. Rev.* **52**: 375-414.
- Luo D, Das S, Vincent SR (1995) Effects of methylene blue and LY83583 on neuronal nitric oxide synthase and NADPH-diaphorase. *Eur. J. Pharmacol.* **290**: 247-251.
- Luo D, Vincent SR (1994) NMDA-dependent nitric oxide release in the hippocampus *in vivo*: interactions with noradrenaline. *Neuropharmacology* **33**: 1345-1350.

- Lynch G, Larson J, Kelso S, Barrionuevo G, Schottler F (1983) Intracellular injections of EGTA block induction of hippocampal long-term potentiation. *Nature* **305**: 719-721.
- Lynch MA (2004) Long-term potentiation and memory. *Physiol Rev* **84**: 87-136.
- MacMicking J, Xie QW, Nathan C (1997) Nitric oxide and macrophage function. *Annu. Rev. Immunol.* **15**: 323-350.
- Magee JC, Avery RB, Christie BR, Johnston D (1996) Dihydropyridine-sensitive, voltage-gated Ca²⁺ channels contribute to the resting intracellular Ca²⁺ concentration of hippocampal CA1 pyramidal neurons. *J. Neurophysiol.* **76**: 3460-3470.
- Makara JK, Katona I, Nyiri G, Nemeth B, Ledent C, Watanabe M, de VJ, Freund TF, Hajos N (2007) Involvement of nitric oxide in depolarization-induced suppression of inhibition in hippocampal pyramidal cells during activation of cholinergic receptors. *J. Neurosci.* **27**: 10211-10222.
- Malen PL, Chapman PF (1997) Nitric oxide facilitates long-term potentiation, but not long-term depression. *J. Neurosci.* **17**: 2645-2651.
- Malenka RC, Kauer JA, Zucker RS, Nicoll RA (1988) Postsynaptic calcium is sufficient for potentiation of hippocampal synaptic transmission. *Science* **242**: 81-84.
- Malenka RC (1991) Postsynaptic factors control the duration of synaptic enhancement in area CA1 of the hippocampus. *Neuron* **6**: 53-60.
- Malenka RC, Bear MF (2004) LTP and LTD: an embarrassment of riches. *Neuron* **44**: 5-21.
- Marsh N, Marsh A (2000) A short history of nitroglycerine and nitric oxide in pharmacology and physiology. *Clin. Exp. Pharm. Physiol.* **27**: 313-319.
- Martens-Lobenhoffer J, Sulyok E, Czeiter E, Buki A, Kohl J, Firsching R, Troger U, Bode-Boger SM (2007) Determination of cerebrospinal fluid concentrations of arginine and dimethylarginines in patients with subarachnoid haemorrhage. *J. Neurosci. Methods* **164**: 155-160.
- Martin SJ, Grimwood PD, Morris RG (2000) Synaptic plasticity and memory: an evaluation of the hypothesis. *Annu. Rev. Neurosci.* **23**: 649-711.
- Massberg S, Sausbier M, Klatt P, Bauer M, Pfeifer A, Siess W, Fassler R, Ruth P, Krombach F, Hofmann F (1999) Increased adhesion and aggregation of platelets lacking cyclic guanosine 3',5'-monophosphate kinase I. *J. Exp. Med.* **189**: 1255-1264.
- Matsuoka I, Giuili G, Poyard M, Stengel D, Parma J, Guellaen G, Hanoune J (1992) Localization of adenylyl and guanylyl cyclase in rat brain by in situ hybridization: comparison with calmodulin mRNA distribution. *J. Neurosci* **12**: 3350-3360.
- Mayer B, Brunner F, Schmidt K (1993) Novel actions of methylene blue. *Eur. Heart J.* **14 Suppl I**: 22-26.
- McKinney BC, Murphy GG (2006) The L-Type voltage-gated calcium channel Ca_v1.3 mediates consolidation, but not extinction, of contextually conditioned fear in mice. *Learn. Mem.* **13**: 584-589.
- McKinney BC, Sze W, Lee B, Murphy GG (2009) Impaired long-term potentiation and enhanced neuronal excitability in the amygdala of Ca_v1.3 knockout mice. *Neurobiol. Learn. Mem.* **92**: 519-528.
- McNaughton BL, Douglas RM, Goddard GV (1978) Synaptic enhancement in fascia dentata: cooperativity among coactive afferents. *Brain Res.* **157**: 277-293.
- Mergia E, Friebe A, Dangel O, Russwurm M, Koesling D (2006) Spare guanylyl cyclase NO receptors ensure high NO sensitivity in the vascular system. *J. Clin. Invest.* **116**: 1731-1737.

- Mergia E, Russwurm M, Zoidl G, Koesling D (2003) Major occurrence of the new alpha2beta1 isoform of NO-sensitive guanylyl cyclase in brain. *Cell Signal*. **15**: 189-195.
- Mermelstein PG, Bito H, Deisseroth K, Tsien RW (2000) Critical dependence of cAMP response element-binding protein phosphorylation on L-type calcium channels supports a selective response to EPSPs in preference to action potentials. *J. Neurosci*. **20**: 266-273.
- Michel JB, Feron O, Sacks D, Michel T (1997a) Reciprocal regulation of endothelial nitric-oxide synthase by Ca²⁺-calmodulin and caveolin. *J. Biol. Chem*. **272**: 15583-15586.
- Michel JB, Feron O, Sase K, Prabhakar P, Michel T (1997b) Caveolin versus calmodulin. Counterbalancing allosteric modulators of endothelial nitric oxide synthase. *J. Biol. Chem*. **272**: 25907-25912.
- Micheva KD, Buchanan J, Holz RW, Smith SJ (2003) Retrograde regulation of synaptic vesicle endocytosis and recycling. *Nat. Neurosci*. **6**: 925-932.
- Micheva KD, Holz RW, Smith SJ (2001) Regulation of presynaptic phosphatidylinositol 4,5-bisphosphate by neuronal activity. *J. Cell Biol*. **154**: 355-368.
- Miki N, Kawabe Y, Kuriyama K (1977) Activation of cerebral guanylate cyclase by nitric oxide. *Biochem. Biophys. Res. Commun*. **75**: 851-856.
- Milligan CJ, Edwards IJ, Deuchars J (2006) HCN1 ion channel immunoreactivity in spinal cord and medulla oblongata. *Brain Res*. **1081**: 79-91.
- Mitchell D, Tymk K (1996) Nitric oxide release in rat skeletal muscle capillary. *Am. J. Physiol* **270**: H1696-H1703.
- Mitchell HH, Shonle HA, Grindley HS (1916) The origin of the nitrates in the urine. *J. Biol. Chem*. **24**: 461-490.
- Moore PK, al-Swayeh OA, Chong NW, Evans RA, Gibson A (1990) L-NG-nitro arginine (L-NOARG), a novel, L-arginine-reversible inhibitor of endothelium-dependent vasodilatation *in vitro*. *Br. J. Pharmacol*. **99**: 408-412.
- Moosmang S, Haider N, Klugbauer N, Adelsberger H, Langwieser N, Muller J, Stiess M, Marais E, Schulla V, Lacinova L, Goebbels S, Nave KA, Storm DR, Hofmann F, Kleppisch T (2005a) Role of hippocampal Ca_v1.2 Ca²⁺ channels in NMDA receptor-independent synaptic plasticity and spatial memory. *J. Neurosci*. **25**: 9883-9892.
- Moosmang S, Lenhardt P, Haider N, Hofmann F, Wegener JW (2005b) Mouse models to study L-type calcium channel function. *Pharmacol. Ther*. **106**: 347-355.
- Moran MM, Xu H, Clapham DE (2004) TRP ion channels in the nervous system. *Curr. Opin. Neurobiol*. **14**: 362-369.
- Morgan SL, Teyler TJ (1999) VDCCs and NMDARs underlie two forms of LTP in CA1 hippocampus *in vivo*. *J. Neurophysiol*. **82**: 736-740.
- Morgan SL, Teyler TJ (2001) Electrical stimuli patterned after the theta-rhythm induce multiple forms of LTP. *J. Neurophysiol*. **86**: 1289-1296.
- Morley D, Keefer LK (1993) Nitric oxide/nucleophile complexes: a unique class of nitric oxide-based vasodilators. *J. Cardiovasc. Pharmacol*. **22 Suppl 7**: S3-S9.
- Moroz LL, Meech RW, Sweedler JV, Mackie GO (2004) Nitric oxide regulates swimming in the jellyfish *Aglantha digitale*. *J. Comp. Neurol*. **471**: 26-36.

Morris RG, Anderson E, Lynch GS, Baudry M (1986) Selective impairment of learning and blockade of long-term potentiation by an N-methyl-D-aspartate receptor antagonist, AP5. *Nature* **319**: 774-776.

Morris RG, Garrud P, Rawlins JN, O'Keefe J (1982) Place navigation impaired in rats with hippocampal lesions. *Nature* **297**: 681-683.

Moser EI, Krobot KA, Moser MB, Morris RG (1998) Impaired spatial learning after saturation of long-term potentiation. *Science* **281**: 2038-2042.

Murphy TH, Worley PF, Baraban JM (1991) L-type voltage-sensitive calcium channels mediate synaptic activation of immediate early genes. *Neuron* **7**: 625-635.

Murthy KS (2001) Activation of phosphodiesterase 5 and inhibition of guanylate cyclase by cGMP-dependent protein kinase in smooth muscle. *Biochem. J.* **360**: 199-208.

Musleh WY, Shahi K, Baudry M (1993) Further studies concerning the role of nitric oxide in LTP induction and maintenance. *Synapse* **13**: 370-375.

N'Gouemo P, Yasuda R, Faingold CL (2010) Seizure susceptibility is associated with altered protein expression of voltage-gated calcium channel subunits in inferior colliculus neurons of the genetically epilepsy-prone rat. *Brain Res.* **1308**: 153-157.

Nakane M, Arai K, Saheki S, Kuno T, Buechler W, Murad F (1990) Molecular cloning and expression of cDNAs coding for soluble guanylate cyclase from rat lung. *J. Biol. Chem.* **265**: 16841-16845.

Nakane M, Saheki S, Kuno T, Ishii K, Murad F (1988) Molecular cloning of a cDNA coding for 70 kilodalton subunit of soluble guanylate cyclase from rat lung. *Biochem. Biophys. Res. Commun.* **157**: 1139-1147.

Nakazawa K, Quirk MC, Chitwood RA, Watanabe M, Yeckel MF, Sun LD, Kato A, Carr CA, Johnston D, Wilson MA, Tonegawa S (2002) Requirement for hippocampal CA3 NMDA receptors in associative memory recall. *Science* **297**: 211-218.

Nedvetsky PI, Sessa WC, Schmidt HH (2002) There's NO binding like NOS binding: protein-protein interactions in NO/cGMP signaling. *Proc. Natl. Acad. Sci. U. S. A* **99**: 16510-16512.

Neitz A, Mergia E, Eysel UT, Koesling D, Mittmann T (2011) Presynaptic nitric oxide/cGMP facilitates glutamate release via hyperpolarization-activated cyclic nucleotide-gated channels in the hippocampus. *Eur. J. Neurosci.* **9**: 1611-1621.

Neves G, Cooke SF, Bliss TV (2008) Synaptic plasticity, memory and the hippocampus: a neural network approach to causality. *Nat. Rev. Neurosci.* **9**: 65-75.

Nicolarakis PJ, Lin YQ, Bennett MR (1994) Effect of nitric oxide synthase inhibition on long-term potentiation at associational-commissural and mossy fibre synapses on CA3 pyramidal neurones. *Br. J. Pharmacol.* **111**: 521-524.

Nicoll RA (2003) Expression mechanisms underlying long-term potentiation: a postsynaptic view. *Philos. Trans. R. Soc. Lond B Biol. Sci.* **358**: 721-726.

Nicoll RA, Schmitz D (2005) Synaptic plasticity at hippocampal mossy fibre synapses. *Nat. Rev. Neurosci.* **6**: 863-876.

Nikonenko I, Boda B, Steen S, Knott G, Welker E, Muller D (2008) PSD-95 promotes synaptogenesis and multiinnervated spine formation through nitric oxide signaling. *J. Cell Biol.* **183**: 1115-1127.

Nikonenko I, Jourdain P, Muller D (2003) Presynaptic remodeling contributes to activity-dependent synaptogenesis. *J. Neurosci.* **23**: 8498-8505.

Nimmegeers S, Sips P, Buys E, Brouckaert P, Van d, V (2007) Functional role of the soluble guanylyl cyclase $\alpha 1$ subunit in vascular smooth muscle relaxation. *Cardiovasc. Res.* **76**: 149-159.

Ninan I, Arancio O (2004) Presynaptic CaMKII is necessary for synaptic plasticity in cultured hippocampal neurons. *Neuron* **42**: 129-141.

Norman JA, Ansell J, Phillips MA (1983) Dihydropyridine Ca^{2+} entry blockers selectively inhibit peak I cAMP phosphodiesterase. *Eur. J. Pharmacol.* **93**: 107-112.

Notomi T, Shigemoto R (2004) Immunohistochemical localization of I^h channel subunits, HCN1-4, in the rat brain. *J. Comp Neurol.* **471**: 241-276.

Nugent FS, Penick EC, Kauer JA (2007) Opioids block long-term potentiation of inhibitory synapses. *Nature* **446**: 1086-1090.

O'Dell TJ, Hawkins RD, Kandel ER, Arancio O (1991) Tests of the roles of two diffusible substances in long-term potentiation: evidence for nitric oxide as a possible early retrograde messenger. *Proc. Natl. Acad. Sci. U. S. A* **88**: 11285-11289.

O'Dell TJ, Huang PL, Dawson TM, Dinerman JL, Snyder SH, Kandel ER, Fishman MC (1994) Endothelial NOS and the blockade of LTP by NOS inhibitors in mice lacking neuronal NOS. *Science* **265**: 542-546.

O'Keefe J (2007) Hippocampal neurophysiology in the behaving animal. In: *The hippocampus book* (Andersen P, Morris R, Amaral D, Bliss TVP, O'Keefe J, eds), pp 475-548. Oxford: Oxford University Press.

Oka M, Itoh Y, Ukai Y, Kimura K (1999) Blockade by NS-7, a neuroprotective compound, of both L-type and P/Q-type Ca^{2+} channels involving depolarization-stimulated nitric oxide synthase activity in primary neuronal culture. *J. Neurochem.* **72**: 1315-1322.

Okada D (1992) Two pathways of cyclic GMP production through glutamate receptor-mediated nitric oxide synthesis. *J. Neurochem.* **59**: 1203-1210.

Olken NM, Marletta MA (1993) NG-methyl-L-arginine functions as an alternate substrate and mechanism-based inhibitor of nitric oxide synthase. *Biochemistry* **32**: 9677-9685.

Ota KT, Pierre VJ, Ploski JE, Queen K, Schafe GE (2008) The NO-cGMP-PKG signaling pathway regulates synaptic plasticity and fear memory consolidation in the lateral amygdala via activation of ERK/MAP kinase. *Learn. Mem.* **15**: 792-805.

Ozawa Y, Hayashi K, Kobori H (2006) New generation calcium channel blockers in hypertensive treatment. *Curr. Hypertens. Rev.* **2**: 103-111.

Palmer RM, Ferrige AG, Moncada S (1987) Nitric oxide release accounts for the biological activity of endothelium-derived relaxing factor. *Nature* **327**: 524-526.

Pape HC, Mager R (1992) Nitric oxide controls oscillatory activity in thalamocortical neurons. *Neuron* **9**: 441-448.

Parent A, Schrader K, Munger SD, Reed RR, Linden DJ, Ronnett GV (1998) Synaptic transmission and hippocampal long-term potentiation in olfactory cyclic nucleotide-gated channel type 1 null mouse. *J. Neurophysiol.* **79**: 3295-3301.

Park JF, Luo ZD (2010) Calcium channel functions in pain processing. *Channels (Austin)* **4**: 510-517.

Park JH, Straub VA, O'Shea M (1998) Anterograde signaling by nitric oxide: characterization and *in vitro* reconstitution of an identified nitrergic synapse. *J. Neurosci.* **18**: 5463-5476.

- Parra P, Gulyas AI, Miles R (1998) How many subtypes of inhibitory cells in the hippocampus? *Neuron* **20**: 983-993.
- Pawlik G, Rackl A, Bing RJ (1981) Quantitative capillary topography and blood flow in the cerebral cortex of cats: an *in vivo* microscopic study. *Brain Res.* **208**: 35-58.
- Perez-Reyes E, Kim HS, Lacerda AE, Horne W, Wei XY, Rampe D, Campbell KP, Brown AM, Birnbaumer L (1989) Induction of calcium currents by the expression of the alpha 1-subunit of the dihydropyridine receptor from skeletal muscle. *Nature* **340**: 233-236.
- Petersen CC, Malenka RC, Nicoll RA, Hopfield JJ (1998) All-or-none potentiation at CA3-CA1 synapses. *Proc. Natl. Acad. Sci. U. S. A* **95**: 4732-4737.
- Petros A, Bennett D, Vallance P (1991) Effect of nitric oxide synthase inhibitors on hypotension in patients with septic shock. *Lancet* **338**: 1557-1558.
- Phillips KG, Hardingham NR, Fox K (2008) Postsynaptic action potentials are required for nitric-oxide-dependent long-term potentiation in CA1 neurons of adult GluR1 knock-out and wild-type mice. *J. Neurosci.* **28**: 14031-14041.
- Pifarre P, Garcia A, Mengod G (2007) Species differences in the localization of soluble guanylyl cyclase subunits in monkey and rat brain. *J. Comp. Neurol.* **500**: 942-957.
- Pigott B, Garthwaite J (2009) Activity-dependent long-term potentiation produced by exogenous nitric oxide during NMDA receptor blockade in hippocampal slices. *Proc. Physiol. Soc.* **15**: Abstract C109.
- Poss KD, Thomas MJ, Ebralidze AK, O'Dell TJ, Tonegawa S (1995) Hippocampal long-term potentiation is normal in heme oxygenase-2 mutant mice. *Neuron* **15**: 867-873.
- Potter LR (2011) Guanylyl cyclase structure, function and regulation. *Cell Signal.* **23**: 1921-1926.
- Pozo K, Goda Y (2010) Unraveling mechanisms of homeostatic synaptic plasticity. *Neuron* **66**: 337-351.
- Prast H, Philippu A (2001) Nitric oxide as modulator of neuronal function. *Prog. Neurobiol.* **64**: 51-68.
- Priestley J (1775) Experiments and observations on different kinds of air. Volume published by W. Bowyer and J. Nichols for J. Johnson, London.
- Pyriochou A, Papapetropoulos A (2005) Soluble guanylyl cyclase: more secrets revealed. *Cell Signal.* **17**: 407-413.
- Rameau GA, Chiu LY, Ziff EB (2004) Bidirectional regulation of neuronal nitric-oxide synthase phosphorylation at serine 847 by the N-methyl-D-aspartate receptor. *J. Biol. Chem.* **279**: 14307-14314.
- Rameau GA, Tukey DS, Garcin-Hosfield ED, Titcombe RF, Misra C, Khatri L, Getzoff ED, Ziff EB (2007) Biphasic coupling of neuronal nitric oxide synthase phosphorylation to the NMDA receptor regulates AMPA receptor trafficking and neuronal cell death. *J. Neurosci.* **27**: 3445-3455.
- Rampe D, Kane M (1994) Activators of voltage-dependent L-type calcium channels. *Drug Dev. Res.* **33**: 344-363.
- Rapoport RM, Draznin MB, Murad F (1983) Endothelium-dependent vasodilator-and nitrovasodilator-induced relaxation may be mediated through cyclic GMP formation and cyclic GMP-dependent protein phosphorylation. *Trans. Assoc. Am. Physicians* **96**: 19-30.

- Raymond CR (2007) LTP forms 1, 2 and 3: different mechanisms for the "long" in long-term potentiation. *Trends Neurosci.* **30**: 167-175.
- Razani B, Woodman SE, Lisanti MP (2002) Caveolae: from cell biology to animal physiology. *Pharmacol. Rev.* **54**: 431-467.
- Regehr WG, Tank DW (1992) Calcium concentration dynamics produced by synaptic activation of CA1 hippocampal pyramidal cells. *J. Neurosci.* **12**: 4202-4223.
- Robello M, Amico C, Bucossi G, Cupello A, Rapallino MV, Thellung S (1996) Nitric oxide and GABAA receptor function in the rat cerebral cortex and cerebellar granule cells. *Neuroscience* **74**: 99-105.
- Rodrigo J, Springall DR, Uttenthal O, Bentura ML, badia-Molina F, Riveros-Moreno V, Martinez-Murillo R, Polak JM, Moncada S (1994) Localization of nitric oxide synthase in the adult rat brain. *Philos. Trans. R. Soc. Lond B Biol. Sci.* **345**: 175-221.
- Rodriguez-Crespo I, Straub W, Gavilanes F, Ortiz de Montellano PR (1998) Binding of dynein light chain (PIN) to neuronal nitric oxide synthase in the absence of inhibition. *Arch. Biochem. Biophys.* **359**: 297-304.
- Romberg C, Raffel J, Martin L, Sprengel R, Seeburg PH, Rawlins JN, Bannerman DM, Paulsen O (2009) Induction and expression of GluA1 (GluR-A)-independent LTP in the hippocampus. *Eur. J. Neurosci.* **29**: 1141-1152.
- Routh BN, Johnston D, Harris K, Chitwood RA (2009) Anatomical and electrophysiological comparison of CA1 pyramidal neurons of the rat and mouse. *J. Neurophysiol.* **102**: 2288-2302.
- Roy B, Garthwaite J (2006) Nitric oxide activation of guanylyl cyclase in cells revisited. *Proc. Natl. Acad. Sci. U. S. A* **103**: 12185-12190.
- Rozov A, Burnashev N, Sakmann B, Neher E (2001) Transmitter release modulation by intracellular Ca²⁺ buffers in facilitating and depressing nerve terminals of pyramidal cells in layer 2/3 of the rat neocortex indicates a target cell-specific difference in presynaptic calcium dynamics. *J. Physiol.* **531**: 807-826.
- Ruiz-Stewart I, Tiyyagura SR, Lin JE, Kazerounian S, Pitari GM, Schulz S, Martin E, Murad F, Waldman SA (2004) Guanylyl cyclase is an ATP sensor coupling nitric oxide signaling to cell metabolism. *Proc. Natl. Acad. Sci. U. S. A* **101**: 37-42.
- Russwurm M, Behrends S, Harteneck C, Koesling D (1998) Functional properties of a naturally occurring isoform of soluble guanylyl cyclase. *Biochem. J.* **335**: 125-130.
- Russwurm M, Wittau N, Koesling D (2001) Guanylyl cyclase/PSD-95 interaction: targeting of the nitric oxide-sensitive $\alpha 2\beta 1$ guanylyl cyclase to synaptic membranes. *J. Biol. Chem.* **276**: 44647-44652.
- Sato M, Hida N, Umezawa Y (2005) Imaging the nanomolar range of nitric oxide with an amplifier-coupled fluorescent indicator in living cells. *Proc. Natl. Acad. Sci. U. S. A* **102**: 14515-14520.
- Sato M, Nakajima T, Goto M, Umezawa Y (2006) Cell-based indicator to visualize picomolar dynamics of nitric oxide release from living cells. *Anal. Chem.* **78**: 8175-8182.
- Sattler R, Xiong Z, Lu WY, Hafner M, MacDonald JF, Tymianski M (1999) Specific coupling of NMDA receptor activation to nitric oxide neurotoxicity by PSD-95 protein. *Science* **284**: 1845-1848.
- Savchenko A, Barnes S, Kramer RH (1997) Cyclic-nucleotide-gated channels mediate synaptic feedback by nitric oxide. *Nature* **390**: 694-698.

- Schafe GE (2008) Rethinking the role of L-type voltage-gated calcium channels in fear memory extinction. *Learn. Mem.* **15**: 324-325.
- Schlossmann J, Ammendola A, Ashman K, Zong X, Huber A, Neubauer G, Wang GX, Allescher HD, Korth M, Wilm M, Hofmann F, Ruth P (2000) Regulation of intracellular calcium by a signalling complex of IRAG, IP3 receptor and cGMP kinase Ibeta. *Nature* **404**: 197-201.
- Schlossmann J, Feil R, Hofmann F (2005) Insights into cGMP signalling derived from cGMP kinase knockout mice. *Front Biosci.* **10**: 1279-1289.
- Schmachtenberg O, Diaz J, Bacigalupo J (2003) NO activates the olfactory cyclic nucleotide-gated conductance independent from cGMP in isolated rat olfactory receptor neurons. *Brain Res.* **980**: 146-150.
- Schmidt K, Desch W, Klatt P, Kukovetz WR, Mayer B (1997) Release of nitric oxide from donors with known half-life: a mathematical model for calculating nitric oxide concentrations in aerobic solutions. *Naunyn Schmiedebergs Arch. Pharmacol.* **355**: 457-462.
- Schrammel A, Behrends S, Schmidt K, Koesling D, Mayer B (1996) Characterization of 1H-[1,2,4]oxadiazolo[4,3-a]quinoxalin-1-one as a heme-site inhibitor of nitric oxide-sensitive guanylyl cyclase. *Mol. Pharmacol.* **50**: 1-5.
- Schulz PE, Cook EP, Johnston D (1994) Changes in paired-pulse facilitation suggest presynaptic involvement in long-term potentiation. *J. Neurosci.* **14**: 5325-5337.
- Schulz PE, Cook EP, Johnston D (1995) Using paired-pulse facilitation to probe the mechanisms for long-term potentiation (LTP). *J. Physiol. Paris* **89**: 3-9.
- Schulz S, Chinkers M, Garbers DL (1989) The guanylate cyclase/receptor family of proteins. *FASEB J.* **3**: 2026-2035.
- Schuman EM, Madison DV (1991) A requirement for the intercellular messenger nitric oxide in long-term potentiation. *Science* **254**: 1503-1506.
- Seidel B, Stanarius A, Wolf G (1997) Differential expression of neuronal and endothelial nitric oxide synthase in blood vessels of the rat brain. *Neurosci. Lett.* **239**: 109-112.
- Senter PD, Eckstein F, Mulsch A, Bohme E (1983) The stereochemical course of the reaction catalyzed by soluble bovine lung guanylate cyclase. *J. Biol. Chem.* **258**: 6741-6745.
- Serulle Y, Zhang S, Ninan I, Puzzo D, McCarthy M, Khatri L, Arancio O, Ziff EB (2007) A GluR1-cGKII interaction regulates AMPA receptor trafficking. *Neuron* **56**: 670-688.
- Shors TJ, Matzel LD (1997) Long-term potentiation: what's learning got to do with it? *Behav. Brain Sci.* **20**: 597-614.
- Silva AJ, Paylor R, Wehner JM, Tonegawa S (1992a) Impaired spatial learning in alpha-calcium-calmodulin kinase II mutant mice. *Science* **257**: 206-211.
- Silva AJ, Stevens CF, Tonegawa S, Wang Y (1992b) Deficient hippocampal long-term potentiation in alpha-calcium-calmodulin kinase II mutant mice. *Science* **257**: 201-206.
- Sokolova IV, Lester HA, Davidson N (2006) Postsynaptic Mechanisms Are Essential for Forskolin-Induced Potentiation of Synaptic Transmission. *J. Neurophysiol* **95**: 2570-2579.
- Son H, Hawkins RD, Martin K, Kiebler M, Huang PL, Fishman MC, Kandel ER (1996) Long-term potentiation is reduced in mice that are doubly mutant in endothelial and neuronal nitric oxide synthase. *Cell* **87**: 1015-1023.

- Song Y, Zweier JL, Xia Y (2001) Heat-shock protein 90 augments neuronal nitric oxide synthase activity by enhancing Ca²⁺/calmodulin binding. *Biochem. J.* **355**: 357-360.
- Southam E, East SJ, Garthwaite J (1991) Excitatory amino acid receptors coupled to the nitric oxide/cyclic GMP pathway in rat cerebellum during development. *J. Neurochem.* **56**: 2072-2081.
- Southam E, Garthwaite J (1993) The nitric oxide-cyclic GMP signalling pathway in rat brain. *Neuropharmacology* **32**: 1267-1277.
- Southam E, Morris R, Garthwaite J (1992) Sources and targets of nitric oxide in rat cerebellum. *Neurosci. Lett.* **137**: 241-244.
- Specht CG, Schoepfer R (2001) Deletion of the alpha-synuclein locus in a subpopulation of C57BL/6J inbred mice. *BMC. Neurosci.* **2**: 11.
- Spruston N, McBain C (2007) Structural and functional properties of hippocampal neurons. In: The hippocampus book. (Andersen P, Morris RG, Amaral D, Bliss TVP., O'Keefe J, eds), pp 133-201. Oxford: Oxford University Press.
- Stanarius A, Topel I, Schulz S, Noack H, Wolf G (1997) Immunocytochemistry of endothelial nitric oxide synthase in the rat brain: a light and electron microscopical study using the tyramide signal amplification technique. *Acta Histochem.* **99**: 411-429.
- Steinert JR, Chernova T, Forsythe ID (2010) Nitric oxide signaling in brain function, dysfunction, and dementia. *Neuroscientist* **16**: 435-452.
- Stephenson DT, Coskran TM, Wilhelms MB, Adamowicz WO, O'Donnell MM, Muravnick KB, Menniti FS, Kleiman RJ, Morton D (2009) Immunohistochemical localization of phosphodiesterase 2A in multiple mammalian species. *J. Histochem. Cytochem.* **57**: 933-949.
- Stone JR, Marletta MA (1994) Soluble guanylate cyclase from bovine lung: activation with nitric oxide and carbon monoxide and spectral characterization of the ferrous and ferric states. *Biochemistry* **33**: 5636-5640.
- Straub VA, Grant J, O'Shea M, Benjamin PR (2007) Modulation of serotonergic neurotransmission by nitric oxide. *J. Neurophysiol.* **97**: 1088-1099.
- Striessnig J (1999) Pharmacology, structure and function of cardiac L-type Ca²⁺ channels. *Cell Physiol. Biochem.* **9**: 242-269.
- Stuehr DJ (1999) Mammalian nitric oxide synthases. *Biochim. Biophys. Acta* **1411**: 217-230.
- Stuehr DJ, Marletta MA (1985) Mammalian nitrate biosynthesis: mouse macrophages produce nitrite and nitrate in response to Escherichia coli lipopolysaccharide. *Proc. Natl. Acad. Sci. U. S. A* **82**: 7738-7742.
- Suma C, Hayashi S, Ukai Y, Yoshikuni Y, Kimura K (1997) Na⁺ and high-voltage-activated Ca²⁺ channel blocking actions of NS-7, a novel neuroprotective agent, in NG108-15 cells. *Eur. J. Pharmacol.* **336**: 283-290.
- Sunahara RK, Beuve A, Tesmer JJ, Sprang SR, Garbers DL, Gilman AG (1998) Exchange of substrate and inhibitor specificities between adenylyl and guanylyl cyclases. *J. Biol. Chem.* **273**: 16332-16338.
- Susswein AJ, Katzoff A, Miller N, Hurwitz I (2004) Nitric oxide and memory. *Neuroscientist* **10**: 153-162.

- Suvarna NU, O'Donnell JM (2002) Hydrolysis of N-methyl-D-aspartate receptor-stimulated cAMP and cGMP by PDE4 and PDE2 phosphodiesterases in primary neuronal cultures of rat cerebral cortex and hippocampus. *J. Pharmacol. Exp. Ther.* **302**: 249-256.
- Szabadits E, Cserep C, Ludanyi A, Katona I, Gracia-Llanes J, Freund TF, Nyiri G (2007) Hippocampal GABAergic synapses possess the molecular machinery for retrograde nitric oxide signaling. *J. Neurosci.* **27**: 8101-8111.
- Takahashi S, Mendelsohn ME (2003a) Calmodulin-dependent and -independent activation of endothelial nitric-oxide synthase by heat shock protein 90. *J. Biol. Chem.* **278**: 9339-9344.
- Takahashi S, Mendelsohn ME (2003b) Synergistic activation of endothelial nitric-oxide synthase (eNOS) by HSP90 and Akt: calcium-independent eNOS activation involves formation of an HSP90-Akt-CaM-bound eNOS complex. *J. Biol. Chem.* **278**: 30821-30827.
- Takasugi Y, Kawata K, Okuda T, Koga Y, Mizuguchi N, Yamanaka S, Watanabe S (2003) Strain differences to effects of aging on concentrations of amino acids in cerebrospinal fluid between Sprague Dawley rat and Wistar Kyoto rat. *Exp. Anim.* **52**: 429-432.
- Tang YP, Shimizu E, Dube GR, Rampon C, Kerchner GA, Zhuo M, Liu G, Tsien JZ (1999) Genetic enhancement of learning and memory in mice. *Nature* **401**: 63-69.
- Tao HW, Poo M (2001) Retrograde signaling at central synapses. *Proc. Natl. Acad. Sci. U. S. A* **98**: 11009-11015.
- Taqatqeh F, Mergia E, Neitz A, Eysel UT, Koesling D, Mittmann T (2009) More than a retrograde messenger: nitric oxide needs two cGMP pathways to induce hippocampal long-term potentiation. *J. Neurosci.* **29**: 9944-9350.
- Tatsumi S, Itoh Y, Ma FH, Higashira H, Ukai Y, Yoshikuni Y, Kimura K (1998) Inhibition of depolarization-induced nitric oxide synthase activation by NS-7, a phenylpyrimidine derivative, in primary neuronal culture. *J. Neurochem.* **70**: 59-65.
- Teyler TJ, Cavus I, Coussens C (1995) Synaptic plasticity in the hippocampal slice: functional consequences. *J. Neurosc. Methods* **59**: 11-17.
- Teyler TJ, Cavus I, Coussens C, DiScenna P, Grover L, Lee YP, Little Z (1994) Multideterminant role of calcium in hippocampal synaptic plasticity. *Hippocampus* **4**: 623-634.
- Teyler TJ (1999) Use of brain slices to study long-term potentiation and depression as examples of synaptic plasticity. *Methods* **18**: 109-116.
- Thevenod F, Jones SW (1992) Cadmium block of calcium current in frog sympathetic neurons. *Biophys. J.* **63**: 162-168.
- Thomas MK, Francis SH, Corbin JD (1990) Substrate- and kinase-directed regulation of phosphorylation of a cGMP-binding phosphodiesterase by cGMP. *J. Biol. Chem.* **265**: 14971-14978.
- Topel I, Stanarius A, Wolf G (1998) Distribution of the endothelial constitutive nitric oxide synthase in the developing rat brain: an immunohistochemical study. *Brain Res.* **788**: 43-48.
- Treiman M, Caspersen C, Christensen SB (1998) A tool coming of age: thapsigargin as an inhibitor of sarco-endoplasmic reticulum Ca²⁺-ATPases. *Trends Pharmacol. Sci.* **19**: 131-135.
- Trezise D, Dale T, Main M (2010) Ion channels: principles, terminology and methodology. In: Ion channels from structure to function (Kew J, Davies C, eds), pp 3-17. Oxford: Oxford University Press.
- Tsien JZ, Huerta PT, Tonegawa S (1996) The essential role of hippocampal CA1 NMDA receptor-dependent synaptic plasticity in spatial memory. *Cell* **87**: 1327-1338.

Vaandrager AB, Ehlert EM, Jarchau T, Lohmann SM, de Jonge HR (1996) N-terminal myristoylation is required for membrane localization of cGMP-dependent protein kinase type II. *J. Biol. Chem.* **271**: 7025-7029.

Vallance P, Leiper J (2002) Blocking NO synthesis: how, where and why? *Nat. Rev. Drug Discov.* **1**: 939-950.

Valtschanoff JG, Weinberg RJ, Kharazia VN, Nakane M, Schmidt HHHW (1993) Neurons in rat hippocampus that synthesize nitric-oxide. *J. Comp. Neurol.* **331**: 111-121.

van Staveren WC, Markerink-Van IM, Steinbusch HW, de VJ (2001) The effects of phosphodiesterase inhibition on cyclic GMP and cyclic AMP accumulation in the hippocampus of the rat. *Brain Res.* **888**: 275-286.

van Staveren WC, Steinbusch HW, Markerink-Van IM, Behrends S, de VJ (2004) Species differences in the localization of cGMP-producing and NO-responsive elements in the mouse and rat hippocampus using cGMP immunocytochemistry. *Eur. J. Neurosci.* **19**: 2155-2168.

van Staveren WC, Steinbusch HW, Markerink-Van IM, Repaske DR, Goy MF, Kotera J, Omori K, Beavo JA, de VJ (2003) mRNA expression patterns of the cGMP-hydrolyzing phosphodiesterases types 2, 5, and 9 during development of the rat brain. *J. Comp. Neurol.* **467**: 566-580.

Venema RC, Venema VJ, Ju H, Harris MB, Snead C, Jilling T, Dimitropoulou C, Maragoudakis ME, Catravas JD (2003) Novel complexes of guanylate cyclase with heat shock protein 90 and nitric oxide synthase. *Am. J. Physiol Heart Circ. Physiol* **285**: H669-H678.

Verma A, Hirsch DJ, Glatt CE, Ronnett GV, Snyder SH (1993) Carbon monoxide: a putative neural messenger. *Science* **259**: 381-384.

Vincent SR (2010) Nitric oxide neurons and neurotransmission. *Prog. Neurobiol.* **90**: 246-255.

Vincent SR, Kimura H (1992) Histochemical mapping of nitric oxide synthase in the rat brain. *Neuroscience* **46**: 755-784.

Visser GJ, Peters PH, Theuvsen AP (1993) Cadmium ion is a non-competitive inhibitor of red cell Ca²⁺-ATPase activity. *Biochem. Biophys. Acta* **1152**: 26-34.

Wagner DA, Young VR, Tannenbaum SR (1983) Mammalian nitrate biosynthesis: incorporation of ¹⁵NH₃ into nitrate is enhanced by endotoxin treatment. *Proc. Natl. Acad. Sci. U. S. A* **80**: 4518-4521.

Walker M, Chan D, Thom M (2007) Hippocampus in human diseases. In: *The hippocampus book* (Andersen P, Morris RG, Amaral D, Bliss TVP, O'Keefe J, eds), pp 769-812. Oxford: Oxford University Press.

Walther C, Gielen S, Hambrecht R (2004) The effect of exercise training on endothelial function in cardiovascular disease in humans. *Exerc. Sport Sci. Rev.* **32**: 129-134.

Wang HG, Lu FM, Jin I, Udo H, Kandel ER, de VJ, Walter U, Lohmann SM, Hawkins RD, Antonova I (2005) Presynaptic and postsynaptic roles of NO, cGK, and RhoA in long-lasting potentiation and aggregation of synaptic proteins. *Neuron* **45**: 389-403.

Wang LY, Salter MW, MacDonald JF (1991) Regulation of kainate receptors by cAMP-dependent protein kinase and phosphatases. *Science* **253**: 1132-1135.

Watanabe M, Fukaya M, Sakimura K, Manabe T, Mishina M, Inoue Y (1998) Selective scarcity of NMDA receptor channel subunits in the stratum lucidum (mossy fibre-recipient layer) of the mouse hippocampal CA3 subfield. *Eur. J. Neurosci.* **10**: 478-487.

- Watanabe Y, Saito H, Abe K (1995) Nitric oxide is involved in long-term potentiation in the medial but not lateral amygdala neuron synapses *in vitro*. *Brain Res.* **688**: 233-236.
- Wedel B, Harteneck C, Foerster J, Friebe A, Schultz G, Koesling D (1995) Functional domains of soluble guanylyl cyclase. *J. Biol. Chem.* **270**: 24871-24875.
- Wedel B, Humbert P, Harteneck C, Foerster J, Malkewitz J, Bohme E, Schultz G, Koesling D (1994) Mutation of His-105 in the beta 1 subunit yields a nitric oxide-insensitive form of soluble guanylyl cyclase. *Proc. Natl. Acad. Sci. U. S. A* **91**: 2592-2596.
- Weisskopf MG, Bauer EP, LeDoux JE (1999) L-type voltage-gated calcium channels mediate NMDA-independent associative long-term potentiation at thalamic input synapses to the amygdala. *J. Neurosci.* **19**: 10512-10519.
- Wendland B, Schweizer FE, Ryan TA, Nakane M, Murad F, Scheller RH, Tsien RW (1994) Existence of nitric oxide synthase in rat hippocampal pyramidal cells. *Proc. Natl. Acad. Sci. U. S. A* **91**: 2151-2155.
- Westenbroek RE, Ahljianian MK, Catterall WA (1990) Clustering of L-type Ca^{2+} channels at the base of major dendrites in hippocampal pyramidal neurons. *Nature* **347**: 281-284.
- Whitlock JR, Heynen AJ, Shuler MG, Bear MF (2006) Learning induces long-term potentiation in the hippocampus. *Science* **313**: 1093-1097.
- Wigstrom H, Gustafsson B, Huang YY, Abraham WC (1986) Hippocampal long-term potentiation is induced by pairing single afferent volleys with intracellularly injected depolarizing current pulses. *Acta. Physiol. Scand.* **126**: 317-319.
- Williams JH, Li YG, Nayak A, Errington ML, Murphy KP, Bliss TV (1993) The suppression of long-term potentiation in rat hippocampus by inhibitors of nitric oxide synthase is temperature and age dependent. *Neuron* **11**: 877-884.
- Wilson EM, Chinkers M (1995) Identification of sequences mediating guanylyl cyclase dimerization. *Biochemistry* **34**: 4696-4701.
- Wilson GW, Garthwaite J (2010) Hyperpolarization-activated ion channels as targets for nitric oxide signalling in deep cerebellar nuclei. *Eur. J. Neurosci.* **31**: 1935-1945.
- Wilson RI, Godecke A, Brown RE, Schrader J, Haas HL (1999) Mice deficient in endothelial nitric oxide synthase exhibit a selective deficit in hippocampal long-term potentiation. *Neuroscience* **90**: 1157-1165.
- Wojtaszek P (2000) Nitric oxide in plants. To NO or not to NO. *Phytochemistry* **54**: 1-4.
- Wolf ME (2003) LTP may trigger addiction. *Mol. Interv.* **3**: 248-252.
- Wood KC, Batchelor AM, Bartus K, Harris KL, Garthwaite G, Vernon J, Garthwaite J (2011) Picomolar nitric oxide signals from central neurons recorded using ultrasensitive detector cells. *J. Biol. Chem.* Epub, DOI: 10.1074/jbc.M111.289777.
- Wood PJ, Marks V (1978) Direct measurement of cGMP in blood plasma and urine by radioimmunoassay. *Ann. Clin. Biochem.* **15**: 25-30.
- Wood PL, Emmett MR, Rao TS, Cler J, Mick S, Iyengar S (1990) Inhibition of nitric oxide synthase blocks N-methyl-D-aspartate-, quisqualate-, kainate-, harmaline-, and pentylenetetrazole-dependent increases in cerebellar cyclic GMP *in vivo*. *J. Neurochem.* **55**: 346-348.

Woodside BL, Borroni AM, Hammonds MD, Teyler TJ (2004) NMDA receptors and voltage-dependent calcium channels mediate different aspects of acquisition and retention of a spatial memory task. *Neurobiol. Learn. Mem.* **81**: 105-114.

Wu HH, Williams CV, McLoon SC (1994) Involvement of nitric oxide in the elimination of a transient retinotectal projection in development. *Science* **265**: 1593-1596.

Wu LG, Saggau P (1994a) Adenosine inhibits evoked synaptic transmission primarily by reducing presynaptic calcium influx in area CA1 of hippocampus. *Neuron* **12**: 1139-1148.

Wu LG, Saggau P (1994b) Presynaptic calcium is increased during normal synaptic transmission and paired-pulse facilitation, but not in long-term potentiation in area CA1 of hippocampus. *J. Neurosci.* **14**: 645-654.

Wu SP, Lu KT, Chang WC, Gean PW (1999) Involvement of mitogen-activated protein kinase in hippocampal long-term potentiation. *J. Biomed. Sci.* **6**: 409-417.

Xue F, Fang J, Delker SL, Li H, Martasek P, Roman LJ, Poulos TL, Silverman RB (2011) Symmetric double-headed aminopyridines, a novel strategy for potent and membrane-permeable inhibitors of neuronal nitric oxide synthase. *J. Med. Chem.* **54**: 2039-2048.

Xue F, Fang J, Lewis WW, Martasek P, Roman LJ, Silverman RB (2010a) Potent and selective neuronal nitric oxide synthase inhibitors with improved cellular permeability. *Bioorganic Medicinal Chem. Lett.* **20**: 554-557.

Xue F, Li H, Delker SL, Fang J, Martasek P, Roman LJ, Poulos TL, Silverman RB (2010b) Potent, Highly Selective, and Orally Bioavailable Gem-Difluorinated Monocationic Inhibitors of Neuronal Nitric Oxide Synthase. *J. Amer. Chem. Society* **132**: 14229-14238.

Xue L, Farrugia G, Miller SM, Ferris CD, Snyder SH, Szurszewski JH (2000) Carbon monoxide and nitric oxide as coneurotransmitters in the enteric nervous system: evidence from genomic deletion of biosynthetic enzymes. *Proc. Natl. Acad. Sci. U. S. A* **97**: 1851-1855.

Zabel U, Kleinschnitz C, Oh P, Nedvetsky P, Smolenski A, Muller H, Kronich P, Kugler P, Walter U, Schnitzer JE, Schmidt HH (2002) Calcium-dependent membrane association sensitizes soluble guanylyl cyclase to nitric oxide. *Nat. Cell Biol.* **4**: 307-311.

Zabel U, Weeger M, La M, Schmidt HH (1998) Human soluble guanylate cyclase: functional expression and revised isoenzyme family. *Biochem. J.* **335 (Pt 1)**: 51-57.

Zakharenko SS, Patterson SL, Dragatsis I, Zeitlin SO, Siegelbaum SA, Kandel ER, Morozov A (2003) Presynaptic BDNF required for a presynaptic but not postsynaptic component of LTP at hippocampal CA1-CA3 synapses. *Neuron* **39**: 975-990.

Zakharenko SS, Zablow L, Siegelbaum SA (2001) Visualization of changes in presynaptic function during long-term synaptic plasticity. *Nat. Neurosci.* **4**: 711-717.

Zarrindast MR, Karami M, Sepehri H, Sahraei H (2002) Influence of nitric oxide on morphine-induced conditioned place preference in the rat central amygdala. *Eur. J. Pharmacol.* **453**: 81-89.

Zhan X, Li D, Johns RA (1999) Immunohistochemical evidence for the NO cGMP signaling pathway in respiratory ciliated epithelia of rat. *J. Histochem. Cytochem.* **47**: 1369-1374.

Zhang HQ, Fast W, Marletta MA, Martasek P, Silverman RB (1997) Potent and selective inhibition of neuronal nitric oxide synthase by N omega-propyl-L-arginine. *J. Med. Chem.* **40**: 3869-3870.

Zhang Y, Hogg N (2005) S-Nitrosothiols: cellular formation and transport. *Free Radic. Biol. Med.* **38**: 831-838.

Zhuo M, Hu Y, Schultz C, Kandel ER, Hawkins RD (1994) Role of guanylyl cyclase and cGMP-dependent protein kinase in long-term potentiation. *Nature* **368**: 635-639.

Zhuo M, Small SA, Kandel ER, Hawkins RD (1993) Nitric oxide and carbon monoxide produce activity-dependent long-term synaptic enhancement in hippocampus. *Science* **260**: 1946-1950.

Zucker RS, Regehr WG (2002) Short-term synaptic plasticity. *Annu. Rev Physiol* **64**: 355-405.